An integrated sensor system

for monitoring washing processes

G.R. Langereis

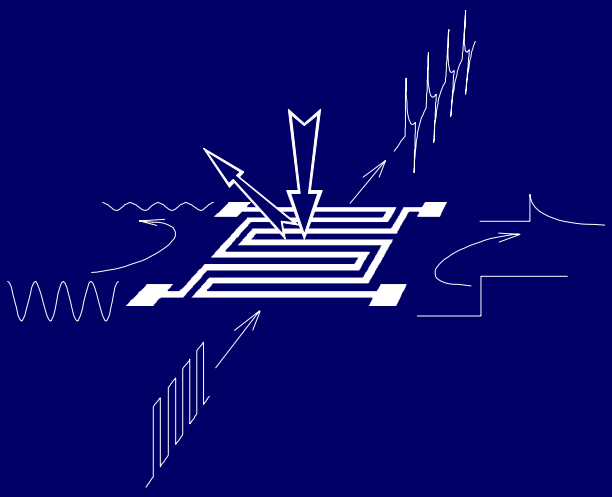

ISBN 90 - 365 - 1272 - 7
April 8, 1999

AN INTEGRATED SENSOR SYSTEM FOR MONITORING WASHING PROCESSES

The research described in this thesis was financially supported by Unilever Nederland B.V.

Cover illustration:
Artist impression of the operation of an integrated sensor array

Title: An integrated sensor system
for monitoring washing processes

Author: Langereis, Gerardus Rudolph
ISBN: 90-365-1272-7

AN INTEGRATED SENSOR SYSTEM FOR MONITORING WASHING PROCESSES

PROEFSCHRIFT

ter verkrijging van
de graad van doctor aan de Universiteit Twente,
op gezag van de rector magnificus,
prof.dr. F.A. van Vught
volgens besluit van het College voor Promoties
in het openbaar te verdedigen
op donderdag 8 april 1999 te 15.00 uur.

door

Gerardus Rudolph Langereis

geboren op 11 april 1970
te Apeldoorn

Dit proefschrift is goedgekeurd door

de promotor:	Prof.dr.ir. P. Bergveld
de assistent promotor:	Dr.ir. W. Olthuis

Voor Tara en Erin

Contents

CHAPTER 1

Introduction

In general, with single sensor applications, problems with calibration and stability are experienced. By combining sensors and using smart measuring methods, these problems might be solved since the coupled set of measured variables gives more information on the system than the separate sensors do. This additional information can be used to reduce the needs for stability, and to obtain calibration data.
Before integration is applied to sensors for monitoring washing processes as described in the rest of this thesis, this chapter gives a motivation for designing such an integrated sensor array. Different methods of integration are defined, justifying the structure of this thesis.

1.1 Motivation

In conventional washing processes, the operator adds a certain amount of detergent to the laundry and chooses a machine program together with a washing temperature. After the washing program is completed, the wash is inspected with human sensors (eyes, nose and hands). According to the obtained information, a decision is made whether the result is satisfying or not. Important criteria are the brightness and the smell of the laundry. When the result is not sufficient, the next washing cycle will be performed with adapted inputs (more or less detergent, other program). However, in the case that the result is judged as sufficient, a human operator will never know if the laundry was already clean ten minutes before the end of the washing process.
It can be questioned whether or not it is possible to replace the human sensors by electronic sensors which will give an independent decision on the final cleanness of the laundry. While the human operator is not able to examine the laundry during the washing process, such sensors placed in the tub would give an on-line monitoring of the process during washing. The advantage is that an objective decision can be made at what time the wash is clean. When also the washing process can be adapted, both the program and the detergent, this will result into a more efficient (environmental friendly) use of detergent and energy.
Although the intelligent human sensors, in the case of determining wash cleanness, can never be replaced by artificial ones, nevertheless the sensors to be developed should give signals from which decisions can be made which are comparable to the human analysis.

1.2 Trends in sensor design

The described motivation for using sensor arrays in washing machines is in line with the global trend in industry to introduce sensors in consumer products. Up to now, the sensor implementation is already very successful in the car industry, but it is also observed to a certain extent in other branches of sophisticated products. For example, sensors can already be found in computers and kitchen equipment.
More and more, the research on sensors is not restricted to simply measuring the parameter that is asked for. The use of integrated sensor arrays with an increased functionality by a smart data interpretation is typical for today's sensor research projects. The trend from developing single sensors towards such sensing systems can be illustrated by a small overview of the projects conducted in the Biosensor Group of the faculty of Electrical Engineering at the University of Twente. Figure 1.1 shows the sequence of all the Ph. D. projects of this group from 1970 to 2001.

The most important thread is the series of projects based on ISFET-like devices. The group was initiated in 1970 by the invention of the ISFET [1], a field effect transistor with a pH modulated threshold voltage. However, a number of assignments appeared to be necessary for understanding its operation and optimising the fabrication process [2, 3]. It was not until 1986 when the first application of an ISFET-based measurement system was developed which explicitely used actuators in combination with sensors [4]. This measurement system is able to measure a new parameter, being the weak acid concentration, by interpreting the pH response on a controlled proton release. Although the research on single devices capable of sensing new parameters went on [5, 6, 7], the research on the combination of sensors and actuators was carried out in later projects [8, 9]. For measurements using enzymes, introducing a selective recognition system with a low detection limit, the use of a stimulus-response measurement appeared to be essential [10, 11]. Therefore, the integration of sensors and actuators became for the second time a hot item. Although the research on particular problems like the packaging of sensors [12] and new sensors will not disappear [13, 14], the research on the integration of sensors and actuators has reached maximum attention. The projects on miniaturised analysis systems, being the development of a chipcard based system [15] and a microdialysis system [16], are just examples.

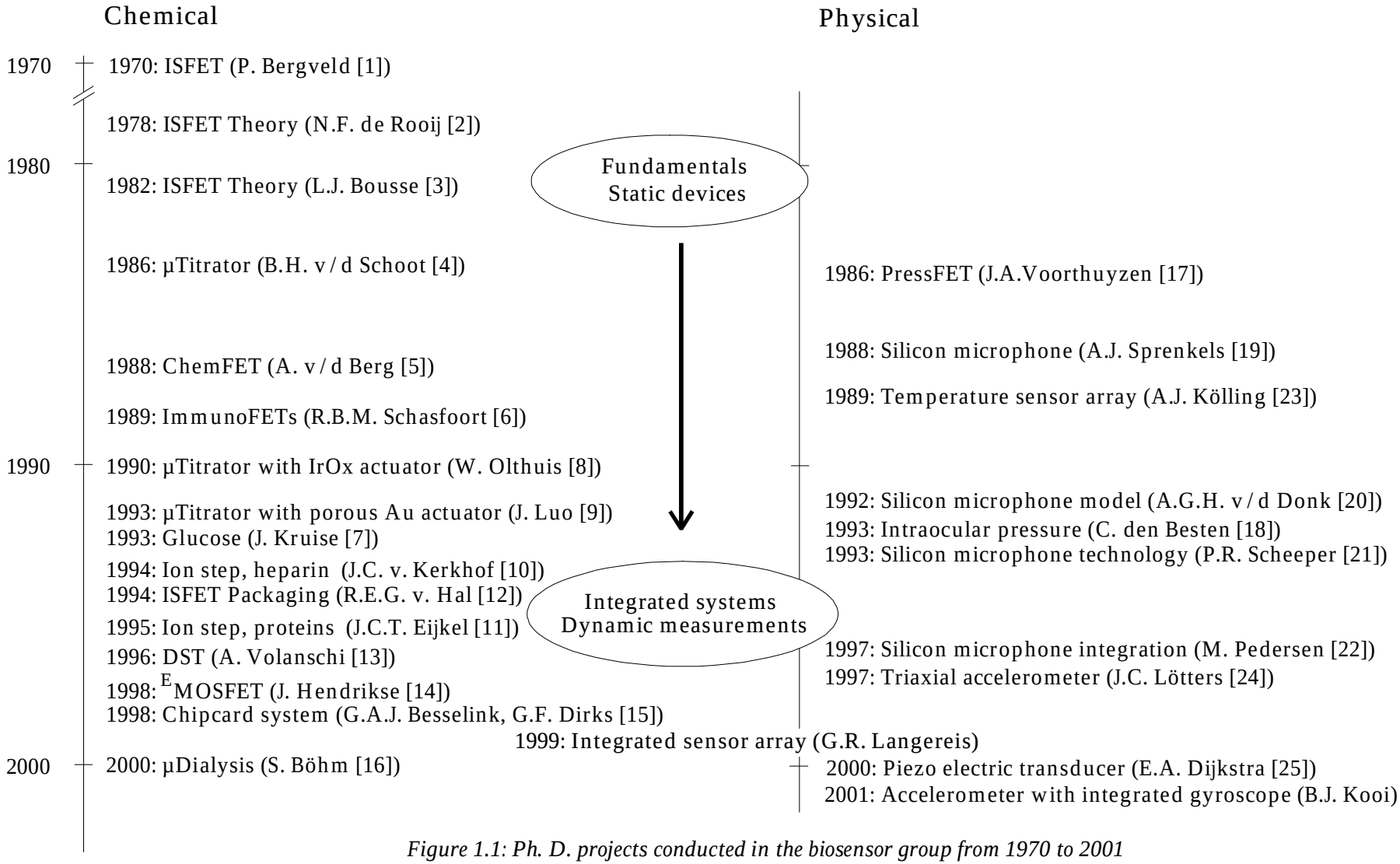

Figure 1.1: Ph. D. projects conducted in the biosensor group from 1970 to 2001

This global trend in the development of chemical sensors, going from device fundamentals and static devices to integrated sensor-actuator systems capable of performing dynamic (stimulus-response) measurements, is also observed in the projects on physical sensors. When trying to deploy the potentiometric FET sensor concept for the sensing of pressure [17, 18] and sound [19], the branch of physical sensors had started. The measurement of sound using a miniaturised microphone, which had nothing to do with ISFETs anymore, needed a more fundamental research on the modelling [20] and processing [21] before integration became possible [22]. Whereas with chemical sensors, the need for integration appeared to focus on the area of sensor-actuator systems, with physical sensors integration is more the integration of sensors with the accompanying electronics. However, also the integration of more than one of the same type appears to be interesting. For example, the development of an array of temperature sensors was initiated for measuring a temperature profile [23]. Another example is the development of a single device capable of measuring acceleration along three axes [24]. The integration of physical sensors is still continued. For determining the position of a spinal cord stimulator, this stimulator will be integrated with an ultrasonic stimulus-response distance detector [25], and the already mentioned three-axial accelerometer is currently expanded with the function to measure rotational speeds as well.

So, the trend from single devices to completely integrated systems capable of performing stimulus-response measurements is both observed in the field of chemical and physical sensors. The next section describes some general sensor concepts and the advantages of stimulus-response measurements.

1.3 General sensor concepts

Generally, a sensor should give an output signal as a function of an input signal, related by a certain sensitivity parameter. If a linear relation is assumed as represented in figure 1.2, two things are important: the slope of this relation and the intercept at zero input.
The operational model of a device gives the operator information about the input when the output is being measured. This requires a characterisation of the slope and the y-axis intercept, either by calibration or complete determination of the model. When according to the model a guaranteed zero output is observed at zero input, as usually observed with self-generating sensors, a one point calibration will be sufficient, else at least a two point calibration must be performed.

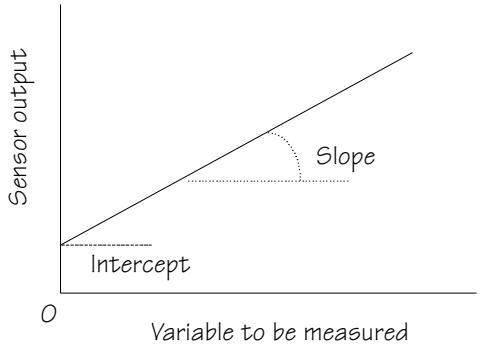

Figure 1.2: Simplistic representation of the transducing function of a sensor

The origin of a non zero y-axis intercept comes from the fact that the sensor is then of the modulating type where a reference is often not well defined. The dependency on stable references and calibration are the key problems in sensor applications. In the following subsections some sensor principles are being considered from the calibration and stability point of view.

1.3.1 Self-generating versus modulating sensors

If a sensor is seen as a transducer of information from one domain to another, two types can be distinguished. The first are sensors which convert energy from one domain to another. As a result, the output signal will be zero when no input is present because the only energy applied is the energy of the signal itself. This is called a self-generating transducer [26]. Examples are the thermocouple and the dynamo.
The second group of transducers consists of devices to which energy is applied by a source, which is subsequently modulated by a physical or chemical parameter. These are modulating transducers [26], examples are the pH sensing ISFET and the Pt-100 thermoresistive temperature sensor.
Because self-generating transducers have no output signal at zero input, there will be no offset (intercept in figure 1.2) and only the slope has to be known, for example by a one point calibration.

1.3.2 Differential measurements

With modulating transducers, the offset can sometimes be eliminated by measuring the output with respect to another element which is not sensitive to the measured parameter. In that case, a zero output means that the conditions at the measuring device are equal to that at the other device. This is a relative measurement with which common undesired signals, like unstable references, can be eliminated.
An often used differential set-up is the Wheatstone bridge as drawn in figure 1.3 [27].

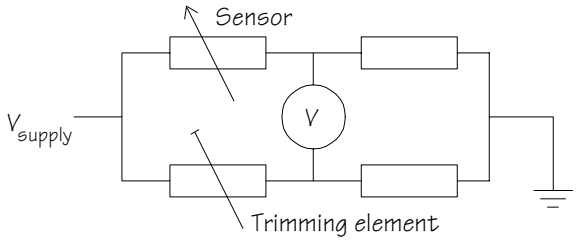

Figure 1.3: The Wheatstone bridge

The advantage of bridge set-ups is that the output voltage V can be set to zero at a desired sensor output by adjusting the trimming element. In addition, interfering signals that are common to the branches are being eliminated.

1.3.3 Dynamic measurements

Normally, when using voltammetric methods, a potential reference electrode is needed. Since reference electrodes are fragile and bulky elements, in practical sensor systems it is desired to find an alternative. A nice example is the coulometric sensor-actuator device [4, 8, 9, 28] which uses a special principle. Two ISFETs, placed in a sample solution of a weak acid, are differentially measured where one is modulated with locally generated hydroxyl ions. The sensed parameter is the time needed to reach the end point of a titration curve, where the pH difference has an abrupt change. The differential measurement of the locally occuring end point results in an elimination of the demands on a potential reference, and a pseudo reference can be used instead.
This technique is an example of a dynamic measurement. In a dynamic measurement, generally a known stimulus is created on which the system under test reacts with a certain response. Some parameters of the system will determine this response. So by observing the response, these parameters can be calculated. In some cases, the advantage is that parameters can be measured which could not be measured using a direct, static, method. Another example of a dynamic measurement application using an ISFET is the ion-step technique [6, 10, 11, 29] where a non-equilibrium situation is accomplished by changing the ion concentration in a flow system.
Other advantages can be in the smart utilising of the sensors. Sometimes, drifting offsets are passed by, when only the reaction on a stimulus is observed. This increases the accuracy of the sensor. The problem, however, is that the accuracy is now dependent on the accuracy of the actuator. Although the used sensors can be either of the modulating or self generating type, the whole system can be seen as a

stimulus-response measurement which is modulated by the parameter of interest.

Chrono amperometric measurements are electrochemical determinations of a concentration where the potential of a metal working electrode in an electrolyte is stepped to another potential while the current is observed [30]. The observed current response has a linear relation to the inverse of the square root of the time. This linear relation can be utilised by only evaluating the slope (instead of absolute values) from which information about concentrations can be determined. Therefore, this is also an example of a dynamic measurement, where a property of the response on a stimulus is used for determining information without being dependent on a stable reference.

1.3.4 Sensor integration

For stimulus-response purposes and differential set-ups, as mentioned in the previous subsections, the integration of multiple devices in a single system is required. With modern silicon technology the realisation of more than one device on a single substrate does not necessarily result into a more complicated process or a more expensive production process. The addition of a new structure of the same material is only a matter of adapting the masks for photolithography.

In addition to the advantages of integration concerning calibration and stable reference definition as mentioned before, there are some other advantages which can be obtained when combining the information of a number of sensor outputs. When more sensor principles for determining a single parameter are present in a sensor array, the combination of the obtained data can be used for the detection of errors or to decrease the error in the measured parameter. On the other hand, measuring two different parameters of a single chemical or physical process gives the possibility of eliminating certain interferences or calculating a new parameter. An example is the elimination of a temperature dependency by implementing a temperature sensor.
When a single structure is used to sense two parameters, which is in fact an array as well, the amount of connecting wires will be reduced. Furthermore, the data obtained from this single structure certainly came from the same location in the sample. This kind of integration is interesting because it simplifies the measuring system.

The realisation of devices on a single substrate results in sensors which have an extremely good similarity. The devices in the sensor array will come from the same batch and have the same processing history.

1.3.5 Sensor miniaturisation

After the required sensors and actuators are designed to be integrated into a single fabrication process, they can easily be miniaturised. Miniaturisation itself is benificial, because with silicon processing, a larger number of devices per wafer reduces the cost per device, at a fixed set of processing steps.
Besides the positive effect on the costs, there might also be some functional advantages. Geometric miniaturisation results in different weight factors of effects. While some effects may be neglected when using macro electrodes, with micro electrodes they might be of interest. So, phenomena can be reduced or magnified when scaling down. An example is the effect of the diffusion of ions which can be exploited in systems smaller than the average diffusion length.
Fast responses can be expected because the "micro experiments" are performed in a local environment. For example a measurement can be repeated at elevated temperature since heating of the local environment is possible with a relatively low consumption of energy. The heating will be fast because of the volume involved is small.

1.3.6 Conclusion

The most commonly observed difficulties when designing sensor systems concern the definition of a stable reference and the calibration of the system. Promising results for solving these problems are obtained by using either differential set-ups or stimulus-response measurements. For both methods, the integration of sensors is essential. For the second one also the integration with at least one actuator is needed.
Integration is not limited to just bringing sensors together, they can be integrated to a higher level by also matching their fabrication processes. An array of integrated sensors, fabricated using for example silicon technology, can be miniaturised easily. Miniaturisation does not only make the array cheaper, but might also lead to new parameters which could not be measured using larger structures. In addition, when sensors and actuators have some geometric resemblance and they are made of the same materials, sometimes the number of contacting leads can be decreased by designing a single multi functional structure.

1.4 Levels of integration

In the previous section, some different kinds of integration were already mentioned. A sensor-actuator system is an example of an integrated system, while also the smart use of multiple data obtained with several sensors is a method of integration. In the first case, the integration is the

joining of structures, while in the second case integration is in the data interpretation.
To separate the problem of designing an integrated sensor system into smaller parts, it is necessary to have a more fundamental view on the integration process. Therefore, the sequences passed through when retrieving a set of data defining the state of a certain environment are schematically drawn in figure 1.4.

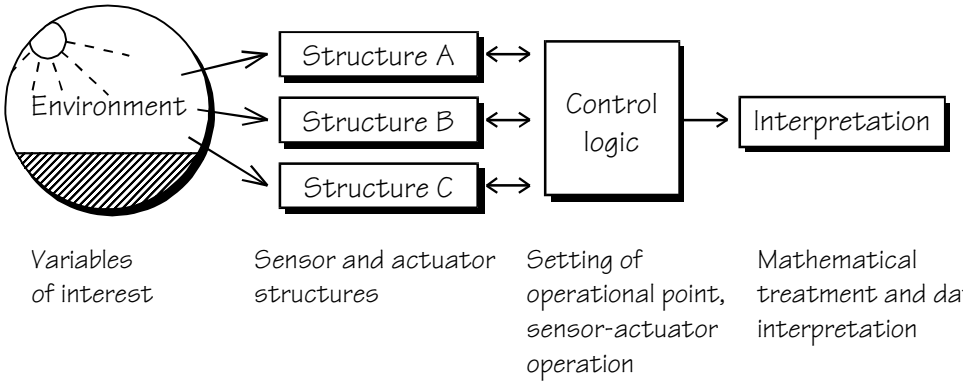

Figure 1.4: Schematic representation of the sequences in a multi sensor system

Four levels can be distinguished. The first level is the choice of a set of environmental variables to be measured. In case of the sensing of a washing process, these will be the washing parameters. The first encountered problem is already in this level. Some washing parameters can never be measured directly. For example, there is no sensor for an indeterminate parameter like “rinsing effectiveness”. Concessions like the conductivity or the turbidity of the washing water are in that case second to best. Another example is the water hardness. Water hardness is defined as the total concentration of multivalent ions, expressed as if they were all calcium ions. Since calcium ions will determine the hardness for the major part, one can suffice with a calcium ion sensor, although this does not measure the real hardness parameter.
So, for the representation of a certain set of washing parameters, a set of measurable variables must be chosen. Fortunately, there are also some variables which can be measured directly. Examples are temperature and pH. For these variables, the desired washing parameter is equal to a measurable variable.

In order to actually sense variables, certain structures have to be placed in the environment of interest. This is represented in figure 1.4 by three structures A, B and C. These structures will in the next level, the control level, be utilised for retrieving data from the environment. Examples of structures for sensing are a platinum resistor, of which the value can be measured in order to obtain the temperature using the thermoresistive

effect, and a parallel plate set-up, which can be used to measure electrolyte conductivity when this cell is immersed in water.
This sensing structure level is the first level on which integration is possible. When the structures are cleverly chosen, and structures for actuating operations are included as well, the structures might be combined into a multi purpose sensor-actuator structure. In order to do this, the structures to combine must be realisable using the same technology and fabrication process, and they must have some geometric resemblance. The result will be a geometrically integrated multi purpose structure, the design of which is the main subject of this thesis.

The next level is the control level which uses the structures for converting chemical or physical data of the washing system into usable electrical signals. This is done by scheduling these structures using certain operational modes. For example, the platinum resistor structure which was mentioned before is scheduled into a temperature sensor by applying a voltage over this resistor and measuring the resulting current. Another example is the ISFET which must be supplied with a drain current and a gate-source voltage in order to be able to read out the pH dependent threshold voltage. Besides setting an operational point, the control logic can also take care of linearising and modifying the signal. This is referred to as a "signal modifier".
Being able to access both sensor and actuator functions, yields the possibility of performing stimulus-response measurements. This kind of integration, which is located in the control level, can be referred to as functional integration since sensor and actuator functions are combined in order to create new functions.

Finally, the information obtained from all the sensors and stimulus-response measurements has to be evaluated in order to utilise this data optimally. An important action is to calculate the variable of interest from the measured electrical signals using the calibration data. Another action is to find new information by combining the information from the several measurements at the control level.
In this interpretation level, the data coming from the included elements are combined, and therefore one can speak of the integration of information.

In the interpretation level, a set of parameters is calculated with which the washing process can be understood in order to control it later. So, actually, the outcome of the interpretation level is the set of chosen washing parameters. While the structures level consists of devices, the control level must be implemented as electronics. For implementing the

interpretation level, a sophisticated piece of electronics can be used, or either a more flexible set-up consisting of a microprocessor where the calculations are performed in software.

1.5 Outline of this thesis

In chapter 2, the first level of figure 1.4 will be evaluated for washing systems. A set of washing parameters will be chosen, together with their practical ranges observed during washing. Their measurable equivalents will be described as well.
To implement the structures level, in chapter 3 a set of sensors is chosen which are based on matched structures with respect to their materials and fabrication technology. This matching of structures is required since geometric integration is desired. The design of a geometrically integrated multi purpose sensor-actuator structure, based on the chosen fabrication technique and set of materials, is presented in chapter 4.
Then, for the continuity, chapter 5 concerning bleach detection is added since it refers to a sensor which is included in the array of chapter 4. Actually, this chapter describes a technique which covers all four levels of sensor integration including stimulus-response measurements and smart data interpretation.
In addition to the shape and material of the structure itself, packaging is also part of the structure level. In chapter 6, one aspect of the packaging is focused on. The thermal properties of the substrate material appeared to determine the heating actuator operation. Some aspects concerning heat conduction and storage are explained which surprisingly results into a new sensing operation for determining the movement of the washing water.
The straight forward scheduling of sensor and actuator functions implemented in the multi purpose structure of chapter 4 is described in the same chapter. Straight forward means, that only one function is used for the detection or control of one parameter at the same time. More interesting for showing the universal applicability of the multi purpose structure is chapter 7 concerning sensor-actuator operations. This chapter accounts for all the possible sensor-actuator combinations and the potential achievements of these combinations.
Chapter 8 gives an example of the interpretation of the results obtained from a sensor-actuator operation: the electrolyte conductivity is monitored as a function of the imposed temperature.
In the supplementary results presented in chapter 9, the estimation of tap water hardness based on an electrolyte conductivity measurement is described. In addition, a design for a conductivity cell using a cheaper alternative fabrication technology as chosen before is tested. Finally, the

experiment of chapter 8, which is performed there using laboratory equipment, is repeated using the relatively cheap structure of chapter 4. In conclusion, the achievements will be summarised and evaluated in chapter 10. The set of variables which can be measured using the designed and tested implementation of the integrated multi purpose sensor-actuator structure is compared to the desired set of washing parameters. Based on this comparison, the structure can be qualified as being suitable for monitoring washing processes, and some suggestions for further research can be formulated.

1.6 References

[1] P. Bergveld, De OSFET en de ISFET: veld-effekt transistor elektroden voor elektrofysiologische toepassingen, thesis, University of Twente, 1973

[2] N.F. de Rooij, The ISFET in electrochemistry, The influence of ionic compositions of solutions on the response of the ion-sensitive field effect transistor, thesis, University of Twente, 1978

[3] L.J. Bousse, The chemical sensitivity of electrolyte / insulator / silicon structures, fundamentals of ISFET operation, thesis, University of Twente, 1982

[4] B.H. van der Schoot, Coulometric sensors, integration of a chemical sensor-actuator system, thesis, University of Twente, 1986

[5] A. van den Berg, Ion sensors based on ISFETs with synthetic ionophores, thesis, University of Twente, 1988

[6] R.B.M. Schasfoort, A new approach to immunoFET operation, thesis, University of Twente, 1989

[7] J. Kruise, Perspectives of glucose sensing based on a charge-modulating competition reaction, thesis, University of Twente, 1993

[8] W. Olthuis, Iridium oxide based coulometric sensor-actuator systems, thesis, University of Twente, 1990

[9] J. Luo, Employment of a porous gold acuator in ISFET-based coulometric sensor-actuator systems, thesis, University of Twente, 1993

[10] J.C. van Kerkhof, The development of an ISFET-based heparin sensor, thesis, University of Twente, 1994

[11] J.C.T. Eijkel, Potentiometric detection and characterization of adsorbed protein using stimulus-response measurement techniques, thesis, University of Twente, 1995

[12] R.E.G. van Hal, Advanced packaging of ISFETs, thesis, University of Twente, 1994

[13] A. Volanschi, Dynamic surface tension measured with single nucleation site electrodes, thesis, University of Twente, 1996

[14] J. Hendrikse, The ^{E}MOSFET: a potentiometric transducer based on chemically induced work function changes of electrochemically active films, thesis, University of Twente, 1998

[15] G.F. Dirks, G.A.J. Besselink, W. Olthuis and P. Bergveld, Development of a disposable biosensor chipcard system, In: A. van den Berg and P. Bergveld, Sensor technology in the Netherlands: State of the art, Proceedings of the Dutch sensor conference held at the University of Twente, The Netherlands, 2 - 3 March 1998, Kluwer Academic Publishers, Dordrecht, The Netherlands, 1998

[16] S. Böhm, W. Olthuis and P. Bergveld, A µTAS based on microdialysis for on-line monitoring of clinically relevant substances, In: D.J. Harrison and A. van

den Berg, Micro Total Analysis Systems ’98, Proceedings of the µTAS ’98 workshop, held in Banff, Canada, 13-16 October 1998, Kluwer Academic Publishers, Dordrecht, The Netherlands, 1998
[17] J.A. Voorthuyzen, The PRESSFET: an integrated electret-MOSFET structure for application as a catheter tip blood-pressure sensor, thesis, University of Twente, 1986
[18] C. den Besten, Sensor systems for the measurement of intraocular pressure, thesis, 1993
[19] A.J. Sprenkels, A silicon subminiature electret microphone, thesis, University of Twente, 1988
[20] A.G.H. van der Donk, A silicon condenser microphone: modelling and electronic circuitry, thesis, University of Twente, 1992
[21] P.R. Scheeper, A silicon condenser microphone: materials and technology, thesis, University of Twente, 1993
[22] M. Pedersen, A polymer condenser microphone realised on silicon containing preprocessed integrated circuits, thesis, University of Twente, 1997
[23] A.J. Kölling, A two-lead CMOS temperature sensor array for use in hyperthermia, thesis, University of Twente, 1989
[24] J.C. Lötters, A highly symmetrical capacitive triaxial accelerometer, thesis, University of Twente, 1997
[25] E.A. Dijkstra, J. Holsheimer, W. Olthuis, and P. Bergveld, Ultrasonic distance detection for a closed-loop spinal cord stimulation system, Proceedings 19th international conference - IEEE / EMBS, page 1954-1957, 1997
[26] S. Middelhoek and S. Audet, Silicon sensors, microelectronics and signal processing, Academic Press Limited, London, 1989
[27] R.S.C. Cobbold, Transducers for biomedical measurements: principles and applications, John Wiley & sons, New York, 1974
[28] B.H. van der Schoot and P. Bergveld, An ISFET-based microlitre titrator: integration of a chemical sensor-actuator system, Sensors and Actuators, 8 (1985), page 11 - 22
[29] J.C. van Kerkhof, P.Bergveld, R.B.M. Schasfoort, Determination of heparin concentrations with the ion-step measuring method, Technical digest of the fourth international meeting on chemical sensors, september 1992, Tokyo, Japan, page 370 - 373
[30] A.J. Bard and L.R. Faulkner, Electrochemical methods: fundamentals and applications, John Wiley & sons, New York, 1980

CHAPTER 2

Specification of the washing environment

This chapter describes the washing process, with the application of relevant sensors in mind. While the importance of integrating sensors was explained in the previous chapter, the need for placing sensors in washing systems is illustrated here. Another aim of this chapter is to show the field of application of the sensors to be designed. The washing process will define the variables to be measured and the ranges of these variables which can be expected.

2.1 Washing

Washing, in this context, is the removal of soil from textiles [1]. The machine washing system can be separated into several elements which together determine the efficiency of washing. The most important element is the detergent which primary task is the actual removal of soil from clothes. However, the detergent effect is manipulated by the washing machine and is dependent on the washing medium being water. Therefore, before the detergent effect can be explained in the next section, first the washing machine, the water and the types of soil must be considered.

2.1.1 The washing machine

Although in Europe front loading washing machines are the most common, the major machine market consists of twin and simple tub washing machines (China, USA and India). The European washing machines using a horizontal axis of rotation consume less water than the vertical axis (tub) types. It appears that with the European washing habits the best result is obtained.

On demand of the user, the washing machine executes a certain program. Normal washing machines can control only a few parameters. There is the possibility to control the volume of water in the tub, either by opening an inlet with tap water or by opening the drain. Next, the water in the tub can be heated using a feedback via a thermostat. The tub can be rotated on demand, sometimes with a variable speed. At a relatively high speed of 60 cycles per minute, using a 60 cm tub, the speed at the outside of the tub is equal to 1.9 m/s. So the mixing of

laundry and water can never be faster than this. Finally, the inlet of detergent and softener can be timed by flushing, using a water inlet.

The steps gone through in a typical washing program can be visualised by observing the water conductivity in a washing machine during washing as shown in figure 2.1.

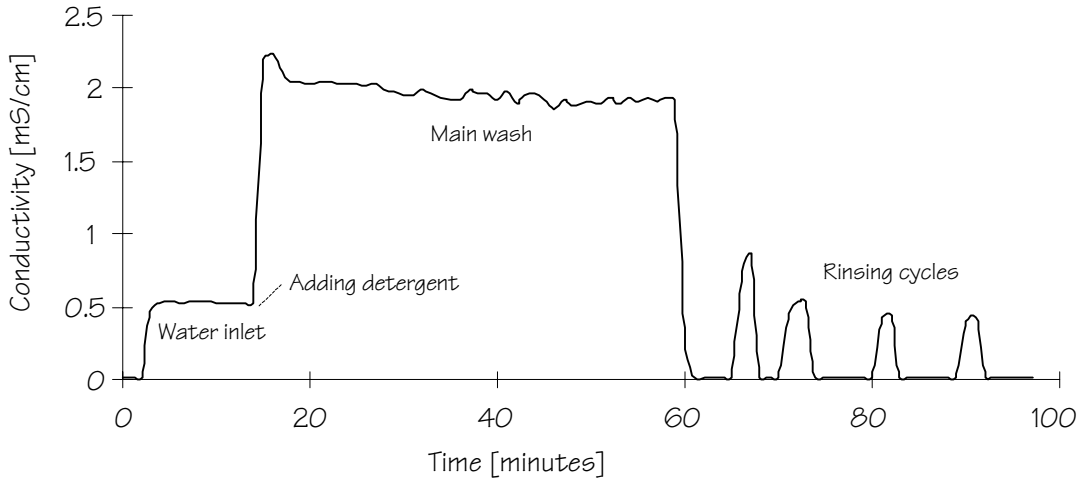

Figure 2.1: Water conductivity during washing

At first instance the conductivity sensor is dry and shows a zero electrolyte conductivity. When the tap water is inserted, the conductivity increases to at least the conductivity of tap water (in this case 500 µS/cm, but lower values can be expected in regions with a lower water hardness), while also the dirt of the laundry might increase the observed value. During the main wash, which starts after applying the detergent, the conductivity increases to about 2 mS/cm. So a conductivity sensor needs to cover about one decade. The building effect (capturing of ions) can be seen during the main wash as a slow decrease in the observed conductivity. During the rinsing cycles, the conductivity lowers to the conductivity of tap water, alternated by dry periods. According to the decreasing heights of the rinsing pulses, a decision can be made on whether the rinsing is effective.

Trends in washing machine developments are aiming at saving energy and detergent. Energy saving can be done by reducing the used amount of water, since then a smaller amount of water has to be heated. To do this, the effectiveness and the volume of the tub must be adapted to the process. Some USA washing machines are using 150 litres of water, while new types do the same with 50 litres. Detergent saving aims at a decrease of loss and better programming of the machine, but also reduction of water will decrease the necessary amount.

2.1.2 The water

The medium in which the whole washing process takes place is water. Water functions as a transport medium for the detergents and must remove the released soil. To guarantee proper transport to and from the laundry, the water must wet the substrate completely. Since water has a very high surface tension (72 mN/m), wetting can only take place rapidly and effectively if the surface tension is reduced by surfactants, which thus become key components of any detergent.

The temperature of tap water is about 10°C but can be lower (down to 5°C) in winter. During the main wash the water will be heated to either 40, 60 or 90°C.

The hardness of water is defined as the amount of multivalent ions, with calcium and magnesium ions the most dominating. The problem with these ions is that they have bad effects on washing machines since they can precipitate as carbonates on heating coils. In addition, they form residues in the laundry, which requires the addition of softener for avoiding stiff fabrics. Another problem is that a high concentration of calcium reduces the efficiency of detergents.
Figure 2.2 shows the distribution of the hardness ions in the tap water of 44 Dutch cities in 1986 [2]. The calcium concentration, which is significantly larger than the magnesium concentration, appears to be normally distributed around 1.4 mM.

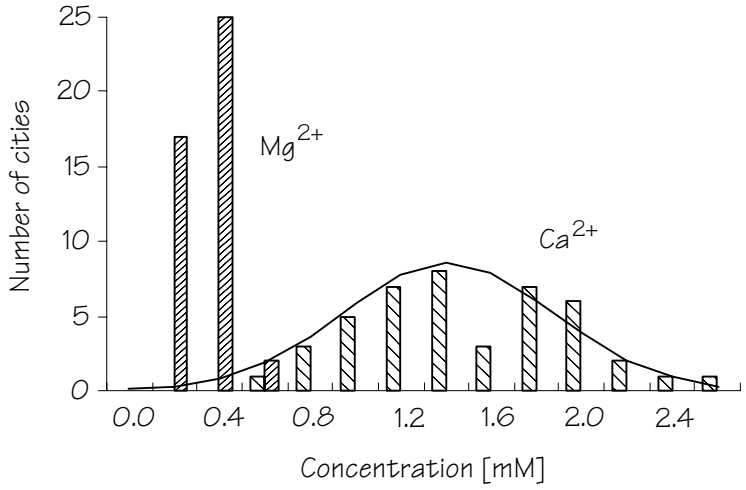

Figure 2.2: Concentration distribution of hardness-ions in tap water of 44 Dutch cities in 1986 [2]

Other elements present in water which decrease the washing efficiency, are iron, copper and manganese ions. These ions catalyse the decomposition of bleaching agents. To avoid this effect complexing agents and ion exchangers are added to the detergent. One of their

functions is to bind multivalent alkaline-earth and heavy-metal ions through chelation or ion exchange.

An impression of the most important ions present in tap water is obtained by observing the conductivity. The conductivity distribution of tap water coming from the same Dutch cities as used for figure 2.2, is plotted in figure 2.3a [2]. The normal distribution curve for the average of 0.49 mS/cm and with a standard deviation of 0.16 mS/cm is drawn as well.

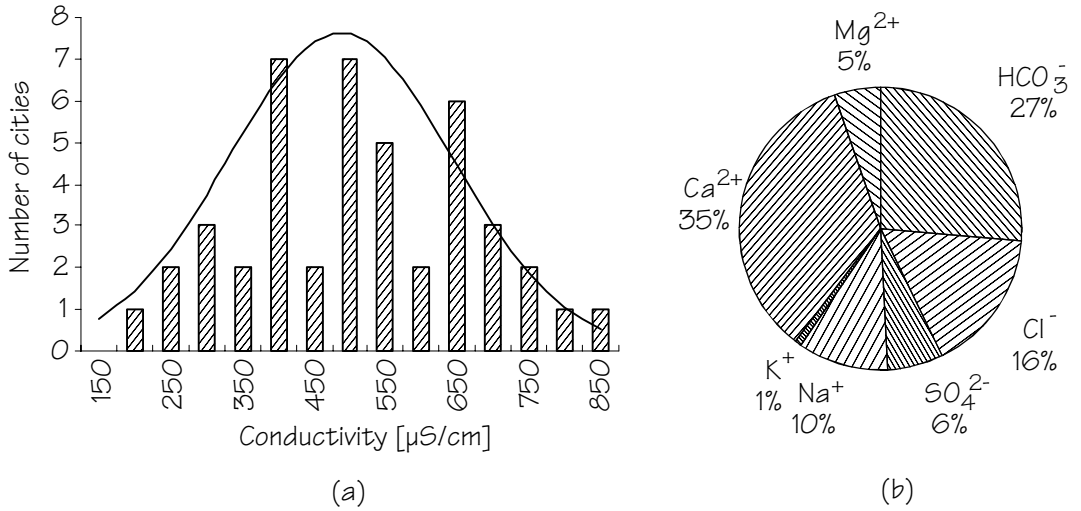

Figure 2.3: (a) Distribution of conductivity in Dutch tap water in 44 cities and (b) the average contribution of the separate ions to this conductivity

The ions that contribute to the conductivity can be found in figure 2.3b. It appears that Ca^{2+}, Na^{+}, Cl^{-} and HCO_3^{-} determine the conductivity of tap water for almost 90% on the average.

2.1.3 Types of soil

Initially, the soils to be removed by washing are present on the fabrics placed in the drum. The aim of washing is to move them from the textile into the water. Finally, they are removed by rinsing.
The types of soil can be distinguished by their chemical and physical behaviour. First, there are water-soluble materials like inorganic salts, sugar, urea and perspiration. Another category of soils are the pigments like metal oxides, carbonates, silicates, humus and soot (carbon black) which can have very intense colours. Fatty contaminations, for example coming from oil or food, can be removed using surfactants. At washing temperatures most oily and greasy fats are liquid. Proteins can also be present, originating from foods, like eggs and milk, or from humans, for example by blood or skin residues. Carbohydrates, especially starches,

form a category themselves. Finally, there are the bleachable dyes from fruit, vegetables, wine, coffee and tea.
Every component in the detergent will account for a certain type of soil. The removal of soils can be either chemical, like bleaching, or physical. Examples of physical soil removal are the washing of fat by the non-specific adsorption of surfactants, the specific adsorption of chelating agents on certain polar soil components and calcium capturing by ion exchangers. The detergent components will be discussed in more detail in the next section.

2.2 Detergents

Removal of soil from a surface can either be achieved with a chemical reaction (for example a redox process like bleaching) or without. In many cases the soil consists of substances that can not simply be removed by chemical treatment, in that case only displacement by interfacial processes will clean the substrate. Modern detergents include this requirement and contain besides bleaches also surfactants, water soluble complexing agents and water insoluble ion exchangers. An enhancement of soil removal is made by the increase of the wash time, temperature or the movement of the washing water.

A division is made into surfactants, builders, bleaching agents and auxiliary agents. These will be described in the next subsections.

2.2.1 Surfactants

In the first phase of washing the textile fibres and soil must be wetted as good as possible by the washing liquor. As a measure for the wetting the contact angle can be taken. If the contact angle is zero it is referred to as complete wetting and the liquid will spread spontaneously over the surface. Only liquids with a surface tension equal or less than the critical surface tension of a surface will cause thorough wetting.
Besides the wetting operation, surfactants take also care of a washing mechanism themselves. Since surfactants are an interface between polar (hydrophilic) and apolar particles, they are capable of making apolar soils, like oil and fat, soluble in water.

The surfactants are water soluble surface active agents. They consist of a long (alkyl) chain which is hydrophobic, and a hydrophilic functional group. In general both adsorption and wash effectiveness increase with increasing chain length. Surfactants with little branching in their alkyl chains generally show good wash effectiveness but relatively poor wetting characteristics, whereas more highly branched surfactants are

good wetting agents but have unsatisfactory detergency. Surfactants can be categorised in anionic, non-ionic, cationic and amphoteric surfactants. Some examples are drawn in figure 2.4.

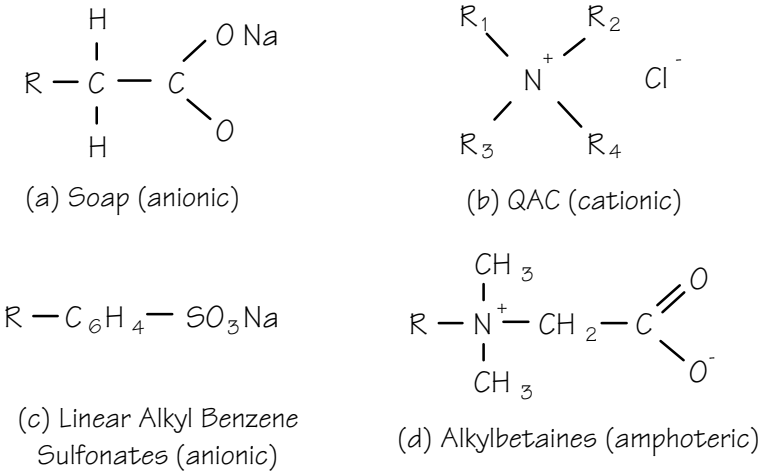

Figure 2.4: Examples of surfactants

2.2.2 Builders

One purpose of the detergent is to keep the concentration of hardness ions (especially calcium) in the water low, so that a maximal concentration gradient is present between soil and water. Then, the solubility equilibrium is shifted in the desired direction. This is done by the capture of multivalent ions by water soluble complexing agents. Next the ions are transported to insoluble ion exchangers which exchange for example one Ca^{2+} ion in two Na^{+} ions. Examples of components which are added to perform this operation, referred to as “builders”, are ethylenediaminetetraacetic acid (EDTA), sodium phosphates and sodium aluminium silicate (zeolite 4A).
When the laundry is being soaked by the water, the calcium concentration rises to the magnitude of about 10 mM (pCa ≈ 2). After applying detergent, the concentration of free Ca^{2+} is being reduced, because of the builder effect, to 0.1-0.01 mM. Using phosphate based builders the pCa becomes 5.6 in general, with zeolite based builders this value is about 4.2. So for measuring hardness before and during washing, a calcium sensor is needed which measures for over four decades. The empirical relation $Mg^{2+} : Ca^{2+} = 1 : 4$ can be used during all phases of the washing process to have an idea of the magnesium concentration.

The function of builders is the support of detergent action. Besides the capturing of hardness ions, an additional operation of builders is the increase of pH to about 12. Therefore, specific alkaline substances like sodium carbonate and sodium silicate are added. Their activity is based

on the fact that soil and fibres become more negatively charged as the pH increases, resulting in increased mutual repulsion. An additional advantage of an alkaline medium is that ions that contribute to the hardness will precipitate.

2.2.3 Bleaches

Bleaches are added to detergents to get a lighter shade in the colour of an object, which physically implies an increase of the reflectance of visible light. Chemical bleaching is the removal of non-washable soils by reductive or oxidative decomposition of chromophoric elements. The oxidative bleaches are more common in washing processes, since in laundry, components are present that become colourless if they are bleached reductively and return to their coloured forms when oxidised by air.

In many countries outside Europe the most common bleaching component is sodium-hypochlorid. In Europe the dominant bleaches are active oxygen based. The active bleaching component is the intermediate hydrogen peroxide anion which is obtained from hydrogen peroxide in alkaline medium:

$$H_2O_2 + OH^- \leftrightarrow H_2O + OH_2^- . \qquad (2.1)$$

The most important source for hydrogen peroxide is sodium perborate ($NaBO_3 \cdot 4H_2O$) which is present in the crystalline form as the peroxodiborate ion. This ion has excellent dry life time and hydrolyses in water to hydrogen peroxide.

Peroxide is most active at 90°C. To wash at lower temperatures (< 60°C) a bleach activator must be added. When present in wash liquor of pH 9-12, these activators react preferentially with hydrogen peroxide to form organic peroxy acids which have a higher oxidation potential than hydrogen peroxide. An example is TetraAcetylEthyleneDiamine (TAED) which can activate bleaching by replacing hydrogen peroxide by peroxyacetic acid as shown in figure 2.5.
Another approach for lowering the bleaching temperature is by using bleaching catalysis, where the bleaching power of sodium perborate is increased by some heavy metal complexes.

The concentration of bleaching compounds is generally 6 - 8 mM for perborate based systems (hydrogen peroxide) and 1 - 2 mM for peracid based systems.

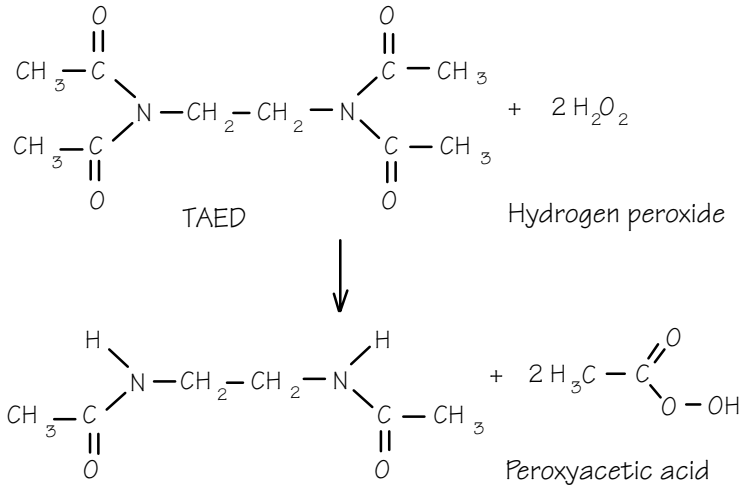

Figure 2.5: The reaction of TAED and hydrogen peroxide to peroxyacetic acid

2.2.4 Auxiliary agents

The last group of detergent compounds are the auxiliary agents which are added in small amounts. They all have a quite specific function.

Enzymes are used to cleave proteins (proteolytic enzymes) from sources like milk, cocoa, blood and grass. The effectiveness of enzymes is based on enzymatic hydrolysis of peptide and ester linkages. The addition of enzymes to detergent required a lot of research, since the presence of hydrogen peroxide, complexing agents and surfactants reduces proper enzymatic cleaning. Especially the bleaching effect destroys the proteolytic enzymes immediately. In addition, the alkaline medium (pH between 9 and 11) and the relatively high temperatures (90°C) will endanger the stability of the enzymes. Also, the enzyme must be storable thus having a little autolysis tendency.

After removal of the soil an antiredeposition technique must be used. Already mentioned are the ion exchangers which capture the ions to an insoluble phase. Other antiredeposition agents are polymers which are being adsorbed to the substrate and become a protecting layer. An example is carboxymethyl cellulose (CMC).

Historically, foam was a good indication of the washing effectiveness. However, with modern synthetic surfactants, foam is not desired because loss of the detergents by foaming out of the system will be the case. So in drum type washing machines, foam is inhibited by foam regulators. This type of regulator is called foam inhibitor. With hand washing the consumer wants to generate lots of foam, so in that case foam boosters are added.

Various machine components are made of metals. To prevent corrosion of these parts, modern detergents are supplemented with corrosion inhibitors. These materials deposit an inert layer on metallic surfaces to prevent attack by hydroxide ions.

After bleaching a yellowish tinge remains. In detergents often fluorescent whitening agents (FWA) are added. They can be categorised as cotton-, chlorine resistant-, polyamide- and polyester whiteners.

Fragrances are added to the detergent to give both the powder and the clean laundry a nice smell. In addition it masks the unpleasant odours produced during the washing.

To sell a product that can be distinguished from other products, the powder is coloured by dyes. The preferred colours for both powders and liquids are blue, green and pink. Green coloured detergent particles are also added to give the consumer the illusion that this product is environmental friendly.

In powdered detergents fillers are present. These inorganic salts (sodium sulphate) give the detergent a good flowability and flushing properties, high solubility, little caking of the powder under humid circumstances and prevent dusting. In liquid detergents phase separation and precipitation due to temperature changes are prevented by formulation aids.

2.3 Sequential dosing and interfacing

In nowadays washing processes a total washing powder is applied containing all detergent elements. The amount of detergent is dosed by the user according to the water hardness and the amount of laundry. In this way, when the builder dosage for lowering the hardness has to be increased, also the amount of surfactant is increased. This does not have much effect because the surfactant effectiveness is a matter of time rather than of concentration. This ineffective way of dosing does not fit with the aim of reducing detergent.

The solution for this problem is sequential dosing, where all the detergent ingredients can be supplied separately on demand. For effective sequential dosing some restrictions must be made. For example if bleaching elements are already supplied, the proteolytic enzymes are destroyed at the moment they are added. So the bleaching must be initiated after the enzymatic cleaning.

A logical sequence for inserting the components starts with the builder. The dosing is according to the water supply and must be applied during the washing to capture Ca^{2+} ions. The enzymes are added in an early stage to avoid the "burn in" effect, which is the unremovable adherence of oxidised (by bleach) peptides like blood contaminants. If the surfactants are added thereafter, this leaves the possibility to raise the temperature in the last phase of the washing for optimal bleaching.

An interesting new design is made by AEG which company has introduced a two-component washing system, on the market available as the ÖKO-LAVAMAT 6953 [3]. The advantage is that the high temperature step, required for accurate bleaching, is only performed a short time. To do this, besides the softener (builder) which is already dosed separately in many washing machines, the detergent is split into two components: one for bleaching and one for the other detergent operations. In figure 2.6 the wash cycle is schematically drawn.

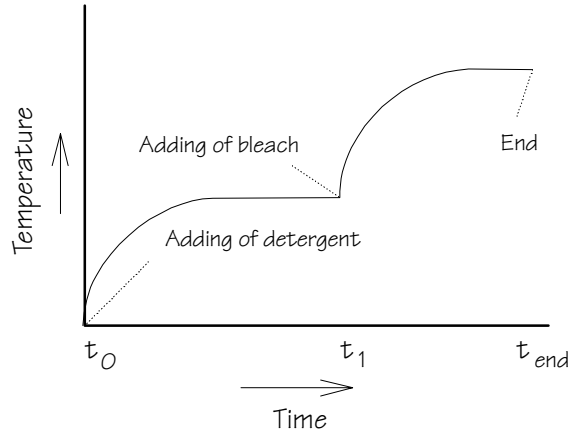

Figure 2.6: Temperature during the two component system

In the first period from t_0 to t_1 the temperature is relatively low (< 40°C) and only detergent is added. An optimal environment for enzymatic cleaning is obtained. At time t_1 the temperature is risen to the temperature necessary for accurate bleaching. So only from t_1 to t_{end} the temperature is high which reduces energy consumption.

Besides the possibility of controlling the dosing, a more efficient use of sequential dosing is accomplished by interfacing between the washing program and the state of the washing water. A washing machine which is capable of sensing the state of the washing water, is able to adjust the program to the laundry load. Interfacing will yield a further reduction of consumed detergent components, energy and used water.
An example of an interfacing washing machine is the Siwamat plus 4000 designed by Bosch-Siemens in co-operation with Unilever. This machine includes the Automatic Dosing System (ADS) [4] which is based on the

separate supply of four detergent components. The interfacing between process and laundry is not achieved by sensors, but by a dialogue keyboard on which the user specifies the contents of the tub and the quality of the tap water. After the completion of the dialogue keyboard, the machine starts to execute a washing program which is optimally adjusted to the load. A decrease of detergent consumption of 50% is claimed by the manufacturers.

However, for optimal interfacing between the program and the washing of the laundry, a real time monitoring by the use of sensors of the washing water is necessary. Only in that case, the program can be adjusted during washing.

2.4 Conclusion and selection of washing parameters

In conventional washing machines, the cleaning is achieved by mechanical input, carried out by the machine, and chemical input, carried out by the detergent. Control of the washing process is done by the user, by choosing the accurate detergent and adjusting the dosing, as well as by choosing the right program and temperature. There is no interaction between detergent and the program executed by the machine.
In order to achieve an optimal reduction of the consumption of water, detergent and energy, an interfacing washing machine is needed. Such a washing machine will monitor the state of the tub contents, resulting into information concerning the load, tap water and washing effectiveness. The process can be adjusted according to this information. For monitoring, sensors must be placed in the washing water.

To make a decision about the sensors that will be needed for monitoring washing processes, table 2.1 gives an impression of desired washing parameters, mentioned implicitly in this chapter.
Before the washing is initiated, the contents of the tub consists of soaked laundry. Parameters of interest are the amount, colour and type of fabrics. Also the quality of the tap water and the type of soil, partially already present in the water, are important parameters based on which the washing has to be adapted. After the detergent is added, the measured parameters will give information on the effectiveness of washing. A fast lowering of bleach activity indicates that many bleachable components are present. Finally, when the washing is done, the dirty water has to be removed by rinsing. This rinsing has to be monitored in order to detect an end point.

Table 2.1: Washing parameters before and during a washing process

Before washing	Type of fabric	The type of fabric (wool, cotton, etc.) present in the tub is hard to determine. Probably this can be left to the operator.
	Colour of fabric	In general, two types of wash are being performed: white wash and coloured wash. Because the difference is very hard to measure, this will be left to the operator.
	Load weight	The torque on the motor that rotates the tub gives information about the load weight.
	Amount of soil	An impression can be obtained by evaluating pH, turbidity and conductivity. For a more accurate measurement, specific sensors for soil contaminants will be needed.
	Type of soil	Specific sensors for detecting bleachable, fatty and stain-like soils are necessary.
	Water quality	Hardness, conductivity and turbidity have to be measured.
During washing	Water level	An explicit water-level indicator will not be necessary when a torque sensor is present (for the load weight). The mass of the tub will be dependent on the amount of water in the tub.
	Temperature	For control of the temperature a sensor will be needed.
	Detergent effectiveness	The measurement of surfactant level, enzyme activity, bleach activity, pH and hardness (builder dosage) gives an idea of the effectiveness of washing.
	Turbidity	Turbidity can only be sensed optically.
	Mixing effectiveness	A flow sensor is needed for measuring mixing effectiveness.
During rinsing	Rinsing effectiveness	For rinsing effectiveness, a secondary parameter must be found which is an indication for how many dirty water is exchanged by tap water. Conductivity and pH might be good indicators.

Terms like water quality, machine load, etc. can not be determined from sensors directly, which was mentioned in chapter 1 as the difference between washing parameters and measurable variables. So from this set of washing parameters, a set of equivalent measurable variables must be found. Table 2.2 gives a list of variables with which the washing parameters from table 2.1 can be approximated.

Torque sensor principles will be omitted in the rest of this thesis, since such sensors will probably not be placed in the sensor array, but will be realised in combination with the tub motor. Sensors for measuring the type of laundry (colour, fabric) are omitted as well. The reason is, that some techniques for fabric type determination are based on the water resorption characteristics (from a water level versus applied water curve), so they will also not be placed in the sensor array. In addition, it

is no big task for the user to tell the machine what type of fabric is in the tub, since a basic selection of fabrics must be made anyway.

Table 2.2: List of measurable variables which give an impression of the washing process

	Measurable variables	Washing parameters
Physical	Temperature	Temperature
	Flow	Mixing, turbulence or flow
	Conductivity	Water quality, rinsing effectiveness, soil load
	Dynamic surface tension	Detergent concentration
	Torque on tub-motor	Amount of laundry, water level
Concentrations	pH	pH
	H_2O_2	Bleach activity
	Ca^{2+}, Mg^{2+}	Hardness, builder functioning
	Enzymes	Enzymatic cleaning effectiveness, specific soil detection

Some ranges for the measurable parameters of table 2.2 were mentioned in this chapter:

Temperature: Tap water can be cold, 5°C, in winter and can be heated up to 90°C during some washing processes;

Flow: Using a 60 cm tub, with a rotation speed of 60 per minute, the speed at the edge of the tub is equal to 1.9 m/s;

Conductivity: a range from 100 µS/cm in very soft tap water to 2 mS/cm during the main wash can be expected;

pH: Between the pH of tap water and the pH after the addition of the detergent: pH = 6 - 12;

Bleach activity: For perborate based systems, the hydrogen peroxide concentration is about 6 - 8 mM, for peracid based systems concentrations of 1 - 2 mM are observed;

Hardness: The hardness of tap water is the result of 0.4 to 2.4 mM calcium and 0.1 to 0.6 mM magnesium. During washing the concentration of hardness ions is reduced to a minimum;

The measurable parameters listed as in table 2.2 are the starting point for the next chapter, where the required sensor structures needed for measuring these parameters are investigated.

2.5 References

[1] G. Jakobi and A. Löhr, Detergents and textile washing, principles and practice, VCH Verlagsgesellschaft mbH, Weinheim, Germany 1987

[2] Statistiek wateronderzoek 1986, Vereniging van Exploitanten van Waterleidingbedrijven VEWIN, Rijswijk, 1986

[3] User manual for the ÖKO-LAVAMAT 6953, AEG Hausgeräte AG, Nürnberg

[4] H. Zott, S. Willemse, Automatisches dosiersystem (A.D.S.) für Haushaltwaschmaschinen, in: Tenside surfactants detergents, vol. 27, 1990/1. Carl Hanser Verlag, München

CHAPTER 3

Selection of sensor materials based on a literature overview

The aim of this chapter is to choose the most appropriate set of materials for fabricating an integrated sensor array. Based on these materials, a set of sensors, or even better an integrated structure has to be designed which can be used to measure as much washing parameters as possible. However, the design itself and the interpretation of the sensor outputs, is set aside for a subsequent chapter.

3.1 Introduction

A sensor is a device which converts information from a domain of interest into a useful signal. In general, this conversion takes place in two parts, a selector and a transducer as indicated in figure 3.1. In the selector the information of interest is converted into a form which is measurable by the transducer. As the transducer is non-selective, the selector must introduce the desired selectivity [1].

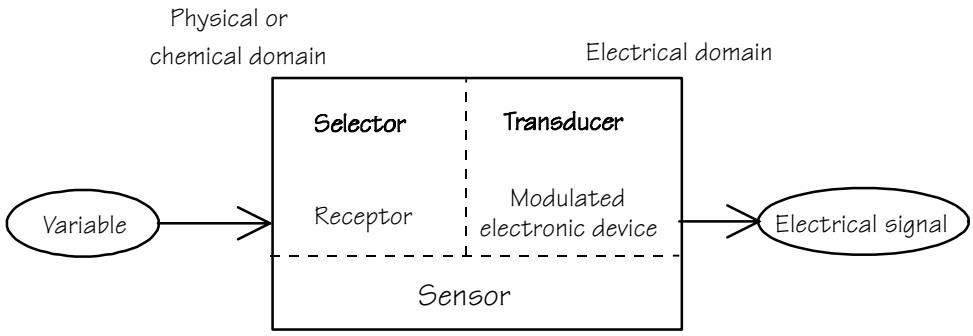

Figure 3.1: Basic structure of a sensor

For many chemical sensors, this two-level interpretation is quite clear. Commonly observed chemical selectors are selective membranes and modified surfaces, examples of transducers are FETs and amperometric working electrodes. Physical sensors have a less defined separation between those two parts. For example, a thermistor acts as a resistor in the transducer part, but a typical selector part is hard to point out. In this case, speaking of selectivity at all is difficult.

Although there are a lot of possible sensors, the ones having an electrical output are the most comfortable. Sensors giving an electrical signal as a measure for the desired chemical or physical parameter can easily be connected to a computer for data evaluation and storage.

When restricting to sensors having an electrical output, one can refer to the transducer part as a modulated electronic device.

For designing an integrated sensor array, the included sensor structures must have some technological compatibility in order to find a single fabrication process. The next three questions may arise considering the sensors to be integrated:

- What variable (washing parameter) is being measured?
- What is the modulated electronic device?
- What material / technology is chosen for the implementation?

The first question is necessary to reduce the enormous amount of known sensors to an orderly set for monitoring washing processes. The second question is added for getting insight in how to read out the sensor using an electronic circuitry. Finally, the third question links the sensor material to the sensor operation since in general the selection process is carried out by the properties of the chosen material.

As an example, table 3.1 gives the answers to the previous questions for three selected sensors. First, the ISFET has a tantalum-oxide layer which transforms the pH of an electrolyte into a surface potential. This surface potential modulates the threshold voltage of the underlying FET structure. Another example is the thermoresistive transducer which uses a conductive material to transform temperature changes into resistance variations. This resistance can be measured by constructing this material in the form of a resistor. With an amperometric working electrode the separation into a selector and an electronic device is more abstract. The receptor can be seen as an evoked specific chemical reaction, in which case the modulated electronic device is a current source with concentration dependent output.

Table 3.1: Some sensors described in the terminology of figure 3.1

Sensor	Measured variable	Modulated electronic device	Material of sensor
ISFET	pH	MOSFET	Ta_2O_5 - layer has a pH-dependent surface potential which modulates the threshold voltage
Pt-100	Temperature	Resistor	Thermoresistive metal of which the resistivity is temperature dependent
Amperometric sensor	Concentration	Current source	Inert metal evokes an electrochemical reaction after applying a potential

The three questions are taken as a guideline for the classification of known sensing methods. The washing parameters as chosen in chapter 2 are used for a first classification. Next, the most common electronic parts are listed, together with their capabilities for chemical and physical sensing. Finally, the most important sensing methods are described, classified by the used materials. Notice that for completeness, now the term “sensing methods” is used, because some mentioned “sensors” are not completely developed devices.
The result will be the choice of a set of materials together with their fabrication technology with which an array of sensors can be fabricated capable of sensing the desired washing parameters.

3.2 Sensor classification by measured washing parameter

In this section, a systematical categorisation of known sensors is performed. This categorising is done with respect to the washing parameters to be measured, as chosen in chapter 2:

- Temperature;
- Flow;
- Conductivity;
- Dynamic surface tension;
- Hydrogen peroxide concentration;
- pH and acid concentrations;
- Water hardness and calcium concentration;
- Enzymes;

3.2.1 Temperature

Most chemical and physical phenomena are temperature dependent. The direct consequence of this is that with almost all sensor output signals, the operational temperature must be given. On the other hand, the large number of temperature dependent phenomena is the reason for the large amount of temperature sensing principles that can be found in literature.
Besides the interest of sensing temperature itself, there are some principles which make use of temperature sensing. Examples can be found in flow measurements [2] and specific heat capacity determination. The specific heat capacity C_V at a constant volume of a substance is defined by [3]:

$$C_V = \left(\frac{\delta U}{\delta T}\right)_V \frac{1}{M} \qquad (3.1)$$

where U is the internal energy, T the temperature and M the mass of the substance. Because a change in internal energy can be identified with the heat supplied at constant volume ($q_{supplied} = \Delta U$), the previous equation can be used to determine the specific heat capacitance. When a known quantity of heat is supplied to a sample and the resulting increase in temperature is observed, the heat capacity can be calculated. An evaluation of the heat capacity of the contents of a washing tub will give information on the laundry type, since the heat capacity of the total tub load is partially determined by this laundry.
The practical realisation of such a determination is quite simple: the washing liquor is heated anyway at the beginning of a washing process by a known amount of heat, only the water temperature should be monitored. The mass of the contents of the tub (both water and soaked laundry) can be determined from the torque on the tub motor which is proportional to the current supplied to this motor.

3.2.1.1 Thermal expansion, glass thermometer

The glass thermometer is based on the thermal expansion of a liquid. At constant pressure, the volume of a certain amount of liquid (originally mercury, but nowadays usually coloured alcohol) changes linearly with temperature. To make the volume change visible for the human eye, the liquid is stored in a small capillary.

3.2.1.2 Thermoresistive effect

The bulk conductivity of many semiconducting materials depends on temperature. This has led to the development of small temperature sensing devices called thermistors.
There are in fact three categories of thermistors: the ceramic negative temperature coefficient (NTC) type, fabricated by high-temperature sintering of certain metallic oxide mixtures, the positive temperature coefficient (PTC) type, made by sintering barium and strontium titanate mixtures, and the single crystal doped semiconductor (silicon) type, which has also a positive temperature coefficient [4]. When accuracy is required and an offset is undesired, the thermistor is placed in a Wheatstone bridge circuitry.

While the temperature dependency of thermistors is exponential, semiconductor temperature sensors based on the spreading resistance technology have a virtually linear temperature characteristic. Discrete devices based on this technology are commercially available [5]. They have a positive temperature coefficient and their nominal resistance is about 1 kΩ at 25ºC.

These sensors use n-type silicon with a doping level between 10^{14} and $10^{15}/cm^3$. Typical chip sizes are about ½ × ½ × ¼ mm. The upper plane of the chip is covered by an insulating silicon dioxide layer in which a hole of about 20 µm has been etched for a metal contact to the silicon. The bottom plane is entirely metallised. When a potential is applied over the device, this structure results into a conical current distribution through the crystal, hence the name "spreading resistance".
Because of the accuracy and reliability, the spreading resistance technology temperature devices are an attractive alternative to the more conventional sensors using NTC or PTC thermistors.

Metal strips do have an almost linear variation in a certain temperature range [4]. A commonly observed implementation is the Pt-100 element, which consists of a platinum resistor with a resistance of 100 Ω at 0 ºC. Practical applications of Pt-100 elements are in a Wheatstone bridge set-up. To remove the effect of lead resistances, the element is supplied with three wires. Two of them are connected to the same side of the Pt resistor, one for the current injection and one for sensing.
Problems with Pt-100 elements come from the self heating when a current flows trough the device. This can be avoided by measuring in a pulsed way.

3.2.1.3 Thermoelectric effect, thermocouple

If two different metals are connected in a closed circuit with their two junctions at different temperatures, a current will be observed [4]. The Seebeck thermal emf, responsible for this current flow, depends on the types of metal involved and is approximately proportional to the temperature difference between the two junctions when the temperature difference is not too large. Since the temperature difference results into a voltage, this type of sensor is self generating.

3.2.1.4 Thermochemical effect

Thermochemical indicators make use of the temperature sensitive chemical changes in some substances. The rapid colour changes that some liquid crystals show occur within relatively small temperature changes. This enables one to measure surface temperatures either by painting or spraying a liquid crystal substance on a surface. In some applications plastic-film encapsulated liquid crystals are used. Registration of the effect is always optical.

3.2.1.5 Pyroelectric effect

Many of the temperature sensors mentioned before are used for temperature measurements by making contact to the medium under test. Applications of thermal sensors using the pyroelectric effect are in the field of IR radiation sensing.
The pyroelectric effect is observed with certain types of materials having a noncentrosymmetric structure where polarisation strongly changes with temperature [4]. Many piezoelectric materials, like ZnO, are also pyroelectric [6]. Other examples are lead zirconate-titanate materials. Under steady state conditions, the surface charge created by the polarisation is neutralised by external charges (due to leakage currents) and no emf is observed across the material. However, if the temperature is changed, the state of polarisation changes and a change in the external emf will be observed.

3.2.1.6 pn-junction

An understanding of the temperature characteristics of pn-junction diodes can be achieved by considering the current I at constant voltage V of a silicon diode in a forward biased operation [7]. The characteristic of a diode depends on the structure of the junction which can vary considerably from type to type. So, an accurate calibration of the temperature dependency is required. Besides that, there is no linear relation with temperature.

3.2.1.7 PTAT set-up

Better results than using a single diode can be obtained with transistors or transistor pairs. For a bipolar junction transistor, the temperature dependency of the V-I characteristics resembles that of the diode. However, by placing two identical transistors in an asymmetrical current mirror, resulting in dissimilar collector currents, the output voltage is proportional to the absolute temperature (PTAT sensor) over a wide range [8, 9]. Besides bipolar PTAT circuits, MOSFET based PTATs are possible as well.

3.2.2 Flow

To get an impression of the stirring effectiveness in a washing machine the flow can be measured. Whether this is mass flow or flow velocity is less important for this purpose. In this subsection an (incomplete) list of flow measurement techniques is given. Some of them are impossible to perform in a washing process, others are more easy. A major source of

flow measurement techniques comes from the field of blood flow determination [10].
In practical applications, normally the flow velocity is determined [11], by additionally using the density of the medium and the cross section of the tube the medium is flowing through, this number can be converted into mass flow.

3.2.2.1 Time of flight

When a liquid (or gas) is locally heated by a heat pulse, the time to detect this pulse at a distance x is a measure for the flow velocity [2]. Other markers like H^+ clouds [12] and small bubbles are reported as well.

3.2.2.2 Pressure gradient

The pressure gradient technique is based on a mathematical relationship between the flow velocity and the pressure gradient along a vessel. This method can only be used in tubes. To increase a pressure gradient, an obstruction is sometimes introduced in the tube.

3.2.2.3 Anemometric measurement

With anemometry, the cooling down of a heated element is used to calculate the flow velocity of a heat conducting medium.

3.2.2.4 Electromagnetic

When a conductor is moved through a magnetic field, an emf is generated within the conductor with a value proportional to the velocity. In case of a conducting fluid moving with a certain velocity, an emf is generated across the diameter of the fluid column, to be measured using appropriate electrodes. The measured emf is proportional to the flow velocity.

3.2.2.5 Ultrasonic

When an ultrasonic sound is applied to a tube with a flowing medium containing particles with a certain mass and size, the sound reflected by these particles has a frequency shift due to the Doppler effect. The Doppler shift in the frequency is proportional to the fluid velocity with a sign dependent on the flow direction [4]. This method is very popular in the medical practice for the measurement of blood flow in human vessels.

3.2.2.6 Indicator dilution methods

The operation of this wide scale of methods is based on the measurement of the dilution of an injected indicator. For proper operation an accurate model of the diffusion and flow behaviour of the indicator is necessary. Examples with different indicators are dye dilution, thermal dilution and conductivity dilution methods (as in use for the measurement of cardiac output [10]).

3.2.3 Conductivity

By measuring the electrical conductivity of the washing liquor, an impression can be obtained of the state of rinsing cycles or about the soil level in the washing tub. Besides that, some conductivity sensors can be used as concentration sensors when they are used in combination with a selective membrane [13].

3.2.3.1 Two-points set-up

A standard conductivity measurement is based on the measurement of the AC potential / current relation (impedance) of an electrolyte. In a two points set-up the electrodes that generate the current are used for measuring the potential as well [14].
The problem with this method is that the two relative unstable electrode interface impedances are in series with the potential difference induced in the electrolyte which gives an unknown error in the measured conductivity.
The insulator Ta_2O_5 has a relatively low oxide / solution impedance, so a two points conductivity measurement based on a Ta_2O_5 on platinum probe is an attractive alternative [15]. Sometimes the probe is realised as a planar interdigitated electrode.

3.2.3.2 Four points set-up

The problem with a two point conductivity set-up is that the impedances of the working electrodes are influencing the measured potential, and so the measured conductivity. In a four points set-up, the current loop and the potential sensing are realised as separate circuits.
The impedances of the electrodes in the measurement loop do not affect the measurement when this loop is sufficiently high-ohmic. Unstable electrode potentials will not affect the measurement if the frequency of the AC current source is chosen high enough.
The potential sensing is realised using either capacitive probes (Ta_2O_5 cell or ISFETs [16]) or metal strips.

3.2.3.3 Using an ISFET

In the small signal model of the ISFET, the electrolyte conductivity between ISFET and reference electrode becomes important [17]. The cut-off frequency of the trans-admittance (the transfer function from the gate-source voltage to the drain current) is equal to

$$f_{-3dB} = \frac{1}{2\pi R C_G} \tag{3.2}$$

with R the resistivity of the electrolyte and C_G the small signal gate capacitance. This small signal gate capacitance consists of the small signal gate to drain and gate to source capacitances in parallel, largely determined by the macroscopic oxide capacitance. A common range for this frequency is 0.1 MHz to 5 MHz which can be adjusted by changing the geometry of the structure.

3.2.4 Dynamic surface tension

The dynamic surface tension (DST) of a liquid is related to the surfactant concentration. This phenomenon was used for the development of a dynamic surface tension sensor [18, 19]. The operation of this sensor is based on monitoring the release frequency of electrolytically generated gas bubbles, which is dependent on the dynamic surface tension.
The DST electrodes are not simple metal films. Two configurations are reported. The first one is the cavity electrode. Bubble nucleation is controlled here by the geometric structure of the electrode. This specific structure is a pyramid shaped hole which is made by an anisotropic etch of silicon (KOH etch) before metal deposition. The second one is the "gas phase nucleation core" electrode where the nucleation is controlled by an initial amount of gas. This device requires an isotropic etch of silicon to make the gas core in the substrate.

3.2.5 Hydrogen peroxide concentration

Some hydrogen peroxide determination methods are well developed in glucose sensors where a GOD-membrane catalyses the glucose concentration to an equivalent hydrogen peroxide concentration. In these systems, the GOD membrane guarantees the selectivity. The resulting hydrogen peroxide concentration is generally measured amperometrically or potentiometrically.
However, in washing systems, the hydrogen peroxide concentration is the parameter of interest itself. So, this measurement technique must be selective for hydrogen peroxide.

3.2.5.1 Amperometric method

A platinum electrode for the electrochemical monitoring of hydrogen peroxide concentration is most widely used for biosensors nowadays. The Pt electrode is biased at 0.7 V versus an Ag/AgCl electrode. This method, however, suffers from interferences of other electro-oxidisable compounds in the solution (such as Fe^{2+}), so a high performance sensor is not possible [20].

3.2.5.2 Chrono amperometric detection

After applying a potential step across an electrolyte-electrode interface, the Cottrell equation [21] can be used to determine the concentration of H_2O_2 from the measured current response. This step must be high enough to deplete the H_2O_2 concentration at the surface completely by means of oxidation or reduction. Under this condition, the current response becomes independent of the applied potential step size. Because the demands on the potential step size are not very critical, the reference electrode might be omitted and a two-strip set-up can be used [22].

3.2.5.3 Potentiometric method

Instead of measuring current, the concentration information can be obtained by measuring potentials as well. Good results are reported [23] using a carbon electrode loaded with Perovskite-type oxides like $LaCo_xNi_yMn_zO_3$. A logarithmic variation with the hydrogen peroxide concentration is observed. Dependent on the used oxide contaminants, the reaction

$$H_2O_2 + 2H^+ + 2e^- \leftrightarrow 2H_2O(l) \qquad (3.3)$$

can be selected. The carbon with a perovskite-type oxide is placed on a conducting material. A current is applied and the emf is being measured in a half cell set-up, using a potentiostat. From the given reaction equation it can be concluded that the pH must be well defined during a measurement.

3.2.5.4 Volumetric titration

The following reaction occurs when a potassium permagnate solution is added to a hydrogen peroxide solution acidified with dilute sulphuric acid [24]:

$$2MnO_4^- + 5H_2O_2 + 6H^+ \leftrightarrow 2Mn^{2+} + 5O_2 + 8H_2O(l) \qquad (3.4)$$

where MnO_4^- has an intense purple colour which is not observed with Mn^{2+}. This is a classical example of a volumetric redox titration. In a laboratory set-up the end point is detected optically when the purple colour of the droplets coming from the burette does not disappear anymore.

3.2.5.5 Chemiluminescence

Certain compounds (molecules) can be detected by mixing them with a reagent with which the molecules react to form excited molecules which decay spontaneously with photo emission [11]. For hydrogen peroxide some of those reagents are available. This method requires a complicated and sensitive optical system.

3.2.6 Acid concentrations and pH

The terminology "acid concentration" and "pH" are both related to acids but are quite different. The pH is defined as the logarithm of the activity of free protons in a solution while the acid concentration concerns the total amount of a certain (weak) acid. For example, an ISFET measures the activity of protons. In a solution of a strong acid this is a direct indication for the acid concentration. However, with a weak acid the amount of free protons is only a fraction of the total acid concentration.
By applying OH^--ions to the chemical system, which can be done by either a volumetric or a coulometric titration, the pH varies with a characteristic shape: the titration curve. From the end point in this curve, which is the moment where the pH has a very steep change, the acid concentration can be determined.
A solid-state version of a titrator is the coulometric sensor-actuator device [12, 25] where hydroxyl ions are electrochemically generated at a noble metal electrode and the resulting change in pH is monitored by an ISFET.
The major part of pH sensors detect proton concentrations by making use of potentiometric techniques.

3.2.6.1 Potentiometric metal oxide sensors

The potentiometric pH sensing capability of metal oxides (PtO_2, IrO_2, RuO_2, OsO_2, Ta_2O_5 and TiO_2) is mentioned many times in literature [26, 27]. The use of antimony-antimony(III) oxide for in vivo pH sensing has become a standard technique in clinical applications [28]. However, the observed near-nernstian behaviour in the pH range 2 - 12 suffers from interferences from oxidising and reducing species and complexing anions. Although a metal oxide structure can be miniaturised easily, the

necessary reference electrode is a voluminous and fragile element. When sensing in a washing environment, the exposure to bleaching (oxidising) agents will be inevitable thus making the successful use of this type of pH sensor improbable.

3.2.6.2 The pH glass electrode

A very well known pH sensor is the pH glass electrode [29], already invented in 1901. This is an ISE (ion selective electrode) with a H^+ selective glass. Inside the electrode there is a pH buffered KCl solution with an Ag-AgCl or calomel electrode as a reference. At the inner side of the glass there is a constant potential because of the constant ion activities of the inner solution. At the outer side of the glass a pH dependent diffusion potential occurs which can be measured with respect to the external reference electrode. The diffusion potential satisfies the Nernst equation and gives a dependency of minus 59 mV per pH at 25°C.

3.2.6.3 The ISFET

The ISFET, which is a transistor based ion sensitive device, has the advantage that it is not made of fragile glass and that it is smaller than the glass electrode [30]. Because the operation is based on surface potentials, rather than diffusion potentials, the operation is faster compared to the glass electrode. The need of a reference electrode, just as with the glass electrode, is unfortunately less elegant. A more rigid system is possible when a solid state reference (a REFET) would be available.

3.2.7 Water hardness and calcium concentration

Historically "hardness" originated from the capacity of multi charged cations in water to replace sodium or potassium in soap [29, 31]. This undesired replacement decreases the efficiency of soap since badly soluble products are the result. Because calcium and magnesium ions generally exceed the concentration of other divalent cations in tap water, in many cases only the contribution of these ions is evaluated in discussions concerning hardness in general. For representing the water hardness as a single number, the hardness is defined as the calcium carbonate concentration equivalent (usually in mg/l) of the total concentration multivalent ions.
Most of the measurement methods listed here are selective for calcium with respect to magnesium but they are widely used for hardness determinations.

3.2.7.1 Volumetric titration with EDTA

A particular property of EDTA (EthyleneDiamineTetraAcetate) as a titrant is that it complexates with metal ions in a 1:1 ratio regardless of the charge of the cation. According to these complexes with a large number of metal ions, the volumetric titration with EDTA is not selective for calcium and magnesium. The general equilibrium is

$$M^{n+} + HY^{3-} \leftrightarrow MY^{(n-4)+} + H^{+} \qquad (3.5)$$

with M^{n+} the metal ion to be titrated and Y^{4-} the EDTA ion. Because of its pH dependency, EDTA titrations are generally performed in buffered solutions (for water hardness a buffered pH of 10).
The key to the measurement of water hardness using an EDTA titration, is the low stability of the complex with magnesium. The last multivalent ion to be titrated is magnesium, and therefore, a magnesium indicator can be used to determine the end point where all the multivalent ions have formed complexes. Such an indicator can either be calmagite or eriochrome black T. Often a small concentration of the EDTA complex with magnesium is included in the buffer to assure the presence of sufficient magnesium ions for improving indicator action [24]. Some test kits for determining the hardness of tap water work in this way.
A back titration, where free calcium is first completely removed by a complex-formation step with EDTA and afterwards quantitatively determined with erio-T is used as well [32].

3.2.7.2 Coulometric titration

This method makes use of the amine mercury(II) complex of EDTA-acid (H_4Y). The complexing agent EDTA is released to the solution as a result of the following reaction of the mercury electrode [24]:

$$HgNH_3Y^{2-} + NH_4^{+} + 2e^{-} \leftrightarrow Hg + 2NH_3 + HY^{3-} \qquad (3.6)$$

which is followed by complexation reaction (3.5). Because the mercury chelate is more stable than the corresponding complex with calcium (also zinc, lead or copper), complexation with this ion will not occur until the electrode process frees the ligand.

3.2.7.3 Potentiometric detection

In analogy with the measurement of protons, the detection of calcium ions can be done using potentiometry. Commercially available ionophores [33] can be used to make a calcium ion selective membrane. The interface potential between this membrane and a contacting electrolyte is nernstian dependent on the electrolyte calcium activity.

Two methods for sensing this interface potential are used. The first one is the calcium selective implementation of the classical *liquid membrane electrode* with an aliphatic di-ester of phosphoric acid as the ion exchanger [29]. In such a set-up, the potential is measured over two reference electrodes in the electrolyte where one of them is placed in a liquid membrane tub. In the liquid membrane tub, calcium ions are buffered resulting in a nernstian interface potential.
When the ion exchanger membrane is placed on an ISFET, this gives a calcium *ChemFET* [34, 35]. Although nernstian responses can be observed, ChemFETs in general do not give promising results for the use in the washing sensor array because the currently used lipophilic membranes will be washed off easily in an environment with soap.

3.2.8 Enzyme detection

Detection of enzymes (or peptides in general) generally requires a two phase method: first the peptide is specifically bound to a membrane and secondly this binding is being detected by an electronic device. In case of a reaction which releases protons or hydroxyl ions, an ISFET can be used for detection (the ENFET). When the ionic strength in the membrane is drastically influenced by the peptide reaction, a conductivity sensor is more adequate.

3.2.9 Summary

The methods evaluated in this chapter are summarised in two separate tables for physical and chemical washing parameters respectively.

Table 3.2: Summary of methods for determining physical washing parameters

Temperature	Flow	Conductivity	Dynamic surface tension
Thermal expansion Thermoresistive effect Thermoelectric effect Thermochemical effect Pyroelectric effect pn-junction	Time of flight Anemometry Pressure gradient Mechanical Electromagnetic Ultrasonic Indicator dilution	Two-points set-up Four points set-up Using an ISFET	Bubble electrode

Table 3.3: Summary of methods for determining chemical washing parameters

H_2O_2	pH and acid conc.	Ca^{2+} and hardness	Enzyme detection
Amperometry	Potentiometry	Volumetric titration	ENFET
Chrono amperometry	ISFET	Coulometric titration	
Potentiometry	Acid-base titration	Potentiometry	
Volumetric titration			
Chemiluminescence			
UV absorption			

3.3 Sensor classification as electronic devices

For the electronic circuitry connected to the sensor, a sensor behaves like a standard electronic component [36]. In chapter 1, sensors were categorised into self generating and modulating devices. While modulating sensing devices are represented by passive electronic components, self generating sensing devices should be represented as current and voltage sources. An exception is the category of transistor based sensors: although these are modulating sensors in general, they are referred to as active components from the electronic point of view.

3.3.1 Resistors

The *thermoresistive effect* of metal strips was already mentioned with the Pt-100 as an application of this effect for sensing temperature. Other materials like metal oxides can be used for thermoresistive set-ups as well.

Chemo resistors are chemically modulated resistors [1]. Standard metal oxide gas sensors consist of a sintered block of the oxide which is heated to a few hundred degrees centigrade. Surrounding gases react with the oxygen on the hot surface causing changes in the resistivity of the material. Gas sensors based on this principle and employing oxides of tin, zinc, zirconium or titanium and with proper doping are known to be sensitive to many types of gases. Metal-oxide gas sensors can be fabricated using thin (silicon) and thick film technology.

3.3.2 Capacitors

The mentioned resistor based sensors are easy to use because they give an immediate (current) response on an applied DC voltage. Capacitor based sensors, however, need an AC operational mode to get information from the device because no DC path is present.

For sensing purposes, two mechanisms are possible: either a change in the geometry or in the dielectric material will result into a change in the observed capacitance.
An example of a sensor based on the change in the geometry of a capacitive structure is the condenser microphone [37]. With this type of microphone, a sound wave brings one plate of a parallel plate capacitor into vibration, while the other plate (the backplate) is made of an inflexible material. The occurring change in the distance between the plates results into a change in the capacitance which can be detected by an electronic circuitry.
The dielectric constant of a material is not always a constant, but sometimes a function of some physical and chemical parameters. Some materials show a temperature dependent dielectric constant which can be measured by using a capacitive sensor structure [1]. Besides capacitive temperature sensors, also capacitive humidity sensors are reported [38, 39]. By placing a water adsorbing material between two metal plates, the capacitance of the created capacitor depends on the amount of the moisture adsorbed on the dielectric material.

3.3.3 Inductors

Inductors are hard to realise in micro technology, maybe that is why no significant chemical and physical sensitive coils were reported in literature. Even in macrotechnology the number of coil based sensors is low, and then only for physical movement detectors like displacement sensors and pick-up elements for both turntables and electrodynamic microphones. In theory it must be possible to determine variations in the magnetic permittivity of materials due to chemical influences. Temperature, moisture and deposition measurements must be possible, but the size of the fluctuations in the magnetic permeability μ_r is small.

3.3.4 Impedances

A sensor like an electrolyte conductivity cell can not be placed in the subsection with resistors or capacitors, because it is modelled as a complex impedance of which the value can only be determined properly by using AC signals. However, sometimes an impedance can be modelled as a network consisting of resistors, capacitors and inductances.
Besides the interest of electrical impedance measurements for determining electrolyte conductivity [14], the measurement of impedances of selective polymer membranes can give specific information on gases and ions [1, 13]. Subsection 3.4.1.4 concerning conducting polymers will discuss such membranes in more detail.

3.3.5 Diodes

The applications of diodes in sensors can be separated into two types. One widely applied physical sensitive diode is the temperature sensor, another chemical sensitive diode-based device is the ion controlled diode.
The diode equation, describing the relation between the voltage across a diode and the resulting diode current is given by [40]

$$I_D = I_0\left(e^{\frac{qV_d}{kT}} - 1\right) \qquad (3.7)$$

with I_0 the saturation current, V_d the diode voltage, q the unity of charge, k the Boltzmann constant and T the temperature. The appearance of the temperature in the diode equation enables temperature sensing using a diode [1].
An *ion controlled diode* (ICD) uses a lateral bipolar transistor covered by an insulating material with a selective membrane on top of it [41, 42]. The size of the depletion regions of the two lateral diodes depends on the interface potential at the ion selective membrane / electrolyte contact. By measuring the differential capacitance of the two space charge regions an impression of the ion concentration is obtained.

3.3.6 Bipolar transistors

In subsection 3.2.1.7 the use of a bipolar junction transistor in a *proportional-to-absolute-temperature* (PTAT) set-up was mentioned as a linear temperature sensor set-up [43].

Not many applications of bipolar transistors for chemical sensing are reported. The ICD described above looks like a bipolar transistor, but is not used in a transistor mode.
A technique called *transistor technique* is sometimes used for a pn junction in contact with an electrolyte to evaluate electrode reactions, because valence band electrons and conduction band electrons can be detected separately [44]. In this set-up only the n-type region is in contact with the liquid, the p-type layer is covered by the n-region. A bipolar junction transistor is formed with the electrolyte as a collector.

3.3.7 MOS transistors

The threshold voltage of MOSFETs is proportional to the difference between the gate metal and silicon work functions, Φ_M and Φ_{Si} [45, 46]. This dependency is essential for the applications of most of the MOSFET

structures in chemical sensors. Variations in these parameters can directly (as a 1:1 relation) be measured in the threshold voltage.
For instance, the ^{E}MOSFET [47] has an iridium oxide gate material which can still operate as a classical MOSFET. In addition, the iridium oxide in contact with an electrolyte results into an oxidation-state dependent work function which can be measured in the threshold voltage of the MOSFET operation.

Gas sensors

Metal work functions change with the contamination of the metal. An application is the use of a palladium gate in a MOSFET structure, the palladium gate IGFET [48]. Since the work function of palladium is dependent on the absorbed hydrogen gas molecules, this device can be used for hydrogen gas measurements by monitoring the threshold voltage.
In a suspended gate GASFET [48], a gap is created between the insulating gate oxide and a platinum gate. When gaseous molecules with a dipole moment diffuse into the gap, they increase the surface potential when adsorbed to either the gate material or the insulator material. While the IGFET is selectively sensitive to hydrogen gas, the suspended gate GASFET is sensitive to all polar molecules.
When the gate metal is omitted and the device exposed to a gas, an Open Gate Field Effect Transistor is created (OGFET) [45]. This device gives responses to polar molecules like water vapour and methanol.
An improvement is obtained when the oxide layer is very thin (5 nm). For thicknesses below this value the device responds to all kind of gases which have a permanent net dipole moment, such as H_2, NH_3, HCl, CO, NO, NO_2 and SO_2. This device is called the ADFET [45].
The problem with these devices is that the gate potential is badly defined. A solution to this problem is the use of the SAFET [45], which has an oxide layer which is partially covered by a metal gate. At the uncovered side, a dependency on polar gases (water, acetone, alcohols) is observed.

Humidity sensor, CFT

The Charge Flow Transistor (CFT) is a MOS-based field effect transistor with the metal gate placed as a ring around a resistive layer [49]. This layer is humidity dependent, so an applied gate voltage appears integrated at the oxide surface, and the resulting time constant can be measured by the field effect transistor as a function of the humidity.

Pressure sensor, PRESSFET
This device contains a floating (mechanical movable) plate hanging above the oxide of an ISFET structure. The influenced parameter is the air gap capacitance in series with the oxide capacitance [50]. This air gap capacitance is dependent on the applied pressure.

pH Sensor, ISFET
The set-up for an ISFET looks like that of the described gas-sensitive FETs but now the oxide is in contact with a liquid [30]. A gate contact is created by placing a reference electrode in the electrolyte. Although the transistor equations of the MOSFET are still valid, an additional term is added to the threshold voltage consisting of the surface dipole moment of the solution and the actual pH dependent electrostatic potential ψ_0. This parameter depends on the pH as follows:

$$\frac{\delta\psi_0}{\delta pH} = -2.303\frac{kT}{q}\alpha \qquad (3.8)$$

with the factor α as a selectivity factor without a dimension being

$$\alpha = \left(\frac{2.3kTC_{dif}}{q^2\beta_{int}} + 1\right)^{-1} \qquad (3.9)$$

where β_{int} represents the intrinsic buffer capacity of the oxide surface and C_{dif} the differential double-layer capacitance [51]. The factor α is between 0 and 1. When this factor equals one, equation (3.8) reduces to minus 59 mV/pH. The pH dependency is the result of the amphoteric sites at the oxide surface.

Reference probe, REFET
For a more elegant use of a pH dependent ISFET, a second modified ISFET is necessary to form a differential set-up which gives a pure pH output. This device, a REFET, should be identical to the ISFET, but with $\alpha = 0$. Although some devices are reported with lowered pH sensitivity ($\alpha < 1$), a good REFET is still not available.

Ion sensor, ChemFET
This device was already mentioned in previous sections. In this context it must be seen as an ISFET with an ion sensitive threshold voltage.

Enzyme based FETs, ENFET, IMFET, BIOFET
When an ISFET is covered by a membrane with immobilised enzymes, the chemical reactions that are specifically catalysed can in some cases be monitored as a pH variation. This is the ENFET [52].

Other ISFET based devices have specific immobilised receptors which give an antigen-antibody response, in early papers they were referred to as IMFET [53, 54], nowadays the word immunoFET is more common. Practical realisations of immuno FETs use a stimulus response technique [55, 56]. The response can also be generated in a bio-active reactor (for instance containing bacteria): the BIOFET.

Conductivity sensor
In the small signal model of the ISFET, the conductivity of the electrolyte is one of the parameters. This can be used to obtain the conductivity from the -3 dB cut-off frequency [17]. The measurable conductivity window can be shifted by modifying the geometry of the electrochemical cell.

3.3.8 Crystal

Quartz crystals have the possibility to vibrate when they are activated by a feed forward electronic circuit. Placed in an oscillator the rather high frequency (about 10 MHz) is very stable, and is often used as clock frequency in many electronic applications.

Crystal oscillator sensors
The resonance frequency of crystals is not only dependent on the properties of the material, but also on the mass of the connecting electrodes. This is why vibrating crystals are sometimes used to determine the mass of deposited material. An example is the monitor-crystal in a vacuum clock for determination of the thickness of a metal film during deposition.
Crystal gas sensors are also reported. They consist of a crystal, coated with materials used in gas-chromatography. This coating will adsorb gases and the mass will thus be increased. The result is an increase in the oscillation frequency. The same is possible in liquids.

SAW devices
Another field of crystal applications are the SAW (surface acoustic wave) devices which are the combination of a crystal actuator and a sensor. SAW devices give information about the propagation of acoustic waves along a surface [57].

3.3.9 Summary

The mentioned devices in the previous section are summarised in table 3.4. With all devices there is a certain current-voltage relation in which a parameter is dependent on an external input. Which parameter this is, is dependent on the device configuration and the chosen materials.

Table 3.4: Overview of electronic devices with their chemical and physical sensitivities

Device	I-V relation	Sensitive parameter	Dependent on	Name
Resistor	$V_R = I_R \cdot R$	R	Temperature Ions Gases	Pt-100 Chemo-res. Chemo-res.
Capacitor	$I_C = C \cdot \frac{dV_C}{dt}$	$C(\varepsilon_r)$	Temperature Moisture	
Inductor	$V_L = L \cdot \frac{dI_L}{dt}$	$L(\mu_r)$	?	
Impedance	$\overline{V_Z} = \overline{I}_Z \cdot \overline{Z}$	Z	Conductivity	Finger elect.
Diode	$I_D = I_0\left(e^{\frac{qV_d}{kT}} - 1\right)$	T I_0	Temperature Ions	 ICD
BJT	$I_C = \alpha_F I_{ES}\left(e^{\frac{qV_{BE}}{kT}} - 1\right) - I_{CS}\left(e^{\frac{qV_{CB}}{kT}} - 1\right)$	T	Temperature	PTAT
MOSFET	$I_D = \mu \frac{W}{L} C_{ox}\left((V_{GS} - V_T)V_{DS} - \frac{V_{DS}^2}{2}\right)$	$V_T(\Phi_M)$	H_2, Polar gases	gas sensitive FETs
		$V_T(\Phi_M)$	Oxidation state	^{E}MOSFET
		$V_T(\psi_0)$	pH	ISFET
		$V_T(\psi_0)$	Ions	ChemFET
		$V_{GS\text{-}eff}$	Humidity	CFT
		C_{Gap}	Pressure	PRESSFET
Crystal		f_{res}	Mass	Deposited layer thickness sensor
		acoustic impedance	Mass	SAW

In the second column of this table, the characteristic current-voltage relations for the electronic components are given [58]. For the resistor, this is just Ohm's law defining a voltage proportional to the applied current. An impedance has a similar characteristic relation, however, written in terms of complex values. A first derivative to the time of the current or the voltage is typical for the inductor or capacitor respectively.

The relation between the current through a diode and the applied voltage over the diode was already shown as equation (3.7). This exponential behaviour is also observed with the bipolar junction transistor (BJT). The equation given for the BJT is known as the Ebers-Moll equation [40, 58] and includes the reverse saturation currents I_{CS} and I_{ES} together with the current gain factor α_F. A MOSFET has a typical behaviour in which the threshold voltage V_T is used as a sensitive parameter in many sensor applications. The given equation describes the drain current as a function of the applied gate-source and drain-source potentials for the transistor in the unsaturated mode [40, 58].

3.4 Sensor classification by materials and technology

In this section, sensing methods are categorised with respect to the material, or material combination, the sensing structure is made of, as well as the technology to make the structure. This enumeration is not completely unbiased. As silicon processing is the most common fabrication technique in the MESA Institute and optical detection methods have not been used very much in the biosensor group, electrochemical methods based on silicon technology are strongly represented in the given sensor overview.
The presented sensor materials and material combinations are categorised by noticing the complexity of the sensor structures. This resulted into the major division of material combinations based on deposited films only, and material combinations having diffusion areas in addition. Under this major division, the classification is done incrementally from single layers to multi layer configurations.
Given a certain combination of materials, sometimes more than one sensor realisation is possible. The measured parameter is not only dependent on the used materials and its configuration, but is also determined by the operational mode, being the electrical bias signal applied to a specific configuration. An attempt is made to mention the known operational modes as complete as possible.

3.4.1 Sensor materials applied by deposition and patterning

First, assume that only deposition and patterning of materials is allowed. The technology can be either thin film (silicon technology), thick film (screen printing) or a macro technology (for example metal electrodes). However, a thin film implementation is preferred because of the availability of required processing equipment. Thin film processing sequences are based on well defined skills which increases reproducibility. In addition, thin film technology is optimised for mass production of small (sensor) structures.

The most important available thin film technology materials are summarised in table 3.5. The following subsections are according to the rows of this table.

Table 3.5: Some sensor materials that can be applied using deposition and patterning in thin film technology

Material	Examples	Deposition	Patterning
Metal films 3.4.1.1	Al, Au, Pt, Cu, ...	Evaporation, sputtering	Lift off, wet or dry etching
Semiconductors 3.4.1.2	Si, group III-V and II-VI compounds	CVD Polysilicon	Wet etching or RIE
Oxides 3.4.1.3	Ta_2O_5, IrOx, SiO_2, ...	Direct sputtering or evaporation with a subsequent oxidation step	Patterning of metal before oxidation, several etching techniques, lift-off
Polymers 3.4.1.4	PVC, Polysiloxane	Spinning, dipping or electrochemical deposition	Photolithography after adding photo initiator, photopoly-merisation
Inorganic membranes 3.4.1.5	chalcogenide glasses, AgX crystals	Depends on material	

3.4.1.1 Metal films in sensor applications

a. Sensing methods using metal films without chemical reactions

First, the sensing methods are listed that can be performed using metal films in such a way that electrochemical modifications of both the metal and the electrolyte are not taking place.

Current through a metal strip

The resistivity of a conducting strip is dependent on temperature. An example is the Pt-100 element [4]. The Pt-100 uses the thermoresistive effect of a platinum strip of 100 Ω. Such a strip has a nearly proportional resistive behaviour over a moderate range of temperature. The temperature coefficient α for platinum is equal to 0.392 %/ºC. Platinum resistance thermometers have a linearity of ±0.2% and are capable of realising an accuracy of 0.001ºC over the range of 0-100ºC. For larger temperature ranges polynomial fits can be used. The application of a platinum strip as a temperature sensor is generally done in a Wheatstone bridge configuration.

Besides the use of the thermoresistive effect for temperature sensing, local heating is also possible. When a current flows through a resistance,

energy is lost in the form of heat. So the resistivity of a metal strip can be used either to sense or to change the local temperature.
Applications of the heat actuator can be found in combination with the temperature sensor. Generally heat is produced and the temperature is measured elsewhere. Examples are specific heat capacitance (with gases), time-of-flight flow measurements and anemometry [2].

In very smooth metal films with thicknesses in the range of the mean free pathway of conduction electrons (≈ 50 nm), electrons will scatter at the surface. This scattering is dependent on adsorbed substances on the film surface, and so is the lateral film resistance. Sensors based on this principle are reported for the sensing of several heavy metal ions [59, 60].

Current between metal electrodes through a liquid
In this context of methods which do not cause chemical reactions, only AC currents are suitable because a DC current would definitely cause an oxidation or reduction.
If an AC current is injected from a metal strip, through a test solution, to a second metal strip, this experiment gives information about the electrical conductivity of the test solution in the potential drop [14]. The problem with this set-up is that the unknown and varying electrode interface impedance is part of the current loop, so this might give an error in the measured conductance. A solution to this problem is the application of a four points set-up or the use of capacitive probes as will be described in a following subsection.
A possible modification is that the current is not forced through an electrolyte, but through a selective membrane which is placed on top of the sensor. Changes in the membrane conductance as a function of some specific reactions from species of the bulk solution with the membrane are being sensed then [13].

Charge step method (coulostatic impulse)
With the charge step method a short current pulse is applied to a cell of two electrodes and the open circuit potential is recorded as a function of time. The current-pulse length is chosen to be sufficiently short that it only causes charging of the electrical double layer. This method has some advantages in the study of electrodes because only non-faradaic processes are selected [21] and the electrical double layer capacitance can be determined.

Schottky diode operation

Although in theory an undoped silicon substrate with a metal layer is a Schottky diode, in practice only doped silicon will be used in this type of diodes. The chemical sensitive Schottky diode will be discussed in section 3.4.2.2 treating the incorporation of doped regions.

b. Sensing methods using metal films that result in chemical modifications

A wide set of sensors can be summarised as devices using controlled potential and controlled current techniques. In principle, electro-chemical experiments can be performed using two electrodes in a liquid. Reactions can take place at both electrode-liquid interfaces and so both will be visible in the measured signal. To monitor the behaviour of a single electrode, a three electrode system using a potentiostat/-galvanostat is necessary.

Two principles for three electrode cell control are drawn in figure 3.2 [21]. When a potential is applied as in figure 3.2a, and the current is monitored in the lead to the counter electrode, the technique is referred to as amperometry and the apparatus to control this is a potentiostat. By choosing the working potential, a certain selectivity is obtained: only chemical reactions with a specific formal potential might occur. The resulting current with amperometric experiments is controlled by mass transport.

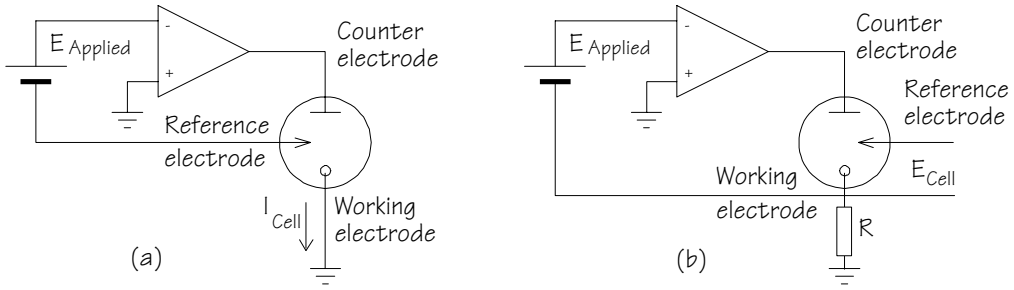

Figure 3.2: Simplified schematics for a potentiostat (a) and a galvanostat (b)

Two major types of amperometry are reported. When the current response to a certain input potential signal (which can be either a step, a sweep or a more sophisticated function) is recorded in time, the technique is referred to as *chrono-amperometry*. When the observed current is plotted as a function of the applied potential, the technique is referred to as *voltammetry* or sometimes *polarography* when a dropping mercury electrode is used.

With the mentioned techniques, macroelectrodes are used with sizes of at least some square millimeters. However, when the size of the working electrode is smaller than the diffusion layer thickness, completely different responses are observed. In general, when a

microelectrode is used, the response is independent on convection in the sample solution [61]. In practical applications, a matrix of electrodes with low packing density is used to increase the signals to be measured.
By taking the integral of the current in one of the controlled potential experiments, the charge involved is obtained, and the technique is called *coulometry*. The achieved information from a coulometric experiment is the amount of reduced or oxidised species.

Figure 3.2b represents the simplest method for applying a current and monitoring the working electrode potential. Techniques based on this set-up are called potentiometric measurements, and the apparatus is referred to as galvanostat.
After applying a constant current to a metal electrode, the electroactive species in the electrolyte will be reduced or oxidised, depending on the direction of the current. The potential of the electrode moves to potentials characteristic for the electroactive couple. After depletion of one species the potential changes until another electrochemical reaction is found. The time to reach depletion is called the transition time and is proportional to the diffusion constant and the square of the concentration. This transition time is described by the Sand equation [21] and the technique is called *chrono-potentiometry*. In general, the word *potentiometry* is reserved for experiments where the applied current is zero. Programmed current techniques using a non-constant current are reported rarely.

Faradaic impedance methods use a small (some millivolts) moderate frequency signal added to a slow ramp signal. A commonly used impedance method is AC-voltammetry, which is called AC-polarography if a dropping mercury electrode is used. The measured values are the magnitude and phase of the AC-current as a function of the frequency. An effective discrimination between faradaic and non-faradaic properties is possible.

The previously described methods monitor the reactions occurring just at the surface of the working electrode. With *stripping analysis*, electrolysis is used to preconcentrate a material on the surface of an electrode, before a voltammetric analysis. In this way very low concentrations can be detected because of the concentrator effect.

Besides sensor applications by electrochemical methods using a metal working electrode, actuator operations can be performed as well. By applying a current, the local electrochemical generation of H^+ or OH^- from water can be controlled:

$$2H_2O + 2e^- \rightarrow H_2(g) + 2OH^- \quad (3.10)$$

$$2H_2O \rightarrow O_2(g) + 4H^+ + 4e^- \quad (3.11)$$

depending on the direction of the current. An application is the coulometric sensor-actuator device were the pH control is used to perform a coulometric acid-base titration, being sensed by ISFETs [12].
The generation of hydrogen gas can be used for a second actuator function. The development of a dynamic surface tension (DST) sensor was conducted in the biosensor group [18, 19]. This device consists of a current controlled working electrode which generates hydrogen gas bubbles. From the fluctuations in either the electrode impedance or the over potential the bubble frequency can be determined. It appears that this frequency is proportional to the surfactant concentration. Actually this device is not a simple metal film. To control gas nucleation an anisotropically etched area is being used.

3.4.1.2 Semiconductors in sensor applications

In this subsection, the combination of semiconducting materials and metal layers is being evaluated. Although in this context actually deposited semiconductor layers should be considered, the most common applications use polycrystalline bulk materials.
Semiconductor materials that are reported mostly are:

- Ge and Si (group IV elements);
- GaAs (III-V compound);
- CdS and Zn, Ti, Sn, Ni, Mn and Co oxides (x -VI compounds);

Since this section is not about doped materials, the semiconductors mentioned here are intrinsic ones (doped semiconductors will be evaluated in the part of this section where diffusion areas are allowed).

a. Sensing methods using a current through a semiconductor

The conductivity of semiconductors changes with temperature [7]. For silicon this dependency is approximately eight percent per degree. This temperature dependency places a limitation on the use of semiconductor devices in some circuits. On the other hand, for some applications this property of semiconductors is used as an advantage. Semiconductors used in this manner are the *thermistor* and the *spreading resistance* temperature sensor.
Silicon and germanium are not used as commercial thermistors because their properties are too sensitive to impurities. Sintered mixtures of NiO, Mn_2O_3 and Co_2O_3 are used instead. Their resistivity changes exponentially with temperature [1].

The resistivity of some semiconductors is dependent on the strain in the material: this is the *piezo-resistive effect*. Strain gauges are generally based on slices of semiconducting material, most often silicon [1].

A well known chemical sensor for gas sensing using a semiconducting material is the tin-oxide CO-gas sensor [1]. This sensor uses a sintered block of the oxide which is heated to a few hundred degrees centigrade. Surrounding gases react with the oxygen on the hot surface causing changes in the resistivity of the material.
Using different dopants, this type of sensor is made sensitive to a wide variety of other gases.

b. Sensing methods using piezo electric operation

Some semiconductor compounds show piezo electric behaviour. This phenomenon can be used in piezo crystals and pressure sensors. Piezo crystals are being used in mass sensors as SAW (surface acoustic wave) devices to measure the mass of deposited materials [1], for instance adsorbed gases.

c. Sensing methods using electrical interaction with an electrolyte

The electron transfer across a semiconductor / liquid interface can easily be understood by looking at the energy levels [44]. The behaviour is dependent on the overlap between energy levels in the liquid and the solid. A semiconductor has a forbidden band gap region, and so only electrons from the valence and the conduction band can interact with the liquid. This results in small currents because the overlap is small. These conditions lead to a rectifying behaviour.
When a semiconductor is completely depleted from free charge at the surface, an insulating layer is created in the semiconductor. In contact with an electrolyte, such an insulating layer behaves similar to the situation that will be described in the next subsection concerning insulating oxides [62]. Actually, many semiconductors will form an insulating oxide layer at their surfaces in contact with an electrolyte or even air.
In literature only a small number of sensor applications of semiconductor / liquid interfaces are reported. A solid state sensor based on a bare semiconductor / liquid interface is the SnO_2 gas sensor [1] which has a dissolved CO-gas dependent resistivity.

3.4.1.3 Oxides in sensor applications

Oxides cover a wide variety of materials with also a wide range of properties. In this overview, the oxides are grouped as insulating and conducting types. Some oxides that show semiconducting properties were mentioned in the previous subsection. Most sensor applications based on oxides make use of metal layers for contacting the oxide, so the oxide-technology must be seen as an addition to the metal layer technology.

a. Sensing methods using insulating oxides

Whereas with conductor/liquid interfaces the potential drop is mainly across the Helmholtz layer, in insulator/liquid interfaces a significant potential difference exists across the insulator. Because of the insulating layer only capacitive measurements can be performed.
Semiconductor oxides are good insulators in general, unless the thickness is smaller than the tunnelling distance of electrons. Silicon oxide (SiO_2) is an insulator which is easy to obtain in silicon processes. Tantalum oxide (Ta_2O_5) is also an insulator but has a lot more surface sites than silicon oxide. The Ta_2O_5/solution interface has a stable and relatively low impedance which is almost completely determined by the activity of protons in the solution. So, noise caused by specific redox processes is reduced. An application is the conductivity sensor using this special oxide in a two points electrolyte conductance measurement [15]. In this case a two point set-up is possible because of the low impedance of the oxide/solution interface. Later, a second application of this oxide will be discussed as a selector material for the ISFET.

b. Sensing methods using conducting oxides

The resistivity of some metal oxides (like SnO_2 and TiO_2) depends on temperature and dissolved gases [1]. The tin-oxide CO gas sensor has become a standard and was mentioned earlier as an application of a semiconductor/electrolyte interface.
Ruthenium oxide (RuO_2) electrodes have an extremely low overpotential for hydrogen evolution and are used for the production of Cl_2 gas and in fuel cells [20].
Generally, conducting oxides can transport ions besides electrons. Therefore, they are sometimes referred to as mixed conductors. The electrochemical properties of conducting oxide-films are completely different from metal films and insulating oxides. A well known conducting oxide in this context is iridium oxide. In theory, all electrochemical methods listed in the metal/liquid section can be

performed. In the iridium oxide film both Ir^{3+} and Ir^{4+} are present. The ratio can be controlled electrochemically, but the total amount is constant. An application is the controlled injection of protons from the IrOx film into the electrolyte (proton actuator). The use of iridium oxide in various oxidation states appeared to give a pH sensitivity dependent on this state [63]. In addition iridium oxide is the basis for workfunction modulated sensors [47].
Many thin film metal oxides have been investigated for use as potentiometric pH electrodes [26, 27] while antimony oxide is already a well known material for pH sensors in biomedical applications [28].

3.4.1.4 Polymers in sensor applications

The application of polymer membranes offers a lot of advantages for sensor technology. These are relatively low cost materials and their fabrication techniques are quite simple (non-cleanroom processes). Polymer membranes can be placed on either metal electrodes, monolithic semiconductors, ceramics and glasses in thick and thin film devices. Most conventional ion selective electrodes (ISEs) contain a polymer membrane.

a. Sensing methods using dielectric properties

After applying a bias potential to some polymers, polarisation occurs. This polarisation can be changed by either mechanical stress or heat radiation (piezo-electric respectively pyro-electric effects). These materials have a wide application in the field of pressure, acceleration, and acoustic sensors [64].
Dielectrics which can hold an applied polarisation for a long time (dipole electrets) can be used in capacitive acoustic sensors [37]. The change in permittivity can be used for humidity sensing [38, 39].

b. Sensing methods using polymers as an ion exchange medium

Polymers like PolyVinylChloride (PVC) and polysiloxane are permeable to ions and gases, so those polymers can be considered as being solid electrolytes. Thus, the liquid to polymer interface will be between two ionic conductors. Some other non-polymeric materials like ZrO_2 and LaF_3 show a similar behaviour [62]. The advantage of these materials lies in the possibility to make ion selective electrodes (ISE's) by creating a selective buffering after inserting ionophoric sites in the membrane resulting in nernstian interface potentials.

Detection of the primary-ion dependent surface potential of such membranes can be done by placing the membrane on an ISFET (referred to as ChemFET [34, 35]).

c. Sensing methods using electrical conductance measurements of polymers

The functioning of membranes used for nernstian potential based sensors (mentioned above) is based on a system which buffers the primary ion concentration in the membrane. Only then, the boundary potential changes according to Nernst law with the concentration of the primary ion in the electrolyte. The same type of membrane, but without the buffering component, can be used with a conductometric detector [13]. Detection is accomplished then by the measurement of the bulk conductance in the membrane which is proportional to the primary ion concentration of the solution due to specific salt extraction.

d. Sensing methods using redox activities of polymers

By impregnating conducting polymers with a metal, the membrane becomes responsive to oxidising and reducing species in an aqueous environment. An example is poly(3-methylthiophene) with metallic platinum [65], or other noble metals. The advantage of poly(3-methylthiophene) is that it is conducting when oxidised (after O_2 exposure) and insulating when reduced (after H_2 exposure). Under aerobic conditions, 1 atmosphere oxygen for example, the device is conducting at low pH and insulating at high pH. Materials like polyaniline and polyacetylene show a metallic regime as well, where the conductivity is about 5 $\Omega^{-1}cm^{-1}$ [66].
Polypyrrole [67] shows another behaviour. It can be used to form membranes with electrically switchable ionic permeability. The ionic permeability is switched by control of the polypyrrole oxidation state with a potential applied to a membrane embedded gold electrode [68].

3.4.1.5 Inorganic selective membranes in sensor applications

Glass (as used for the pH glass membrane electrode) is not the only electrode material capable of a selective nernstian response to specific ions. Table 3.6 gives a summary of some important electrode materials [4]. The ion selective electrodes (ISEs) constructed with these materials are often used as potentiometric sensors.
An important class of inorganic selective materials are the chalcogenide glasses [69]. These are membrane materials (mainly Ag, S, and As alloys) that are highly ionic conductive. They are used for the

determination of heavy metal cations (Ag^+, Cu^{2+}, Pb^{2+}, Cd^{2+} and Fe^{3+}), iodide and bromide.

Table 3.6: Solid-state inorganic membrane electrodes

Ion	Ion-exchange medium	Operating ranges [M]
Ag^+	AgS crystal	$1 - 10^{-7}$
Br^-	AgBr crystal	$1 - 5{\cdot}10^{-6}$
Cl^-	Silverchloride (polycrystalline)	$1 - 5{\cdot}10^{-5}$
Cu^{2+}	CuS-Ag_2S mixture	$1 - 10^{-5}$
F^-	LaF_3 single crystal	$1 - 10^{-6}$
I^-	AgI crystal	$1 - 5{\cdot}10^{-8}$
S^{2-}	AgS crystal	$1 - 10^{-7}$
Heavy metal ions	Chalcogenide glasses	

3.4.2 Adding diffusion areas

After the previous section, which gave a summary of possible sensing techniques which can be performed using deposited and patterned structures on for instance an oxidised silicon or glass substrate, this section gives a summary of sensing methods that can be executed with structures on top of diffused areas in the substrate. While in the previous section the realisation could be in either thin-film, thick-film or macro electrodes on any substrate, now we are restricted to using silicon technology. Although as an exception, thin film transistors can be made on a lot more substrates.
Using diffusion areas, pn-junctions (and thus transistors) can be made. This allows a much wider range of sensors, for example a wide variety of ISFET based devices.

3.4.2.1 Single doped regions in sensor applications

This is an expansion of the semiconductor / liquid interface mentioned in subsection 3.4.1.2. If the semiconductor is doped the application is more convenient because some essential material properties are controlled during fabrication. The semiconductor / electrolyte interface now behaves like a pn-junction. By adding more donor or acceptor states, the semiconductor begins to behave more like a metal. The relation between current and voltage resembles the Schottky behaviour of a metal / semiconductor interface [70] and was studied many times but did not lead to important sensor applications.

3.4.2.2 Metal-semiconductor contacts in sensor applications

A metal layer on a semiconductor (or a heavily doped semiconductor on a semiconductor) is known as the Schottky barrier diode [7]. Two sensing principles were developed using this Schottky diode.
In Schottky diode operation mode, no interaction with an electrolyte is assumed, and only the temperature dependency can be mentioned as sensing possibility.
When the metal layer is catalytically active, a gas dependent behaviour is observed. In practice, the metal is almost exclusively Pd and the semiconductor ZnO, TiO_2 or CdS. The dependency observed is towards dissolved hydrogen gas. Hydrogen molecules in air are dissociated on the Pd surface and some of the atoms diffuse through the thin metal layer. They are adsorbed on the metal-semiconductor interface which results in a change in the Schottky diode properties [71].

3.4.2.3 Single pn-junctions in sensor applications

Two operational modes were developed using a single pn-junction, one with only currents in the bulk, and one with electrochemical interaction with an electrolyte.
For normal pn-junction *diode operation*, currents flowing in the device must be forced to stay in the substrate. When this is the case, only thermal interaction with the surroundings is observed and so a temperature measurement can be performed. High doping of one of the regions gives a more Schottky-like behaviour [7].
With the *transistor technique*, there is a direct chemical interaction with the liquid. The set-up for this technique consists of an n-type region in contact with the liquid which covers a buried p-type layer. A bipolar junction transistor is formed with the electrolyte as a collector. Using this technique, valence band electrons and conduction band electrons can be detected separately [44].

3.4.2.4 Dual pn-junctions in sensor applications

Two pn-junctions together may form a bipolar junction transistor. The structure can be either lateral or in the bulk. In literature, no complete bipolar transistors in contact with liquids were reported (structures that look like a bipolar junction transistor were mentioned before as the transistor technique, but they use a single pn-junction).
Without contact to an electrolyte, a bipolar junction transistor is sometimes used in a circuitry which is proportional to the absolute temperature (PTAT-configuration). This gives a more linear

temperature signal than a single pn-junction, however, four transistors are required [8].

3.4.2.5 Insulator on doped-silicon structures in sensor applications

Many insulators are not chemically inert, but show an equilibrium with protons and hydroxide ions (in case of SiO_2 and Ta_2O_5) when in contact with an electrolyte. A wide variety of sensors is based on insulator on silicon structures. The physical and chemical properties of insulators in contact with an electrolyte were mentioned in section 3.4.1.3a concerning insulating oxides. To convert a chemical or physical parameter into an electronic signal, some diffusion areas are introduced to get a modulated electronic device.

a. The ion controlled diode

The ion controlled diode (ICD) uses the phenomenon that the space charge is modulated by the ion-concentration of an electrolyte. The advantage is that the wires for electronic connection are at the back-side of the device, so insulation from the electrolyte is more easy than with front-side contacts.
ICD's are reported with a PVC membrane with incorporated valinomycin for potassium sensitivity and silicon nitride for pH sensitivity [42].

b. The ISFET and its applications

While the ICD structure resembles a bipolar junction transistor, the ISFET is based on the MOSFET structure and operation. The ISFET is best understood by describing it as a MOSFET with the metal gate substituted by an electrolyte, contacted by a reference electrode which now acts as the gate. With an ISFET, the threshold voltage appears to have a nernstian relation to the pH, due to buffered H^+ and OH^- ions at the oxide-electrolyte interface [30, 25].
If the insulator is thinner than about 30 nm then tunnelling is possible. This would be an ISFET with a an electron leakage through the oxide layer. In literature experiments are reported with ISFETs having a gate of 3 nm. They still acted as ISFETs because the tunnelling current was too low [70].

The use of ISFETs is not limited to pH measurements only. To make an ISFET selective for other species than H^+ and OH^-, a selective membrane must be added. The first option is to add an organic membrane as mentioned in subsection 3.4.1.4b. This device is called a ChemFET with

which a selective ion detection can be performed [34, 35]. A polyHEMA layer is added at the interface between the polymer membrane and the oxide to eliminate pH responses due to changing CO_2 equilibria and to guarantee a stable membrane/insulator interface potential. Ionophores for for example K^+, Na^+, Li^+ Ca^{2+}, Pb^{2+}, Mg^{2+} and NH_4^+ are commercially available. Inorganic membrane based ISFETs are reported as well, making use of materials mentioned in subsection 3.4.1.5.
When an ISFET is stacked with an immobilised enzyme membrane, the chemical reactions that are specifically catalysed can be monitored as a pH variation. This is the ENFET. Other devices (IMFET) have specific immobilised receptors which give an antigen-antibody response. This immuno-reaction can be monitored by the ISFET in case of the application of a (dynamic) concentration stimulator [56]. Besides that the response can be generated in a bio-active reactor (for instance containing bacteria): the BIOFET [45].

The cut off frequency in the small signal model of an ISFET is being determined by three physical parts. These are the small signal input capacitance, the cell constant and the electrolyte conductance (between a reference electrode and the ISFET). This last dependency has led to the realisation of an ISFET-based conductivity sensor [17]. The measurable conductivity window can be shifted by adapting the geometry of the cell. To get a measurable signal, the nominal electrolyte bulk resistance must be reduced using a configuration with a small window.

With ISFETs in the input stage of a differential amplifier, a potential difference in the liquid can be determined. This set-up can be used in combination with two additional metal electrodes which apply a current through the electrolyte. An example is the four points conductivity measurement using two ISFETs [16].

c. Thin film transistors

Thin film transistors (TFTs) are structures that look like MOSFETs but are completely assembled on top of a substrate which does not necessarily has to be silicon [72]. The staggered type can be made in an LPCVD/PECVD reactor without breaking the vacuum. The most common semiconducting material is amorphous silicon. Promising results are obtained using silicon-germanium mixtures.
Applications are in the field of active matrix liquid crystal displays and static memories. The use of TFTs for ion sensing (ISTFTs) and catalytic Pd-gate TFTs has been demonstrated [72]. A similar technology, however not used for transistor structures, is used for light addressable potentiometric sensors (LAPS) [73].

3.4.2.6 Metal-insulator-silicon structures in sensor applications

After having considered insulators and metals on semiconductors, the combination of metals and insulators on semiconductors is given here. The most common application is the classical MOSFET. Historically, this device must be placed before the ISFET.

Without chemical interference with an electrolyte, the device is the actual MOS field effect transistor. Applications in sensing are only in the PTAT set-up [43].

Chemical dependent versions of the MOSFET, sometimes referred to as MISFETs or MIS-capacitors, have a chemical dependent flatband voltage, measurable in their threshold voltage. A sensor is obtained by choosing an appropriate chemically active gate material [1].
Chemical reactivity is known from group VIII elements Ni, Pd and Pt. In this way devices sensitive to hydrogen, carbon monoxide, hydrogen disulphide and ammonia were realised. The behaviour comes from the dipole layer formation at the metal-insulator interface [71]. The device may be realised with single or multilayered dielectrics.
Other MISFET devices only have a very thin layer of insulating material (some nanometers), which is used to prevent undesired formation of intermediate species, while the electrons easily tunnel across this layer.
The MISFET was historically the successor of the chemical sensitive Schottky diode [36] as shown in subsection 3.4.2.2. Because the semiconductor materials ZnO and CdS are not very common in the integrated circuit technology, the combination of silicon and palladium was tried for gas sensing. The problem with this device was a formation of an intermediate silicide layer of Pd_2Si. The solution to this problem was the application of a tunnable SiO_2 layer between palladium and silicon.
A special chemically dependent MOSFET is the ^{E}MOSFET [47]. This device has an iridium oxide gate material enabling classical MOSFET operation. In addition, the iridium oxide is in contact with an electrolyte resulting into an oxidation-state dependent work function which can be measured as a modulation of the threshold voltage of the MOSFET.

3.4.2.7 Summary on sensors with diffusion areas

A summary of the mentioned doped-region structures is given in table 3.7. The most solid state applications are based on the electrolyte-insulator-silicon (ISFET) and metal-insulator-silicon (MOSFET) configuration.

Table 3.7: Sensor structures fabricated using thin films and diffusion areas

Structure	Examples	Modes
Doped region	Impedance measurement	current from silicon to liquid
Metal-silicon contact	Schottky diode, H_2-electrode	currents in the substrate only, gas sensitive metal layer
Single pn-junction	Temperature, transistor technique	current in diode only, current to liquid
Dual pn-junctions	Bipolar junction transistor, PTAT, on chip electronics	no chem. interaction with liquid
Insulator-silicon structure	Ion controlled diode, tunnelling diode, ion sensing ISFET capacitive probe ISFET	thick insulator, thin insulator, "normal" ISFET mode, AC mode
Membrane-insulator-silicon structure	ChemFET	Interaction with liquid
Metal-insulator-silicon structure	MOSFET, PTAT, H_2 sensor (Pd gate)	No chem. interaction with liquid, Interaction with gas
Oxide-insulator-silicon structure	^{E}MOSFET	Redox reaction with liquid

3.4.3 Summary

This section can be divided into two major parts. First subsection 3.4.1 described sensor structures which can be made using just deposition and patterning of (thin) films. The second major group of sensors as described in subsection 3.4.2 consists of semiconductor sensors with doped regions. A nice overview based on this second group was given by Saaman and Bergveld [70] who constructed a two dimensional graph partially covering the information of table 3.7. However, the devices were placed along an "insulator thickness" axis and an "in contact with" axis. For completeness the information of this graph is repeated here in table 3.8.

Table 3.8: Structural overview of insulator on silicon sensors with diffusion areas [70]

Insulator thickness:	*In contact with:* metal (Physical sensors)	electrolyte (Chemical sensors)
none	metal-semiconductor Schottky diode hydrogen gas-sensor	electrolyte-semiconductor TiO_2- cell pH sensitive
thin (<30 nm)	metal-insulator-semiconductor tunnel diode hydrogen gas	electrolyte-insulator-semiconductor. pH sensitive
thick	metal-insulator-semiconductor MISFET hydrogen gas	electrolyte-insulator-semiconductor. ISFET pH sensitive

This type of representation for the contents of subsection 3.4.2, can be expanded to subsection 3.4.1 concerning sensors which are fabricated using deposition and patterning of films on a substrate. In table 3.9 the "insulator thickness" axis is substituted by a material axis, and the "in contact with" axis by the criterion whether there is an observed chemical interaction with the electrolyte.

Table 3.9: Structural overview of film-type sensors without diffused areas

	Chemical interaction with electrolyte	
Material	No (Physical sensors)	Yes (Chemical sensors)
Metal	through metal Thermoresistive sensor Thermoresistive heater Lateral film resistance through electrolyte Electrolyte conductivity Coulostatic impulse using the Si substrate Schottky diode operation	through electrolyte Controlled potential technique Controlled current technique Stripping techniques Micro electrodes proton actuator
Metal + semiconductor	current through semiconduct. Thermistor Spreading resistance piezo effects Strain gauge SAW device	Tin-oxide CO-gas sensor
Metal + oxide	insulating oxides Conductivity cell	conducting oxides Mixed conductor pH electrode proton actuator
Metal + polymer	dielectric properties Electrets Acoustics transducers Acceleration transducers Pressure transducers	ion exchange medium Selective ion sensing conductance of polymer Selective ion sensing Polypyrrole systems
Metal + inorganic selective membr.		Selective ion sensors

3.5 Conclusions

The overview given in this chapter was focused on washing sensor array applications. This is why gas sensors are considered as being less interesting here. In addition, optical techniques are considered as less practical. The application of silicon technology is preferred because it is the most common fabrication technique in the field of microtechnology.

In the introduction the three-axes approach for categorising sensors was proposed to be a logical result of a certain generalisation of sensor operation. The used fabrication materials, the measured washing parameter and the measuring electronic device were chosen to be placed on the three axes. Notice that since these axes do not contain linear information, the order along the axes is arbitrary. Only along the fabrication materials axis, a certain ordering is possible: from simple to multi-layer structures. Figure 3.3 shows a two-dimensional projection of the three-axes graph. The third (measuring electronic device) axis is represented by comments in the graph.
Not all sensors mentioned in this chapter are placed in this final figure. For example the Pd-gate H_2 sensor, the TiO_2 CO-gas sensor, moisture sensors and SAW-based structures are omitted in figure 3.3 because they can not be used for measuring one of the eight chosen washing parameters. Another difference between the text and the figure is the assumption that metal layers are always necessary. Referring to its operation, the ISFET was discussed in the subsection concerning semiconductor materials with insulating oxides. For practical operation, however, the ISFET needs a metal layer for contacting the source and drain.

Remarkable is that the upper row, containing sensors and sensor techniques based on metal films only, cover already a wide range of physical and chemical parameters. As a starting point, consider the possibilities of sensor arrays consisting of metal films. The metals meant here are chemically inert, like platinum and gold. From the first row of figure 3.3 and recalling the washing parameters of chapter 2, it can be seen that the set of washing parameters given in table 3.10 can be measured using this category of sensors.
The required sensors referred to in table 3.10 are actually four types:

- A (planar) interdigitated electrolyte conductivity cell;
- An amperometric working electrode;
- A thermoresistive transducer for both heating and measuring;
- A bubble electrode;

R: Resistor
C: Capacitor
Z: Impedance
D: Diode
I: Current source
V: Voltage source
BJT: Bipolar transistor
FET: Field effect transistor

Metal films	Semiconductors	Insulating metal oxides	Conducting metal oxides	Polymers	Inorganic selective layer	Diffusion areas	Temperature	Flow	Conductivity	DST	H_2O_2	Hardness	pH, $[H^+]$	Enzymes
●							R: Pt-100 R: Heat actuator	R: Time of flight R: Anemometry	Z: Interdigitated structure Z: Four points set-up	V / Z: Bubble electrode	I: Amperometry		H^+, OH^- Actuator	
●	●						R: Thermistor							
●		●							Z: Ta_2O_5 cell					
●			●										H^+ Actuator V: Potentiometry	
●				●								V: ISE		V: ISE
●					●						V: Perovskite oxides			
●						●	D: Diode BJT: PTAT							
●		●				●	FET: PTAT		FET: ISFET (AC mode)				FET: ISFET	
●					●	●							BJT: Si_3N_4 ICD	
●		●		●		●						FET: ChemFET		FET: ENFET

Figure 3.3: Sensors categorised on their materials and measured washing parameters

Table 3.10: Washing parameters that can be measured using metal films only

Washing parameter	Description	Used sensors
Water quality	The conductivity measured in the tap water gives information about the water quality	Interdigitated conductivity cell or four points conductivity set-up
Amount of soil	An impression can be obtained by comparing the conductivity before and after the addition of laundry to the tap water	Same as above
Rinsing effectiveness	For rinsing effectiveness, the change in conductivity might be a good indicator	Same as above
Temperature	The thermoresistive effect of platinum can be used for a reliable temperature measurement	Pt-100 sensor
Bleach activity	Electrochemical detection of hydrogen peroxide seems possible	Amperometric sensor
Surfactant monitoring	Making use of the relation between dynamic surface tension and surfactant concentration	Bubble electrode
Turbulence, movement of medium	Anemometry or time of flight using a heat pulse indicates movement of the medium	Heater and temperature sensor

Notice that only the bubble electrode cannot be implemented as a simple planar structure, since it requires an anisotropic etching of the substrate. Nevertheless, integration is still attractive because all structures use the same materials.

In addition to this integration on material level, geometric integration is conceivable. To retrieve information from the sensors, these four sensors need different electrical operational signals. So it is plausible that a certain shape can be constructed with which all four sensing techniques can be carried out, scheduled by applying and reading out specific electrical signals. Therefore, the next step will be the design of such a single structure, having less connecting wires than the separate sensors would have, with which the mentioned sensing techniques can be performed by imposing certain operational modes.

Although the proposed set of measurable variables gives a rather complete impression of a washing process, two important washing parameters, hardness and pH, are missing. The concessions needed for implementing these washing parameters are unacceptable. For pH sensing, the method found in literature which comes the closest to the metal film only implementation is the potentiometric pH sensing using a conducting metal oxide. However, although an oxidised part of the metal structure can easily be generated in situ, for proper pH sensing a

reference electrode is needed. The application of a reference electrode will partially cancel out the advantages of the simplicity of the chosen metal film implementation.
For hardness determination, the use of a hardness ion selective membrane is not an option. These generally lipophilic membranes will be too fragile for the use in a washing machine where detergents are present for the removal of fatty species. In chapter 7, it is considered whether it is in principle possible to get an impression of the calcium concentration or hardness using a new technique with the available sensors and actuators.

To step back to figure 3.3, the next alternative is the use of a system based on metal deposition on silicon with ion diffusion steps and polymer membranes in addition. Although the use of a matrix of ChemFETs and ISFETs for sensing purposes seems interesting at first glance, the possibilities of functional integration are less interesting than is the case with the metal structures. Actually the creation of such a matrix consequently is just a matter of placing several sensors on a single substrate and there are less possibilities for wire and size reduction. So the choice will be to design a sensor array based on the application of deposited and patterned metal films only.

3.6 References

[1] S. Middelhoek and S. Audet, Silicon sensors, microelectronics and signal processing, Academic Press Limited, London, 1989

[2] J.H. Fluitman, A. van den Berg and T.S. Lammerink, Micromechanical components for µTAS, Proc. Micro total analysis sytems, page 73-83, Kluwer academic publishers, 1995

[3] P.W. Atkins, Physical Chemistry, fifth edition, Oxford university press, 1994

[4] R.S.C. Cobbold, Transducers for biomedical measurements: principles and applications, John Wiley & sons, New York, 1974

[5] Datahandbook Philips Semiconductors, Semiconductor sensors, book SC17, 1995

[6] R.S. Muller, Heat and strain sensitive thin film transducers, Sensors and actuators, 4 (1983), page 173 - 182

[7] S.M. Sze, Semiconductor devices, Physics and technology, John Wiley & Sons, New York, 1985

[8] G.C.M. Meijer, Thermal sensors based on transistors, Sensors and Actuators, 10 (1986), page 103 - 125

[9] A. Kölling, F. Bak, P. Bergveld and E. Seevinck, Design of a CMOS temperature sensor with current output, Sensors and Actuators, A21 - A23 (1990), page 645 - 649

[10] J.G. Webster, Medical instrumentation systems, application and design, Houghton Mifflin Company, Boston, 1992

[11] H.N. Norton, Electronic analysis instruments, Prentice Hall Inc., New Jersey 1992

[12] B.H. van der Schoot and P. Bergveld, An ISFET-based microlitre titrator: integration of a chemical sensor-actuator system, Sensors and Actuators, 8 (1985), page 11 - 22

[13] A.A. Shul'ga, B. Ahlers, K. Cammann, Ion-selective conductometric microsensors based on the phenomenon of specific salt extraction, Journal of Electroanalytical Chemistry, 395 (1995), page 305 - 308

[14] P. Jakobs, A. Varlan and W. Sansen, Transducers and electrodes, design optimisation of planar electrolytic conductivity sensors, Medical & Biological Engineering & Computing 33, nov 1995, page 802 - 810

[15] W. Olthuis, A. Volanschi, J.G. Bomer and P. Bergveld, A new probe for measuring electrolytic conductance, Sensors and Actuators B, 13-14 (1993), page 230 - 233

[16] A. Volanschi, W. Olthuis and P. Bergveld, Design of a miniature electrolyte conductivity probe using ISFETs in a four point configuration, Sensors and Actuators B, 18-19 (1994) page 404-407

[17] A. Volanschi, W. Olthuis and P. Bergveld, Electrolyte conductivity measured with an ISFET, Proceedings conf. Trends in electrochemical biosensors, Trieste, Italy, June 1992

[18] A. Volanschi, W. Olthuis, P. Bergveld, Gas bubbles electrolytically generated at microcavity electrodes (MCE) used for the measurement of dynamic surface tension in liquids, Proc. Transducers '95, Eurosensors IX, June 25-29 1995, Sweden

[19] A. Volanschi, W. Olthuis, R.T.J.M. van der Heijden, P. Bergveld, European Patent Application nr. 94203609.6 deposited at the European Patent Office in Rijswijk, December 13, 1994

[20] M. Lambrechts and W. Sansen, Biosensors: bioelectrochemical sensors, IOP Publishing, Bristol, 1992
[21] A.J. Bard and L.R. Faulkner, Electrochemical methods: fundamentals and applications, John Wiley & sons, New York, 1980
[22] K.D. Klein, Voltage relaxations of bi-electrodes for the long term monitoring of concentrations of hydrogen peroxide, glucose, etc., Sensors and Actuators B 22 (1994) page 127-132
[23] Y. Shimizu, H. Komatsu, S. Michishita, N. Miura and N. Yamazoe, Hydrogen peroxide sensor based on carbon electrode loaded with perovskite-type oxide, Proceedings of Transducers '95, Eurosensors IX, page 981-984, Stockholm, Sweden, June 1995
[24] A.I. Vogel, Vogel's textbook of qualitative inorganic materials, 4th edition, Longman Group Ltd., London 1978
[25] W. Olthuis, B.H. van der Schoot, F. Chavez, P. Bergveld, A dipstick sensor for coulometric acid-base titrations, Sensors and Actuators, 17 (1989), page 279 - 283
[26] K.G. Kreider, M.J. Tarlov, J.P. Cline, Sputtered thin film pH electrodes of platinum, palladium, ruthenium, and iridium oxides, Sensors and Actuators B 28 (1995), page 167-172
[27] A. Fog and R.P. Buck, Electronic semiconducting oxides as pH sensors, Sensors and Actuators, 5 (1984), page 137 - 146
[28] G. Edwall, Improved antimony-antimony (III) oxide pH electrodes, Medical & Biological Engineering & Computing, vol. 16, november 1978, page 661 - 669
[29] D.A. Skoog, D.M.West and F.J. Holler, Analytical Chemistry, Saunders College Publishing, Philadelphia, 1992
[30] P. Bergveld and A. Sibbald, Comprehensive Analytical Chemistry, edited by G. Svehla, Volume XXIII, Analytical and biomedical applications of ion-selective field-effect transistors, Elsevier, Amsterdam, 1988
[31] G. Jakobi and A. Löhr, Detergents and textile washing, principles and practice, VCH Verlagsgesellschaft mbH, Weinheim, Germany, 1987
[32] W. J. Blaedel and V. W. Meloche, Elementary quantitative analysis, Theory and practice, second edition, Harper & Row, New York, 1963
[33] Fluka Chemika, Selectophore, Ionophores for ion-selective electrodes and optodes, catalog edition 1991, Fluka Chemie AG, Buchs, Switzerland, 1991
[34] A. van den Berg, Ion sensors based on ISFETs with synthetic ionophores, thesis, University of Twente, The Netherlands, 1988
[35] C.C. Johnson, S.D. Moss, J.A. Janata, Selective chemical sensitive FET transducers, United States Patent no. 557,545, March 12, 1975
[36] P. Bergveld, Chemically sensitive electronic devices, microanalysis and microelectronics, Proc. of the 2nd int. meeting on chemical sensors, Bordeaux, 1986
[37] A.J. Sprenkels, R.A. Groothengel, A.J. Verloop and P.Bergveld, Development of an electret microphone in silicon, Sensors and Actuators, 17 (1989), page 509 - 512
[38] M. Menken, Aluminium oxide sensor, Electron. Appl. (Germany), vol. 13, no. 6, june 1981, page 48-49
[39] V.K. Khanna and R.K. Nahar, Effect of moisture on the dielectric properties of porous alumina films, Sensors and Actuators, 5 (1984), page 187 - 198
[40] R.S. Muller and T.I. Kamins, Device Electronics for Integrated Circuits, John Wiley & Sons, 1986

[41] I.R. Lauks, in P. Bergveld and J. Zemel (eds.), Proc. NATO-Advanced Study Inst. Chemically Sensitive Electronic Devices, Hightstown, N.J., 1980, Lausanne, Switzerland; Sensors and Actuators, 1 (1980), page 403
[42] I. Lauks, Polarizable electrodes, Part II, Sensors and Actuators, 1 (1981) page 393 - 402
[43] R.W. Murray, Chronoamperometry, chronocoulometry and chrono-potentiometry, From: B.W. Rossiter, J.F. Hamilton, Physical methods of chemistry, 2nd edition, volume II, 1986, page 525 - 589
[44] S. Roy Morrison, Electrochemistry at semiconductor and oxidized metal electrodes, Plenum press, New York, 1980
[45] P. Bergveld, The impact of MOSFET-based sensors, Sensors and Actuators, 8 (1985), page 109 - 127
[46] P. Bergveld, J. Hendrikse and W. Olthuis, Theory and application of the material work function for chemical sensors based on the field effect principle, Meas. Sci. Technol., 9 issue 11 (1998), page 1801 - 1808
[47] J. Hendrikse, W. Olthuis and P. Bergveld, A drift free nernstian iridium oxide pH sensor, proc. Transducers '97, Chicago, Illinois, 1997
[48] A.P.F. Turner, I. Karube and G.S. Wilson, Biosensors, Fundamentals and applications, Oxford University Press, 1987
[49] S.D. Senturia, C.M. Secken and J.A. Wishnenski, The charge flow transistor: a new MOS device, Appl. Phys. Lett., 30 (1977), page 106
[50] A.J. Sprenkels, J.A. Voorthuyzen and P. Bergveld, Theoretical analysis of the electret air-gap field effect structure for sensor applications, Sensors and Actuators, 9 (1986), page 59 - 72
[51] R.E.G. van Hal, J.C.T. Eijkel and P. Bergveld, The pH sensitivity of ISFETs described in terms of buffer capacity and double layer capacitance, Technical digest of the fifth international meeting on chemical sensors, July 1994, Rome (Italy), 249 - 252
[52] Y. Miyahara, F. Matsu and T. Miriizumi, Micro enzyme sensors using semiconductor and enzyme-immobilization techniques, in: T. Seiyama, S. Suzuki, F. Fueki and J. Shiokawa (eds.), Chemical Sensors, Analytical Chemistry Symposia Series, Vol. 17, Elsevier, Amsterdam, 1983, page 501 - 506
[53] E. Engvall and P. Perlman, Enzyme-linked immunosorbant assay (ELISA), Quantitative assay of immunoglobulin G, Immunochemistry, 8 (1971), page 871
[54] J.F. Schenck, Technical difficulties remaining to the application of ISFET devices, in: Theory, design and biomedical applications of solid state chemical sensors, C.R.C. Press, Boca Raton, FL, 1978, page 165
[55] J.C. van Kerkhof, P. Bergveld, R.B.M. Schasfoort, Determination of heparin concentrations with the ion-step measuring method, Technical digest of the fourth international meeting on chemical sensors, September 1992, Tokyo, Japan, page 370 - 373
[56] J.C. van Kerkhof, J.C.T. Eijkel and P. Bergveld, ISFET responses on a stepwise change in electrolyte concentration at constant pH, Sensors and Actuators B, 18 (1994), page 56 - 59
[57] E.A. Hall, Biosensors, Open University Press, Buckingham, 1990
[58] J. Millman and A. Grabel, Microelectronics, McGraw-Hill, Inc., Singapore, 1988
[59] W.J. Anderson and W.N. Hansen, Observing the electrochemical interphase via electrode surface conductance, Electroanalytical Chemistry and Interfacial Electrochemistry, 43 (1973), page 329 - 338

[60] O. Glück, M.J. Schöning, H. Lüth, H. Emons, C. Hanewinkel, D. Schumacher, A. Otto, Trace metal determination with gold microelectrodes fabricated by silicon technology, Eurosensors XI, The 11th European Conference on Solid State Transducers, Warshaw, Poland, September 21-24, 1997, page 615 - 618

[61] W.E. Morf and N.F. de Rooij, Performance of amperometric sensors based on multiple microelectrode arrays, Proc. Eurosensors X, Leuven, Belgium, 8-11 September 1996

[62] M.J. Madou and S.R. Morrison, Chemical Sensing with solid state devices, Academic Press, Inc., 1989

[63] W. Olthuis, M.A.M. Robben, P. Bergveld, M. Bos and W.E. van der Linden, pH sensor properties of electrochemically grown iridium oxide, Sensors and Actuators, B4 (1990), page 247 - 256

[64] Gábor Harsányi, Polymeric sensing films: new horizons in sensorics?, Sensors and Actuators A, 46-47 (1995), page 85-88

[65] J.W. Thackeray and M.S. Wrighton, Chemically responsive microelectro-chemical devices based on platinized poly(3-methylthiophene): variation in conductivity with variation in hydrogen, oxygen, or pH in aqueous solution, J. Phys. Chem. 1986, 90, page 6674-6679

[66] W. Huang, B.D. Humphrey and A.G. MacDiarmid, Polyaniline, a novel conducting polymer, Journal of the Chemical Society, Faraday Trans. 1, 1986, 82, page 2385 - 2400

[67] T. Shimidzu, Derivation of conducting polymers with functional molecules directed via molecular structural control towards a molecular device, Reactive polymers, 11 (1989), page 177-189

[68] P. Burgmayer and R.W. Murray, Ion gate electrodes, polypyrrole as a switchable ion conductor membrane, J. Phys. Chem. 1984, 88, page 2515-2521

[69] Y.G. Vlasov, E.A. Bychkov and A.V. Legin, Mechanism studies on lead ion selective chalcogenide glass sensors, Sensors and Actuators B, 10 (1992), page 55 - 60

[70] A.A. Saaman and P. Bergveld, A classification of chemically sensitive semiconductor devices, Sensors and Actuators, 7 (1985), page 75 - 87

[71] I. Lundström, Hydrogen sensitive MOS-structures, Part 1: principles and applications, Sensors and Actuators, 1 (1981), page 403 - 426

[72] J. Holleman and J.B. Rem, Thin film transistors for matrix sensors and actuators, Proceedings of the 2nd international workshop on materials science (IWOMS'95), Hanoi, Oct. 1995

[73] A. Pecora, G. Fortunato, R. Carluccio and S. Sacco, Hydrogenated amorphous silicon based light-addressable potentiometric sensor (LAPS) for hydrogen detection, Journal of non-crystalline solids, vol. 164 - 166, 1994, page 793 - 796

CHAPTER 4

A multi-purpose sensor-actuator structure[1,2]

Using a single multi purpose sensor-actuator structure, consisting of patterned metal films on a substrate only, three electrolyte parameters are measured. These parameters are temperature, electrolyte conductivity and hydrogen peroxide concentration, where the latter represents one example of many species that can be determined amperometrically. In addition, two actuator functions using the same single structure are possible as well. First, the local environment is thermoresistively heated and secondly a local pH gradient is created by the electrolysis of water. Since the active area of the fabricated devices is only about one square millimetre, the device is small and can be a starting point for a wide range of local measurements and experiments.

4.1 Device modelling and design

From the sensor overview of chapter 3, three sensor principles that can be integrated easily concerning their fabrication technology and methods of sensing are:

- Thermoresistive temperature measurement;
- Electrolyte conductivity determination;
- Amperometric bleach detection.

The following two additional actuator functions can easily be implemented as well:

- Thermoresistive heating of the local environment;
- Generation of a local pH gradient by the electrolysis of water.

These are the individual sensor and actuator operational behaviours which will be the guidelines for designing and testing an integrated sensor-actuator structure. The possibilities of combining these single operations for deducing new parameters is not evaluated in this chapter. Chapter 7 will deal with these possibilities.

As will be explained in a later subsection, the geometry of a conductivity cell determines the operational range for conductivity sensing. With the other two sensing principles, namely thermoresistive sensing and amperometry, the sensor geometry is less critical for proper

---

Parts of this chapter have been published before:
[1] Proc. Transducers '97, Chicago, June 16-19, 1997, page 543 - 546
[2] Sensors and Actuators B, 53/3, page 197 - 203, April 1999

operation. This is the reason that the conductivity cell is chosen as the starting point for the integrated sensor design.

Three configurations for conductivity cells are observed mostly: a structure of two rings with a common axis [1], a parallel plate set-up [1] and a planar interdigitated structure [2]. All three configurations can be adapted in order to create resistive pathways for thermo-resistive experiments as well as a working electrode for amperometry. Figure 4.1 shows the three basic designs.

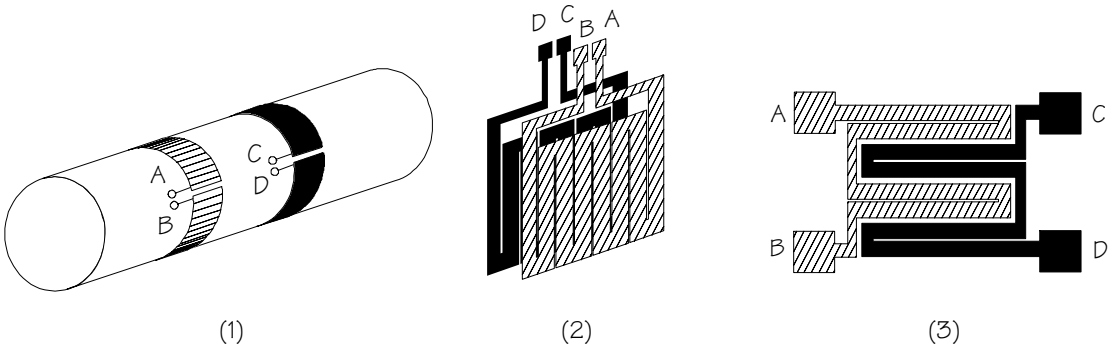

Figure 4.1: Three implementations for conductivity cells, adapted for thermoresistive experiments. Structure 1 is based on the dual ring configuration, structure 2 is a parallel plate set-up and structure 3 is created from an interdigitated configuration.

With all three structures of figure 4.1, the five operational modes can be accessed by connecting two or four of the connecting pads:

- Between pads A and B (or C and D) a resistive path is present for thermoresistive temperature sensing or local heating;
- When pads A and B are short circuited, and C and D as well, the two resulting metal structures will reduce to the original conductivity cell set-up;
- By short-circuiting all four pads, a metal surface is created which can function as a working electrode for electrochemical experiments with respect to an external counter electrode. In certain experiments, also only half of the structure can be used as a working electrode with the other half as the counter electrode.

Although these structures are functionally equal, the third configuration is preferred. The cylindrical set-up is less interesting because this configuration can not be switched into a square planar electrode. A planar working electrode, like one plate of the second set-up or the whole surface of the third set-up, is more convenient because it has the lowest boundary effects. The third configuration is easier to implement than the other two because of its planar shape, which enables processing using deposition and etching techniques resulting in easier miniaturisation. In fact, configurations 1 and 2 are actually macro electrodes.

Now the shape for the multi purpose single sensor structure has been chosen, its dimensions must be optimised. The following design criteria can be formulated:

- The overall size must be small to reduce the device price. Using silicon technology the costs per wafer are fixed irrespective of the number of devices per wafer. So, a high yield per wafer is desired;
- A good electrolyte conductivity cell has a constant impedance over a wide range of frequencies. As will be shown later, a wide operational frequency range means that the cell can be used for measuring a wide range of electrolyte conductivities;
- For heating purposes and sensing temperature, a resistance in the order of a hundred ohms is preferred for the paths A-B and C-D. With a resistance in this order the measurement of the resistance can be done using normal equipment while a considerable heating operation is still possible;
- The working electrode obtained when all the pads are connected, must have an optimal coverage of the device surface. Large gaps between the meander path loops and the conductivity fingers will reduce the effective surface area, and therefore result in lower observed currents;

A certain design freedom is available when implementing the resistive paths because the number of meander loops per conductivity finger is free to choose. So, the implementation can be started with the optimisation of the conductivity cell.

4.1.1 Electrolyte conductivity

The functional configuration of the planar multi purpose structure when switched as an interdigitated conductivity cell is drawn in figure 4.2a. When such a cell is immersed in an electrolyte, the simplified equivalent electrical circuit is as represented by figure 4.2b.

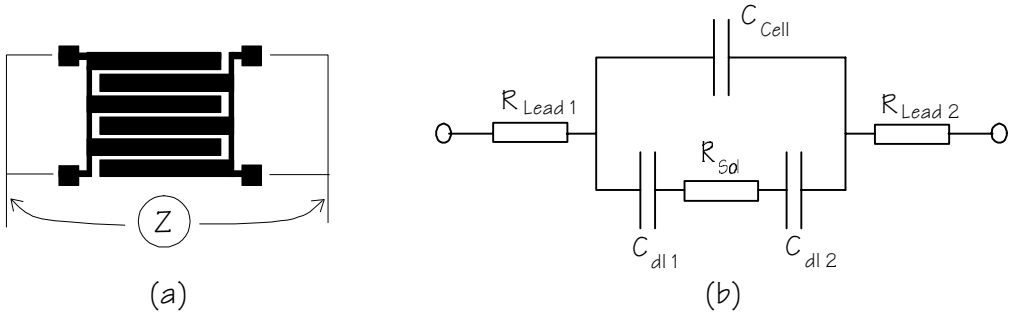

Figure 4.2: (a) Configuration of interdigitated conductivity cell and (b) its equivalent circuit

The electrical components in the equivalent circuit of figure 4.2b represent physical phenomena which determine the total electrical

impedance as will be observed with the conductivity cell shown in figure 4.2a. First, the equivalent model components are expressed in terms of physical quantities.

The solution resistance R_{Sol} is the component of interest for conductivity sensing and is related to the electrolyte conductivity κ_{Sol} by the cell constant K_{Cell}:

$$R_{Sol} = \frac{K_{Cell}}{\kappa_{Sol}}. \qquad (4.1)$$

This cell constant for an interdigitated structure with N fingers, finger spacing S, finger width W and finger length L is equal to [2]

$$K_{Cell} = \frac{2}{(N-1)L} \cdot \frac{K(k)}{K\left(\sqrt{1-k^2}\right)} \qquad (4.2)$$

with

$$K(k) = \int_0^1 \frac{1}{\sqrt{(1-t^2)(1-k^2t^2)}}\,dt \qquad \text{and} \qquad k = \cos\left(\frac{\pi}{2} \cdot \frac{W}{S+W}\right)$$

where the function K(k) is the incomplete elliptic integral of the first kind [3]. So, the cell constant entirely depends on the geometry of the sensor.

The lead resistance R_{Lead} is the result of the series resistances of the connecting wires (± 50 cm), the copper tracks on the printed circuit board where the device will be mounted on, and the bonding wires. A practical value of 1 Ω is observed for both $R_{lead\ 1}$ and $R_{lead\ 2}$.

Direct capacitive coupling between the two electrodes is represented by the cell capacitance C_{Cell} being equal to

$$C_{Cell} = \frac{\varepsilon_0 \varepsilon_{r,Sol}}{K_{Cell}} \qquad (4.3)$$

with $\varepsilon_{r,Sol} \approx \varepsilon_{r,Water} = 80$. One model component which is not drawn in figure 4.2b is a capacitor representing the direct capacitive coupling between the connecting wires. This capacitor comes in parallel with C_{Cell} and will therefore virtually increase the observed cell capacitance.

The impedances describing the interface phenomena occurring at the electrode-electrolyte interfaces, are simplified to the double layer capacitances C_{dl}. These depend on the electrode material and the electrolyte but can for smooth electrode surfaces be approximated by

$$C_{dl} = 0.5 \cdot A \cdot C_{dl,square} = 0.5 \cdot W \cdot L \cdot N \cdot C_{dl,square} \quad (4.4)$$

where A is the electrode surface and $C_{dl,square}$ the characteristic double layer capacitance of the electrode-electrolyte system. Notice that the factor 0.5 is the result of C_{dl} being determined by only half of the electrode surface A. The characteristic double layer capacitance $C_{dl,square}$ can assumed to be equal to the characteristic capacitance of the Stern layer for electrolytes having a quite high ionic strength. This characteristic capacitance of the Stern layer is approximated by $C_{stern,square}$ = 10-20 $\mu F / cm^2$ [4, 5].

Based on the equivalent circuit of figure 4.2b, the total observed impedance can be expressed as

$$Z(j\omega) = 2R_{Lead} + \frac{x}{j\omega C_{Cell} x + 1}$$
$$x = R_{Sol} + \frac{2}{j\omega C_{dl}} \quad (4.5)$$

which has a characteristic frequency response as theoretically drawn in figure 4.3.

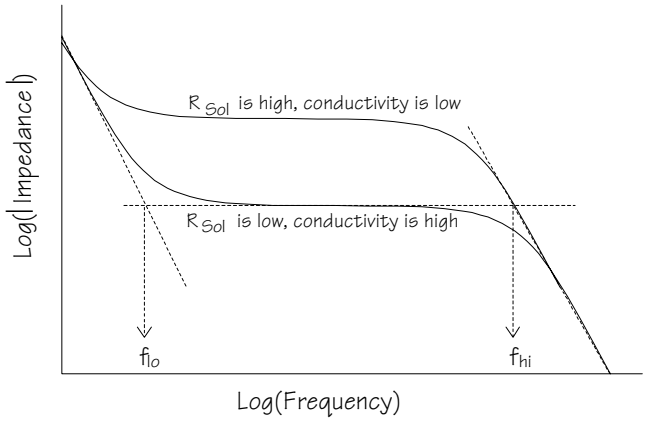

Figure 4.3: Characteristic frequency response of a two electrode conductivity cell

Above the frequency f_{lo}, the term referred to as x in equation (4.5) reduces to R_{Sol} while below f_{hi} the influence of C_{Cell} is not yet significant. This results into a frequency band, restricted by f_{lo} and f_{hi}, in which the conductivity can be found from the observed impedance using

$$Z(j\omega) = 2R_{Lead} + R_{Sol} \quad (4.6)$$

with R_{Sol} proportional to the inverse of the electrolyte conductivity. When the conductivity increases, the R_{Sol} decreases and the plateau shifts to a lower impedance. In addition, a change in the height of the plateau implies a change in the boundary frequencies f_{lo} and f_{hi}. In practice this results in the restriction of the conductivity measurement

range at a single operational frequency. Optimisation of a conductivity cell is the maximisation of the plateau width.

The boundary frequencies can be calculated from equation (4.5):

$$f_{lo} \approx \frac{1}{2\pi\left(R_{Lead}C_{dl} + 2R_{Lead}C_{Cell} + \frac{1}{2}R_{Sol}C_{dl}\right)} \approx \frac{1}{\pi R_{Sol}C_{dl}} \qquad (4.7)$$

$$f_{hi} = \frac{1}{2\pi R_{Sol}\dfrac{C_{dl}C_{Cell}}{C_{dl}+2C_{Cell}}} \approx \frac{1}{2\pi R_{Sol}C_{Cell}} \qquad (4.8)$$

or in terms of conductivity parameters:

$$f_{lo} \approx \frac{\kappa_{sol}}{\frac{1}{2}\pi W \cdot L \cdot N \cdot C_{dl,square}K_{Cell}} \qquad (4.9)$$

$$f_{hi} \approx \frac{\kappa_{sol}}{2\pi\varepsilon_0\varepsilon_{r,Sol}} \qquad (4.10)$$

In the derivation of the lower boundary frequency (4.7), the assumption is made that $C_{dl}{\cdot}R_{Sol}{\cdot}C_{Cell}{\cdot}R_{Lead} << 1$, which is practically always true with realistic R and C values.
Note that the higher boundary frequency, f_{hi}, is not dependent on the geometry in principle, when the wiring capacitance is not present. Obviously, maximising the width of the plateau can only be done by lowering the lower boundary frequency. In order to make the lower boundary frequency (4.9) as low as possible, the geometrical term

$$W \cdot L \cdot N \cdot K_{Cell}(N, L, S, W) \qquad (4.11)$$

should be maximised. When using a square structure of L×L, one variable can be eliminated because

$$L = N \cdot (W + S). \qquad (4.12)$$

Expression (4.11) is written in terms of the finger width W, the finger spacing S, the length of the fingers L and the number of fingers N.

However, it is more illustrative to introduce a factor $\alpha = S/W$. Using the substitutions

$$S = \frac{L}{N}\frac{\alpha}{\alpha+1} \qquad \text{and} \qquad W = \frac{L}{N}\frac{1}{\alpha+1},$$

which are based on equation (4.12) together with the ratio α, expression (4.11) becomes

$$\frac{2 \cdot L}{N-1} \cdot \frac{K\left(\cos\left[\frac{\pi}{2}\frac{1}{\alpha+1}\right]\right)}{(\alpha+1) \cdot K\left(\cos\left[\frac{\pi}{2}\frac{\alpha}{\alpha+1}\right]\right)} \qquad (4.13)$$

where the function K has the same meaning as it had in equation (4.2). This optimisation expression, which has to be maximised in order to minimise f_{lo}, can be split into two parts. The first is the factor $2L/(N-1)$, showing that the cell size L×L must be as large as possible while the number of fingers must be reduced. Since there is no maximum in the desired cell size, with respect to the optimisation of f_{lo}, the value L can be chosen arbitrarily. A cell size of about 1×1 mm² will be taken. The optimal number of fingers N has a maximum for N = 2 since this is the lowest possible number of fingers. However, when using one meander of the final structure as shown in figure 4.1c as a heater, a larger number of fingers will result in a more homogenous heating of the local environment. As a compromise, N = 5 and N = 9 fingers where chosen, resulting in an increase of the f_{lo} by a factor four respectively eight from the optimal f_{lo}.

The factor $2L/(N-1)$ is related to the sum $W+S$ according to equation (4.12), the second factor in expression (4.13) has only the ratio $W/S=\alpha$ as a parameter. In figure 4.4 this factor is plotted as a function of α, with α ranging from 0 to 5.

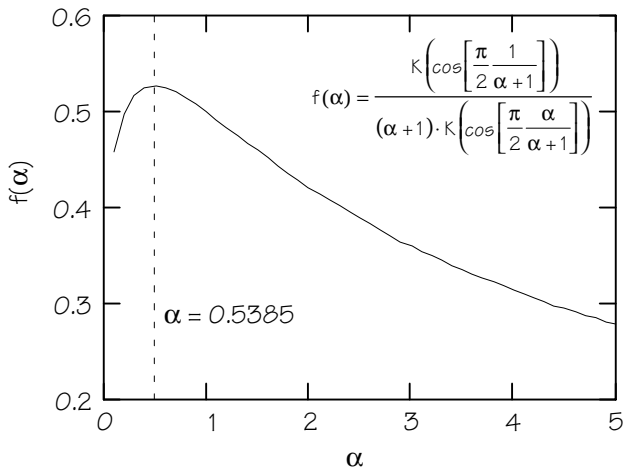

Figure 4.4: Optimisation of the S/W ratio α

For α = 1, the finger width is equal to the gap between them. It can be seen that this is not the optimal ratio, for α = 0.5385 the optimisation function has a maximum which means that the finger width should be approximately twice the gap width $W=2S$. This maximum for the function denoted in the figure as f(α) is equal to 0.521.

Therefore, when designing a square structure, the design rule, based on the maximum frequency range criterion becomes according to equation (4.12): L = 1.5NW. When also the minimum number of fingers , N = 2, is taken into account, the design rule becomes: L = 3W. The resulting lowest possible frequency f_{lo} becomes

$$f_{lo} = \frac{\kappa_{sol}}{0.521\pi \cdot C_{dl,square} L} \tag{4.14}$$

which is equal to 770 Hz for L = 1 mm, $C_{dl,square}$ = 10 $\mu F/cm^2$ and κ_{Sol} = 1.26 mS/cm (the conductivity of a 10 mM KNO_3 solution).

However, since the coverage of metal parts must be as large as possible for optimal working electrode operation, large gaps are not desired. Fortunately, a deviation from the optimal S/W ratio has not a dramatic effect on the lower boundary frequency, as can be seen in figure 4.4. At a ratio S/W of 0.15 the lower boundary frequency will differ a factor 1.13 from the optimal frequency, while at a ratio 0.025 this factor is still not larger than 1.6. Therefore, these two ratios were taken as acceptable, but the ratio with the largest loss was applied on the device with the lowest number of fingers N and vice versa. This resulted into two devices where the first one (type A) has the largest deviation from the lowest possible lower boundary frequency (4.14) due to a mediocre S/W ratio, and the second one (type B) has the largest deviation due to a number of fingers which is not optimal. Notice that the overall increase of the lower boundary frequency is the lowest for device type A (a factor 4 × 1.6 resulting in f_{lo} = 4.8 kHz).

The finally chosen sets of geometrical parameters are given in table 4.1. For calculating some of the resulting equivalent circuit parameters, an electrolyte conductivity of 10 mM KNO_3 is taken as an example. A characteristic double layer capacitance of 10 $\mu F/cm^2$ is assumed.

So between the frequencies f_{lo} and f_{hi} the measured impedance of the system has a resistive nature according to (4.6), which is proportional to the electrolyte resistance R_{Sol}. This electrolyte resistance depends on the conductivity as given by equation (4.1). Far below the frequency f_{lo}, the impedance is equal to

$$\left|Z(j\omega)\right| = \frac{1}{\pi f C_{dl}} \tag{4.15}$$

with a phase angle of 90 degrees. Far above f_{hi}, the impedance is given by

$$\left|Z(j\omega)\right| = \frac{1}{2\pi f C_{Cell}} \qquad (4.16)$$

where the phase angle has returned to 90 degrees again after being zero at the frequency independent plateau. This plateau and the asymptotic approximations of the impedances, as given by equations (4.15) and (4.16), were already shown in figure 4.3.
It is needless to say that the latter two measured values, C_{dl} and C_{Cell} respectively, are of no interest for the intended goal, although a measurement of C_{dl} might be of interest to observe possible adsorption of certain species to the electrode. In addition, determination of C_{Cell} is actually the calibration of the cell, since equation (4.3) shows that the cell capacitance is related to the cell constant. These additional determinations are however beyond the scope of the presented research.

*Table 4.1: Chosen parameters for the planar conductivity cell. For the numbers marked with *), a conductivity of κ_{Sol} = 1.26 mS·cm^{-1} (≈ 10 mM KNO_3) is chosen*

		Type A	Type B
Finger spacing	S [µm]	5	15
Finger width	W [µm]	200	100
S / W ratio	α	0.025	0.15
Length of fingers	L [µm]	1025	1035
Number of fingers	N	5	9
Resulting cell constant	K_{Cell} [cm^{-1}]	1.65	1.28
Theoretical cell capacitance	C_{Cell} [pF]	4.30	5.54
Theoretical solution resistance*)	R_{Sol} [kΩ]	1.31	1.02
Theoretical double layer capacitance	C_{dl} [nF]	51.3	46.6
Assumed lead resistance	R_{Lead} [Ω]	1	1
Resulting lower cut-off frequency *)	f_{lo} [kHz]	4.76	6.76
Resulting upper cut-off frequency	f_{hi} [MHz]	28.3	28.3

4.1.2 Temperature sensing

When the fingers are cut along as shown in figure 4.5 for creating two resistive paths, two conditions must be met in order not to lose the optimised conductivity operation:

- The cuttings must be narrow for maintaining the double layer capacitance and the cell constant K_{Cell} as calculated for the non-cut device;
- The resistance of the cutted fingers must remain much lower than the resistance of the liquid because else a voltage drop along the

fingers might become a dominant factor in the conductivity cell impedance;

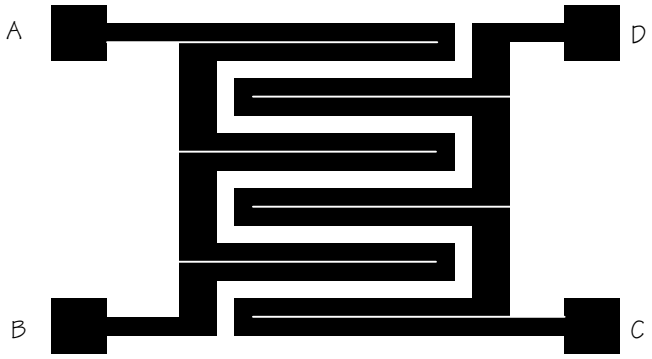

Figure 4.5: Basic multi purpose sensor shape

In general, the resistance of a metal strip is equal to

$$R_0 = \frac{\rho l}{wh} \tag{4.17}$$

with w the width, h the thickness and l the length of the strip and ρ the specific resistivity of the metal. For platinum, the specific resistivity at room temperature is $1.06 \cdot 10^{-5}$ Ω·cm [6].
Temperature sensing is done by observing the change in resistance due to temperature variations. The resistance can be written as

$$R = R_0\left(1 + \alpha\left(T - T_0\right)\right) \tag{4.18}$$

with α the temperature coefficient. This coefficient is 0.00392 $°C^{-1}$ for platinum with a non-linearity of 0.2% between 0-100 °C [7].

Since implementation B has a finger width of 100 µm, when cut along with a cutting gap of 10 µm the width w of the resistive path will be 45 µm. The length l is 8.28 mm for each meander. With an intended platinum thickness of 250 nm, the nominal resistance between pads A and B (and C and D) will be approximately 78 Ω at room temperature.
Structure A has a much larger finger width and less fingers. To avoid a very low meander resistance, each finger is double cut in order to create two resistive loops per finger. The lengths of these pathways are 10.25 mm, the cutting gap is 5 µm, the width of the path 47 µm. At room temperature the resulting meander resistance will be about 92 Ω. Both values are in the intended range of 100 Ω, while these are also much lower than typically observed solution resistances. The decrease in electrode surface due to the cutting is 7%. So the conditions which were to be met for not losing the efficiency of the conductivity sensing and having an easy to measure resistance for temperature measurements are fulfilled.

Figure 4.6 shows the enlarged mask layouts for the sensors of type A and B, with the conductivity sensing geometrics as given in table 4.1 and the modified fingers for enabling thermoresistive measurements. The geometrical factors and resulting calculated meander resistances are summarised underneath this figure.

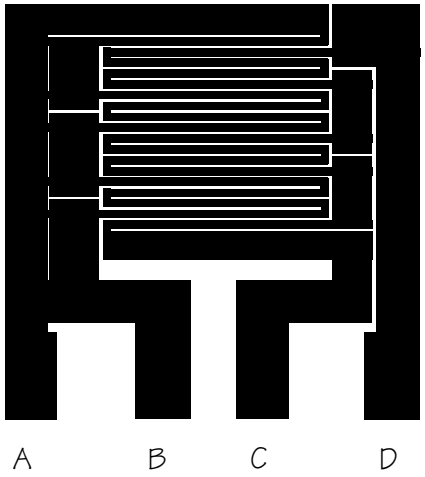

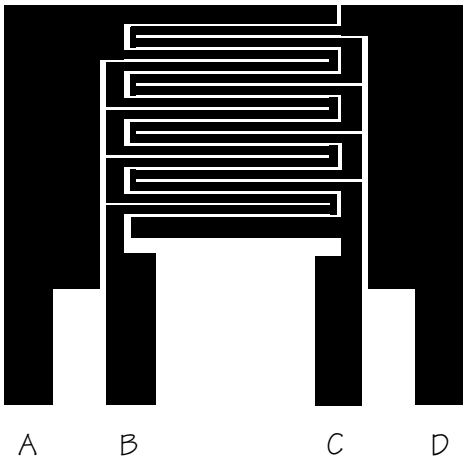

Type A		*Type B*	
Thickness of Pt layer	*250 nm*	*Thickness of Pt layer*	*250 nm*
Size of meander area	*1×1 mm²*	*Size of meander area*	*1×1 mm²*
Width of wire	*47 µm*	*Width of wire*	*45 µm*
Width of cutting gap	*5 µm*	*Width of cutting gap*	*10 µm*
Width of finger gap	*5 µm*	*Width of finger gap*	*15 µm*
Fingers for conductivity cell	*5*	*Fingers for conductivity cell*	*9*
Resistance A to B	*92 Ω*	*Resistance A to B*	*78 Ω*
Resistance C to D	*92 Ω*	*Resistance C to D*	*78 Ω*
Cell constant	*1.65 cm⁻¹*	*Cell constant*	*1.28 cm⁻¹*

Figure 4.6: Enlarged mask layout for structure type A and B

For a practical resistance measurement, as well as for heating, a potential must be applied while monitoring the current, or vice versa. Since the metal layer is in contact with the electrolyte, this applied potential drop along the meander might evoke an electrochemical reaction at the metal-electrolyte interface. A solution might be to use only very small potentials, but when using the meander for heating purposes, this applied voltage becomes in the order of volts. However, with an AC operational mode of sufficiently high frequency, electrochemical reactions are not likely because the alternation of the potential will be too fast. Therefore, faradaic processes are not occuring when the operational frequency is chosen sufficiently high.

4.1.3 Amperometric working electrode

By applying an insulating material on top of the metal structure, a window can be defined where the metal is in contact with the electrolyte. Since the meander structures cover an area of about 1×1 mm^2 (0.96 and 0.84 mm^2 exactly for type A and B respectively), a square planar working electrode can be defined.
The primary aim of the working electrode is to detect hydrogen peroxide as a measure for bleaching activity. For showing the use of the integrated sensor device as a working electrode, the relatively simple method of chrono-amperometry using a three electrode set-up is used here. The application of a more sophisticated method for amperometric detection is postponed to the next chapter.

The involved reaction for the reduction of hydrogen peroxide is:

$$H_2O_2 + 2H^+ + 2e^- \leftrightarrow 2H_2O \tag{4.19}$$

which is evoked after applying a negative potential step to the working electrode. In case of a potential step which is high enough to deplete the reacting species (hydrogen peroxide) at the electrode surface completely during this step, the resulting current response for a planar electrode is given by the Cottrell equation [5]:

$$i(t) = nFAC_{Ox}\sqrt{\frac{D_{Ox}}{\pi t}} \tag{4.20}$$

with F the Faraday constant, n the number of electrons transferred, A the working electrode size, C_{Ox} the bulk H_2O_2 concentration and D_{Ox} the diffusion coefficient of H_2O_2 (approximately $1.6 \cdot 10^{-5}$ cm^2/s at pH<10 [8]). So, after applying a voltage step, the monitored current response is proportional to the hydrogen peroxide concentration.

4.1.4 Generation of a local pH gradient

By applying a current to all four short circuited pads of the structure with respect to an external counter electrode, the anodic or cathodic electrolysis of water can be selected:

$$2H_2O \rightarrow O_2 + 4H^+ + 4e^- \tag{4.21}$$

$$2H_2O + 2e^- \rightarrow 2OH^- + H_2 \tag{4.22}$$

where the first reaction decreases and the second increases the local pH. Notice that the reaction of equation (4.22) will not happen as long as hydrogen peroxide is present since equation (4.19) will occur first. This

is not a practical problem because the resulting pH change as a result of a certain applied current is equal for both reactions.
A method for showing a pH actuator operation using the second reaction, is a coulometric acid to base titration of a weak acid with the electrochemically produced OH^- as base. The measured electrode potential can be used as an end-point indicator because the corresponding Nernst equation has a pH dependent term:

$$E = E^0 - 0.059 \cdot pH . \tag{4.23}$$

For such a chrono potentiometric titration, the end point is determined by the Sand equation [5]:

$$t_{end} = \left[\frac{C_{HA,bulk} F \sqrt{\pi D_{HA}}}{2 j_c} \right]^2 \tag{4.24}$$

with $C_{HA,bulk}$ the acid bulk concentration, F Faraday's constant, D_{HA} the diffusion coefficient of the acid and j_c the actuator current density.

4.1.5 Local heating

The dissipated energy in a resistor, when supplied with an AC current or voltage, is equal to

$$P = V_{eff} \cdot I_{eff} = I_{eff}^2 R \tag{4.25}$$

with V_{eff} the effective value of the applied voltage over the resistor, I_{eff} the resulting effective value of the current and R the resistance. The assumption is made that the voltage and current are in phase which is plausible for a resistor. This energy is released as heat and will result in a rise of temperature. So the increase in temperature will be proportional to the square of the applied current.

For heating purposes, matching of relevant thermal properties between the electrolyte and the substrate is important. For example, when the substrate consists of a relatively large piece of material with a much higher heat conductivity than the electrolyte, the produced heat of the resistor will immediately be lost into this undesired heat sink. A more complete thermal evaluation is postponed to chapter 6, where it is deduced that a glass substrate, having the same heat resistance and heat capacitance as the electrolyte, will result in an optimal thermal behaviour. Under this condition, the heating of substrate and electrolyte will be equal and since there is no difference in heat storage, there will be no undesirable heating delay. Therefore, glass is a quite optimal substrate material because of its thermal properties.

4.2 Experimental

The devices as shown in figure 4.6 were realised and tested. To compare the modified conductivity cells (with cuttings) to the original cells, some cells without resistive pathways and having the dimensions as given in table 4.1 were produced as a reference.
Only the testing of direct sensor and actuator functions is reported here. Possible combinations of actuating and sensing will be introduced in chapter 7 and worked out in chapter 8 and 9 respectively.

4.2.1 The fabrication process

The devices are realised on a Hoya® SD-2 glass substrate with a thickness of 500 µm. A datasheet of the properties of this material is included in appendix 4.A. Before the platinum film can be evaporated, a 20 nm tantalum layer is applied for adhesion purposes. After deposition of a 250 nm thick platinum film, a second 20 nm tantalum layer is applied. This second tantalum layer is the base for a tantalum oxide layer which is necessary for a good adhesion of a polyimide insulation layer. The sandwich tantalum / platinum / tantalum is patterned photo-lithographically using reactive ion etching for tantalum and wet chemical etching for platinum. The upper tantalum layer is oxidised by dry thermal oxidation at 500 °C during one hour. A polyimide layer is spun on and patterned by photolithography to open the active area and the contact pads. The tantalum oxide on the platinum in the opened areas can now be removed by reactive ion etching. Notice that the whole process takes only two masks: one for the conductor definition and one for the opening of the actual sensor surface and the contacting holes. Figure 4.7 shows a schematic cross-sectional view of the device. In appendix 4.B there is a step by step description of the whole cleanroom process.

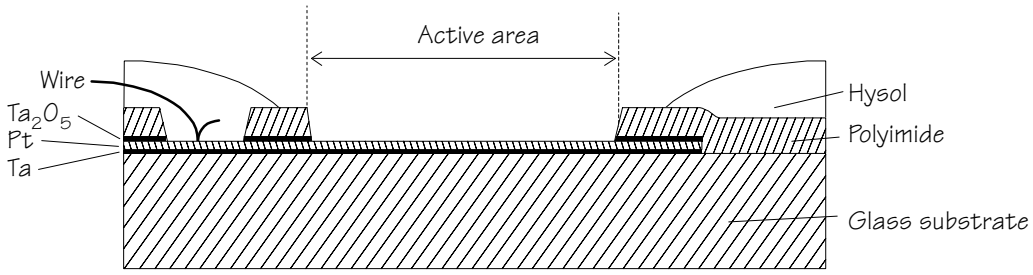

Figure 4.7: Cross-section of the multi purpose sensor-actuator device realised on a glass substrate using thin film technology

After sawing, the devices are mounted on a printed circuit board, bonded and encapsulated with Hysol® resin. Figure 4.8a shows the devices just after sawing. In the middle row there are four structures:

from left to right type A, type B, type A and a reference structure containing an unmodified conductivity cell. Figure 4.8b was taken after packaging. The bonding wires and copper traces are visible under the transparent resin.

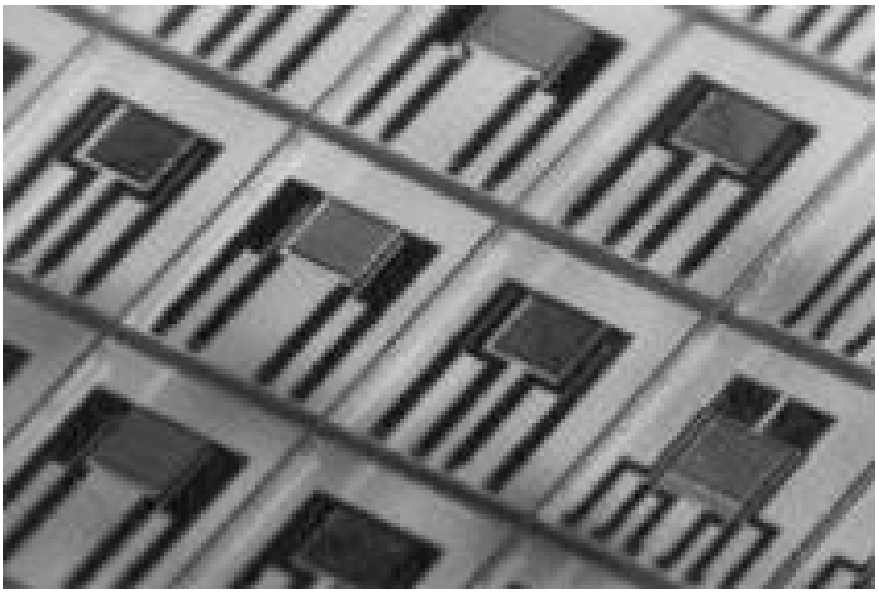

Figure 4.8a: Photograph of realised sensor structures just after sawing

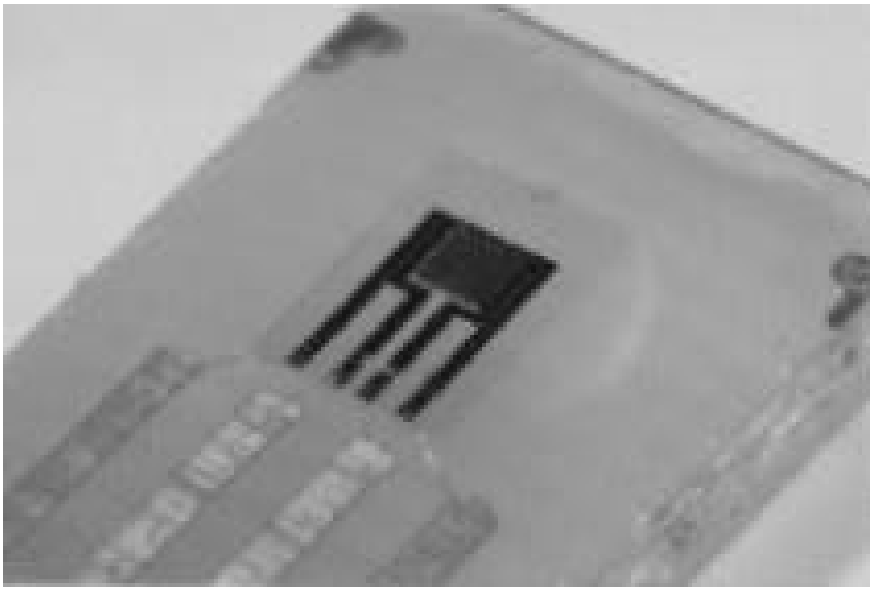

Figure 4.8b: Photograph of a sensor structure after packaging on a printed circuit board

Knowledge of the thickness of the metal layer is quite important for a quantitative assessment of the device properties. This thickness was measured using a Dektak surface profiler and appeared to be 255 nm, so within the intended value of 270 nm (consisting of a 250 nm platinum layer and a 20 nm thick tantalum adhesion layer). From the same analysis the thickness of the polyimide layer was determined to be 850 nm.

4.2.2 Conductivity measurement

Measurement set-up

The measurements were carried out using a Hewlett Packard impedance/gain-phase analyser type HP4194A, controlled by a computer using the graphical programming environment LabView. As a reference, the electrolyte conductivities where measured using a Consort K820 commercial conductivity meter.

Measurement of model parameters

Impedance versus frequency sweeps were made for sensors A and B in potassium nitrate solutions of 0.5, 1.0, 5.0 and 10 mM. The equivalent electrical conductivities of the sample solutions were measured using the Consort conductivity meter, being 72, 143, 681 and 1264 µS/cm respectively, slightly differing from the theoretical conductivities (72, 145, 725 and 1450 µS/cm respectively for the intended concentrations).

Figure 4.9 shows the measured impedance plots as a function of the applied frequency. The amplitude of the oscillator voltage was 100 mV, the sample temperature 20°C. The theoretical curves, based on the intended geometrics as summarised in table 4.1 and impedance equation (4.5), are added as dotted lines. The characteristic shape as predicted in figure 4.3 is observed: a capacitive nature for low frequencies determined by the double layer capacitances, a resistive behaviour for moderate frequencies and finally again a capacitive behaviour for high frequencies. However, some deviations from theory are observed:

- The curves in the measured plots are not as sharp as can be expected from theory using ideal electrical components. This results in plateaus which are not completely frequency independent;
- The observed higher boundary frequency is significantly lower than was found in theory;
- From the heights of the plateaus observed with sensor type A, it must be concluded that the theoretical cell constant does not match the observations. This error is much smaller for sensor type B;

Especially for the double layer impedances, it is known that an ideal capacitor is not the correct model. This might explain the first difference. Later on, the other two errors will be discussed quantitatively when the equivalent circuit components are fitted.

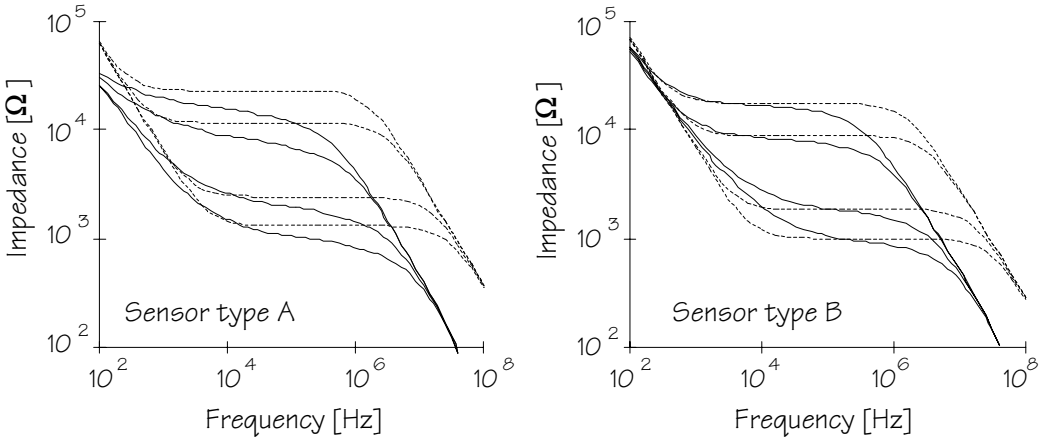

Figure 4.9: Impedance versus frequency sweeps for the multi purpose sensor structures. From top to bottom: 0.5, 1.0, 5.0 and 10 mM KNO_3

Both boundary frequencies f_{lo} and f_{hi} can be fitted from the impedance plots. This was done by drawing three slope lines in each curve for the three regions as was already done in the theoretical plot of figure 4.3. By observing the intercepts of these slope lines the boundary frequencies are found. The solution resistance is determined from the same graph by taking the impedance at the most horizontal part of the curve, where the first derivative shows a maximum. From the boundary frequencies and the measured solution resistance, the cell constant, the double layer capacitance per square unit $C_{dl,square}$ and equivalent electrical components can now be calculated using equations (4.7) through (4.10). The results are summarised in table 4.2.

Table 4.2: Measured conductivity parameters with theoretical values in parentheses at a conductivity of 1.26 mS/cm

	Type A	Type B
Measured		
f_{lo} [kHz]	5.53 (4.76)	7.69 (6.76)
f_{hi} [MHz]	7.81 (28.4)	8.13 (28.4)
R_{Sol} [kΩ]	1.07 (1.30)	0.98 (1.01)
Calculated from measurement		
$C_{dl,square}$ [μF / cm²]	10.5 (10)	9.07 (10)
K_{Cell} [cm⁻¹]	1.35 (1.65)	1.24 (1.28)
C_{Cell} / / C_{wires}[pF]	19.0 (4.30)	20.0 (5.54)
C_{dl} [nF]	53.8 (51.3)	42.2 (46.6)

The agreement with the theoretical values of table 4.1 is large. Notice that the observed high cut-off frequency does not correspond to the theoretical one, since the theory assumed no influence of the wiring capacitance. The “cell capacitance”, which can be calculated from this high cut-off frequency, consists of the actual cell capacitance with the

wiring capacitance in parallel, as was already mentioned in subsection 4.1.1. From the difference between the observed capacitance $C_{Cell}//C_{wires}$ and the calculated C_{Cell}, the parasitic capacitance of the connecting wires, including the parallel copper tracks on the PCB, appears to be about 15 pF.
An unmodelled source of possible errors is the relatively high relative dielectric constant of the used substrate material. The metal structure itself on the substrate introduces a parallel parasitic capacitance with the substrate material as a dielectric material. The capacitive coupling through the substrate material has a capacitance which can be calculated using equation (4.3). With ε_r of the glass equal to 6, this results into capacitances in the order of 0.1 pF. So, this effect is completely overruled by the presence of the wiring capacitance of 15 pF.

As was concluded from figure 4.9, the mismatch in the cell constant for type A is larger than for type B. The observed slope in the plateau can be explained as a result of the double layer impedance, modelled as being a perfect capacitor C_{dl}. This assumed model, resulting in the asymptote (4.15), is apparently a simplification of the actual electrical double layer behaviour.

Despite the obviously over simplified model, the existence of a wiring capacitance and the mismatch in the cell constant, the devices can still be used for conductivity measurements. The widths of the observed plateaus show that it is in principle possible to determine the electrolyte resistance (and so the conductivity) at a single operational frequency of 500 kHz for almost one and a half decade of concentrations. For another range of concentrations, another operational frequency has to be chosen. However, it is also possible to adapt the operational frequency for each individual concentration. This can be done by determining the impedance at the frequency where the first derivative of the impedance curve shows a maximum.

Comparison to an unmodified conductivity cell
For determining the effect of introducing the resistive pathways into a planar conductivity cell, an unmodified cell was processed. Figure 4.10 shows the two measured curves in 10 mM potassium nitrate, where sensor type B_{Ref} stands for type B without cut fingers. Although the dimensions of the cells B and B_{Ref} are similar, the connecting wires on the substrate connecting the cell to the bond pads are not identical, resulting in dissimilar wiring capacitances.

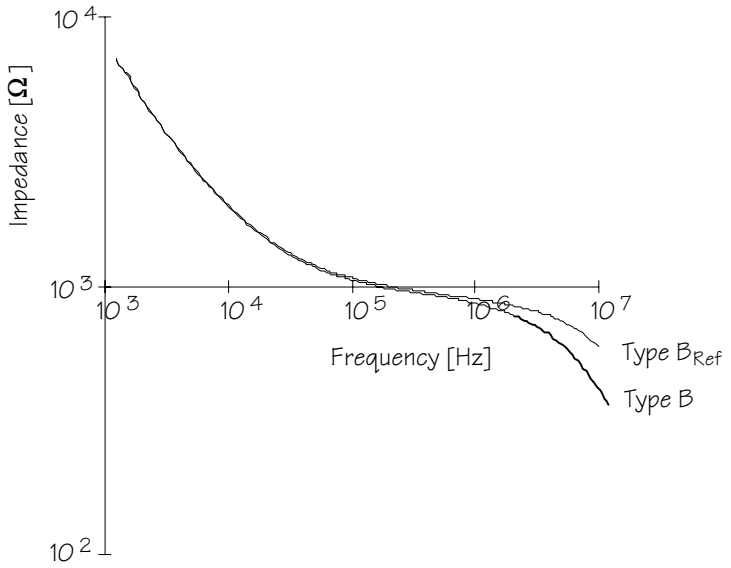

Figure 4.10: Comparison of a type B cell with an unmodified conductivity cell (type B_{Ref})

It appears that the introduction of the resistive path does not influence the low frequency behaviour. Whether or not the cell capacitance is affected by introducing the cuttings in the fingers can not be seen by noticing the shift in the higher boundary frequency. The wiring capacitances are not exactly equal for sensor type B and B_{Ref} which overrules small changes in the cell capacitance. However, because the height of the plateau is not changed, it may be concluded that the cell constant is not affected. Since the cell capacitance is related to the cell constant as given in equation (4.3), this capacitance is obviously not changed either.

Measurement of the operational range

Practical observed conductivities in washing systems range from 100 - 900 µS/cm in tap water to 2 mS/cm during the main wash (chapter 2). The tap water range is already verified by the measurements of figure 4.9 ranging from 72 to 1264 µS/cm, the complete range is shown in figure 4.11 including measurements up to 20 mM KNO_3 (equivalent to 2.9 mS/cm). The plotted admittances were taken from impedance versus frequency plots by taking the admittance at the horizontal part of the frequency curves where the first derivative shows a maximum. At this frequency, the measured admittance is related to the electrolyte conductivity with respect to the cell constant as given by equation (4.1).

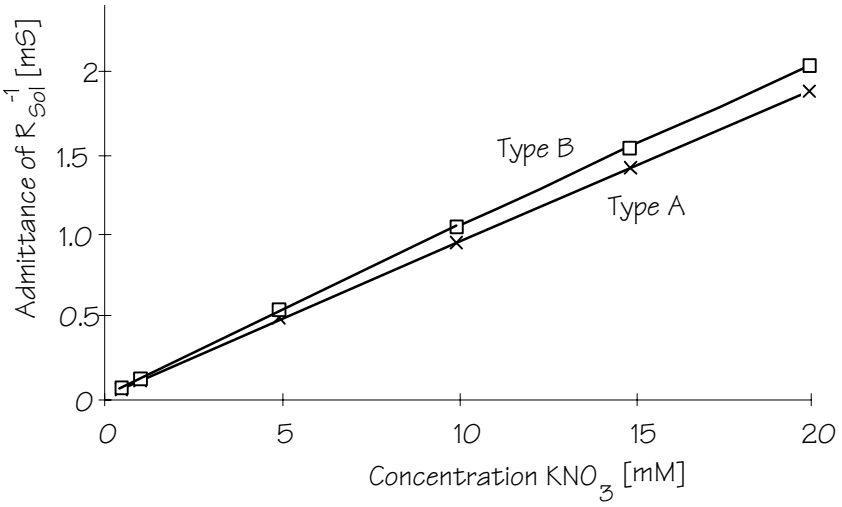

Figure 4.11: Admittance versus potassium-nitrate concentration, measured at the frequency where the first derivative of the impedance plot shows a maximum. The range from 0.5 to 20 mM KNO_3 is equivalent to 0.072 to 2.9 mS/cm

4.2.3 Chrono amperometry

Measurement set-up

The chrono amperometric experiments were carried out using the planar structure as a working electrode in a three electrode set-up with a conventional glass Ag/AgCl reference electrode and a platinum counter electrode of 1.0×0.5 cm^2. Although the use of this liquid filled reference electrode is not desirable in a final sensor system, the three electrode set-up is used here for evaluating the amperometric operation of the designed working electrode operation. In the next chapter an amperometric sensing technique will be discussed which does not need this reference electrode.

The measurement set-up consists of an EG&G potentiostat/galvanostat model 173 under computer control. Measurements are carried out directly after dilution from a 30 wt% hydrogen peroxide stock solution. Before each experiment, the solution was saturated with nitrogen gas in order to minimise the initial oxygen concentration. For the chrono amperometric experiments a 100 mM potassium nitrate supporting electrolyte is used to reduce the ohmic drop, and to prevent migration. During the measurement, the solution is not stirred.

Experimental

For finding the optimal step size for the chrono-amperometric detection, an orientating cyclic voltammogram is made in a 10 mM hydrogen peroxide solution with 10 mM potassium nitrate as an ionic strength adjuster (figure 4.12).

Starting at 0 Volt and following the direction of the arrows, the first observed peak (1) is the result of the reduction of hydrogen peroxide as given by equation (4.19) which is partially reversed at peak number (3). Peak (1) is the measure of interest since it is proportional to the bleaching capability of the solution. Peaks (2) and (4) are the result of the reduction and oxidation of water respectively. Since it is unavoidable that there is some dissolved oxygen present, the reduction of oxygen results in peak (5).

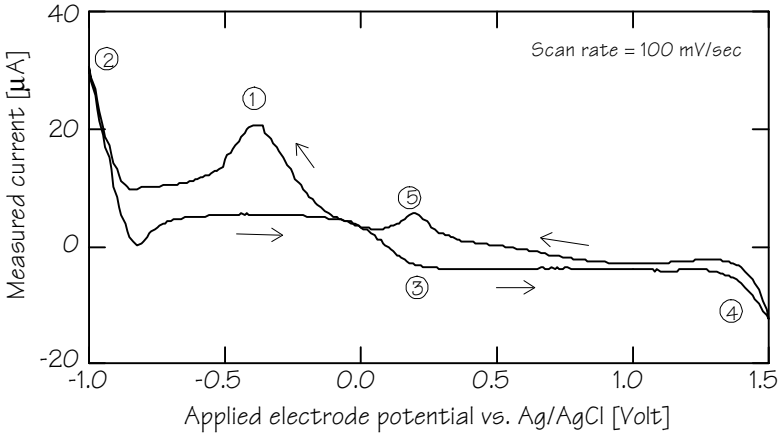

Figure 4.12: Measured cyclic voltammogram of 10 mM hydrogen peroxide

From the cyclic voltammogram it will be clear that stepping from zero to minus 0.5 volts will result into a current response due to hydrogen peroxide reduction at the working electrode according to equation (4.19). This experiment gives the desired hydrogen peroxide concentration information as described by the Cottrell equation (4.20).

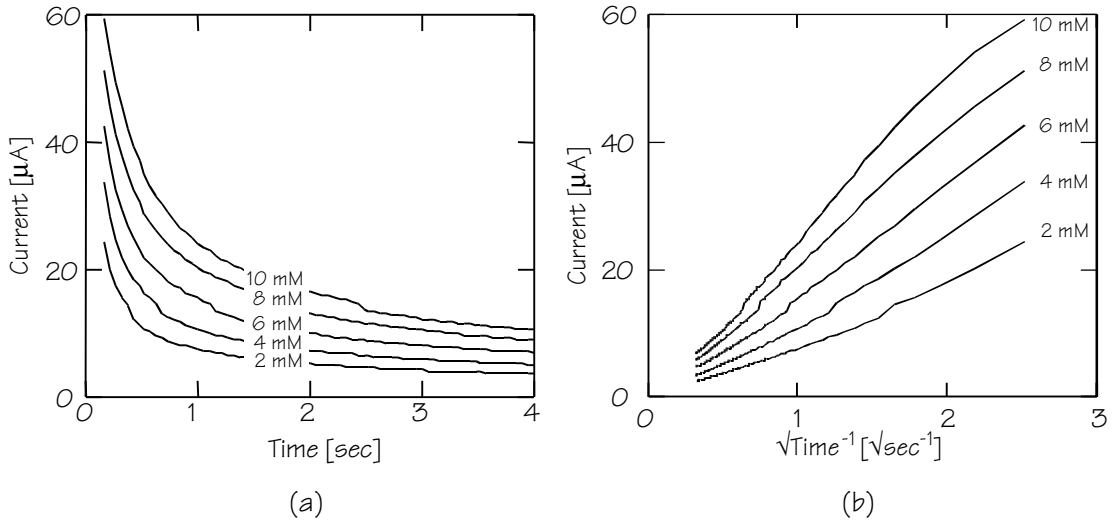

Figure 4.13: Chrono amperometric H_2O_2 measurement results:(a) the current relaxation curves for sensor type B as a function of the H_2O_2 concentration, (b) the same data but plotted on a non-linear time axis

Figure 4.13a shows the recorded current responses for hydrogen peroxide concentrations of 2, 4, 6, 8 and 10 mM for a sensor of type B. The characteristic $1/\sqrt{t}$ shape is observed and confirmed by figure 4.13b where the recorded current is plotted as a function of the inverse of the square root of time. The slopes of these curves are plotted in figure 4.14 as a function of the applied hydrogen peroxide concentration. In addition the similar data is recorded using a sensor of type A and plotted in the same graph.

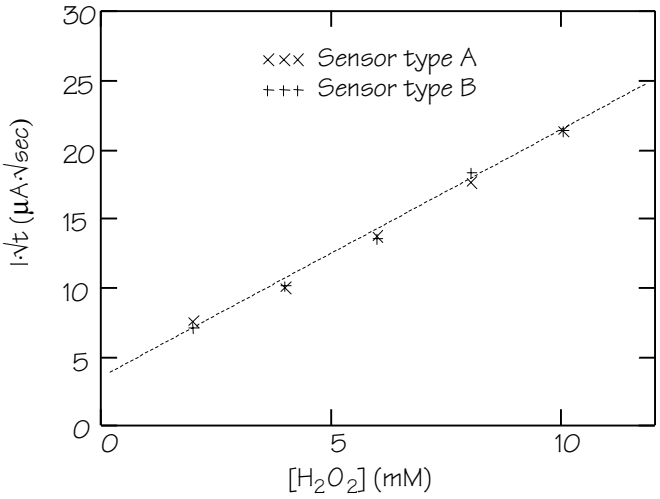

Figure 4.14: Measured calibration curve for chronoamperometric responses

Data evaluation

Figure 4.14 is constructed from figure 4.13a by plotting the recorded current versus $1/\sqrt{t}$ and determining the slope. These slopes plotted as a function of the H_2O_2 concentration give the calibration curve for the sensor. This curve shows an offset (extrapolating to a zero concentration does not give a zero slope) probably due to a double layer capacitance loading current. Table 4.3 summarises the observed sensitivities.

Table 4.3: Measured sensitivity and electrode surface

Sensor	Slope [µA·sec^{½}·mM^{-1}]	Area [mm^2]
Type A	1.754	0.96
Type B	1.842	0.84

From the Cottrell equation (4.20) the diffusion coefficient of hydrogen peroxide can be determined as a verification. Using the slope of sensor B, being equal to 1.842 µA·sec^{½}·mM^{-1}, this results in

$$D_{H_2O_2} = \pi\left(\frac{\text{slope}}{nFA}\right)^2 = 1.62 \cdot 10^{-5} \cdot \text{cm}^2 \cdot \text{sec}^{-1}$$

which is equal to the theoretical value of $1.6 \cdot 10^{-5}$ cm^2/sec [8].

Conclusions

Chrono amperometry appears to be a reliable method for the detection of the hydrogen peroxide concentration as indicated by the straight calibration curve of figure 4.14. The tested concentration range of 2 to 10 mM hydrogen peroxide covers the actual values during washing being 6 to 8 mM. Because the bleaching process is the oxidation of stains, and this method measures reduction of hydrogen peroxide (the oxidising operation), this method measures the bleach activity directly. Although the model, represented by the Cottrell equation (4.20), was actually derived for an infinite electrode surface, the used structure still satisfies the theory. In chapter 5 a technique will be derived which does not need a liquid filled reference electrode.

4.2.4 Measurement of temperature

Measurement set-up

Using an automated set-up the resistance of the structure while heating the solution is recorded. The set-up consists of a Radiometer CDM210 conductivity meter configured for measuring resistance. This meter has also the possibility to measure temperature using a separate probe. The set-up is controlled using the graphical programming environment LabView 3.1 for high reproducibility. The sensor, together with the temperature probe for reference, is placed in a glass on a heater with stirring option. The measurements are carried out in water, starting with melting ice.

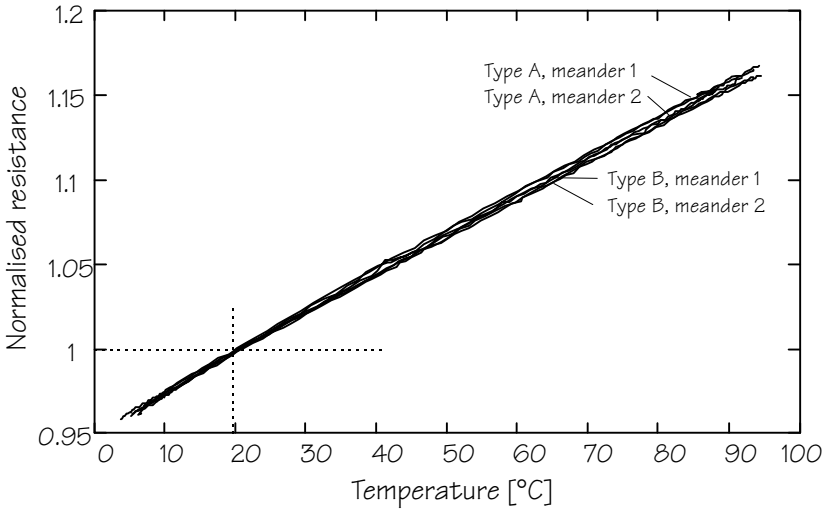

Figure 4.15: Measured normalised resistance versus temperature for both meanders of sensor type A and B

Measurement results
The measurements as shown in figure 4.15 are constructed by recording both the sensor resistance and the reference temperature while heating the water under stirred conditions starting with melting ice. This results in a tested range of 5 to 95°C.

Data evaluation
At 20ºC the resistance of sensor A is equal to 69.8 Ω, for type B this is 63.8 Ω. This is slightly less than the theoretical values based on the bulk resistivity of platinum. Since the platinum layer was somewhat thicker than the intended thickness and there is a tantalum adhesion layer between the platinum and the substrate, this difference is not very surprising. In addition, since the temperature information is in the change in resistance, the nominal value is not of interest.
After choosing a reference temperature, the experimentally determined temperature coefficient α can be found using equation (4.18). For a reference temperature of T_0 = 20ºC, the observed value is equal to α = 0.00231°C^{-1} where the worst point has only a deviation from the fitted straight line of less than 0.5%.

Conclusion
The curves for both meanders of sensors of type A and type B show an impressive similarity. Apparently, the temperature coefficient of α = 0.00231°C^{-1} can be used for all sensor structures. However, the theoretical value of α = 0.00392°C^{-1} is not observed. An explanation can be that this value is given for bulk platinum and we are dealing here with a thin film. In addition, an adhesion layer of tantalum is present which has a different temperature dependency and might even form an alloy with platinum which changes also the temperature dependency.

4.2.5 Generation of a local pH gradient

Measurement set-up
The pH actuator operation is tested by performing a coulometric acid to base titration. Therefore, the multi purpose sensor structure is used as a potentiometric working electrode by connecting inputs A, B, C and D to the working electrode lead of an EG&G PAR 173 potentiostat. A three electrode set-up is used with a platinum 1.0×0.5 cm^2 counter electrode and a conventional Ag/AgCl reference electrode. In practice, a two electrode set-up can be used as well, if the counter electrode is placed at a certain distance from the working electrode. The used working electrode is of type A with an area as given in table 4.3.

The titration is carried out in a 0.10 M acetic acid (HAc) solution with 0.10 M potassium nitrate as a supporting electrolyte. An applied current of 100 µA is used.

Measurement
The recorded working electrode potential V_{Pt} during the current injection is plotted in figure 4.16. After 9.71 seconds the end point t_{end} is observed.

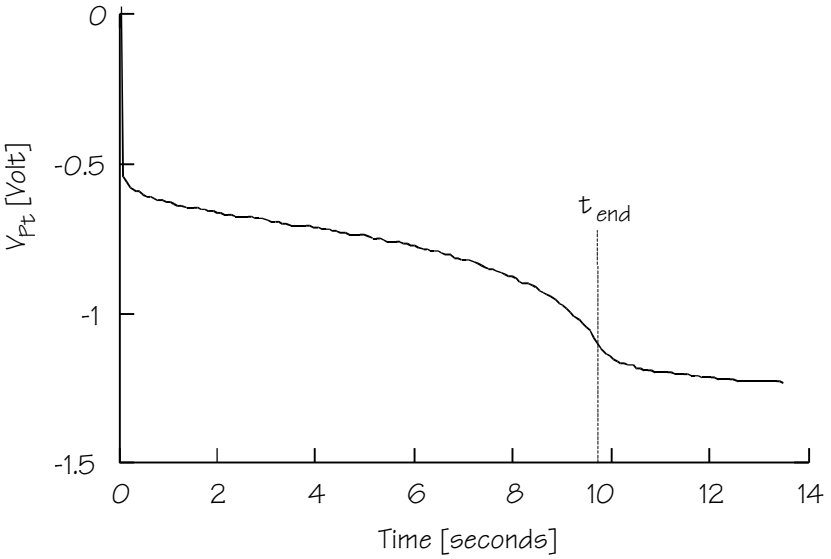

Figure 4.16: Measured potentiometric titration curve in 100 mM acetic acid

From the Sand equation (4.24) the bulk concentration acetic acid can be calculated using its diffusion constant being $1.21 \cdot 10^{-9}$ m^2 sec^{-1} [9]. The calculated value is 0.109 M which is almost equal to the used concentration.

4.2.6 Local heating

Measurement set-up
After the thermo resistive pathways were calibrated for temperature measurement as described in subsection 4.2.4, the dissipated heat can be measured. This is done by applying an AC current to one branch (pads A and B), while measuring the resistance of another (pads C and D). An AC actuator current is chosen in order to avoid electrochemical reactions in the contacting electrolyte. The electrolyte, which is not stirred during a measurement, is tap water.

Experimental
Figure 4.17a shows the transient response when heating with a sine wave of 1 kHz and an effective current of 35 mA. The measured resistance was converted to an equivalent temperature using the

calibration curve of figure 4.15. The 95% response time appears to be 8.9 seconds. Figure 4.17b shows the linear relation between the square of the applied current and the measured temperature. The increase in temperature is limited here by the sine wave generator which can not apply more than 35 mA. To determine the effect of the heater current frequency, the experiment was performed using heater currents of 10, 100 and 1000 Hz.

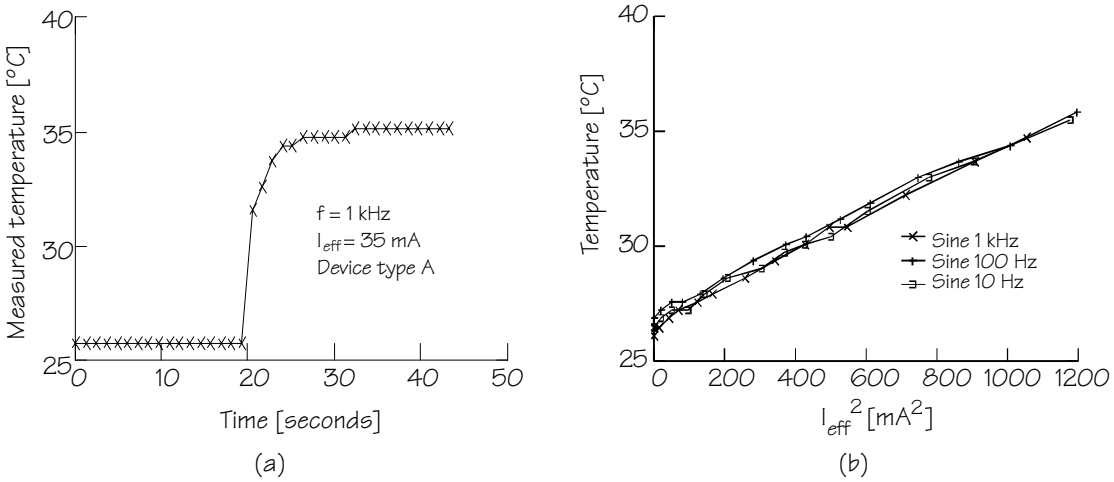

Figure 4.17: Thermoresistive heating of water::(a) transient response, (b)power response

Conclusion

As indicated by equation (4.25), the injected heat is proportional to the square of the effective value of the heater current. There is no observed dependency on the frequency within the tested range of 10 to 1000 Hz.
The conclusions here are rather short, since chapter 6 is devoted to thermoresistive heating. The verification that it is in principle possible to heat the local environment is sufficient in this context.

4.3 Conclusions

In the previous chapter a material for the fabrication of an integrated sensor device was chosen. Structures consisting of a planar metal film, fabricated by deposition and patterning of a noble metal, appeared to be a promising starting point for integration. This chapter described the choice of an integrated sensor structure lay-out and the optimisation of the geometry for proper sensing operation in the desired practical ranges.

The choice is a planar structure, since this gives the possibility to realise the devices using standard silicon processing equipment. Planar structures can be made on a (glass) wafer with a high reproducibility.

Two implementations are proposed, originating from an optimisation process for the electrolyte conductivity sensing operation where two concessions were made. These concessions were made in favour of optimal heating operation and the potential use of the device as a working electrode. The observed resulting differences between these two implementations for measuring and actuating are minimal. Although, when used as a conductivity cell, sensor type A has a slightly wider operational frequency range than type B, the observed sensor and actuator behaviour does not result in the rejection of one of the two implementations. Note that the higher efficiency concerning the band width observed with sensor type A was predicted in subsection 4.1.1 where the consessions were introduced.

In table 4.4 the practical ranges of the sensed parameters as given in chapter 2 are repeated together with the tested ranges.

Table 4.4: Observed ranges during washing and tested values

	During washing process	Tested range
Conductivity	100 - 2000 µS/cm	70 - 2900 µS/cm
Bleach activity	6 - 8 mM	2 - 10 mM
Temperature	5 - 90°C	5 - 95°C

Using the proposed multi purpose sensor-actuator structure, three parameters were successfully measured in the range of interest. The integrated structure yields the possibility of very local measurements because the active sensing area is only 1×1 mm^2. Besides the three basic sensing operational modes, two actuator modes were performed as well. A quantitative analysis of the actuator behaviour is meaningless at this moment, because a direct use of the actuator functions during washing processes is beyond the scope of this chapter. A coulometric determination (using potentiometry as an end point indicator method) of a 100 mM acetic acid solution verified the pH gradient actuator operation in an arbitrary way. An also arbitrary heating experiment was done as well. An application of the heating operation is described in chapter 6.

The three sensor operations and two actuator modes are obtained by connecting the structure to advanced laboratory equipment. A disadvantage is that for the chrono amperometric experiment a conventional reference electrode had to be used. In the next chapter, a technique is derived which does not need a conventional reference any more.

The actuator modes are not meaningful at this moment, but they can be used for local sensor-actuator experiments as described in chapter 7 and in the supplementary results of chapter 9. Some practical results using the device as a sensor-actuator system can also be found in chapter 9. Together with the sensor modes this gives a real multi purpose integrated sensor-actuator device with which many local experiments can be performed in order to analyse a solution more completely than was possible using some particular single sensors.

4.4 References

[1] Yokogawa Electrofact b.v., Cursusboek Geleidendheid in theorie en praktijk, November 1987

[2] P. Jacobs, A. Varlan, W. Sansen, Design optimisation of planar electrolytic conductivity sensors, Medical & Biological Engineering & Computing, November 1995, page 802 - 810

[3] M. Abramowitz and I. Stegun, Chapter 17: “Elliptic integrals”, Handbook of mathematical functions, Dover Publications Inc., New York, 1965

[4] E.A.M.F. Dahmen, Electroanalysis, Theory and applications in aqueous and non-aqueous media and in automated chemical control, Elsevier, Amsterdam, 1986

[5] A.J. Bard and L.R. Faulkner, Electrochemical methods, fundamentals and applications, John Wiley and Sons, New York, 1980

[6] D.R. Lide, Handbook of chemistry and physics, 74th edition 1993 - 1994, CRC Press, Boca-Raton, Florida

[7] R.S.C. Cobbold, Transducers for biomedical measurements: principles and applications, John Wiley & sons, New York, 1974.

[8] V.G. Prabhu, L.R. Zarapkar and R.G. Dhaneshwar, Electrochemical studies of hydrogen peroxide at a platinum disc electrode, Electrochimica Acta, Vol. 26, No. 6, page 725 - 729, 1981

[9] V. Vitagliano and P.A. Lyons, Diffusion in aqueous acetic acid solutions, J. Am. Chem. Soc., 78 (1956) 4538

4.A Hoya® glass wafer SD-1 and SD-2 datasheet

			SD-1	SD-2
Thermal properties				
Coefficient of linear thermal expansion	$\alpha_{30\text{-}300}$	$\times 10^{-7}$ / °C	30.5	32.0
	$\alpha_{30\text{-}450}$	$\times 10^{-7}$ / °C	32.5	34.1
Transformation point		°C	725	721
Sag point		°C	788	787
Strain point ($10^{14.5}$ poise)		°C	673	669
Thermal conductivity	20 °C	cal / sec·cm·°C	0.0029	0.0026
Specific heat	20 °C	cal / g·°C	0.175	0.176
Mechanical properties				
Specific gravity			2.59	2.60
Knoop hardness	Hk	kgf / mm^2	640	638
Young's modulus	E	kgf / mm^2	9010	8860
Modulus of rigidity	G	kgf / mm^2	3620	3560
Poisson's ratio			0.244	0.244
Abrasion factor	FA		42	44
Optical properties				
Refractive index (at 587.56 nm)	η_d		1.532	1.531
Abbe number (at 587.56 nm)	ν_d		59	59
Physical properties				
Volumetric resistivity	20 °C	Ω·cm	$6.0 \cdot 10^{14}$	$4.1 \cdot 10^{14}$
(DC 500V)	100 °C	Ω·cm	$1.4 \cdot 10^{12}$	$4.2 \cdot 10^{12}$
	200 °C	Ω·cm	$3.5 \cdot 10^{9}$	$3.8 \cdot 10^{9}$
Dielectric constant	20 °C		6	6
(1 MHz)	100 °C		6	7
	200 °C		7	7
Dielectric loss	20 °C		$0.8 \cdot 10^{-2}$	$1.0 \cdot 10^{-2}$
(1MHz)	100 °C		$1.6 \cdot 10^{-2}$	$1.9 \cdot 10^{-2}$
	200 °C		$3.9 \cdot 10^{-2}$	$4.9 \cdot 10^{-2}$
Chemical properties				
Alkali durability[1]				
(Surface method)	NaOH	mg / 15 cm^2	0.02	0.01
Acid durability[2]				
(Surface method)	HNO_3	mg / 15 cm^2	1.95	1.20

1: The test pieces of glass are 43.7 mm diameter with both surfaces polished, and are soaked for 15 hours in a well-mixed 50°C 0.01 N NaOH solution. The weight loss is measured.

2: The same method as the alkali durability test except that the test piece is soaked for 50 hours in a 50°C 30% HNO_3 solution.

4.B The fabrication process

1. Wafer cleaning

Hoya® glass Wafer:

Size:	3 inch
Thickness:	500 µm

Wafer Cleaning:
1 min 1% HF
5 min O_2 plasma

2. Sputtering of Ta/Pt/Ta

Adhesion layer:	20 nm Ta
Pt Thickness:	250 nm
Adhesion layer:	20 nm Ta

3. Lithography using mask 1
"Conductors"

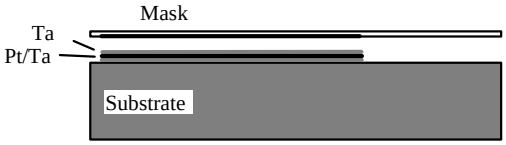

Resist:
spinning HMDS, 4000 rpm 20 sec
pos. resist (1813), 4000 rpm 20 sec
pre bake at 90 ºC during 20 min
exposure 8 sec mask 1
60 sec in 351 developer
post bake at 120 ºC during 30 min

Etching:

Ta:	RIE
Pt:	HCl/HNO_3 mixture
Ta:	RIE

Stripping of resist:
15 min O_2 plasma

4. Oxidation of Ta

Thermal, dry oxidation:
1 hour 500 ºC in O_2
Dry surface in vacuum oven 150 ºC

5. Polyimide

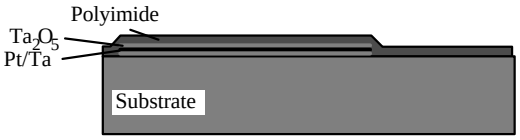

Primer:
19 ml methanol
1 ml water
1 droplet APS
(3-triethoxysilylpropylamin)
Polyimide:
PI : NMP (n-methylpyrolidon) = 4 : 1
Spinning of primer 4000 rpm 20 sec
Spinning of PI 4000 rpm 60 sec
Pre bake 90 ºC 25 min

6. Lithography using mask 2
"Contact holes and liquid-exposure areas"

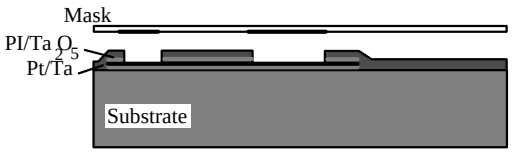

15 sec exposure using mask 2
Dry at 90 ºC during 10 min
Devel. polyimide in PI-developer
during 2 min
Dry 30 min in vacuum oven 300 ºC
Remove Ta_2O_5 by RIE

7. Sawing, packaging and bonding

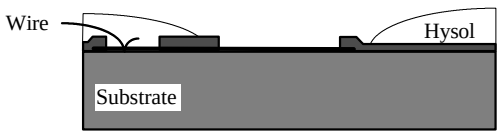

Material: Two component resin Hysol®

CHAPTER 5

Amperometric bleach detection

In this chapter the progresses that were made for sensing bleach activity using amperometry are summarised. Hydrogen peroxide is used as a representative bleaching agent for evaluating the measurement techniques. The final result is a two electrode set-up with which bleach activity can be monitored after interpreting a measured current response on a voltage sweep.

5.1 General concepts

Amperometry is an attractive tool for monitoring bleach activity since it can be used to measure the bleaching components in the way they are intended to do their work during washing: reductively or oxidatively decomposing a target species. It does not really matter what component is included in the detergent for the bleaching operation, the operator just wants to know the effectiveness of stain removal by redox mechanisms. In addition, the implementation of an amperometric detector fits with the integrated sensor structure consisting of metal films only, as described in chapter 4.
A sensing method is derived for measuring bleach activity in general, where hydrogen peroxide is used as a model for bleaching agents. The reason is that in Western European detergents the oxidative bleaching by hydrogen peroxide based systems is the most common.

The measurement of hydrogen peroxide is frequently applied in glucose sensors. In general, glucose sensors consist of a membrane which selectively catalyses glucose to gluconic acid and hydrogen peroxide by the use of glucose oxidase (GOD), where the hydrogen peroxide is detected by a subsequent amperometric method [1-3]. This amperometric method is normally not selective for hydrogen peroxide, which is not necessary since the GOD membrane takes care of the selection process. Nevertheless, for measuring hydrogen peroxide in a solution, simply omitting the membrane will not result into a selective hydrogen peroxide sensor in principle. In this chapter, a certain level of selectivity is obtained by interpreting the current response while applying a smart potential signal to a bare noble metal working electrode.
In addition to the selectivity problem with the amperometric measurement of bleach, there is the commonly observed reference definition problem. In general, with amperometric techniques, a liquid

filled reference electrode is needed together with a metal counter electrode in order to impose a desired electrode potential. Under certain conditions in practical cases, sometimes the counter electrode potential can be used as a reference point. For example, with glucose detection, interfering species are filtered out by the GOD membrane which simplifies the demands on the reference electrode enabling the use of a two (metal) electrode system [4]. However, when measuring hydrogen peroxide in the bulk of a solution, the stability of the counter electrode potential is no longer guaranteed.

The use of a carefully chosen working potential together with a smart interpretation of the measured current appeared not only to be a method for getting sufficient selectivity, but also for defining a reference point in the applied potential. Before focusing on measurement techniques, first an overview of the electrochemical behaviour of the used bleaching model (being hydrogen peroxide) is given.

5.2 The chemistry of hydrogen peroxide

The reaction mechanisms and the chemical properties of hydrogen peroxide are quite difficult to understand since it can both act as an oxidator and a reductor, where the reaction products are electrochemically active as well. To separate the influence of the reaction products and the single electrochemical modes, this section is divided into two subsections. The first one considers the thermodynamic equilibrium description of the electrochemical and acid-base properties of hydrogen peroxide, represented by a Pourbaix diagram. The other subsection shows an example of the encountered interpretation problems during the actual measurement of a cyclic voltammogram where the reaction kinetics and the produced oxygen influences the measurement.

5.2.1 The Pourbaix diagram

An elegant representation for the reaction and equilibrium formulas of hydrogen peroxide is a Pourbaix diagram [5]. This diagram contains information on both the acid-base behaviour and electrochemical reactions, together plotted in a potential versus pH graph. All numerical values for the electrode potentials and acid or base constants are taken from [5, 6].

The acid-base behaviour is determined by the decomposition of hydrogen peroxide into the intermediate hydrogen peroxide anion, which satisfies

$$H_2O_2 \leftrightarrow HO_2^- + H^+, \qquad (5.1)$$

with the acid constant defined as

$$k_a = \frac{[HO_2^-]\cdot[H^+]}{[H_2O_2]} = 2.4 \cdot 10^{-12}. \qquad (5.2)$$

It can be calculated that at pH = 10 the hydrogen peroxide is dissociated for only 2.3%. The logarithm of equation (5.2) yields the first equation for the construction of the Pourbaix diagram:

$$\log \frac{[HO_2^-]}{[H_2O_2]} = -11.63 + pH. \qquad (5.3)$$

It appears that for pH = 11.63 the ratio $[HO_2^-]/[H_2O_2] = 1$.

In addition to the acid-base behaviour, electrochemical half cell reactions are involved which can occur at a biased electrode or take place in conjunction with other half cell reactions [7]. They can be divided in reactions using H^+ and reactions using oxygen. For both HO_2^- and H_2O_2 an electrochemical interaction with water and H^+ can be observed:

$$H_2O_2 + 2H^+ + 2e^- \leftrightarrow 2H_2O \qquad E^0 = 1.776 \qquad (5.4a)$$

$$HO_2^- + 3H^+ + 2e^- \leftrightarrow 2H_2O \qquad E^0 = 2.119 \qquad (5.5a)$$

with E^0 the standard electrode potential. For electrolyte concentrations not equal to 1 molar and gas pressures not equal to 1 atmosphere, the standard electrode potentials must be transformed to the half-cell potentials E. This results in the following potential-concentration dependencies:

$$E = 1.776 + \frac{RT}{2F\log(e)}\log[H_2O_2] - \frac{RT}{F\log(e)}pH \qquad (5.4b)$$

$$E = 2.119 + \frac{RT}{2F\log(e)}\log[HO_2^-] - \frac{3RT}{2F\log(e)}pH, \qquad (5.5b)$$

with R, T and F having their usual meaning. Since pH is defined using a logarithm of base ten, and Nernst's law is defined using the natural logarithm, the factor log(e) appears in the denominators of the terms. This factor is sometimes approximated as a factor 2.3 in the numerator.
Furthermore, HO_2^- and H_2O_2 can react with dissolved oxygen according to

$$O_2 + 2H^+ + 2e^- \leftrightarrow H_2O_2 \qquad E^0 = 0.695 \qquad (5.6a)$$

$$O_2 + H^+ + 2e^- \leftrightarrow HO_2^- \qquad E^0 = 0.338 \qquad (5.7a)$$

with the corresponding potential-concentration equations

$$E = 0.695 + \frac{RT}{2F\log(e)}\log\frac{pO_2}{[H_2O_2]} - \frac{RT}{F\log(e)}pH \qquad (5.6b)$$

$$E = 0.338 + \frac{RT}{2F\log(e)}\log\frac{pO_2}{[HO_2^-]} - \frac{RT}{2F\log(e)}pH \qquad (5.7b)$$

where pO_2 is the oxygen pressure in Atmospheres.

When equations (5.3), (5.4b), (5.5b), (5.6b) and (5.7b) are plotted into a single potential versus pH plot, this plot is referred to as a Pourbaix diagram [5]. Some values for the partial oxygen pressure pO_2 and for the concentrations of H_2O_2 and HO_2^- are assumed. Figure 5.1 shows the complete Pourbaix diagram for the system of hydrogen peroxide in water.

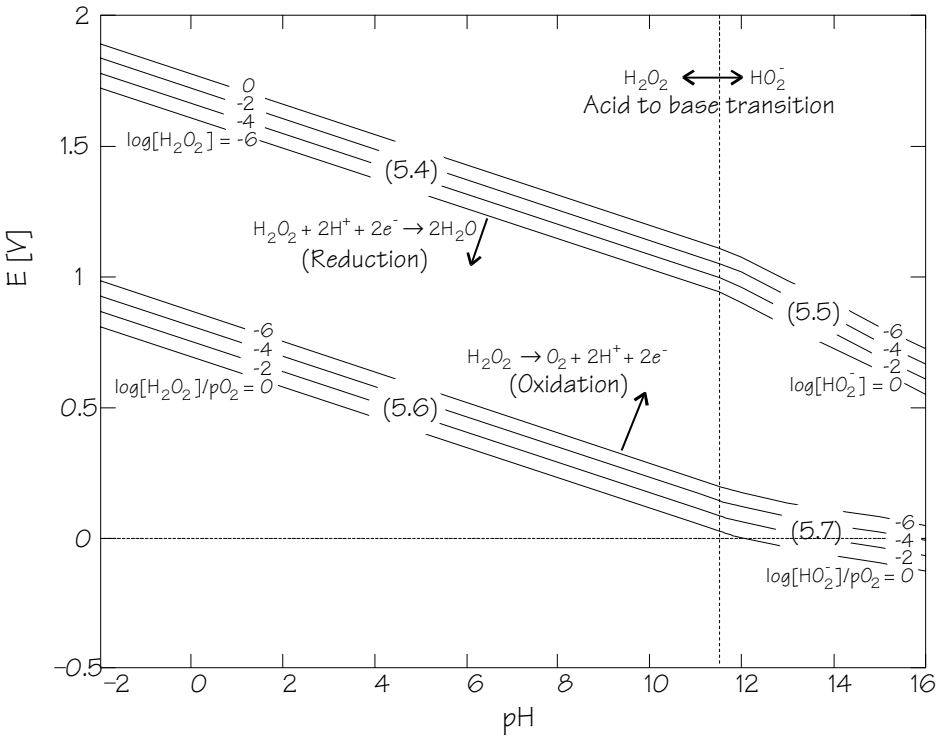

Figure 5.1: The Pourbaix diagram for the system H_2O_2 / water at 25ºC

From this graph it can be concluded that below the lines of equation (5.4), hydrogen peroxide can act as an oxidising agent with the formation of water. In general, this is the bleaching effect of hydrogen peroxide where coloured stains are oxidised into soluble non-coloured elements. Therefore, when the bleaching effectiveness has to be measured, it is this reaction that has to be observed.

However, the oxidation of hydrogen peroxide itself is an interfering phenomenon. Since above the lines of the equation (5.6), hydrogen peroxide is a reducing agent with the formation of dissolved oxygen, there is a common area with the oxidising behaviour. In this common area, hydrogen peroxide is said to be double unstable and can decompose into water and oxygen according to

$$\begin{array}{ll} H_2O_2 + 2H^+ + 2e^- & \leftrightarrow 2H_2O \\ H_2O_2 & \leftrightarrow O_2 + 2H^+ + 2e^- \\ \hline 2H_2O_2 & \leftrightarrow 2H_2O + O_2 \end{array}$$

Therefore, at a metallic surface with an electrode potential in the range of double instability, the decomposition of hydrogen peroxide is being catalysed without a resulting electrode current. Because the decomposition process is much slower than electrochemical reactions involved with amperometric experiments, this phenomenon is not likely to be of interest during a measurement. The spontaneous decomposition rate of hydrogen peroxide without a catalytic electrode is even lower.

Since the electrochemical operation (5.4) representing the bleaching capability has to be measured, without the interference of reaction (5.6), the measurement technique has to be chosen carefully. One option for selecting half cell reactions is to use a dynamic measurement by applying a potential step or sweep. With a controlled potential, a single line in the Pourbaix diagram can be crossed, and the measured response is the result of the corresponding half cell reaction only. In practice, this is not as simple as suggested, because reaction products will interfere during the dynamic measurement. The interpretation of the cyclic voltammogram at different pH's will explain this complexity.

5.2.2 The cyclic voltammogram

The influence of oxygen on measurements of hydrogen peroxide at a platinum (rotating) disk electrode is well described in literature [8-11]. Oxygen is present as a product of the catalysed or spontaneous decomposition of hydrogen peroxide or as dissolved atmospheric oxygen.

Figure 5.2a/b shows the recorded cyclic voltammograms in four 100 mM hydrogen peroxide solutions at different pH's. The experiments are carried out at a 0.5 mm^2 Pt working electrode in a 100 mM KNO_3 supporting electrolyte with a scan rate of 100 mV/sec and there was no stirring during the recording of the curve. The solution is saturated with nitrogen gas just before the measurement in order to minimise the initial

oxygen concentration, so the oxygen observed during the measurement can only be generated during this measurement.

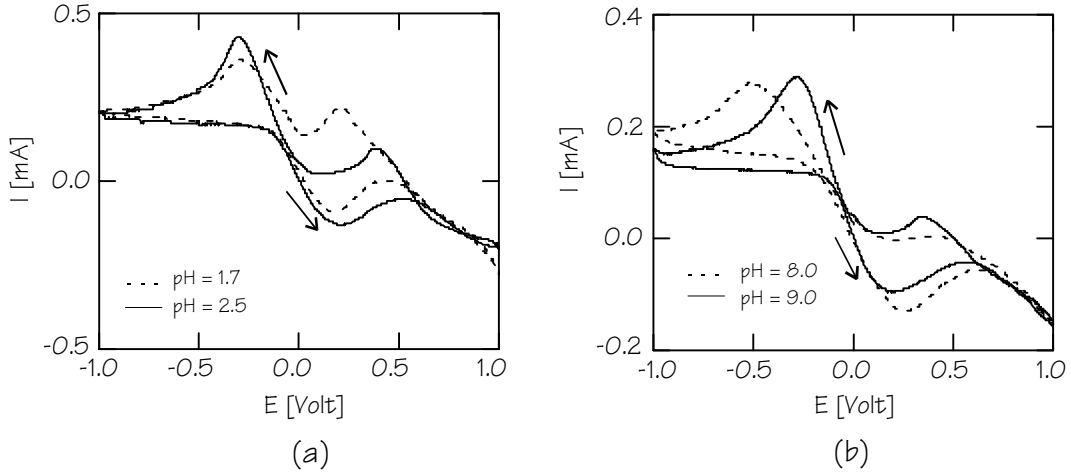

Figure 5.2: Cyclic voltammograms in H_2O_2 at four different pH's

In figure 5.2a, the pH is lowered to 1.7 and 2.5 by adding nitric acid. This results into a certain pH buffering operation because of the large background H^+ concentration. In figure 5.2b, the pH is increased by adding sodium hydroxide up to pH = 8.0 and pH = 9.0, which results also into a pH buffering effect. For each voltammogram, an identical potential sweep is chosen. The starting potential is 0 Volt versus an Ag/AgCl reference electrode. After an equilibrium time of 5 sec, the potential is lowered to minus 1 Volt resulting into a cathodic wave. Next, the potential sweeps from -1 Volt to +1 Volt, showing an anodic wave in the right half of the voltammogram. Finally, the potential is swept back to 0 Volt.

The cathodic wave

In terms of the Pourbaix diagram, the initial potential is below the lines of equation (5.4), and even below the lines of equation (5.6). This means that reduction of hydrogen peroxide is possible. In addition, the reduction of oxygen, present due to the spontaneous decomposition of hydrogen peroxide during the 5 seconds equilibrium time, is not implausible.

Direct reduction of hydrogen peroxide as given by equation (5.4a) is only observed at pH < 6 which was shown by others using rotating disc experiments [8]. Only in that case, the nernstian dependency on the pH as expected from equation (5.4b) is observed. This is confirmed by the cyclic voltammograms in figure 5.2a since the electrode potential at which the cathodic peak is observed shifts about 47 mV which is equivalent to the change from pH = 2.5 to 1.7 with -59 mV/pH.

For pH > 6, the presence of oxygen becomes of interest resulting into an indirect mechanism for the reduction of hydrogen peroxide [8]. This oxygen can be reduced to hydrogen peroxide according to

$$O_2 + 2H^+ + 2e^- \rightarrow H_2O_2 \qquad (5.8)$$

or to water according to

$$O_2 + 4H^+ + 4e^- \rightarrow 2H_2O\,. \qquad (5.9)$$

The overall observed reaction becomes

$$\begin{array}{ll} 2H_2O_2 & \rightarrow 2H_2O + O_2 \\ O_2 + 2H^+ + 2e^- & \rightarrow H_2O_2 \\ \hline H_2O_2 + 2H^+ + 2e^- & \rightarrow 2H_2O \end{array}$$

for the reduction of oxygen to hydrogen peroxide, or

$$\begin{array}{ll} 2H_2O_2 & \rightarrow 2H_2O + O_2 \\ O_2 + 4H^+ + 4e^- & \rightarrow 2H_2O \\ \hline H_2O_2 + 2H^+ + 2e^- & \rightarrow 2H_2O \end{array}$$

for the reduction of oxygen to water. Both results are equal to the direct reduction of hydrogen peroxide, but due to the indirect mechanism the cathodic peak in the cyclic voltammogram will not necessarily be observed at the equilibrium half-cell potential E. Figure 5.2b shows indeed a shift in the potential at which the cathodic peak is observed which can not be explained with a nernstian dependency. This indicates a more complex, indirect mechanism.

However, independent of the responsible reaction mechanism, the peak current observed when lowering the electrode potential is the result of the reduction of the species of interest. Whether the location and shape of this peak is caused by dissolved oxygen or by the hydrogen peroxide concentration does not matter: the process responsible for this peak represents the oxidative capability of the electrolyte under test. Therefore, the height of this peak, which was not considered up to now, is a measure for the bleach activity. So, a method for determining the bleach activity in washing water, which is generally alkaline, is to record the current through a working electrode which is biased at a potential lower than the location of the cathodic peaks in figure 5.2.

The anodic wave

Concerning the anodic currents, the interpretations in literature are less coherent. Both the oxidation of hydroxyl ions in alkaline media and hydrogen peroxide is possible in principle. In the case of the cyclic voltammograms of figure 5.2, the chemical histories before arriving at

the anodic sweep potentials are completely different, resulting in irreproducible conditions (local oxygen and hydrogen peroxide concentrations). Because in addition the interpretation of the anodic wave is of no interest in this context, no attempt is made to explain the behaviour.

5.2.3 Conclusion

So, the most appropriate method for determining bleach activity is the application of a negative potential to a working electrode while monitoring the current. This way of measuring is the closest to the actual bleaching operation which is the oxidation of stains. What type of bleaching system is present in a certain detergent is not of interest, an electrode biased at a sufficiently negative potential will record an electrical current which is proportional to the bleach effectiveness.
As can be seen from some measured cyclic voltammograms, an applied potential of -0.5 Volt versus an Ag/AgCl reference electrode is a correctly chosen electrode potential when hydrogen peroxide is the bleaching agent. However, a reliable reference electrode is necessary for assuring that the applied potential is indeed at this chosen potential, in order to "select" the desired bleaching mechanism. Since such a reference electrode is not desired, an indication whether the applied potential is in the desired region must be obtained from another source. The search for such an indication is described in the next section.

5.3 Controlled potential measurement techniques

With controlled potential techniques, the working electrode potential is swept from one potential to another while the current is being monitored under non-stirred conditions. A three electrode set-up using a potentiostat is used for applying the desired potential across the working electrode-electrolyte interface as shown in figure 5.3. No current flows through the reference electrode and in general, the working electrode is grounded.

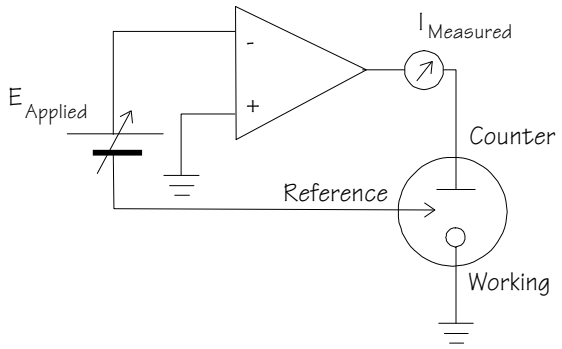

Figure 5.3: Three electrode set-up with a potentiostat

The differences in the controlled potential techniques are in the applied potential signals and the way the measured currents are represented. In the following subsections, the most appropriate amperometric technique for determining the hydrogen peroxide concentration will be selected. The selection criterion will be whether the technique can be used in a small sensor system. In a sensor system, the measurement may not be too time consuming and the use of a glass reference electrode is not desired.

5.3.1 Chrono amperometry and sampled current voltammetry

When the current is monitored while a potential step is applied to a working electrode, this stimulus-response technique is referred to as chrono amperometry [7]. With hydrogen peroxide in the electrolyte, a potential step can be applied which immediately depletes hydrogen peroxide at the electrode surface according to (5.4a). The observed chrono amperometric current response has a $1/\sqrt{t}$ shape and is linearly dependent on the hydrogen peroxide concentration. In general, for the chemical reaction evoking a species in the oxidised state to the reduced state according to

$$Ox + ne^{-} \rightarrow Red, \tag{5.10}$$

the observed current is given by the Cottrell equation [7]

$$i(t) = nFAC_{Ox}\sqrt{\frac{D_{Ox}}{\pi t}} \tag{5.11}$$

with n the number of electrons transferred, F Faraday's constant, A the electrode area, C_{Ox} the bulk concentration and D_{Ox} the diffusion coefficient of the species in the oxidised state. This equation is derived for an infinitely large, planar electrode and an applied potential step large enough to deplete the particles in the oxidised state immediately at the electrode surface.

In chapter 4, chrono amperometric detection of hydrogen peroxide was demonstrated by applying potential steps of -0.5 V in a three electrode configuration with an Ag/AgCl reference electrode. The step size was chosen empirically by first taking a cyclic voltammogram using the same set-up. Because a reference electrode was used, it was sufficient to choose the potential step size once and use it in all the subsequent experiments. However, the final aim is to find a detection technique which does not need a conventional reference electrode. So, it is preferred to have a technique which gives information on both the hydrogen peroxide concentration itself and on whether the applied

potential is the correct one, since then information on the validity of the experiment is available.

This idea is shown by a series of chrono amperometric experiments, each with a different step size. Consider the measured chrono amperometric curves as shown in figure 5.4a, recorded at various potential step sizes ranging from 0.0 to -1.0 volt. The electrolyte consists of 10 mM hydrogen peroxide with 10 mM potassium nitrate as a supporting electrolyte. A platinum sensor of type B (as described in chapter 4) was used as the working electrode.
A snap shot of the sampled currents after two seconds is given in figure 5.4b, which is commonly referred to as the sampled current voltammogram [7]. For step sizes between 0.0 and -0.3 Volts the observed sampled current is dependent on the applied potential. Between -0.3 and -0.8 Volts there is a step size independent plateau which indicates that the Cottrell equation is valid. This is the most common area for chrono amperometry. Finally, the applied electrode potential becomes negative enough to evoke the reduction of water.

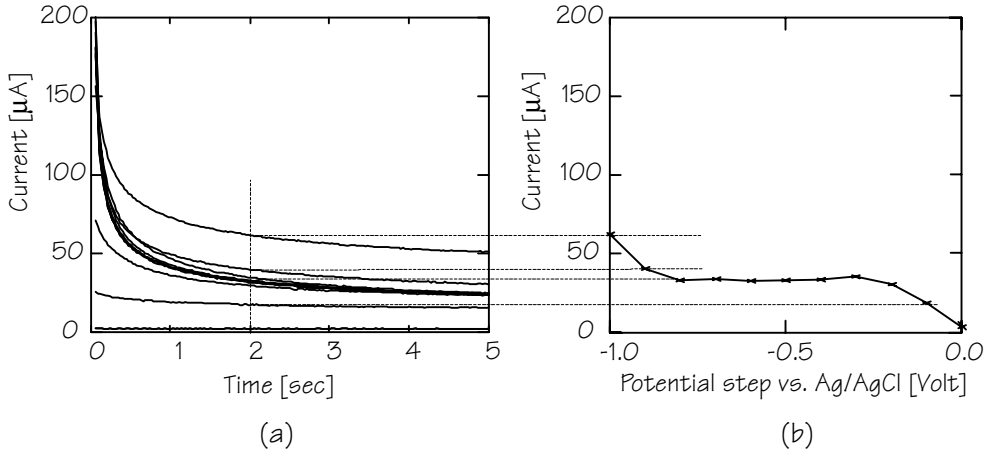

Figure 5.4: Chrono amperometric curves (a) in 10 mM H_2O_2 at various potential steps and the sampled currents (b) after t = 2 sec

From this curve it becomes clear that under certain conditions the actual value of the applied potential is not of interest for a concentration measurement. When the plateau in figure 5.4b is detected, the chrono amperometric experiment is meaningful and the concentration can be calculated without knowing the absolute potential. So, if the stable Ag/AgCl reference electrode is being replaced by a simple platinum electrode, and consequently the voltammogram will shift with an unpredictable value along the potential axis, the measured current will still give the same information. Notice that this potential shift must remain constant during all the chrono amperometric experiments. As a compromise, this condition is met in the three electrode set-up where no

current flows through this platinum reference electrode, so no time or current dependent electrode potential is expected. The platinum electrode can probably act as a pseudo reference in a three electrode set-up.

A better idea than using a series of chrono amperometric experiments, however, is to use a single potential sweep instead of a series of potential steps, since then the drift in the pseudo reference electrode is less likely. In addition, the application of a potential sweep and the recording of the current response is less laborious than the construction of a sampled current voltammogram.

5.3.2 Potential sweep voltammetry

A method that has some resemblance with sampled current voltammetry, is potential sweep voltammetry [7]. While with the sampled current technique a set of chrono amperometric experiments has to be done for constructing the voltammogram, sweeping the electrode potential linearly will give a potential-current curve directly. Although the mechanisms determining the shapes of sampled current and potential sweep methods are completely different, the possibility of substituting the conventional reference electrode for a pseudo reference electrode remains unchanged.

Because of its different kinetics, the linear potential sweep technique shows no plateaus, but peaks. Figure 5.5 shows the typical shape of a cathodic linear sweep voltammogram. The peak current I_{peak} is determined by [7]:

$$I_{peak} = kn^{3/2}AD_{Ox}^{1/2}v^{1/2}C_{Ox} \qquad (5.12)$$

under unstirred conditions, with

- k the Randles-Sevcik constant ($k = 2.69 \cdot 10^5$ ampere·volt$^{-½}$·sec·mol^{-1});
- n the number of electrons involved in the reduction;
- A the electrode surface area;
- D_{Ox} the diffusion constant of the particle to be reduced;
- v the potential sweep speed;
- C_{Ox} the bulk concentration of the particles to be reduced.

The appearance of a peak in the current, while this was not the case with the sampled current voltammogram, is due to the depletion of the target particles near to the electrode surface. Because the diffusion layer thickness of the particles to be reduced increases with the applied potential, the mass flux rate decreases.

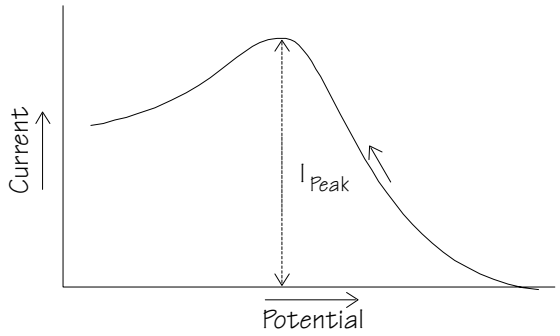

Figure 5.5: Drawing of a typical linear cathodic sweep voltammogram for a reversible system

Notice that for the theoretical evaluation of the peak current, equation (5.12) can not simply be used for hydrogen peroxide when the pH is larger than 6. In that case, the observed cathodic wave is not determined by a single reduction process, but by a complex indirect mechanism as was described in subsection 5.2.2. If the current would have been the result of the direct reduction of hydrogen peroxide, the height of the current peak would be equal to 2.1 mA for an electrode of size 1×1 mm^2, a scan rate of 500 mV/sec, a hydrogen peroxide concentration of 100 mM and an assumed diffusion constant of $1.6 \cdot 10^{-5}$ $cm^2 \cdot sec^{-1}$. With an indirect reduction mechanism, via the reduction of oxygen, this peak can only get lower since another time consuming step is introduced in the electrochemical process.

5.3.3 Conclusion

Amperometry is a suitable technique for measuring bleach activity since the bleaching is measured in the way it is supposed to work. The recorded current through a working electrode is a measure for an imposed bleaching action.
When using controlled potential techniques, an orientation point in the current response is sometimes present, that is independent of a reference electrode potential. With sampled current voltammetry, this is a potential step independent region, with linear sweep voltammetry this is a peak in the observed current. For constructing a sampled current voltammogram, a series of chrono amperometric experiments is needed. Therefore, the use of the sweep technique is preferred, since it can be recorded in a single experiment. By determining the peak and measuring the peak value, the concentration indication becomes independent of the used reference electrode.
Two options are possible for carrying out the experiments with a platinum reference. First, a three electrode set-up can be used as given in figure 5.3 where the Ag/AgCl reference is replaced by a platinum plate. In that case, no current flows through the platinum reference electrode, and therefore it is not likely that the potential of this electrode

will change during a measurement. However, when the counter electrode is much larger than the working electrode, at equal current, the current density through the counter electrode surface area will be much lower. Since electrochemical phenomena are dependent on the current density, the reactions occurring at this counter electrode will not introduce significant changes in electrode potentials. So, a second option can be to use a large counter electrode as the reference which results into a very simple two electrode set-up. The choice between these two set-ups is made by comparing some practical experiments as presented in the next section.

5.4 Experimental

The conclusion of the previous section is that it should be possible to measure the hydrogen peroxide concentration amperometrically without knowing the exact electrode potential. In this section some measurements are reported which verify this idea. The measurements were done in both a three and a two electrode set-up.

5.4.1 Three electrode set-up

In a set-up with three electrodes, as represented in figure 5.3 some potential sweep experiments are performed. The working electrode is a sensor of type B (as described in chapter 4) switched as a one square millimetre large platinum surface. A platinum plate of 0.5 cm^2 is used as a counter electrode. For the reference electrode a commercial Radiometer Ag/AgCl electrode or a second platinum 0.5 cm^2 electrode has been chosen. The measurements are performed by an EG&G potentiostat/galvanostat model 173 under computer control. Before each measurement, the solution is saturated with nitrogen gas in order to minimise the initial oxygen concentration. A 100 mM potassium nitrate supporting electrolyte is used to reduce the ohmic drop in the electrolyte and to prevent migration. During the recording of a sweep, the solution is not stirred. With all following measurements, the scan rate is 500 mV/sec. The bulk pH in the non-buffered 100 mM hydrogen peroxide solution is 6.3.

The solid loop in figure 5.6, being the cyclic voltammogram (CV) using the Ag/AgCl reference electrode, shows the dominant current peak at minus 0.5 Volt. As explained in subsection 5.2.2, the corresponding overall reaction is the one given by equation (5.4a). When using the CV as a fingerprinting technique for locating a reaction peak, the absolute potential is not of interest and therefore no attempt is made for completely understanding the location of this peak.

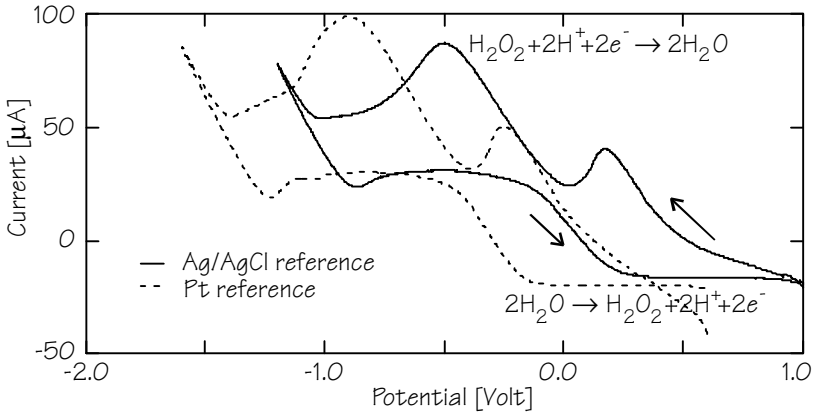

Figure 5.6: Cyclic voltammogram in 0.1 M H_2O_2 with 0.1 M KNO_3 as a supporting electrolyte

Now the primary reaction is located in the CV using this fingerprinting method, the experiment is repeated with the reference electrode replaced by a simple platinum plate (dashed line in figure 5.6). The start and end potentials are changed after some initial experiments in order to limit the currents of water electrolysis. As predicted from theory, the shape of the CV is not significantly changed, only the potential of the reference is shifted. So, although the platinum reference has an unknown electrode potential, this potential is at least sufficiently constant during the potential sweep which takes two seconds. However, one indication that the platinum reference does not stay completely stable during the recording of the CV, is the crossing of lines at a potential of about 0.4 Volt.

Next, this experiment is repeated for other concentrations of hydrogen peroxide. Only parts of the sweeps in the negative direction are plotted in figure 5.7, the reversal sweeps are also performed but not included in the graphs.

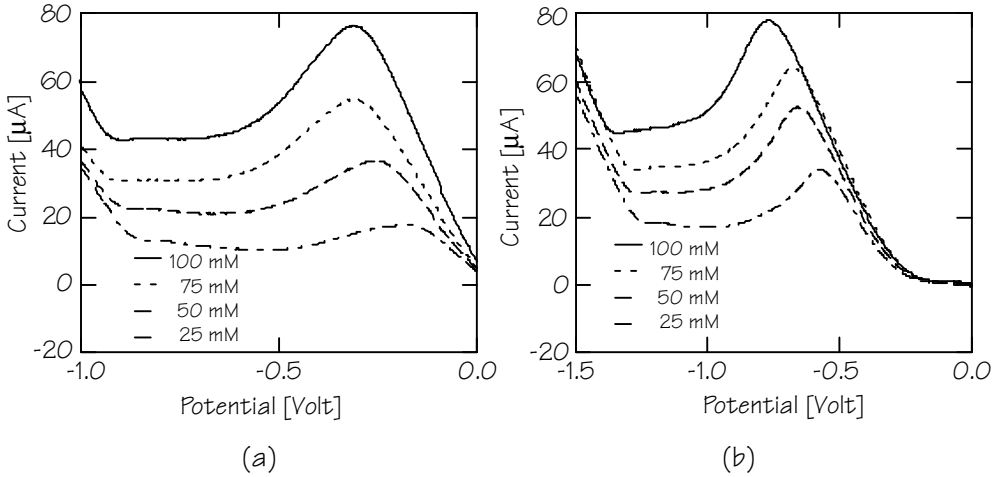

Figure 5.7: Potential sweep voltammograms in various concentrations H_2O_2 with (a) Ag/AgCl reference and (b) Pt reference electrode

The peak currents can easily be read from these curves and plotted into a peak current versus hydrogen peroxide concentration graph (figure 5.8). However, the theoretical peak heights can not be plotted in this graph, because equation (5.12) can not completely be evaluated. For a complete evaluation of this equation, the peak height determining species must be known. In the case of a pH larger than 6, the mechanism determining the peak is indirect, so equation (5.12) is too simplistic for calculating the height of the peak.

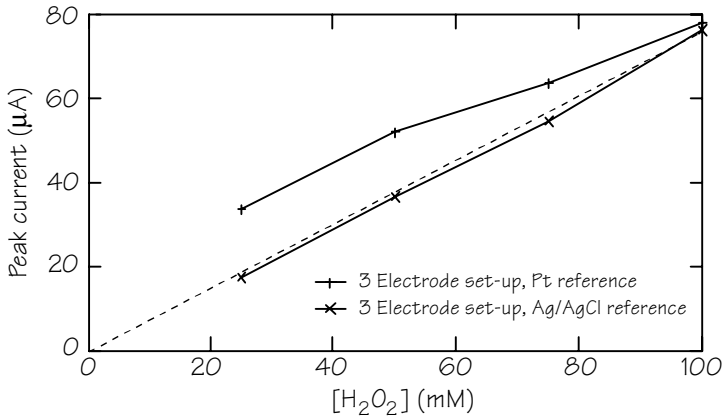

Figure 5.8: Measured values for the peak currents as a function of the H_2O_2 concentration

Figure 5.8 shows that the height of the current peak is an indication for the hydrogen peroxide concentration in these three electrode systems. However, when using a platinum electrode as a reference, the measured points are not on a straight line as can be observed when using a Ag/AgCl reference electrode. The peak current not being proportional to the concentration can not be explained by differences in double layer charging. There is no current flowing through the platinum reference electrode in a three electrode set-up which could charge the electrical double layer. So, the deviation from a straight line indicates that the platinum reference electrode potential does change during the recording of a sweep. However, this change is still of such a level that an almost linear relationship between the observed peak current and the applied hydrogen peroxide concentration is observed.

5.4.2 Two electrode set-up

The advantage of a three electrode set-up is that the potential across the working electrode-electrolyte interface can be measured or applied directly. In a two electrode set-up, the measured or applied potential will be distributed over two current carrying electrode-electrolyte interfaces.
However, in the case of the current peak detection method, the knowledge of the separate interface potentials is not needed. In

addition, the size of the counter electrode can be chosen much larger than the size of the working electrode which results in a much lower current density at this counter electrode. Therefore, it is not likely that the reactions at the counter electrode will be present significantly in the voltammogram.

This assumption is verified by a potential sweep experiment with a two electrode set-up where the separate electrode potentials were determined by monitoring the electrolyte potential using an Ag/AgCl reference electrode. A two electrode set-up is created by connecting both the counter lead and the reference lead of the potentiostat to a single (0.5 cm^2) platinum plate while the working electrode is a type B sensor structure (1.0 mm^2). The Ag/AgCl reference electrode is connected to the auxiliary input of an EG&G PAR potentiostat type 273. Using this set-up, the recorded auxiliary voltage is the potential of the working electrode with respect to the Ag/AgCl electrode, referred to as $V_{WE\text{-}Ref}$. The counter/reference electrode potential with respect to this Ag/AgCl electrode ($V_{CE\text{-}Ref}$) is obtained from the applied potential ($V_{WE\text{-}CE}$) and the measured auxiliary voltage by noticing that

$$V_{WE-Ref} - V_{CE-Ref} = V_{WE-CE}\,.$$

Figure 5.9 shows the current flowing through the two electrode cell, together with the determined separate electrode potentials during a potential sweep experiment.

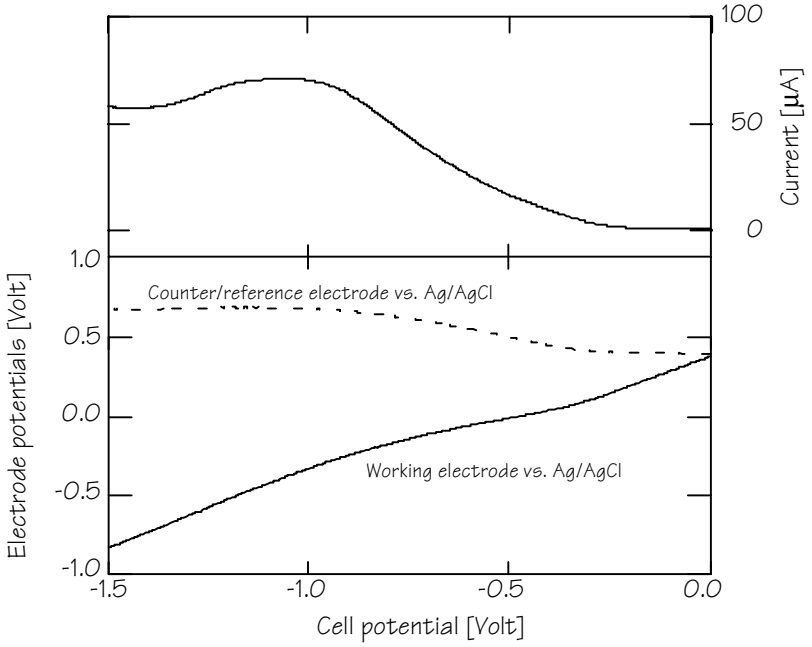

Figure 5.9: Potential sweep voltammogram in a two electrode set-up with an Ag/AgCl reference electrode for measuring the separate electrode potentials

The same conditions as in the previous experiments were chosen: a 500 mV/sec scan rate, a 0.1 M hydrogen peroxide solution with a 0.1 M

potassium nitrate supporting electrolyte. Before the measurement the solution was bubbled with nitrogen gas. Of course, the bulk pH in the non-buffered 100 mM hydrogen peroxide solution is 6.3 again.

The upper curve in figure 5.9 represents the cathodic current flowing through the working electrode, and therefore also through the counter / reference electrode. As could be expected, this current sweep has the same shape as the sweeps given in figure 5.7 for systems using three electrodes, since the conditions are the same. Even the height of the current peak is similar: the peak current of about 75 mA is also observed for the other set-ups when used in a 100 mM hydrogen peroxide solution.
However, the interesting information is in the lower part of the plot. The dotted curve represents the potential of the 0.5 cm^2 counter / reference anode with respect to a Ag / AgCl reference electrode, the solid line shows the potential of the working electrode (cathode) with respect to the same reference. A single x-axis is used for all three curves, on which the applied cell potential is written. Consequently, the difference between the working electrode potential and the counter / reference electrode potential is equal to the applied cell potential at all time.
In the ideal case, the dotted curve, representing the counter / reference electrode potential, is a horizontal line. However, at this anode, the pH will decrease during the sweep. Therefore, the electrode potential will increase, which can be seen in figure 5.9 as the dotted curve going up when decreasing the cell potential from 0 to -1.5 Volt (note, that the time elapses from right to left in figure 5.9). As a consequence, this shift in the counter / reference potential can be seen in the potential of the working electrode with respect to the Ag / AgCl reference as well.

Fortunately, this effect, which introduces a drift in the counter / reference electrode, is much lower than the intended reference operation. With respect to the potential of the working electrode, the counter / reference electrode remains almost constant. The applied cell potential drops almost completely over the working electrode-electrolyte interface with the subtraction of an offset.
The conclusion is that by introducing a difference in current density through the two electrodes (due to the different sizes), the potential of the counter electrode is forced to be indifferent with respect to the working electrode potential. So, during this experiment the relatively large counter electrode behaves more or less like a reference electrode.

Theoretically, an interfering phenomenon will be the charging current of the electrical double layers both for the working electrode and the

counter / reference electrode. Since a potential change is applied over these interfaces with a capacitive nature, a charging current will be observed. Assuming the interface capacitance of a metal-liquid interface equal to the capacitance of the Stern layer, which is a reasonable assumption for electrolytes with a rather high ionic strength (see also chapter 4), the capacitance of the working electrode can be approximated by about 100 nF. Then the counter / reference electrode, which is a factor 50 larger, will have a capacitance of approximately 5.0 μF. The potential change across the working electrode is equal to the scan rate being 500 mV / sec, resulting into a charging current of about 50 nA. For the counter / reference electrode the potential change is lower (about 400 mV / sec in the steepest part in figure 5.9) resulting in a charging current of approximately 2.0 μA. So, probably none of these currents will interfere significantly with the observed peak current which is about 75 μA.

Potential sweeps are made at hydrogen peroxide concentrations of 25, 50, 75 and 100 mM using the model 173 potentiostat again. The same conditions as for the experiments of figure 5.7 are used. As a reference, a sweep in a 100 mM hydrogen peroxide solution using a three electrode set-up and an Ag / AgCl reference electrode is plotted together with the two electrode measurements in figure 5.10.

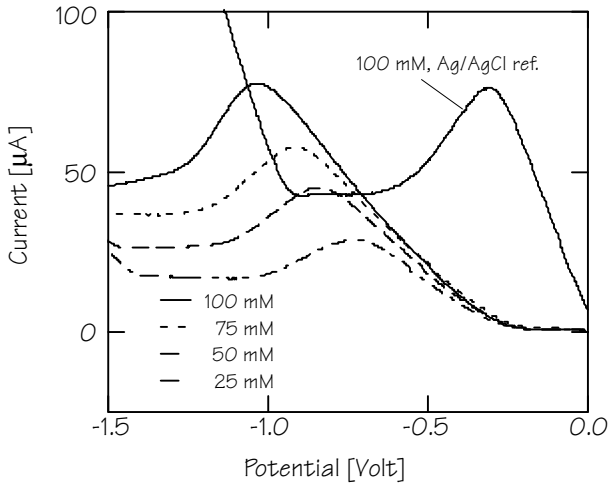

Figure 5.10: Potential sweep voltammograms in a two electrode system

At 100 mM hydrogen peroxide, the same peak current can be measured using either a three electrode set-up or a two electrode set-up. The potential at which this peak is observed, however, has moved. The peak currents observed with the two electrode set-up are plotted together with the results of the other experiments in figure 5.11.

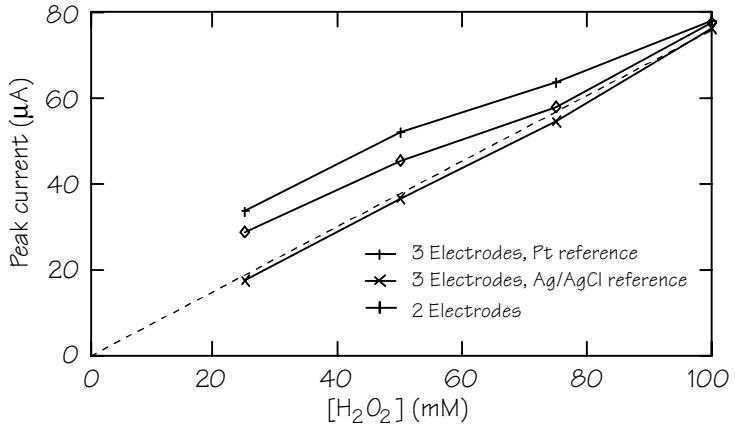

Figure 5.11: Summary of all measured peak currents

Since the results of the two electrode set-up are between the curves for the three electrode set-ups, it must be concluded that the two electrode method is better than the three electrode set-up with the platinum reference electrode. However, the two electrode method is not as good as the three electrode set-up with a glass reference electrode, which could be expected since figure 5.1 already showed a non-constant counter/reference electrode potential. A non-constant reference potential is not a problem itself, because this would only give a horizontal movement of the peak, but it indicates a chemical interference which will determine partially the observed current.

5.4.3 Measurement in a commercially available detergent

In the previous sections, the measurements were all performed in a perfectly conditioned electrolyte. The used electrolytes are based on demi water, the initial oxygen concentration is minimised, a supporting electrolyte is added and the bleaching component is simplified by using hydrogen peroxide. However, it was also stated that it does not matter what is the bleaching mechanism: an amperometric detection technique using a sufficiently negative biased working electrode, will measure the oxidative capability of the electrolyte. Therefore, it must be quite easy to reproduce the previous experiments in a more practical environment, being a sample of washing water.

A series of solutions is made by dissolving 1, 2, 3, 4 or 5 gram detergent per litre tap water. The chosen detergent is Dobbelman® Compact, a synthetic powder with bleach, on which package the use of 5 gram per litre is advised for the application in hand washes. Before each measurement, the solution is heated up to 40 °C since this is also the case during washing. While a potential sweep is made, the solution is not stirred. A sensor of type A, as described in chapter 4, is used in a two electrode set-up with a 1×0.5 cm^2 platinum counter electrode. The recorded sweeps at 100 mV/sec are presented in figure 5.12a.

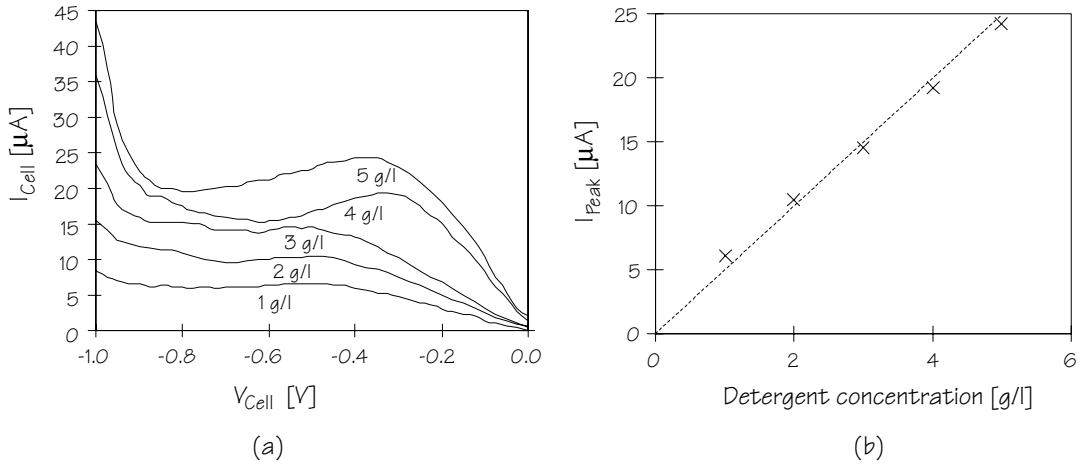

Figure 5.12: Measurements in 1 to 5 g/l detergent (Dobbelman® Compact) heated to 40 °C. (a) Recorded currents during applied potential sweeps, (b) sampled peak currents

The cell potential at which a peak is visible changes unpredictably. Between 3 g/l and 4 g/l an adventitious step in this potential is observed which can not be explained better than to ascribe it to a coincidental change in the counter / reference electrode potential.
However, the heights of the peaks are almost perfectly proportional to the applied detergent concentration. Figure 5.12b shows a very small deviation of the peak currents from a straight line without offset.

5.4.4 Conclusion

A two electrode set-up, consisting of a small 1×1 mm^2 platinum working electrode and a relatively large 1×0.5 cm^2 platinum counter / reference electrode, can be used for determining the bleach activity. Owing to the difference in electrode size, it is not necessary to include a separate reference electrode: the large counter electrode remains relatively stable during a potential sweep. The height of the observed current peak, when lowering the cell voltage from 0 to -1 Volt, is an indication for the bleach activity. This was verified in a non-conditioned detergent solution.

5.5 Summary

Potential sweep voltammetry appears to be a technique which does not need a conventional reference electrode when only the concentration of a redox active component has to be measured. In the described technique, the reference potential does not have to be well defined, but must at least remain constant during the potential sweep. Then, the information can be deduced from the current response by determining the amplitude of a peak at an arbitrary voltage.

This technique can be used with either a three or two electrode system, where the second one is more interesting because this can reduce the measurement probe to a simple stick with a small electrode on the upper side (for example the multi purpose integrated sensor structure) and a much larger platinum (or gold-plated copper) counter electrode on the back side.

5.6 References

[1] D.A. Skoog, D.M. West and F.J. Holler, Analytical Chemistry, Saunders College Publishing, Philadelphia, 1992

[2] M.J. Madou and S.R. Morrison, Chemical Sensing with solid state devices, Academic Press, Inc., 1989

[3] E.A.H. Hall, Biosensors, Open University Press, Buckingham, 1990

[4] K.D. Klein, Voltage relaxations of bi-electrodes for the long term monitoring of concentrations of hydrogen peroxide, glucose, etc., Sensors and Actuators B, 22 (1994) page 127-132

[5] M. Pourbaix, Atlas of electrochemical equilibria in aqueous solutions, Pergamon Press, New York, 1966

[6] D.R. Lide, H.P.R. Frederikse, Handbook of chemistry and physics, 74th edition, 1993-1994, CRC Press, Inc., Boca Raton, Florida, 1993

[7] A.J. Bard and L.R. Faulkner, Electrochemical methods, fundamentals and applications, John Wiley and Sons, New York, 1980

[8] V.G. Prabhu, L.R. Zarapkar and R.G. Dhaneshwar, Electrochemical studies of hydrogen peroxide at a platinum disc electrode, Electrochimica Acta, Vol. 26, No. 6, page 725 - 729, 1981

[9] G. Raspi and L. Nucci, Polarographic behaviour of H_2O_2 on a platinum microelectrode with periodic renewal of the diffusion layer, La Ricerca Scientifica, Vol. 37, No. 6, June 1967

[10] J. Koryta, M. Brezina and N. Kirz, Electrode processes of hydrogen peroxide on platinum disk electrode in alkaline and acid medium, Revue Roumaine de Chimie, 17, page 171 - 178, 1972

[11] M. Forbes, S. Lynn, Oxygen reduction at an anodically activated platinum rotating disk electrode, AIChE Journal, vol. 21, No. 4, page 763 - 769, July 1975

CHAPTER 6

Thermoresistive heating

A theoretical view on heating is given in order to understand the heating operation of the integrated sensor structure. First, the thermoresistive heating of a medium by a planar dissipator is observed. As an introduction a finite volume is evaluated. Subsequently, this model is expanded to the more practical system by introducing heat conduction and storage within an infinite volume. It appears that the differential equation describing this system is also applicable to other phenomena like the diffusion of ions in a solution and the propagation along an electrical transmission line. Although this equivalence is not explicitly needed in this context, it fits nicely within the multidisciplinary interfaces encountered when designing a sensor array. The kinetics of heating are illustrated by some temperature profiles which are the result of using a square planar heater in water. Next, the model for heating is expanded with a thermal analysis in the frequency domain which appears to be a suitable tool for modelling the effect of the substrate material on the heating of water. This frequency domain analysis is used for optimising the integrated sensor structure by choosing the most appropriate substrate material. Finally, the sensor-actuator operation consisting of measuring temperature while heating is used for determining a new parameter being the movement (turbulent flow) of the medium.

6.1 Heating a finite volume

The quantity of heat ΔQ produced by a thermoresistive heater is equal to the dissipated energy in the heater, being the power P of the heater multiplied by the time:

$$\Delta Q = P \cdot t = I^2 R t \qquad (6.1)$$

with R the resistance of the heater, I the current through the heater and t the time in which the current is switched on. Consider the planar resistor structure of figure 6.1 which is functionally equal to the integrated sensor device of chapter 4 switched with the two resistive paths in series.

In correspondence with the symbols used in chapter 4, the planar heater covers a square area of $L \times L$. Therefore, when the number of branches is equal to n, the total length of the conducting strip is approximately equal to $n \cdot L$, and also

$$n \cdot (s + w) = L \qquad (6.2)$$

with w the width of the strip and s the spacing between the branches. Notice that the capitals S and W are reserved for the spacing and width of the fingers of the same structure used as a conductivity cell as described in chapter 4.

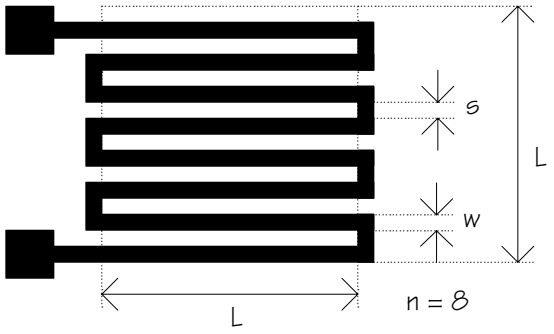

Figure 6.1: Structure of a heating element

Now the resistance R of the heater can be expressed in geometrical terms [1] as

$$R = \frac{n \cdot L}{\sigma h w} = \frac{n \cdot L}{\sigma h\left(\frac{L}{n} - s\right)} \approx \frac{n^2}{\sigma h} \tag{6.3}$$

with σ the electrical conductivity of the metal and h the thickness of the strip. In the last step of this expression, the assumption w >> s is made.

The calculation of the required heat for changing the temperature of a finite medium placed on top of the heater can be done by observing the heat capacity of this medium [2] defined as

$$c_m = \frac{1}{m}\frac{\Delta Q}{\Delta T} \tag{6.4}$$

which represents the absorbed heat ΔQ due to a temperature change ΔT normalised to the mass m. The temperature change ΔT as a result of heat injection ΔQ in a cubic volume with cross section L^2 and height z becomes

$$\Delta T = \frac{\Delta Q}{m c_m} = \frac{\Delta Q}{L^2 z \rho c_m} \tag{6.5}$$

where the density ρ of the medium is being introduced. If the heat is injected by the resistive heater of figure 6.1 according to (6.1), and inserting the theoretical resistance as expressed by (6.3), the change in temperature becomes

$$\Delta T = \frac{I^2 R t}{L^2 z \rho c_m} = \frac{I^2 n^2 t}{L^2 z \rho c_m \sigma h} \approx \frac{I^2 w^2 t}{z \rho c_m \sigma h} \tag{6.6}$$

again with the assumption that w >> s. However, this expression is only valid for a homogeneously heated volume since conduction and storage of heat is not implemented. So, although the time t and distance to the heater z are in this equation, it can not be used for determining the temperature profile in an infinitely large volume along the z-axis (perpendicular to the heater surface).

6.2 Heating an infinite volume

When there is no homogeneous heating of the medium, conduction and storage of heat must be included in the model. Therefore, the heat diffusion dynamics are now described by a differential equation.

6.2.1 The diffusion equation

The derivation of the differential equation describing implicitly the temperature distribution, consists of joining the equations for the thermal conductivity and the heat capacitance [3]. If Q is the amount of heat and T the temperature, then the one dimensional heat flow through a cross section A can be expressed using the thermal conductivity λ:

$$\frac{dQ}{dt} = \lambda A \frac{dT}{dx} \tag{6.7}$$

with dT/dx the gradient of temperature. Consider a volume with a cross section A and a thickness dl as indicated in figure 6.2. This volume is filled with a medium with a heat capacity c_m. When a heat flow is applied in the x direction, a temperature gradient occurs.

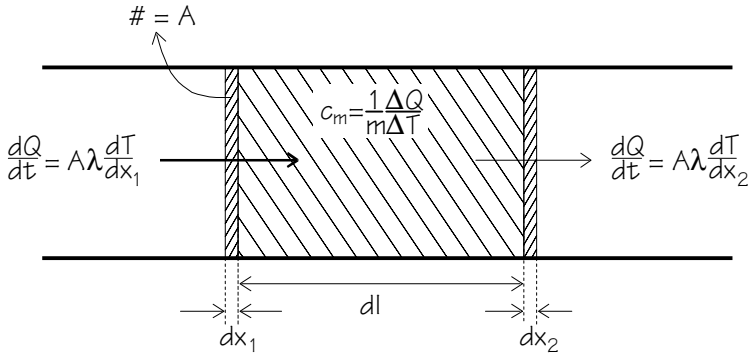

Figure 6.2: Representation of one dimensional heat conduction and storage

The difference between the influx and the outflux is according to (6.7)

$$\left.\frac{dQ}{dt}\right|_1 - \left.\frac{dQ}{dt}\right|_2 = \lambda A\left(\frac{dT}{dx_1} - \frac{dT}{dx_2}\right) \tag{6.8}$$

which reduces to

$$\left.\frac{dQ}{dt}\right|_{dl} = \lambda A \frac{d^2T}{dx^2} dl \qquad (6.9)$$

for an infinitesimally small slice with thickness dl and cross section A. This difference is equal to the change in the amount of stored heat in the slice A·dl which can be found from (6.4):

$$\left.\frac{dQ}{dt}\right|_{dl} = c_m \cdot m \cdot \frac{dT}{dt} = c_m \cdot \rho \cdot A \cdot dl \cdot \frac{dT}{dt} \qquad (6.10)$$

where the mass is written in terms of the density ρ. From equations (6.9) and (6.10) it can be found that

$$\frac{dT}{dt} = \frac{\lambda}{c_m \cdot \rho} \frac{d^2T}{dx^2} \qquad (6.11)$$

with

- ρ the density of the medium [kg/m^3],
- c_m the heat capacity [J/kgK] and
- λ the thermal conductivity of the medium [W/Km].

For the three dimensional case the differential equation becomes

$$\frac{dT}{dt} = \kappa \nabla^2 T \qquad (6.12)$$

where $\lambda/\rho \cdot c_m$ is now substituted by the constant κ. Since equation (6.12) is the equation for the diffusion of heat, the constant κ is the diffusion constant of heat in a certain medium with the unit [m^2/sec]. This equation can be used for conduction of heat in solids. When applied to the conduction of heat in liquids, it must be realised that it only implements heat transfer by diffusion. If also convection is present, equation (6.12) is no longer valid.

6.2.2 Diffusion of ions and electrical transmission lines

The described behaviour of a quantity being conducted by a medium in which it can also be stored, is observed in other branches of science as well. For example Fick's second law of diffusion [4] which describes the diffusion of ions in water, is a similar differential equation where the diffusion constant D is determined by the mobility of ions. With electrical transmission lines [5], being networks consisting of an infinite number of capacitors and resistors, the potential distribution along the network shows a diffusion like differential equation. In table 6.1 the equivalents are summarised.
Note that the first two rows deal with the one dimensional case, whereas in the last row, the three dimensional differential equation is given.

Table 6.1: Equivalent phenomena in the field of heat conduction, ion diffusion and the propagation along an electrical transmission line

	Conduction of heat	Diffusion of ions	Electrical transmission line
Flow through a cross section A	$\frac{dQ}{dt} = \lambda A \frac{dT}{dx}$	$I = \frac{dq}{dt} = D \cdot A \cdot F \frac{dC}{dx}$	$I = \frac{dq}{dt} = A \cdot \sigma E = \frac{1}{R_l} \frac{dU}{dx}$
Through slice with thickness dl	$\left.\frac{dQ}{dt}\right\|_{dl} = \lambda A \frac{d^2T}{dx^2} dl$	$I = \left.\frac{dq}{dt}\right\|_{dl} = D \cdot A \cdot F \frac{d^2C}{dx^2} dl$	$I = \left.\frac{dq}{dt}\right\|_{dl} = \frac{1}{R_l} \frac{d^2U}{dx^2} dl$
Storage in slice	$\left.\frac{dQ}{dt}\right\|_{dl} = c_m \rho A \frac{dT}{dt} dl$	$I = \left.\frac{dq}{dt}\right\|_{dl} = A \cdot F \frac{dC}{dt} dl$	$I = \left.\frac{dq}{dt}\right\|_{dl} = C_l \frac{dU}{dt}$
Differential equation	$\frac{dT}{dt} = \frac{\lambda}{c_m \rho} \nabla^2 T$	$\frac{dC}{dt} = D \nabla^2 C$	$\frac{dU}{dt} = \frac{1}{R_l C_l} \nabla^2 U$
	Q : heat dQ / dt : heat flow T : temperature A·dl : slice λ : thermal conductivity ρ : density c_m : specific heat capacity	q : charge I : current C : ion concentration A·dl : slice D : diffusion coefficient F : Faraday's constant	q : charge j : current density U : potential A·dl : slice R_l : resistance per unit length C_l : capacitance per unit length σ : electrical conductivity

The diffusion coefficient describing the conduction of heat in a solid, or a liquid where convection can be neglected, is equal to $\kappa = \lambda / \rho \cdot c_m$, for the diffusion of an ion in water this coefficient is referred to as D. In practice, the value for κ is much larger than the value for D, which means that diffusion of heat is faster than diffusion of ions in a solution. In the theory concerning electrical transmission lines, the term diffusion coefficient is not used in general, although the factor $(R_l C_l)^{-1}$ is equivalent to the diffusion coefficients in the other systems. Evaluation of transmission lines is more common in terms of (characteristic) impedances and phase differences.

6.2.3 Example solutions for the diffusion equation

For solving equation (6.12) the standard solution, being a Green's function, for diffusion from an instantaneous heat point source [3] can be used:

$$T_{Point}\left(\overline{R}\right) = \frac{e^{-\frac{\left|\overline{R}-\overline{R}'\right|^2}{4\kappa t}}}{(4\pi\kappa t)^{\frac{3}{2}}} \qquad (6.13)$$

with $|\overline{R} - \overline{R}'|$ the distance between the source point $\overline{R}'$ and the point of measurement $\overline{R}$. For a finite instantaneous plane source with size $L \times L$ the resulting temperature at a certain location can be found from equation (6.13) by integration, using carthesian co-ordinates:

$$T_{Square} = \int_{-\frac{L}{2}}^{\frac{L}{2}} \int_{-\frac{L}{2}}^{\frac{L}{2}} T_{Point} \cdot dxdy\,. \qquad (6.14)$$

For a non-instantaneous source, the temperature can be calculated using convolution with the injected heat function Q(t):

$$T(t) = \int_0^t Q(\tau) \cdot T_{Square}(t-\tau)d\tau\,. \qquad (6.15)$$

This injected heat function for a point source in a plane of size $L \times L$, can be found from the dissipated power P(t) in the heater at time t using the density and heat capacity of the heated medium [3]. If the heater is a resistive heater with resistance R, heated by a current I, the power is equal at any time, and the injected heat function can be written as

$$Q(t) = \frac{P(t)}{\rho c_m L^2} = \frac{I^2 R}{\rho c_m L^2} \qquad (6.16)$$

with ρ and c_m the density and heat capacity of water. Again, the width between the fingers of the heater is chosen much smaller than the width

of the resistive path s << w. When the centre of this actuator is chosen as the origin of space, the temperature at location (x, y, z) at time t can be found from substituting equation (6.14) and (6.16) into (6.15) resulting in

$$T(x,y,z,t) = \frac{I^2R}{\rho c_m L^2 (4\pi\kappa)^{\frac{3}{2}}} \int_0^t \int_{-\frac{L}{2}}^{\frac{L}{2}} \int_{-\frac{L}{2}}^{\frac{L}{2}} \frac{e^{-\frac{(x-x_0)^2+(y-y_0)^2+z^2}{4\kappa(t-\tau)}}}{(t-\tau)^{3/2}} dx_0 dy_0 d\tau . \qquad (6.17)$$

The integrations in space can be re-arranged according to

$$T(x,y,z,t) = \frac{I^2R}{\rho c_m L^2 (4\pi\kappa)^{\frac{3}{2}}} \int_0^t \frac{e^{-\frac{z^2}{4\kappa(t-\tau)}}}{(t-\tau)^{3/2}} \left(\int_{-\frac{L}{2}}^{\frac{L}{2}} \int_{-\frac{L}{2}}^{\frac{L}{2}} e^{-\frac{(x-x_0)^2+(y-y_0)^2}{4\kappa(t-\tau)}} dx_0 dy_0 \right) d\tau$$

and subsequently be solved giving

$$T(x,y,z,t) = \frac{I^2R}{8\rho c_m L^2 \sqrt{\pi\kappa}} \int_0^t \frac{e^{-\frac{z^2}{4\kappa(t-\tau)}}}{\sqrt{t-\tau}} \chi d\tau \qquad (6.18)$$

$$\chi = \left(\mathrm{erf}\left(\frac{L/2-y}{\sqrt{4\kappa(t-\tau)}} \right) + \mathrm{erf}\left(\frac{L/2+y}{\sqrt{4\kappa(t-\tau)}} \right) \right) \left(\mathrm{erf}\left(\frac{L/2-x}{\sqrt{4\kappa(t-\tau)}} \right) + \mathrm{erf}\left(\frac{L/2+x}{\sqrt{4\kappa(t-\tau)}} \right) \right)$$

where the χ-term represents the effect of a finite actuator and the exponential term the time delay due to the diffusion into the medium.

Solution on the z-axis

On the z-axis (perpendicular to the surface of the heater) the χ-term simplifies because x = y = 0. The result is

$$\chi_{z-axis} = 4 \cdot \mathrm{erf}^2 \left(\frac{L/2}{\sqrt{4\kappa(t-\tau)}} \right) \qquad (6.19)$$

so

$$T(z,t) = \frac{I^2R}{2\rho c_m L^2 \sqrt{\pi\kappa}} \int_0^t \frac{e^{-\frac{z^2}{4\kappa(t-\tau)}}}{\sqrt{t-\tau}} \mathrm{erf}^2 \left(\frac{L/2}{\sqrt{4\kappa(t-\tau)}} \right) d\tau . \qquad (6.20)$$

Using the approximation

$$\mathrm{erf}^2(\xi) \approx 1 - e^{-\frac{4}{\pi}\xi^2} \qquad (6.21)$$

(where the introduced error is not larger than 1.4% for any ξ) it is found that

$$T(z,t) = \frac{I^2R}{2\rho c_m L^2 \sqrt{\pi\kappa}} \int_0^t \frac{e^{-\frac{z^2}{4\kappa(t-\tau)}}}{\sqrt{t-\tau}} \left(1 - e^{-\frac{L^2}{4\pi\kappa(t-\tau)}} \right) d\tau \qquad (6.22)$$

which can be written as

$$T(z,t) = \frac{I^2 R}{2\rho c_m L^2 \sqrt{\pi\kappa}} \left(\int_0^t \frac{e^{-\frac{z^2}{4\kappa(t-\tau)}}}{\sqrt{t-\tau}}\, d\tau - \int_0^t \frac{e^{-\frac{z^2+L^2/\pi}{4\kappa(t-\tau)}}}{\sqrt{t-\tau}}\, d\tau \right). \qquad (6.23)$$

Although the shown integrals do have the analytical solution [6]

$$\int_0^t \frac{e^{-\frac{\eta}{t-\tau}}}{\sqrt{t-\tau}}\, d\tau = 2\sqrt{t}\cdot e^{-\frac{\eta}{t}} - 2\sqrt{\pi\eta}\left(1 - \operatorname{erf}\sqrt{\frac{\eta}{t}}\right) \qquad (6.24)$$

substitution does not lead to a useful expression. However, the practical value for κ in water is $1.455 \cdot 10^{-7}$ $m^2 \cdot sec^{-1}$ [6], which means that for L = 1 mm and a time t smaller than 0.5 seconds, equation (6.23) can be simplified since $t < L^2/4\pi\kappa$. The temperature distribution then reduces to

$$T(z,t) = \frac{I^2 R}{2\rho c_m L^2 \sqrt{\pi\kappa}} \int_0^t \frac{e^{-\frac{z^2}{4\kappa(t-\tau)}}}{\sqrt{t-\tau}}\, d\tau \qquad (6.25)$$

since the exponential term containing the heater size L is not significant anymore.

For a square 1 mm^2 heater of 0.1 Watt, and using the non-simplified expression (6.23), the temperature distribution becomes as shown in figure 6.3. Since equation (6.13) gives the temperature due to a point source, the result T(z,t) thus represents the temperature due to the heater only. So T(z,t) = 0 means that the absolute temperature is equal to room temperature.

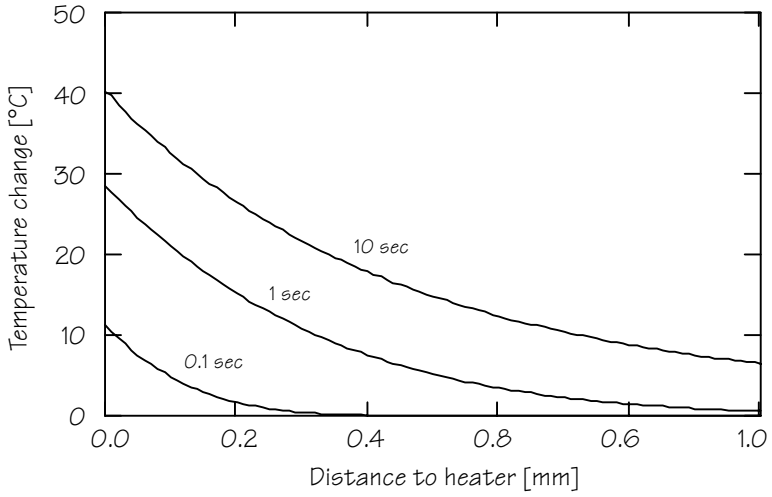

Figure 6.3: Temperature distribution along the z-axis using a 0.1 Watt heater in water

Solution on the x or y axis

On the x-axis where z = 0 (similar to the y-axis) the general solution (6.18) becomes

$$T(x,t) = \frac{I^2 R}{4\rho c_m L^2 \sqrt{\pi\kappa}} \int_0^t \frac{\operatorname{erf}\left(\frac{L/2}{\sqrt{4\kappa(t-\tau)}}\right)}{\sqrt{t-\tau}} \left(\operatorname{erf}\left(\frac{L/2-x}{\sqrt{4\kappa(t-\tau)}}\right) + \operatorname{erf}\left(\frac{L/2+x}{\sqrt{4\kappa(t-\tau)}}\right)\right) d\tau \qquad (6.26)$$

which is plotted in figure 6.4 for a 1 mm² heater of 0.1 Watt.

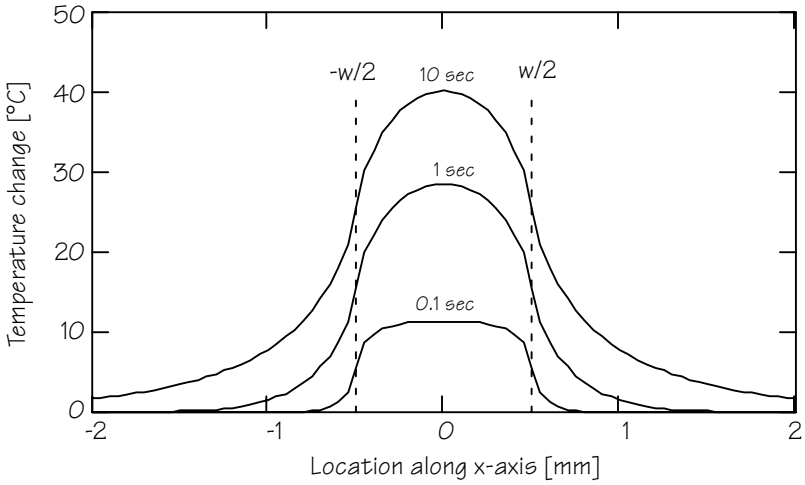

Figure 6.4: Temperature distribution along the x-axis (z = 0) using a 0.1 Watt heater

6.2.4 Conclusions

A constant power dissipated in a planar heater results into an inhomogeneous temperature distribution in the solution. Although this will certainly result into convection, this effect is assumed to be small.
Another effect which is neglected, is absorption of heat by the substrate material. It is not easy to expand the derived temperature distribution to a situation where the substrate material can absorb heat as well. Therefore, later in this chapter, the analytically found solution of the temperature distribution is not used for experimentally verifying the properties of the heater. Instead, the thermal diffusion coefficient and the thermal impedance are used, because the equivalence shown in the previous subsection showed that it is correct to use the well-developed impedance mathematics.

6.3 The substrate material

According to equation (6.11) the diffusion constant of a medium for heat is equal to

$$\kappa = \frac{\lambda}{c_m \cdot \rho}. \qquad (6.27)$$

Some numerical values of different substrates for the heat capacity c_m, the density ρ, the thermal conductivity λ and the thermal diffusion coefficient κ can be found in table 6.2.

Table 6.2: Some thermal diffusion properties [6]

Material	c_m Heat capacity [10^3 J·kg^{-1}·K^{-1}]	ρ Density [10^3 kg·m^{-3}]	λ Thermal conductivity [Watt·K^{-1}·m^{-1}]	κ Thermal diffusion coefficient [m^2·sec^{-1}]	δ Diffusion depth (in 1 ms) [µm]
Water	4.18	0.998	0.6071	$1.455 \cdot 10^{-7}$	17.1
Silicon	0.702	2.328	148	$9.055 \cdot 10^{-5}$	425.6
SiO_2 *)	0.745	2.660	12	$6.055 \cdot 10^{-6}$	110.0
Hoya® SD-1	0.733	2.59	1.214	$6.396 \cdot 10^{-7}$	35.8
Hoya® SD-2	0.737	2.60	1.089	$5.683 \cdot 10^{-7}$	33.7
Quartz	0.740	2.2	0.22	$1.351 \cdot 10^{-7}$	16.4
PCB	1	1.85	0.4	$2.162 \cdot 10^{-7}$	20.8

*) Thermally grown

In this table, water is included because it is the medium to be heated, while silicon, quartz and the Hoya® glasses are the most common bulk materials. A typical set of parameters for printed circuit boards (PCB) is included as well since, in general, devices are mounted on a small piece of PCB. Finally, the parameters for silicon dioxide are given because this must always be used in combination with silicon for creating an electrically insulating layer.

For the evaluation of the diffusion of ions in a solution, sometimes the diffusion depth is used [7] representing how far the ions have moved, on the average, in a certain time from their origin. This diffusion depth can also be used for the diffusion of heat. It is given by

$$\delta = \sqrt{2\kappa t} \qquad (6.28)$$

and is an important measure for how fast a medium will absorb the heat. Therefore, this value is included in table 6.2 as well for the arbitrary time of one millisecond.
Equation (6.28) can also be used to get an expression of the time needed for complete heating of the substrate. For example, a 380 µm thick

silicon wafer is completely passed through by the heat produced at the surface in 0.8 ms. For a quartz and a Hoya® SD-2 wafer, which are 500 µm thick in general, this heating time is 0.53 and 0.22 seconds respectively.

From the diffusion depths it can be concluded that only a quartz substrate has the same very low heat penetration as water. Silicon, on the other hand, takes up the heat very well. One can imagine that a low heat absorption is desired in order to heat the water instead of the substrate material. The first alternative for expensive quartz wafers are the Hoya® glasses which are much cheaper. Surprisingly, a printed circuit board as a substrate material seems interesting with respect to its thermal behaviour. However, the fabrication of a metal structure on a PCB is a process different from the intended silicon technology, and this option is therefore not evaluated here. Therefore, Hoya® glass will be the best option.

6.3.1 Frequency domain analysis

In order to verify the prediction as given in the previous section, two systems are compared as shown in figure 6.5. The first one has a metal heater on a quartz substrate, but also the Hoya® materials are used in a similar set-up. For a silicon wafer, an electrically insulating layer is used for avoiding a shortcut between metal traces on top of the wafer. In both cases, the printed circuit board where the device is mounted upon is omitted, because considering their thermal properties printed circuit boards resemble the properties of water as was shown in table 6.2.

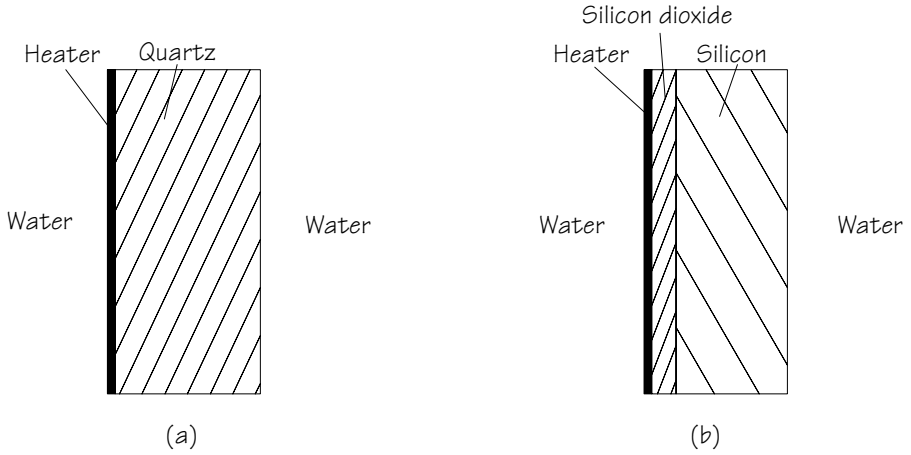

Figure 6.5: Two structures to be modelled: (a) a heater on a quartz wafer, (b) a heater on a silicon wafer electrically insulated by a silicon dioxide layer

In both figure 6.5a and figure 6.5b the thermal behaviour of present water can be modelled as a semi infinite transmission line of heat

resistors and heat capacitances. The input impedance of such a semi infinite transmission line is equal to [5]

$$Z_{Water}(j\omega) = \sqrt{\frac{R_W}{j\omega C_W}} = \sqrt{\frac{(\lambda_W \cdot A)^{-1}}{j\omega c_{m.W}\rho_W A}} \tag{6.29}$$

with R_W the thermal resistance per meter and C_W the heat capacitance per meter. The resistance is equal to the inverse of the thermal heat conductivity for water, λ_W, multiplied by the heater size A, the capacitance is equal to the heat capacity of water $c_{m.W}$ multiplied by the density ρ_W and the heater size A. The heater size A is equal to L × L as was indicated in figure 6.1.
Using the thermal input impedance is a practical tool, since it gives the relation between the inserted heating power P and the resulting temperature. The temperature in the frequency domain can be found from

$$T(j\omega) = Z_{Water}(j\omega) \cdot P(j\omega) \tag{6.30}$$

in equivalence with an electrical impedance which gives the relation between potential and current.

The thermal impedances of substrate materials can also be calculated. A thermal resistor equivalent to a finite heat conducting element is given by

$$R_{Substrate} = \frac{d}{\lambda A} \tag{6.31}$$

with d the thickness of the material, A the cross sectional size and λ the thermal conductivity. A thermal capacitor describing the heat storage in a finite bulk of material is given by

$$C_{Substrate} = c_m \rho A d \tag{6.32}$$

with c_m the heat capacity and ρ the density of the material. The next step is how to implement the network of thermal resistors and capacitors. With a quartz substrate, as shown in figure 6.5a, this substrate acts both as a thermal resistor and a heat capacitor for heat storage. On the other hand, when having silicon dioxide on silicon, as in figure 6.5b, the materials accounting for heat storage and conduction are separated. In the relatively thick silicon bulk, conduction of heat is relatively fast considering the thermal conductivity of silicon as given in table 6.2. Since the mass of the silicon bulk is much larger than the mass of the silicon dioxide layer, this bulk will have a capacitive behaviour. In the thin silicon dioxide layer, storage of heat is relatively low while it has a

much lower heat conductivity than silicon. So a thermal resistor is the most appropriate model component for the silicon dioxide layer.

The equivalent model, described in electrical components, for a planar heater on a finite substrate in water is given in figure 6.6. The impedance for the semi infinite transmission lines representing water was given by equation (6.29), the current source represents the injection of heat, equal to dQ/dt with Q the quantity of heat. In case of a quartz substrate, $R_{Substrate}$ and $C_{Substrate}$ are the thermal resistor and capacitor representing quartz. In case of a silicon dioxide layer on a silicon substrate, the thermal resistor is determined by the silicon dioxide layer, while the heat capacitor is determined by the silicon bulk.

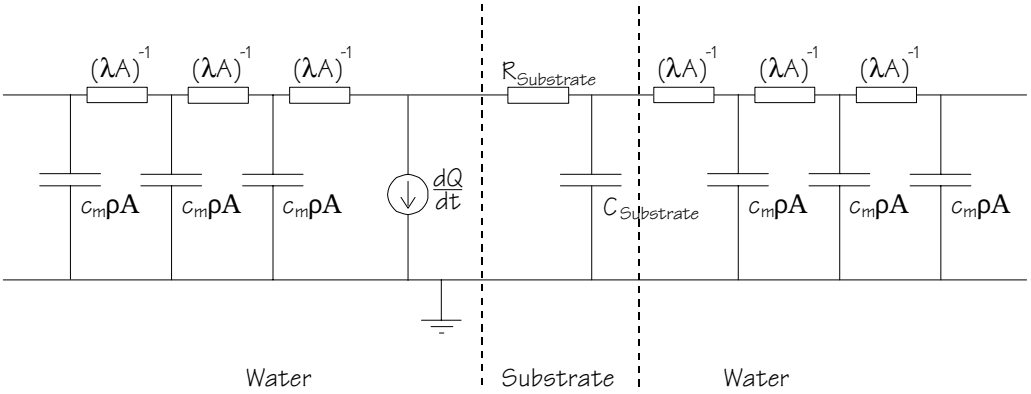

Figure 6.6: Equivalent model for a planar heater on a finite substrate heating an infinite volume of water

In figure 6.7 the thermal impedances as seen by the heater are plotted for both the system of figure 6.5a and figure 6.5b. As an alternative for the quartz substrate, a Hoya® SD-2 substrate is included as well. The impedance of a semi infinite transmission line is drawn as a dotted line labelled as Z_{Water}. This is the impedance as seen by the source when $R_{Substrate} = \infty$. When $R_{Substrate} = C_{Substrate} = 0$, the source is loaded by two Z_{water} transmission lines in parallel. This is represented by the dotted line labelled as $\frac{1}{2} Z_{water}$.

The used numerical values are:

- A square planar heater of A = 1×1 mm², resulting in a water heat resistance per metre of $1.65 \cdot 10^6$ K·watt^{-1}·m^{-1} and a water heat capacitance per metre of 4.17 watt·sec·K^{-1}·m^{-1} for a one dimensional transmission line;
- A thermal resistance for the bulk material as given by equation (6.31) using the surface area A of the heater. The thickness d of the silicon dioxide layer is chosen equal to 1 µm, for the quartz and the Hoya® SD-2 substrate this thickness is the thickness of the wafer which is equal to 500 µm. Using silicon dioxide this results into a thermal

resistance of $83.3 \cdot 10^{-3}$ K·watt^{-1}, for a quartz substrate $2.27 \cdot 10^{3}$ K·watt^{-1} and for SD-2 this is $0.459 \cdot 10^{3}$ K·watt^{-1};

- The thermal capacitance of the bulk material is found by using equation (6.32) and substituting the volume of the bulk material being A×d. Normally, wafers are cut to pieces of 3×4 mm^2, although the metal structures are much smaller. Using a thickness of 380 µm for the silicon wafer and 500 µm for quartz and Hoya®, the heat capacitances become $7.45 \cdot 10^{-3}$, $9.77 \cdot 10^{-3}$ and $11.50 \cdot 10^{-3}$ watt·sec·K^{-1} respectively;

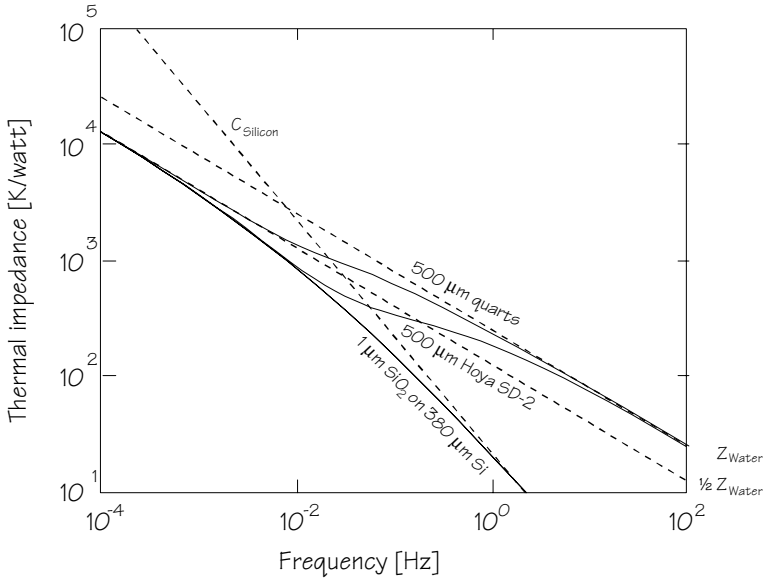

Figure 6.7: Theoretical thermal impedance plots for both a quartz and a silicon substrate

As can be seen from figure 6.7, for low frequencies (smaller than 0.01 Hz, equivalent to more than 100 seconds after switching on the heater) the impedances to be expected are equal. Only then, they are completely determined by the two semi infinite water transmission lines. In this region the heat will be absorbed by the water, the thermal properties of the substrate do not contribute to the local heating at the surface.

For higher frequencies (so during the seconds directly after switching on the heater), there is a fundamental difference between a silicon bulk and a quartz bulk. Using a silicon bulk at higher frequencies, the thermal impedance to be expected is dominated by the heat capacitance of this bulk material. A silicon substrate appears to become a heat sink for fast temperature changes. The impedance of the heat capacitor consisting of the silicon bulk material is represented in the figure by the dotted line marked by $C_{Silicon}$.

Using a quartz substrate at higher frequencies, however, the influence of the bulk material is much lower. The expected impedance is determined then by just one transmission line, representing the thermal impedance of the water in contact with the heater.

A Hoya® SD-2 wafer can be seen as a (cheaper) alternative of the quartz material. At about 0.01 Hz there is a certain tendency to the undesired heat sink behaviour, but this is not observed for higher frequencies as with the silicon bulk material.
So, especially in the first seconds after switching on the heater, a silicon bulk (covered by an insulating silicon dioxide layer) will absorb the produced heat because of its low thermal impedance. A more efficient heating of the water in contact with the heater is obtained when a quartz substrate is used, where a Hoya® SD-2 wafer is a cheaper alternative. According to equation (6.23), a higher observed thermal impedance for quartz and Hoya® SD-2 results into a higher temperature increase after switching on the heater.

6.3.2 Temperature distribution in water

The evaluation in the previous subsection is used to determine which medium will absorb the produced heat. Based on the absorption characteristics, the best substrate material could be chosen. However, besides having a model for optimising the design, a model for the temperature distribution in the electrolyte during practical use is also useful. The time domain analysis of section 6.2 does not account for heat absorption in the substrate material. On the other hand, the frequency domain analysis of the previous subsection does only give the temperature at the heater surface by equation (6.30). In case of the experiments described in the next subsection this is not a problem, since the temperature is measured at this surface. However, when the temperature at another point in the solution is desired in a system where the substrate material is absorbing heat, the two theories must be combined.

An estimation of the temperature distribution in the electrolyte can be deduced by observing the instantaneous impedance in time. Using a quartz substrate, immediately after switching on the heater (up to 1 second, equivalent to frequencies above 1 Hz) the instantaneous impedance is equal to the thermal impedance of Z_{Water} as can be seen in figure 6.7. This is the situation as calculated in section 6.2, so the temperature distribution will be as plotted in figure 6.3. After approximately 100 seconds (equivalent to frequencies below 0.01 Hz), the instantaneous impedance has become more like the thermal impedance of two semi infinite volumes of water ½ Z_{Water}. Therefore, the resulting temperature distribution will be half as high as the distribution observed with Z_{Water}.
Using the model of an instantaneous thermal impedance, the temperature profile can be calculated. First, the impedance which loads

the source in figure 6.6 is divided by the impedance of a semi infinite volume of water. This ratio gives the efficiency of the dissipated heat for heating the solution. In fact, the solution is heated by a constant power multiplied by this ratio. The instantaneous power, produced by the loaded heater, which heats the solution at a certain time can now be calculated by transforming to the time domain. Using this loaded heater, the convolution of equation (6.15) can be used to give the temperature at every point in the solution.
In figure 6.8 the calculated temperature profiles on the axis perpendicular to the heater, 10 seconds after switching on this heater, are plotted for several substrates using the dimensions given in the previous subsection. The upper curve represents a perfectly insulating substrate which is equal to the one drawn in figure 6.3 for the situation after 10 seconds.

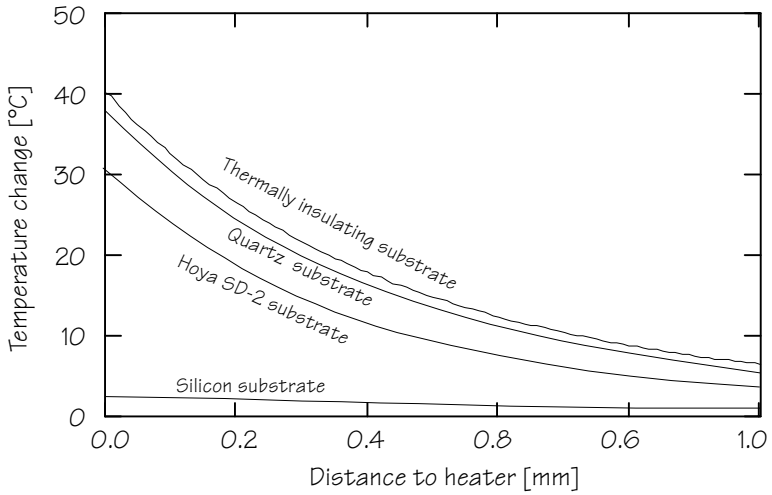

Figure 6.8: Temperature profile perpendicular to the 0.1 W heater after 10 seconds

The expected succession in the substrate materials can be seen. First, quartz does not differ very much from a perfectly insulating substrate, with Hoya® SD-2 the next in quality. A silicon substrate covered by a silicon oxide layer, however, results into a bad transport of heat to the water.

6.3.3 Experimental

Two devices of type B, as described in chapter 4, will be compared with respect to their heating capabilities. One device is realised on a 500 µm thick Hoya® SD-2 substrate, while the other one has the same shape, but is realised on an oxidised silicon substrate. The thickness of the silicon material is 380 µm which is oxidised by a wet thermal oxidation step resulting in a 1 µm thick SiO_2 insulation layer. The substrates are cut into pieces of 3×4 mm^2.

One meander of each device is first calibrated for measuring temperature by placing the devices in a beaker with tap water which is heated to 40° under stirred conditions. The recorded resistance of the meander, together with the corresponding water temperature, serves as the calibration curve.
Next, the resistance is measured, while a power of 200 mW (a sine wave of 1 kHz) is applied to the other meander. This is done in water at room temperature under non-stirred conditions. In figure 6.9 the transient responses for both configurations are shown. To show the differences between devices coming from the same batch, the experiments are repeated using other devices with a Hoya® and a silicon bulk. These experiments are plotted in the same graph.

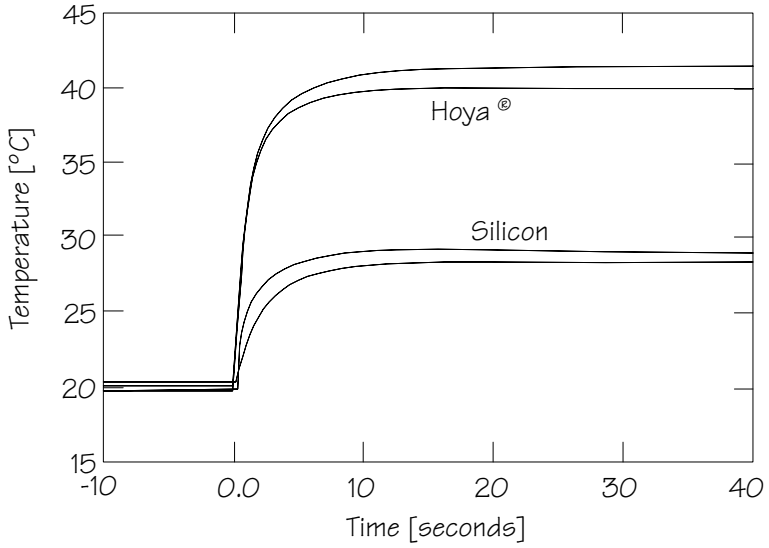

Figure 6.9: Measured transient responses of sensor type B on both a Hoya® and a silicon substrate

6.3.4 Discussion and conclusion of the transient experiment

The first conclusion which can be made from figure 6.9 is that the observed difference in the transient responses for different substrates is much larger than the spreading in the experiments using the same substrate. So the temperature measured at the device surface is indeed dependent on the chosen substrate material.
When using a Hoya® SD-2 substrate, the heating is more efficient, since an equal amount of supplied power results into a higher temperature. This was already expected by the interpretation of the impedances of figure 6.7 and the knowledge that the resulting temperature is equal to the inserted heat multiplied by the thermal impedance as shown by equation (6.30). Because the thermal impedance (at frequencies above 0.01 Hz) for a silicon substrate is relatively low, the heater can not

increase the temperature as much as with a substrate having a high thermal impedance.
Theoretically, the observed thermal impedance should become independent on the substrate material for very low frequencies (< 0.01 Hz), equivalent to hundreds of seconds after switching on the heater. This effect, however, was not observed. The reason is probably due to convection of water. Since an inhomogeneous temperature distribution results into an inhomogeneous density of water, the water will begin to move. The result is that the derived differential equation which includes diffusion only, is not valid anymore.

6.4 Mass flow measurement

Besides convection due to the inhomogeneous temperature distribution, there can be an additional flow or movement of the medium which comes from another, external, source. The result on the measurement described in the previous section will be that the produced heat is distributed over a larger volume resulting into a lower observed temperature increase. This effect can be used for measuring flow because the measured temperature change at a constant heating power will be a measure for the mass flow of the liquid.
Since the integrated sensor-actuator device as described in chapter 4 is in principle not used in a channel, one can not speak of a flow in one direction. An observed decrease in temperature will only indicate motion (turbulence) of the fluid rather than a certain flow rate.
Without completely describing the theoretical background of this measurement, the experiment will simply be done.

6.4.1 Experimental

A fluid flow along the sensor-actuator devices is generated by placing the devices on the inner wall of a beaker in which water is stirred. Since the distance of the devices from the centre of the beaker is about 2.5 cm, a stirring speed of 100 min^{-1} equals a flow rate at the device surface of 0.26 m / s.
The theory describing the operational mechanism of this experiment is not worked out. Therefore, it is not obvious whether the direction of the flow is of influence. To investigate the influence of the flow direction, the devices are placed in the beaker using two different orientations. With the first device, the water flows from left to the right in figure 6.1. The second device is rotated 90°, resulting into a flow in the direction from the top to the bottom in figure 6.1.
The measurements are carried out using devices of type A in a beaker with a 6 cm diameter. The used medium is tap water. A magnetic stirrer

is used with a 4 cm magnet in the beaker. The heater element of the sensor-actuator device is supplied with a 5 V top to top, 1 kHz signal, equal to about 184 mW for this 68 Ω heater. Under non-stirred conditions, this resulted into a temperature increase of 14 °C. The value of the measuring resistor is read out 15 seconds after every change in the rotational speed since figure 6.9 showed that this time is needed for setting up an equilibrium in an unstirred environment. The results are in figure 6.10.

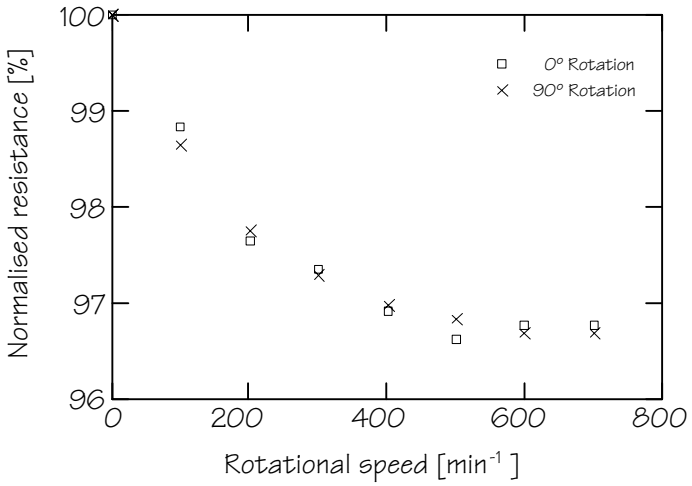

Figure 6.10: Measurement of the speed of rotation (mass flow) with a heating-sensing set-up

6.4.2 Discussion and conclusion of the flow measurement

There is no significant flow direction dependency. Obviously the system does not measure the time of flight of a heat cloud from one to another finger, because then no flow effect would be measured in the direction along the fingers (0° rotation). What is probably being measured is the transportation of a generated heat cloud, larger than all the separate fingers, covering whole the device. Only that mechanism confirms the observed independence on the flow direction.

The relation between rotational speed and sensor output is not linear. At rotational speeds above 500 min^{-1} (equivalent to about 1.3 m/s), the changes in the output signal become very small. Probably the heat cloud has moved away then and the environmental temperature of water is measured. In chapter 4, the sensitivity of the temperature sensors was determined to be 0.23 %/°C. This means that the decrease in figure 6.10 of about 3.2 % corresponds to about 14 °C, which confirms that the environmental water temperature is measured since the non stirred temperature is 14 °C above the environmental temperature. The range of speeds that can be measured can probably be increased up to a certain limit by increasing the heater current. Notice that the found

upper limit of the measurable speed is already in the range of the maximum speeds observed in washing machines. For example a washing tub with a diameter of 60 cm, rotating at a speed of 30 min^{-1}, has a speed at the edges of 0.94 m/s. The water can never move faster than this speed.
So, in the range of turbulent movement speeds in a washing tub, a signal can be measured which is an indication for this movement. This can be interesting because the movement of the washing medium (water) is important for the washing effectiveness. First, the movement itself causes a mechanical washing which removes larger particles. Secondly, the transportation of detergent components to the laundry and the removal of dirt from the laundry is completely dependent on the movement of the water. The mechanical washing was already mentioned as an important washing parameter in chapter 2.

6.5 Summary

This chapter started with a description of the diffusion of heat in a medium. Some theoretical plots were made showing the temperature distribution in a liquid when using a square planar heater, assuming that the substrate does not absorb heat. For modelling the absorption of heat into the substrate, which is necessary for choosing the best material, this transient analysis in the time domain could not be used easily at first instance.
The differential equation describing the thermal behaviour in a medium appeared to be equal to the differential equation describing the diffusion of ions in water and the equation for the potential distribution along an electrical transmission line. This equivalence could later on be used for modelling the thermal behaviour of a multi-layer structure consisting of a planar heater on a substrate in water. While an analysis in the time domain did only give some examples of temperature profiles, in the thermal impedance domain the available substrate materials could be compared with respect to their thermal properties.
The conclusion was that a substrate consisting of quartz (with Hoya® SD-2 as a cheaper alternative) results into a more efficient heating of the contacting water than a substrate consisting of silicon with an oxide layer as an electrical insulation. This was proven experimentally.
Besides giving a clarification concerning whether the produced heat flows into the substrate or into the water, the impedance method could be used for a transient analysis in the time domain. Based on impedance considerations, the loss of heat into the substrate material was determined. The resulting amount of heat is injected into the water and was used to calculate the temperature profile.

Convection of water, which is the result of the inhomogeneous temperature distribution, is not implemented in the model. This type of convection was assumed to be negligible. However, an externally imposed movement of water could be measured. When the fluid to be heated is moving, the heating becomes less efficient since virtually a much larger volume absorbs the heat. This effect can be exploited by measuring one of the resistors while applying a constant amount of energy to the other resistor. The decrease in the observed resistance is a measure for the movement of the medium. This value can be either flow or turbulence, depending on the configuration. In a washing machine it can be an indication for the mechanical washing effectiveness.

6.6 References

[1] S.M. Sze, Semiconductor devices, Physics and technology, John Wiley & Sons, New York, 1985

[2] D.A. Skoog, D.M. West and F.J. Holler, Analytical Chemistry, Saunders College Publishing, Philadelphia, 1992

[3] H.S. Carslaw and J.C. Jaeger, Operational methods in applied mathematics, Dover publications, Inc. New York, 1947

[4] P.W. Atkins, Physical Chemistry, fifth edition, Oxford university press, 1994

[5] D.K. Cheng, Field and wave electromagnetics, second edition, Addison-Wesley Publishing Company, Reading, Massachusetts, 1989

[6] D.R. Lide, Handbook of chemistry and physics, 74th edition 1993 - 1994, CRC Press, Boca-Raton, Florida

[7] A.J. Bard and L.J. Faulkner, Electrochemical methods, fundamentals and applications, John Wiley & Sons, New York, 1980

CHAPTER 7

Stimulus-response measurements

Until now, the reported measurements using the integrated sensor-actuator device as described in chapter 4 used only one single operational mode at the same time. However, in chapter 1, the advantage of the functional integration of sensors and actuators was mentioned. By combining actuator functions with sensor functions, on-line calibration can be done. In addition, the interpretation of the response on an imposed temporary disturbance of a solution under test might give completely new information.
First the effect of an actuator step is evaluated mathematically. After this, the actuator functions as available in the integrated sensor-actuator device are taken as starting points for possible stimulus-response implementations.

7.1 Mathematical generalisation of differential measurement systems

A generalised set-up for differential measurements is given in figure 7.1. The picture shows a tube which has the possibility to shift a sample solution in steps or continuously along sensors and actuators. In the simplest case, two sensors and only one actuator are implemented, resulting in the set-up where a sample is measured before and after the actuator step.

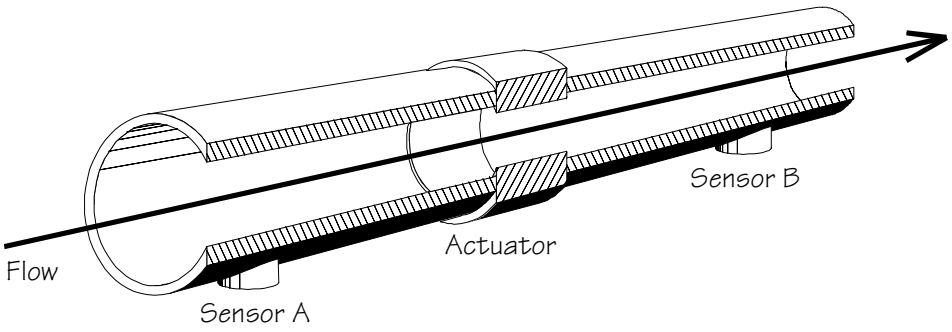

Figure 7.1: Generalised set-up for spatial differential measurements using one actuator

Because of the assumed small diameter of the tube the modification by the actuator will be accomplished over the whole cross-section of this tube. When the input solution does not change (with respect to the measured variable) during a measurement, the sample measured at sensor B differs from that at sensor A only due to the modification induced by the actuator. If the modification is complete at the time the sample is at sensor B, there is no effect of time observed in the difference in sensor outputs. Therefore, one can speak of a spatial differential measurement, sampled at a single moment.

Apart from spatial differential systems, there exist time differential systems. When the flow direction of the liquid can be reversed, only one sensor is needed because then the sample can be measured before and after the actuation step using the same sensor. This requires also a composition of the input sample which is not changing due to other factors than the stimulus. When this single sensor is integrated with the actuator, as is the case with the integrated sensor-actuator device described in chapter 4, even the tube can be omitted since no controlled flow is needed. In such single sensor set-ups, one should speak of a time differential system sampled at the same location instead of a spatial differential system. Notice that this does not change the mathematical operation describing the system since in both cases a difference between the sample before and after a modification stimulus is measured.

For the generalisation of spatial or time differential systems, figure 7.2 will be used. Variable x_1 is the input of interest and is modified by the actuator to x_2 which has the same dimension as x_1. The function describing the stimulus operation of the actuator is referred to as $f_\alpha(x)$, so $x_2 = f_\alpha(x_1)$. This stimulus operation will be dependent on both the actuator and the properties of the solution. If a controllable actuator is used, the controlled parameter is represented by the subscript α.

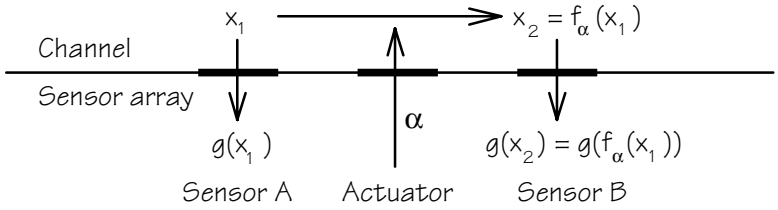

Figure 7.2: Mathematical representation of a differential measurement system

Assume that both the original sample variable x_1 and the modified variable x_2, are being sensed using two similar sensors. This means that the sensor outputs are both given by the same operation g(x) on the sensed variable. These sensors do not influence the sample.
So two operations are involved: the sensor operation function g(x) and the stimulus function $f_\alpha(x)$. These operations will be discussed here separately.

7.1.1 Evaluation of the sensor operation g(x)

The sensor operation g(x) can be any function in principle, nevertheless the number of functions observed with practical sensors is limited. Some special cases of g(x) functions will be evaluated here.
Although it was assumed that both sensors have the same measurement principle, they might have a different sensitivity or offset. This results in

the same g(x) function, but with different parameters. The difference in the sensor operation function for sensor A and B is indicated by a superscript A or B.
For a spatial differential system, the sensors A and B are different devices and might therefore have dissimilar parameters, for example due to a not perfectly reproducible fabrication process or an unequal temperature while measuring. With a time differential system, sensor A is the same device as B, but read out at another moment. So variations in fabrication processes are cancelled out, only drift in the sensor parameters will change the function g(x).

(a) g(x) is known
When the sensor operation g(x) is completely known, the inverse function g^{-1} can be determined and variable x can exactly be calculated from the sensor output. In this case, the use of an actuator and a second sensor is not needed for measuring x_1. However, with practical sensors, the g(x) function is only known directly after calibration since drift in both the sensitivity and the offset will change this function.

(b) g(x) is a linear function with an offset
The operation of many sensors can be approximated by

$$g(x) = a_g \cdot x + b_g \tag{7.1}$$

for at least a certain range of x. In many sensors the drift and inter device deviation in the sensitivity a_g is much lower than the uncertainty in the offset b_g both due to drift and differences in processing. For example, when x is the pH which is measured using a pH sensor, the sensitivity is equal to about a_g = -59 mV / pH. This sensitivity is much more constant than the offset, which is among other things also determined by the stability of the reference electrode.
The offset b_g of the sensor is determined by two parts. The first one is the part that is common for both sensor A and B. For example, the effect of an interfering parameter, like temperature, results in such a common offset. The second one is a constant term which is different for sensor A and B. Using a differential measurement it can be found that the output is equal to

$$g^B(x_2) - g^A(x_1) = a_g \cdot \left(x_2 - x_1\right) + b_g{}^B - b_g{}^A \tag{7.2}$$

assuming identical sensitivities a_g for both sensors. The observed offsets of the individual sensors, $b_g{}^A$ and $b_g{}^B$, consist of the summation of offsets which are common for both sensors and offsets which differ from sensor to sensor. By a differential measurement, common parts in the offsets b_g are filtered out and only the non-common offsets remain.

In practice, common offsets are the result of undesired external influences, while non-common offsets are constant for the individual devices.
Equation (7.2) shows that actually only the difference between the input x_1 and output x_2 can be measured, but when the actuator function $f_\alpha(x)$ is chosen well (for example $f_\alpha(x) = a_f \cdot x$), an absolute value for x_1 can be found as will be shown later.

(c) g(x) is a logarithmic function
In case of a pH measurement using a potentiometric technique, the output of the sensor (glass electrode or ISFET) is linearly dependent on the pH. This is a linear sensing principle which has its origin in the Nernst equation [1] which expresses the linear relation between an interface potential and the pH. Actually, with all potentiometric ion selective electrodes (ISEs), the output is dependent on the logarithm of a concentration. When a concentration is the variable of interest, and not the logarithm of a concentration, the sensor output must be written as

$$g(x) = a_g \cdot \log(x) + b_g \tag{7.3}$$

and the differential output becomes

$$g^B(x_2) - g^A(x_1) = a_g \cdot \log\left(\frac{x_2}{x_1}\right) + b_g{}^B - b_g{}^A \tag{7.4}$$

assuming the same sensitivity a_g for both sensor A and B. So when using logarithmic sensors, the differential output shows the same advantage with respect to the sensor offsets. However, with respect to the variable to be measured, x_1, the difference between two logarithmic sensor outputs gives only information on the ratio between the input and output variable x_2 / x_1. So, to measure the absolute value of the input variable x_1, it is not likely that a differential system based on logarithmic sensors will give the desired result[1]. Stimulus functions which can make the output useful must raise the input variable to a certain power. For example $f_\alpha(x) = x^2$ will reduce (7.4) to

$$g^B(x_2) - g^A(x_1) = a_g \cdot \log\left(x_1\right) + b_g{}^B - b_g{}^A . \tag{7.5}$$

However, such stimulus functions are not easy to realise using practical actuators.

---

[1] One can easily confuse this set-up with the successful acid to base titration set-up where the end point is determined by ISFETs and the titrant is generated coulometrically [2]. Although this method measures a concentration using logarithmic sensors, it is not of the generalised configuration as described here.This method uses the pH difference only as an indicator for detecting the end point of the titration. The concentration of interest is calculated from the charge supplied to the actuator when the end point is reached.

7.1.2 Evaluation of the stimulus function $f_\alpha(x)$

A linear stimulus operation will be assumed here because this describes most of the practical observed actuator operations. Consider the stimulus function

$$f_\alpha(x) = a_f(\alpha) \cdot x + b_f(\alpha) \qquad (7.6)$$

where the parameters $a_f(\alpha)$ and $b_f(\alpha)$ are constant at a certain chosen actuator intensity α. The constant $a_f(\alpha)$ represents an intended amplification or attenuation of the species x placed in front of the actuator, and will therefore be without a dimension. The constant $b_f(\alpha)$ is the result of an intended addition, or subtraction of the species x, which is not proportional to the amount placed in front of the actuator. This second constant will have the same dimension as x. The most common actuator operations can be identified and categorised by these constants.
Because the actuator intensity α is assumed to be constant in the following examples, the parameters $a_f(\alpha)$ and $b_f(\alpha)$ will be written from now on as a_f and b_f.

(a) Complete depletion of x: $b_f = 0$, $a_f = 0$
When both a_f and b_f are zero then (7.6) simplifies to $f_\alpha(x) = 0$, or in other words: the species x_1 is completely depleted by the actuator to $x_2 = 0$. An example is the effect of an ion exchanger which captures all ions of interest, when sensors are used which measure these ions selectively. Another example is an electrochemical actuator which evokes the degeneration of hydrogen peroxide into hydrogen gas and oxygen gas, and using sensors which are selective for hydrogen peroxide.
In the case of linear sensors with an equal sensitivity a_g equation (7.2) now gives the absolute value of input variable x_1 because x_2 equals zero. In this case sensor B is solely used as an indifferent reference sensor to filter out offsets which are common to both sensors. Notice that even if the sensors do not have the same sensitivity, the same result is obtained.

(b) Partial depletion or accumulation of x: $b_f = 0$, $a_f \neq 0$
In the case of a fractional depletion or accumulation of species x, the situation resembles the previous one. This situation represents an incomplete ion exchange where always a fraction a_f is not being exchanged. Equation (7.2) becomes equal to

$$g^B(x_2) - g^A(x_1) = a_g\left(a_f - 1\right) \cdot x_1 + b_g{}^B - b_g{}^A \qquad (7.7)$$

with a_f the fraction of depletion (<1) or accumulation (>1) and a_g the sensitivity of the sensors, assumed to be equal. Even when the sensors

do not have an equal sensitivity, the differential output is still linearly proportional to the input variable x_1 according to

$$g^B(x_2) - g^A(x_1) = \left(a_g{}^B \cdot a_f - a_g{}^A\right) \cdot x_1 + b_g{}^B - b_g{}^A. \qquad (7.8)$$

When the fraction a_f is always the same, and there is no drift in the differences between the sensitivities, there is no theoretical difference with the previous situation where $a_f = 0$. Again, the advantage is in the elimination of offsets which are common for both sensors.

(c) Known addition: $b_f \neq 0$, $a_f = 1$

A special situation occurs when the variable x_1 is increased by a constant value. This can be done by injecting a known amount of H^+ ions in a sample which is not buffered, while the H^+ concentration is the measured variable. The differential output (7.2) becomes

$$g^B(x_2) - g^A(x_1) = a_g \cdot b_f + b_g{}^B - b_g{}^A \qquad (7.9)$$

which is not dependent on the input variable x_1. This method which can be referred to as “known addition” can be used to determine the sensitivity a_g of the sensors involved. The condition that the sensitivities of sensor A and B are equal is now necessary, else the difference will still be dependent on the input concentration x_1.

(d) No actuator operation: $b_f = 0$, $a_f = 1$

When the actuator does nothing, the input variable x_1 is exposed to both sensor A and B. Examples are an inactive electrochemical actuator, an inactive heater and a saturated ion exchanger. For non-equal sensor offsets b_g, but with equal sensitivities a_g, equation (7.2) can be written as

$$g^B(x_2) - g^A(x_1) = \left(a_g \cdot x_2 + b_g{}^B\right) - \left(a_g \cdot x_1 + b_g{}^A\right) = b_g{}^B - b_g{}^A. \qquad (7.10)$$

This means that the differential offset due to unequal sensors can be found (and eliminated afterwards) by inactivating the actuator.

7.1.3 Summary

A generalised stimulus-response set-up is that of a flow system with two sensors and a single actuator. The sample solution is pumped along sensor A, the actuator and then sensor B. The assumption is made that the variable of interest in the supplied electrolyte is homogeneously present at both sensor A and B in the absence of a stimulus. Only then, the difference between the outputs of sensor A and B, after the stimulus is applied, can be completely ascribed to the influence of the actuator.

An alternative to this spatial differential system is a time differential system, where using a single sensor, an electrolyte is measured before and after an actuator step. Here, stability of the composition of the sample is necessary. While a difference in space can be measured at the same moment, a difference in time can be measured at the same spot in the solution.
Using a differential measurement system in combination with an actuator, data can be obtained concerning the sample as well as on the sensors itself. To get information on the sensors, the actuator must be controllable in order to select operational modes for collecting calibration data. Important is that both sensors have a similar, but not necessarily identical, operation.

7.2 Some examples based on available actuators

After the theoretical evaluation in the previous section, now three actuators are being categorised in these theoretical terms. The first two are the available actuator operations in the integrated sensor-actuator device as described in chapter 4. These are the electrochemical actuator (for O_2, H_2, H^+ or OH^-) and the thermoresistive heater. In addition, an ion exchanger is taken as a third actuator. Although ion exchanger materials are not controllable actuators, an interesting intended modification of an electrolyte is made by such materials. The operation of ion exchangers can be monitored using the implemented electrolyte conductivity operation of the integrated device.
For the sensors, the three available sensor operations in the integrated sensor-actuator device are taken. The detection of pH is evaluated as well in each subsection, although this can not simply be realised using metal films. Nevertheless, this is done because the measurement of pH shows a logarithmic sensor function which is interesting to compare with the linear operation of a conductivity sensor.
The following list of possible stimulus-response measurements does not contain all the possible options, but is more or less a brainstorm of advantages which can be expected when integrating sensors and an actuator.

7.2.1 Electrochemical actuator

Consider an inert metal working electrode at which the oxidation of water to protons and oxygen gas is controlled by an applied anodic current:

$$2H_2O \rightarrow O_2 + 4H^+ + 4e^- \qquad (7.11)$$

or water is reduced to hydroxyl ions and hydrogen gas by a cathodic current:

$$2H_2O + 2e^- \rightarrow H_2 + 2OH^-. \qquad (7.12)$$

The reaction products H^+ and OH^- can be used for pH control. In the case of equation (7.11), the amount of generated protons follows from integrating the anodic current in time. However, in general, this actuator is not of the "known addition" type (c) of subsection 7.1.2 because the protons released will cause chemical equilibria in the solution to change. So, the measured proton concentration increase at sensor B in figure 7.1 is not only dependent on the released amount in general, for example because of the influence of pH buffers and weak acids.

Weak acid concentration determination

The response on an imposed injection of protons of size ΔH^+ in a solution of a weak acid is being considered. As an example, the acetic acid equilibrium is used for the complete description of the system. This equilibrium is given by

$$HAc \leftrightarrow H^+ + Ac^- \qquad k_a = 1.7 \cdot 10^{-5} \qquad (7.13)$$

so, before and after the addition of a ΔH^+ the acid-base equilibrium satisfies

$$\frac{[H^+][Ac^-]}{[HAc]} = k_a. \qquad (7.14)$$

Two equations can be written which describe the balance of the total amount of Ac^- and H^+ respectively:

$$[Ac^-]_{before} + [HAc]_{before} = [Ac^-]_{after} + [HAc]_{after} = C_{Ac} \qquad (7.15)$$

$$[H^+]_{before} + [HAc]_{before} = [H^+]_{after} + [HAc]_{after} - \Delta H^+ = C_H. \qquad (7.16)$$

From equations (7.14), (7.15) and (7.16) the proton concentration before and after the release of H^+ can be found:

$$[H^+]_{before} = -\frac{k_a}{2} + \frac{1}{2}\sqrt{k_a{}^2 + 4k_a C_{Ac}} \qquad (7.17)$$

$$[H^+]_{after} = -\frac{k_a + \Delta H^+}{2} + \frac{1}{2}\sqrt{\left(k_a + \Delta H^+\right)^2 + 4k_a C_{Ac}}. \qquad (7.18)$$

Both a conductivity sensor or a potentiometric pH sensor can be used for determining a shift in the equilibrium. Two pH sensors will measure

$$\Delta pH = -\log[H^+]_{after} + \log[H^+]_{before} \qquad (7.19)$$

which can be expressed in terms of the constants C_{Ac}, k_a and ΔH^+ using (7.17) and (7.18). However, this results in a complicated expression. In this chapter no numerical evaluation will be given on whether this leads to interesting information on C_{Ac} or k_a. Instead, a graphical method is used.

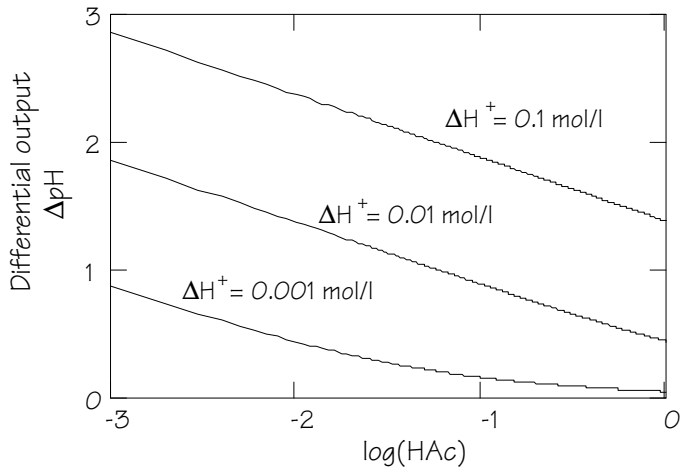

Figure 7.3: Dependency of the differential pH on a "proton step" as a function of the weak acid concentration using the acid constant of acetic acid

Figure 7.3 shows a plot of equation (7.19) for an acetic acid concentration range of three decades and using three different H^+ steps. It appears that the dependency on the logarithm of the weak acid concentration is linear unless the ΔH^+ is much smaller than the weak acid concentration. The lowest curve shows a deviation from a linear behaviour because of a too low ΔH^+. The dependency on the chosen H^+ addition shows that the output signal is only useful in a certain range.

In the parts of the curves in figure 7.3 where the curves are linear, the added amount of H^+ ions is apparently an excess, resulting into a pH which is only dependent on this added excess. Therefore, the pH difference is determined by the pH of the original acetic acid concentration and the pH caused by the excess of H^+ ions. So, the principle of operation is that the pH after the addition of a sufficient amount of H^+ ions (which results into an acetic acid independent “reference” pH) is compared to the pH of the original acetic acid. This method comes the closest to the type complete depletion (a) with b_f not equal to zero.

In fact this method is a part of a coulometric titration which is only sampled at two points, and where the measured information is in the pH change (and not in the supplied amount of titrant). This successful application of a differential measurement system based on logarithmic sensors seems an exception to the conclusion which was drawn from

equation (7.4). However, since the logarithm of the acetic acid concentration is measured, the used sensors are actually linear sensors.

Using a differential conductivity determination the output will be:

$$\Delta\kappa = \kappa_{after} - \kappa_{before} \tag{7.20}$$

with

$$\kappa = [H^+]\lambda_{H^+} + [Ac^-]\lambda_{Ac^-} \tag{7.21}$$

where λ_i is the limiting molar conductivity for ion i. The difference in the conductivity $\Delta\kappa$ before and after the injection of the ΔH^+ can be calculated by evaluating equation (7.21) in both situations. To express the observed $\Delta\kappa$ in terms of the acetic acid concentration C_{Ac}, the acid constant k_a and the injected amount of protons ΔH^+, equations (7.14), (7.17) and (7.18) must be substituted into (7.21) for the situation before and after the H^+ injection. Just like the pH measurement this conductivity measurement gives a complicated expression.

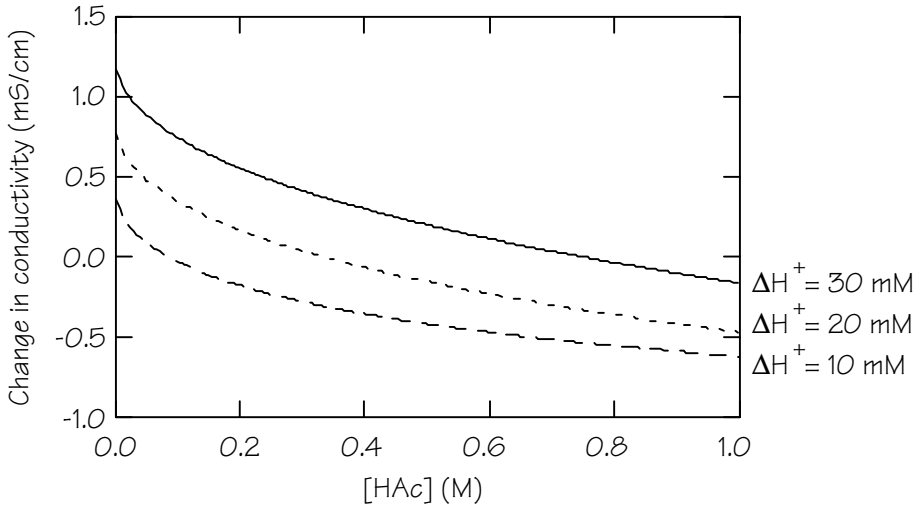

Figure 7.4: Theoretical dependency of the differential conductivity on a "proton step" as a function of the acetic acid concentration

Figure 7.4 shows the simulated relation between the conductivity change and the weak acid concentration. At a zero acetic acid concentration, the injected protons are not captured by acetate ions Ac^-, and the measured change in conductivity is caused by the conductivity of the ΔH^+ only. Since the curves are not linear, the acetic acid concentration corresponding to a measured $\Delta\kappa$ is harder to determine for a higher acetic acid concentration. Therefore, it is more practical to find the necessary amount of ΔH^+ resulting into a $\Delta\kappa$ equal to zero. Empirically, using theoretically obtained data, it was determined that then the corresponding acetic acid concentration can be approximated

by $C_{HAc} = 0.84 \cdot 10^3$ litre / mole $\cdot (\Delta H^+)^2$ over quite a large range of acetic acid concentrations.

Differential temperature measurement

Now the measurement of pH and conductivity is used as an example of differentially monitoring the effect of an electrochemical actuator, also the other two sensors are described in combination with this actuator. The measurement of temperature is only of interest when an endo- or exothermic reaction is evoked by injecting oxygen gas, hydrogen gas, protons or hydroxyl ions. At first sight, such reactions are not likely in a washing system.

Differential amperometric H_2O_2 detection

In the presence of hydrogen peroxide, the oxidation of water at the actuator will not occur before all hydrogen peroxide is oxidised:

$$2H_2O_2 \rightarrow O_2 + 2H^+ + 2e^- . \qquad (7.22)$$

This gives the possibility of the electrochemical capturing of all available hydrogen peroxide at the actuator. The difference measured by two H_2O_2 sensors is equal to the absolute amount of H_2O_2. Under this condition the actuator function is of the type (a) "complete depletion" which has the advantage that common offsets in the sensors are filtered out.

7.2.2 Thermoresistive heating

The thermoresistive heater is a metal strip with a certain resistance. The heat being produced when a current flows through it will be used to put thermal energy in the system.

Equilibria, observed in acid-base systems like equation (7.13) and precipitation systems, are dependent on temperature because the equilibrium constants k_a and k_s are temperature dependent in general. However, a concentration determination based on an imposed disturbance of such an equilibrium will be difficult. An interference is the dependency of the ion mobility on temperature which will complicate the interpretation of a conductivity measurement. Although this is not observed with a differential pH measurement, the logarithmic nature of pH sensing completely suppresses the very small changes in the H^+ concentration.

Differential conductivity measurement

The limiting molar ionic conductivity λ_i is indirectly temperature dependent, according to [3]

$$\lambda_i = \frac{z_i^2 Fe}{6\pi a} \frac{1}{\eta(T)} \qquad (7.23)$$

with

z_i : the charge number of ion i,
F : Faraday's constant,
e : the charge of an electron,
a : the radius of the ion and
$\eta(T)$: the viscosity of the medium,

where the last one depends exponentially on temperature. This results into an increase of λ_i with temperature of 2 to 3% per degree for typical ions around room temperature. The corresponding stimulus function describing the effect of heating on a conductivity measurement, is of the type (b) “accumulation of x” with $a_f(\alpha) > 1$, and $b_f(\alpha) = 0$ in equation (7.6). The parameter α represents the imposed temperature change.

In general, a fitted polynomial temperature dependency for the limiting molar ionic conductivity is more practical than the use of equation (7.23). In the next chapter, it will be shown that using such polynomials, the separate ion concentrations can be calculated of an assumed set of present ions. Therefore, this stimulus-response measurement will not be evaluated here.

Differential pH measurements

In terms of section 7.1, the effect of heating will change the sensitivity a_g of the sensors, since in general a pH measurement has a sensitivity proportional to temperature. The process of interest, the influence of the stimulus function $f_\alpha(x)$, can not be studied separately because pH sensors are temperature dependent.

Differential amperometric H_2O_2 detection

Hydrogen peroxide is in equilibrium with the HO_2^- ion under the dissociation of a proton:

$$H_2O_2 \leftrightarrow H^+ + HO_2^- . \qquad (7.24)$$

When measuring, using two amperometric sensors, this equilibrium is not relevant because whether H_2O_2 or HO_2^- is measured, in both cases the number of electrons released per measured molecule is equal according to equations (5.4a) through (5.7a). What is observed as a response on a heating stimulus when doing chrono amperometry, is probably the effect of a small change in the diffusion coefficient.

Differential temperature measurement
By measuring temperature differentially while heating, the system is of the type “known addition” (c) which does not give any information on the input, but only on the system. An example is the use of the time delay between stimulation and sensing for determining the speed of flow. This is described in section 7.2.4, where a flow measurement is described based on the transport time of a heat marker from the actuator to a temperature sensor.

7.2.3 Ion exchangers or enzymes

The actuator function f(x) for an ion exchanger is of the type "partial depletion or accumulation" (b) because a constant percentage of species x_1 is being captured [4]. It makes a difference whether sensors are used which can measure selectively the captured/released species or the used sensors are not selective (like electrolyte conductivity sensors).
For example, the commercially available ion exchanger Dowex® CCR-2 is originally saturated with H^+ ions, but will release two of them when one Ca^{2+} ion is captured. The operations on the proton and calcium concentrations are

$$[Ca^{2+}]_{out} = a_f[Ca^{2+}]_{in} \tag{7.25}$$

$$[H^+]_{out} = 2\cdot\left(1-a_f\right)\cdot[Ca^{2+}]_{in} + [H^+]_{in} \tag{7.26}$$

where $0 < a_f < 1$. A complete exchange is characterised by $a_f = 0$ and no operation by $a_f = 1$. The last one can be the result of a saturated ion exchanger.

From the field of applications and the available sensors this couple of ions ($2H^+ \leftrightarrow Ca^{2+}$) is very interesting. The ion to be captured should be calcium while this might give information on the water hardness in washing processes. For miniaturised sensors and actuators the exchange of these calcium ions to protons is desired because protons are relatively easy measurable ions and it leaves the possibility of reversing the exchange action by electrochemically generating H^+.

The operation of an enzymatic actuator can be compared to the operation of an ion exchanger because a certain percentage of species is being catalysed while a product is released. This results into a partial depletion operation. All examples in this paragraph use the ion exchange principle.

Differential pH measurement
Measurement of the pH before and after an ion exchange results in

$$\begin{aligned}\Delta\mathrm{pH} &= -\log[\mathrm{H}^+]_{\mathrm{out}} + \log[\mathrm{H}^+]_{\mathrm{in}} \\ &= \log\left(\frac{[\mathrm{H}^+]_{\mathrm{in}}}{2\cdot(1-a_f)\cdot[\mathrm{Ca}^{2+}]_{\mathrm{in}} + [\mathrm{H}^+]_{\mathrm{in}}}\right)\end{aligned} \tag{7.27}$$

So, for a significant measured pH change, the proton concentration must not be very large in relation to the calcium concentration. Secondly, for determining the calcium concentration, the absolute proton concentration must be known.

Differential conductivity measurement
The difference in conductivity induced by the ion exchanger is equal to

$$\begin{aligned}\Delta\kappa &= \Delta[\mathrm{H}^+]\cdot\lambda_{\mathrm{H}^+} + 2\cdot\Delta[\mathrm{Ca}^{2+}]\cdot\lambda_{\mathrm{Ca}^{2+}} \\ &= 2\cdot(1-a_f)\cdot[\mathrm{Ca}^{2+}]_{\mathrm{in}}\lambda_{\mathrm{H}^+} + 2\cdot(a_f-1)[\mathrm{Ca}^{2+}]_{\mathrm{in}}\lambda_{\mathrm{Ca}^{2+}} \\ &= 2(1-a_f)(\lambda_{\mathrm{H}^+} - \lambda_{\mathrm{Ca}^{2+}})[\mathrm{Ca}^{2+}]_{\mathrm{in}}\end{aligned} \tag{7.28}$$

which means that the output is linearly dependent on the calcium concentration.

Differential temperature measurement
The ion exchange process most probably does not influence the temperature of the sample. Therefore it can not be expected that differentially measured temperature changes will occur.

Differential amperometric H_2O_2 detection
For an ideal ion exchange the presence of H_2O_2 will have no effect. However, the pH change due to the exchange of calcium with protons might disturb the amperometric H_2O_2 measurement at sensor B with respect to sensor A.

7.2.4 Additional results

Some additional techniques can be performed, using the same set-up as shown in figure 7.1, or the time differential equivalent, but which do not satisfy the generalised measurement technique. An example is the coulometric sensor-actuator device for performing acid-base titrations [2]. Although this set-up consists of two sensors and one actuator, the determination is done by recording a titration curve instead of using a single differential measurement. In this subsection, two methods are presented where the output is also not determined by simply taking the difference between two sensor outputs.

Coulometric precipitation titration of calcium

Besides the already mentioned acid-base equilibria like described in equation (7.13), also precipitation reactions can be evoked using a H^+ or OH^- stimulus. In that case, the stimulus function $f_\alpha(x)$ is not one of the linear examples of subsection 7.1.2, since in this case $f_\alpha(x)$ describes the non-linear disturbance of a solubility equilibrium. Therefore, the interpretation of a single differential measurement will not be easy. An alternative to get useful information from this stimulus-response measurement, is to control the actuator until the differential measurement indicates an end point. This will be explained with the precipitation of calcium hydroxide as an example.

The bad solubility of calcium ions in an alkaline medium is given by

$$Ca(OH)_2 \leftrightarrow Ca^{2+} + 2OH^- \qquad k_s = 1.3 \cdot 10^{-6}\ mol^3 l^{-3} \qquad (7.29)$$

with k_s the solubility constant of calcium hydroxide. Precipitation of calcium hydroxide can be monitored using a conductivity sensor since an imposed addition of for example sodium hydroxide does not result in the expected conductivity increase when some of the added hydroxyl ions have precipitated with calcium ions.

The measurement of calcium ions is very interesting for qualifying the builder action when monitoring washing processes. As has been explained in chapter 2, the builder effect consists of both exchange and precipitation of calcium ions. While ion precipitation during washing can be monitored by measuring the electrical conductivity of the water, the exchange of ions will not result into a significant electrolyte conductivity change. Therefore, a calcium detection method is desired for monitoring building by means of ion exchange.

The typical shape of a volumetric conductimetric precipitation titration can easily be constructed [5]. Consider a solution containing calcium ions and where all other charged particles are not likely to precipitate. By adding volumes of a sodium hydroxide solution, sodium will introduce a conductivity increase proportional to the added volume and the other ion concentrations will be constant. So, only Ca^{2+} and OH^- will account for a non-linear change in the observed conductivity since they have a certain interaction. Normally, with precipitation titrations, the first addition of titrant is already enough to reach the saturation point and will therefore result into a minimal precipitant.

When adding a small amount of sodium hydroxide, all added hydroxyl ions will precipitate and the remaining effect is the replacement of calcium ions by two sodium ions. The conductivity will slightly decrease since the molar conductivity of sodium ions is higher than that

of calcium ions. After all calcium ions are captured completely, the conductivity will increase because of the added free hydroxyl and sodium ions. So, the end point of the titration, which is a measure for the calcium concentration, can easily be determined from the turn over point where the calcium ions are just exhausted. A theoretical plot of a volumetric precipitation titration with a conductivity measurement as an end point detection is drawn in figure 7.5.

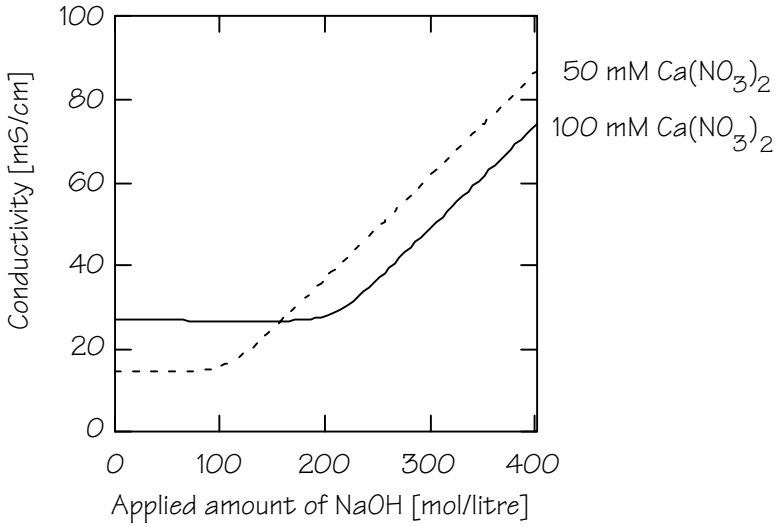

Figure 7.5: Volumetric conductimetric precipitation titration of calcium nitrate with sodium hydroxide

From this figure it can be seen that a fixed addition of sodium hydroxide will not result into an unambiguous change in conductivity, since one does not know whether the end point in the titration curve is passed. A method using a controlled titrant addition (a titration), while monitoring the conductivity as an end point detection, does give more information on the success of the determination. Therefore, it is preferred to measure a precipitation reaction not using the generalised measurement technique of section 7.1.

While a volumetric titration requires a burette for adding the titrant, an alternative is to add the titrant by coulometric generation. Hydroxyl ions for the titration can be generated by the reduction of water according to equation (7.12). A coulometric precipitation titration of calcium with conductivity sensing as the end point detection, seems an ideal method since it can be implemented very simply using solid state components. The precipitation can easily be reversed by subsequently lowering the local pH using an anodic current. The shape of the curve will be different from figure 7.5 since only OH^- is added without a positive counter ion. Charge neutrality is accomplished by migration of positive ions to the working electrode. However, in practice, the precipitation appears to be less controllable than might be expected

from equation (7.29). When the solution is supersaturated, the solubility constant k_s can be exceeded and the theoretical behaviour in the conductivity is not observed. Therefore, in analytical chemistry, a nucleation core is used to prevent supersaturation. How this technique can be applied to a coulometric actuator is not yet clear.

Flow measurement

For the application of the generalised set-up, the assumption was made that there is a flow along the sensors of an input electrolyte which is not changing in composition, and an immediate and complete modification of the electrolyte is generated at the actuator. Only in that case, the measurement is continuous and the distance between sensors and actuator is not of interest. However, when the actuator is switched on and off, the time delay between the actuator and one of the sensors can be observed. This delay is directly proportional to the flow speed of the sample.

In the alternative set-up consisting of an integrated sensor actuator structure, a flow measurement can also be performed. The actuated species will be removed proportionally to the flow speed. This is already used in section 6.4 where a continuous supply of heat is injected into an electrolyte while the temperature is monitored. A lowering of the observed temperature indicates movement of the medium.

Considering the actuators of section 7.2, two markers for determining flow speed are available. Either a heat pulse or an electrochemically generated H^+ or OH^- cloud can be used, since also the sensors for detecting these pulses are available. When using a generated H^+ cloud as a marker, appropriate sensors are the conductivity cell and a pH sensor. The other option is to use a heat pulse and measure this with a temperature sensor.

The difference between time of flight using ions and time of flight using a heat pulse is in the diffusion effect. The diffusion constant of heat in water was given in table 6.2 and is equal to $1.455 \cdot 10^{-7}$ $m^2 \cdot sec^{-1}$, the diffusion constant of protons in water is equal to $9.311 \cdot 10^{-9}$ $m^2 \cdot sec^{-1}$ [6]. So, when using ions as a marker, the spreading of this marker is much smaller than when using a heat pulse. In addition, while heat can leak out of the channel by thermal conduction through the walls, particles like H^+ can not. Therefore, the use of a H^+ marker is preferred, especially for determining very low flow rates.

With time differential systems, using an integrated sensor-actuator structure, the same advantage of an ionic marker will be observed. In correspondence with the flow measurement described in section 6.4, the movement of a generated H^+ cloud due to flow of the medium can be

measured as a decrease in the observed conductivity. In this case the same advantage to the thermal equivalent is observed since no absorption by the substrate material of the generated stimulus is possible.

7.2.5 Summary

Using three actuators and four sensors, twelve combinations for building a differential measurement system are possible. Table 7.1 gives a summary on the possible combinations for implementing the set-up of figure 7.1.

Table 7.1: Summary of sensor-actuator combinations

Sensor / Actuator	Pt-100 Temperature	Finger structure Conductivity	Amperometry H_2O_2	Potentiometry pH
Electrochemically generated H^+, OH^-, O_2 or H_2	0	Weak acid conc. Mass flow Ca^{2+} concentration	H_2O_2	Weak acid conc. Mass flow
Thermoresistive heating	Mass flow	Ion concentrations (with assumed set of ions)	Diffusion constant	Dissociation or acid constant
Ion exchanger	0	Ca^{2+}	0	Ca^{2+} (if pH is known)

The use of a time differential or spatial differential system does not make any difference for the mathematical background of the stimulus-response measurements, with the exception of the flow measurements. However, the spatial differential system measures at one single moment at two different sensors, while a time differential system measures at two different moments at the same spot in the electrolyte.

For the application of temperature sensors in a differential set-up, only mass flow can be detected. The reason is that no heating due to the electrochemical actuator and the ion exchanger is assumed.
The differential conductivity measurement appears to be the most universal technique for measuring. This advantage comes from the non-selectivity, resulting in a difference in conductivity after all three actuator steps. Unless a logarithmic value, like pH of pCa, is desired, the linear nature of sensing of a conductivity cell shows the advantages of linear sensing described in section 7.1.
A hydrogen peroxide measurement using an amperometric technique, shows little new information. Although a cancellation of offsets can be observed when using an electrochemical actuator, either thermoresistive

heating or an imposed ion exchange does not show any promising new results.
Using potentiometric pH sensors, the results do not compete with the coulometric acid-base titrator as was published before [2]. Probably, due to its selectivity and logarithmic dependency on concentrations, the practical application of pH measurements in differential set-ups will give results which do need smart additional manipulation in order to retrieve useful electrolyte information.

For mass flow measurements, the choice of a spatial or a time differential set-up does make a difference. With the sensors and actuator placed in a row, the time of flight of a marker is measured. This results in the restriction that only linear flow can be measured and no turbulent flow. When, however, an integrated sensor-actuator structure is used, there is no time delay due to the geometry, and the flow information is obtained from the dilution of a marker. An example of the second technique was shown in the previous chapter with heat as the marker.

7.3 Conclusions

The mathematical impact of subtracting sensor signals was demonstrated in the first section of this chapter. Promising results could be expected from linear actuators, before and after a stimulus measured by linear sensors. In that case, sensor offsets will cancel out and absolute information on a certain input variable will be present in the differential signal.
This rather theoretical evaluation was illustrated by brainstorming on the combinations possible with three actuators and four simple sensors, resulting into twelve set-ups for implementing differential measurement systems. Some of them resulted into useful ideas.

Weak acid concentration determination was mentioned more than once. Although the used weak acid model solution acetic acid is of course not present in a washing machine, hydrogen peroxide shows also an acid-base behaviour with the anion HO_2^-.
Determination after the addition of H^+, created by an electrochemical actuator, can be done by both a differential pH or conductivity measurement. Although these methods resemble acid-base titrations, the information is in the measured sensor difference and not in the added amount of titrant (indicated by the end-point). The differential pH method gives information on the logarithm of the weak acid concentration, while a differential conductivity sensing gives the weak acid concentration immediately. For efficient use of the second one, the injected current through the actuator before the end-point (defined as

the moment where the difference in conductivity equals zero) can be used. However, the conventional coulometric titration with pH as the end point detection is still much more established and requires a similar set-up.
Weak acid concentration determination by measuring either pH or conductivity while applying a temperature step in order to change the acid equilibrium was suggested. But the practical use of this method is not easy since a temperature step will change much more parameters like the ion mobility and sensor slopes. Moreover, the use of a logarithmic sensor for measuring a concentration is not optimal since a non-linear operation is applied to the signal of interest.

Measuring calcium could not be done using single sensors up to now. Three options where found using stimulus-response measurements. Although it is not a one-spot differential measurement, the most elegant method would be a precipitation titration with conductivity sensing as an end point detection. The measurement of calcium by a precipitation technique is preferred because the possibility to precipitate is the reason that this hardness ion must be measured. Practical use of this titration method might fail, however, since precipitation is slow and furthermore hard to control.
Another method is to compare the conductivity at two temperatures. For this method, the pH must be increased first in order to assure that calcium is partially precipitated, since only then a change in the solubility constant due to the temperature difference can be measured. But now, the same problems will be encountered as with the other calcium precipitation method while in addition the problems with all the other parameters varying with temperature will show up.
What is probably possible for calcium sensing, is the application of an ion exchanger in combination with conductivity sensors. It was shown that an ion exchanger which exchanges one calcium ion by two H^+ ions, gives a conductivity change which is proportional to the absolute calcium concentration which is supplied to this system. Notice that this is an example of a method using linear sensors in combination with a linear actuator. The selectivity of the ion exchanger is used to sense calcium using non-selective conductivity sensors. The advantage of ion exchangers is that they can be reversed. An example is the use of an exchanger for the couple $Ca^{2+} \leftrightarrow 2H^+$, which can simply be reversed using electrochemically generated H^+ ions. A completely saturated ion exchanger gives calibration data on the sensors because the same sample solution is supplied to both sensors.
Since the ion exchanger material needs a certain path-length in order to exchange ions, the sample solution must be pumped through a column.

The result is that this method can not directly be realised in combination with the integrated sensor-actuator device of chapter 4, since it requires a spatial differential system. This pumping and the use of a column will limit the advantages of the “all in one” sensor-actuator device. In addition, the use of a tube introduces a source of possible system break downs since obstructions might occur easily in dirty washing water.

What is interesting is the comparison of flow detection methods based on indicators. When using a cloud of ions as a marker (preferably H^+ since this can be generated electrochemically), this marker can not diffuse out of the tube. A heat pulse instead, can be conducted by the tube material or the substrate of the sensor-actuator, and will be lost for time of flight detection purposes. In addition, because the diffusion of heat is faster than the diffusion of ions, very low flow rates can be determined with a low spreading of the marker. With an integrated sensor-actuator device, the same advantages of an ionic marker will be observed, since there is also no sink via the bulk material.

One method was not worked out, but only mentioned superficially. This is the ion concentration measurement by interpreting the change in conductivity after changing the temperature. In the next chapter this method will be described completely, and verified with some experiments.

7.4 References

[1] A.J. Bard and L.R. Faulkner, Electrochemical methods, fundamentals and applications, John Wiley & Sons, Inc., New York, 1980

[2] B.H. van der Schoot and P. Bergveld, An ISFET-based microlitre titrator: integration of a chemical sensor-actuator system, Sensors and Actuators, 8 (1985), page 11 - 22

[3] P.W. Atkins, Physical Chemistry, fifth edition, Oxford university press, 1994

[4] C.D. Amphlett, Topics in inorganic and general chemistry: Inorganic ion exchangers, Elsevier Publishing Company, Amsterdam, 1964

[5] D.A. Skoog, D.M. West and F.J. Holler, Analytical Chemistry, Saunders College Publishing, Philadelphia, 1992

[6] D.R. Lide, Handbook of chemistry and physics, 74th edition 1993 - 1994, CRC Press, Boca-Raton, Florida

CHAPTER 8

Ion concentration estimation using conductivity and temperature

The combination of a heater function and the measurement of electrolyte conductivity, as available on the integrated sensor structure, can be used to determine specific ion information. In this chapter this combination is used, however, not using the integrated device, but using a commercial conductivity meter and a heater/stirrer plate.
A method is introduced with which a non-selective electrolyte conductivity measurement is used for determining specific information on separate ion concentrations. This method starts with an assumed set of ions. Subsequently, the specific responses on temperature of the conductivities of these ions are related to the measured temperature dependency of the overall electrolyte conductivity.
For the calculation of the ion concentrations from a conductivity versus temperature sweep, an estimation algorithm is introduced based on the linear minimum mean square of the error. Errors in the measured conductivity will propagate through the algorithm into errors in the fitted ion concentrations. For the validation of the estimation method, this propagation of errors is also evaluated.
Finally the method is applied to solutions having two and three different types of ions, and is used to show the possibility of determining pH using a conductivity cell without a reference electrode.

8.1 The effect of temperature on conductivity

A single electrolyte conductivity measurement is not interesting unless the measured value is normalised for temperature. The reason for this is that at a higher temperature, ions become more mobile and will cause an increase in conductivity. So, with the same concentration, an increase in temperature results in an increase in conductivity. Therefore, in practical conductivity measurements, the measured conductivity is compensated to 25°C by using a simultaneous temperature measurement.

The total conductivity of an electrolyte expressed in terms of the limiting molar conductivities of the separate ions can be expressed by

$$\Lambda = \sum_{i=1}^{I} |z_i| c_i \lambda_i(T) \qquad (8.1)$$

with z_i the charge of ion i, c_i the concentration, I the number of different types of ions and $\lambda_i(T)$ the limiting molar conductivity of ion i. This last one is dependent on temperature and specific for every single ion. Since a conductivity measurement can not differentiate between ions, it is not possible to eliminate the temperature effect completely.

Industrial temperature compensation methods use the average temperature dependency of Λ which is about 2%/°C. This linear fit is the most simple approximation of the temperature dependency and is suitable for most pure water applications for over a moderate temperature range [1]. More sophisticated fits compensate by using a third order polynomial, but this method is electrolyte and concentration dependent [2].

A more complicated temperature compensation uses a polynomial fit for the limiting molar conductivities of the separate ions [3]. A third order approximation was proposed by Harned and Owen [4] and tabulated for several ions. The equation is

$$\lambda_i(T) = \lambda_i^0\left[1 + k_{i,1}(T-25) + k_{i,2}(T-25)^2 + k_{i,3}(T-25)^3\right] \qquad (8.2)$$

with λ_i^0 the limiting molar conductivity of ion i at 25°C. This polynomial approach will be used for ion identification.

8.1.1 General description

The generalised polynomial fit of order J with respect to temperature T_0 can be written as

$$\lambda_i(T) = \lambda_i^0 \sum_{j=0}^{J} k_{i,j}\left(T - T_0\right)^j . \qquad (8.3)$$

Together with equation (8.1) the total conductivity of an electrolyte having I types of ions can now be calculated:

$$\Lambda(T) = \sum_{i=1}^{I}\left[|z_i| c_i \lambda_i^0 \sum_{j=0}^{J} k_{i,j}\left(T - T_0\right)^j\right]. \qquad (8.4)$$

Manipulation yields:

$$\Lambda(T) = \sum_{i=1}^{I}\sum_{j=0}^{J}\left[|z_i| c_i \lambda_i^0 k_{i,j}\left(T - T_0\right)^j\right]$$

$$\Lambda(T) = \sum_{j=0}^{J}\sum_{i=0}^{I}\left[|z_i| c_i \lambda_i^0 k_{i,j}\left(T - T_0\right)^j\right]$$

and

$$\Lambda(T) = \sum_{j=0}^{J}\left[\left(T - T_0\right)^j \sum_{i=0}^{I}\left(\left|z_i\right| c_i \lambda_i^0 k_{i,j}\right)\right]. \qquad (8.5)$$

For conductivity measurements at N different temperatures, I types of ions and a polynomial fit of order J, a matrix equation can be formed using equation (8.5):

$$\begin{bmatrix}\Lambda_1\\ \Lambda_2\\ .\\ .\\ \Lambda_N\end{bmatrix} = \begin{bmatrix}1 & (T_1-T_0) & (T_1-T_0)^2 & . & (T_1-T_0)^J\\ 1 & (T_2-T_0) & (T_2-T_0)^2 & . & .\\ . & . & . & . & .\\ . & . & . & . & .\\ 1 & (T_N-T_0) & (T_N-T_0)^2 & . & (T_N-T_0)^J\end{bmatrix} \cdot \begin{bmatrix}k_{1,0} & k_{2,0} & . & k_{I,0}\\ k_{1,1} & k_{2,1} & . & .\\ . & . & . & .\\ . & . & . & .\\ k_{1,J} & k_{2,J} & . & k_{I,J}\end{bmatrix} \cdot \begin{bmatrix}|z_1|c_1\lambda_1^0\\ |z_2|c_2\lambda_2^0\\ .\\ |z_I|c_I\lambda_I^0\end{bmatrix} \qquad (8.6)$$

or

$$\overline{\Lambda} = \overline{\overline{T}} \cdot \overline{\overline{K}} \cdot \overline{c}.$$

The meaning of the terms is:

- $\overline{\Lambda}$ Vector containing measured conductivities at N different temperatures;
- $\overline{\overline{T}}$ Matrix with the temperature information;
- $\overline{\overline{K}}$ Matrix with the polynomial coefficients $k_{i,j}$;
- $\overline{c}$ Vector with the ion concentrations multiplied by the parameters $|z| \cdot \lambda^0$;

The question rises whether it is possible to calculate the vector $\overline{c}$ (containing the concentration information) from a known $\overline{\overline{T}}$ matrix and a measured $\overline{\Lambda}$ vector. It would be interesting to know if the $\overline{\overline{K}}$ matrix can be calculated as well. This would mean that the present ions can be identified by their found $k_{i,j}$ coefficients. The next section, however, shows that this is not possible, unfortunately.

8.1.2 Identification of ions by solving the coefficient matrix $\overline{\overline{K}}$

If equation (8.6) can be solved completely (both $\overline{\overline{K}}$ and $\overline{c}$ separately), the present ions can be identified by comparing the columns of matrix $\overline{\overline{K}}$ to known coefficients. Afterwards, the corresponding concentrations can be found from the vector $\overline{c}$.

The solution for the $\overline{\overline{K}} \cdot \overline{c}$ product is given by

$$\overline{\overline{K}} \cdot \overline{c} = \overline{\overline{T}}^{-1} \cdot \overline{\Lambda} \qquad (8.7)$$

with

$$\overline{\overline{K}} \cdot \overline{c} = \begin{bmatrix} k_{1,0} & k_{2,0} & . & k_{I,0} \\ k_{1,1} & k_{2,1} & . & . \\ . & . & . & . \\ . & . & . & . \\ k_{1,J} & k_{2,J} & . & k_{I,J} \end{bmatrix} \cdot \begin{bmatrix} |z_1| c_1 \lambda_1^0 \\ |z_2| c_2 \lambda_2^0 \\ . \\ |z_I| c_I \lambda_I^0 \end{bmatrix}. \qquad (8.8)$$

From this equation it will be clear that the coefficients $k_{i,j}$ can never be calculated without knowing the terms $|z_i| c_i \lambda_i^0$. In other words: for every set of coefficients $k_{i,j}$ another set of concentrations will be found. So, the coefficients must be known for solving the concentrations.
Notice that the number of measurements, N, is not visible in equation (8.8) so increasing the number of measurements will not solve the problem of the unsolvable coefficients either.

8.1.3 Calculation of ion concentrations using tabulated coefficients

When the $\overline{\overline{K}}$ matrix is assumed to be known, which implies a chosen set of ions, equation (8.6) can be written as

$$\begin{bmatrix} \Lambda_1 \\ \Lambda_2 \\ . \\ . \\ \Lambda_N \end{bmatrix} = \begin{bmatrix} \sum_{j=0}^{J} k_{1,j}(T_1 - T_0)^j & \sum_{j=0}^{J} k_{2,j}(T_1 - T_0)^j & . & \sum_{j=0}^{J} k_{I,j}(T_1 - T_0)^j \\ \sum_{j=0}^{J} k_{1,j}(T_2 - T_0)^j & \sum_{j=0}^{J} k_{2,j}(T_2 - T_0)^j & . & . \\ . & . & . & . \\ \sum_{j=0}^{J} k_{1,j}(T_N - T_0)^j & . & . & \sum_{j=0}^{J} k_{I,j}(T_N - T_0)^j \end{bmatrix} \cdot \begin{bmatrix} |z_1| c_1 \lambda_1^0 \\ |z_2| c_2 \lambda_2^0 \\ . \\ |z_I| c_I \lambda_I^0 \end{bmatrix} \qquad (8.9)$$

where the $\overline{\overline{T}} \cdot \overline{\overline{K}}$ matrix is written as a single one. The elements in this matrix are polynomials for the n-th temperature (rows) and the i-th ion (columns). If the $\overline{\overline{T}} \cdot \overline{\overline{K}}$ matrix has an inverse, the concentrations will follow from

$$\overline{c} = \left(\overline{\overline{T}} \cdot \overline{\overline{K}}\right)^{-1} \cdot \overline{\Lambda}. \qquad (8.10)$$

The first condition for having an inverse is that the matrix is square, so the minimal number of necessary experiments is equal to the number of ions to fit (N = I). For N > I an estimator must be used. The second condition is that the determinant is not equal to zero. This is true when the coefficients are different for every ion and the order of the polynomial is equal or larger than I - 1.

So, it is possible to find the concentrations of individual ions in a solution under the following conditions:

- The measured conductivity scan must be a linear combination of the temperature responses for the individual ions. This means that

→ Every ion which is significantly present in the electrolyte conductivity must be represented in the calculations;
→ No two ions may have the same temperature dependency (which will probably never be the case);
→ When I types of ions have to be calculated, the conductivity of the electrolyte must be measured at at least N = I temperatures;
→ The order of the used polynomials is equal to or larger than the number of different ions to fit minus one (J = I - 1);

- The coefficients $k_{i,j}$ of the individual ions must be known. The coefficients for the third order fit are given by Harned and Owen [4] for nine types of ions;

8.1.4 Error propagation

Errors due to systematic errors in conductivity measurements, for example due to an inaccurately assumed sensor slope, representing the sensitivity, can be proportional to the measurand itself. Proportional errors can be written as an undesired multiplication of Λ by ξ. For such proportional errors, equation (8.10) must be expanded to

$$\bar{c}^{\xi} = \left(\bar{\bar{T}} \cdot \bar{\bar{K}}\right)^{-1} \cdot \overline{\Lambda\xi} \qquad (8.11)$$

where $\overline{\Lambda}$ is multiplied per element by the proportional error vector $\bar{\xi}$. When ξ is equal for every single measurement, this results in

$$\bar{c}^{\xi} = \left(\bar{\bar{T}} \cdot \bar{\bar{K}}\right)^{-1} \cdot \overline{\Lambda} \cdot \xi = \bar{c} \cdot \xi\,. \qquad (8.12)$$

From this equation it can be concluded that an x per cent error in the measured conductivity will result in an x per cent error in the calculated ion concentrations.

Other types of errors might introduce a constant offset in the conductivity measurement. The most likely origin of such an error is the unexpected presence of an ion which is not included in the fitting algorithm. In that case, the observed conductivity versus temperature curve can never be a linear combination of the contributions of the assumed set of ions. Therefore, this kind of error will be much more severe than a proportional error. Such a systematic error which manifests as an unknown offset in the measurement can be written as a constant addition ε of Λ. In this case equation (8.10) becomes

$$\bar{c}^{\varepsilon} = \left(\bar{\bar{T}} \cdot \bar{\bar{K}}\right)^{-1} \cdot \left(\overline{\Lambda} + \bar{\varepsilon}\right) \qquad (8.13)$$

and manipulation yields

$$\bar{c}^{\varepsilon} = \left(\bar{\bar{T}} \cdot \bar{\bar{K}}\right)^{-1} \bar{\Lambda} + \left(\bar{\bar{T}} \cdot \bar{\bar{K}}\right)^{-1} \bar{\varepsilon} = \bar{c} + \left(\bar{\bar{T}} \cdot \bar{\bar{K}}\right)^{-1} \bar{\varepsilon} \qquad (8.14)$$

which shows that the faulty fitted vector $\bar{c}^{\varepsilon}$ is equal to the actual vector $\bar{c}$ increased by a constant vector. So, the error vector $\bar{\varepsilon}$ will result in unknown additions to all the elements of $\bar{c}$, which are different for every element.

Random noise in the measurement shows up as unknown offsets as well, like described in equation (8.14). However, the error vector $\bar{c}^{\varepsilon} - \bar{c}$ has another property now: its elements represent random numbers with an average of zero. In other words, when the number of experiments is chosen larger, the average of the elements in $\bar{c}^{\varepsilon} - \bar{c}$ will go to zero. In the next subsection, an estimation algorithm is introduced with which the number of experiments can be increased in order to reduce the error due to random noise in the conductivity measurement.

8.2 A linear minimum mean square estimation

The calculation of ion concentrations using the basic algorithm (8.10) requires conductivity measurements at as much as temperatures as the number of ions to be fitted. It is more accurate to do more measurements (N > I) and use an estimation method. In order to find the best fit from the measurements, some theory concerning parameter estimation is necessary. This is done in the first upcoming subsection. In the next subsection, the estimation algorithm is reduced to a more convenient form. The implementation of the condition that the sum of charge in a solution will be equal to zero is implemented in the third subsection.

8.2.1 Parameter estimation theory

The method introduced here is a matrix based algorithm for minimising the mean square error of the estimation [5]. Consider the generalised system

$$\bar{\Lambda} = \bar{\bar{B}} \cdot \bar{c} + \bar{v} \qquad (8.15)$$

with

- $\bar{\Lambda}$ the vector containing the observations,
- $\bar{\bar{B}}$ a matrix representing the system (in our case equal to $\bar{\bar{T}} \cdot \bar{\bar{K}}$),
- $\bar{c}$ the input vector to be estimated and
- $\bar{v}$ the noise or error in the measurement.

The aim is to find an estimate $\hat{\bar{c}}$ for the vector $\bar{c}$ satisfying the observed vector $\bar{\Lambda}$. Introducing the operator E for the moment of the operand,

which is equal to the average, the average of x can be written as E(x). If the average of the estimate is the true value

$$E\left(\hat{\bar{c}}\right) = \bar{c} \tag{8.16}$$

then the estimate is called unbiased. In the ideal case, the estimate is equal to the true value. In practice, however, an error will be present represented by the error vector, defined as

$$\bar{e} = \hat{\bar{c}} - \bar{c} = \hat{\bar{c}} - E\left(\hat{\bar{c}}\right). \tag{8.17}$$

The aim of the estimation algorithm is to minimise this error vector. In general, a function of $\bar{e}$ is chosen for optimisation, which can be the average mean square error of the components of $\bar{e}$. Consider the moment matrix

$$\overline{\overline{C}}_{\bar{e}} \equiv E\left(\bar{e}\bar{e}^T\right) = E\left[\left(\hat{\bar{c}} - E\left(\hat{\bar{c}}\right)\right)\left(\hat{\bar{c}} - E\left(\hat{\bar{c}}\right)\right)^T\right] \tag{8.18}$$

known as the covariance matrix of the estimate. Notice that the transpose operator ^{T} means that the vector is changed from a column into a row. The diagonal elements of the covariance matrix are the variances of the estimate's components. The best estimate can now be defined as the one having the smallest variances: the minimum variance unbiased estimator.

If $\bar{c}$ and $\bar{\Lambda}$ are random variables with moment matrices

$$\begin{aligned} \overline{\overline{C}}_{\bar{c}} &\equiv E\left(\bar{c}\bar{c}^T\right) \\ \overline{\overline{C}}_{\bar{c}\bar{\Lambda}} &\equiv E\left(\bar{c}\bar{\Lambda}^T\right) \\ \overline{\overline{C}}_{\bar{\Lambda}} &\equiv E\left(\bar{\Lambda}\bar{\Lambda}^T\right) \end{aligned} \tag{8.19}$$

and $\overline{\overline{C}}_{\bar{\Lambda}}$ is non-singular, implying that there is an inverse $\overline{\overline{C}}_{\bar{\Lambda}}^{-1}$, then the minimum variance unbiased estimate $\hat{\bar{c}}$ of $\bar{c}$ using the given data $\bar{\Lambda}$ is according to the Gauss-Markoff theorem [5] equal to

$$\hat{\bar{c}} = \overline{\overline{C}}_{\bar{c}\bar{\Lambda}}\overline{\overline{C}}_{\bar{\Lambda}}^{-1} \cdot \bar{\Lambda}. \tag{8.20a}$$

The associated error matrix of the estimate is

$$\overline{\overline{C}}_{\bar{e}} = \overline{\overline{C}}_{\bar{c}} - \overline{\overline{C}}_{\bar{c}\bar{\Lambda}}\overline{\overline{C}}_{\bar{\Lambda}}^{-1}\overline{\overline{C}}_{\bar{c}\bar{\Lambda}}^T. \tag{8.20b}$$

Now the theorem will be written in terms of the covariance matrices $\overline{\overline{C}}_{\bar{c}}$ and $\overline{\overline{C}}_{\bar{c}\bar{v}}$ because these are the closest to physical interpretation. The first one is the auto covariance of the concentration vector and the second one represents the correlation between concentration and noise. Substituting (8.15) in (8.19) yields

$$\overline{\overline{C}}_{\bar{c}\bar{\Lambda}} = \overline{\overline{C}}_{\bar{c}}\overline{\overline{B}}^T + \overline{\overline{C}}_{\bar{c}\bar{v}} \tag{8.21}$$

and for $\overline{\overline{C}}_{\bar{\Lambda}}$

$$\overline{\overline{C}}_{\bar{\Lambda}} = \overline{\overline{B}}\,\overline{\overline{C}}_{\bar{c}}\overline{\overline{B}}^T + \overline{\overline{C}}_{\bar{c}\bar{v}}{}^T\overline{\overline{B}}^T + \overline{\overline{B}}\,\overline{\overline{C}}_{\bar{c}\bar{v}} + \overline{\overline{C}}_{\bar{v}}. \tag{8.22}$$

The Gauss-Markoff theorem (8.20) can now be written as

$$\hat{\bar{c}} = \left(\overline{\overline{C}}_{\bar{c}}\overline{\overline{B}}^T + \overline{\overline{C}}_{\bar{c}\bar{v}}\right)\left(\overline{\overline{B}}\,\overline{\overline{C}}_{\bar{c}}\overline{\overline{B}}^T + \overline{\overline{C}}_{\bar{c}\bar{v}}{}^T\overline{\overline{B}}^T + \overline{\overline{B}}\,\overline{\overline{C}}_{\bar{c}\bar{v}} + \overline{\overline{C}}_{\bar{v}}\right)^{-1}\cdot\bar{\Lambda} \tag{8.23a}$$

and

$$\overline{\overline{C}}_{\bar{e}} = \overline{\overline{C}}_{\bar{c}} - \left(\overline{\overline{C}}_{\bar{c}}\overline{\overline{B}}^T + \overline{\overline{C}}_{\bar{c}\bar{v}}\right)\left(\overline{\overline{B}}\,\overline{\overline{C}}_{\bar{c}}\overline{\overline{B}}^T + \overline{\overline{C}}_{\bar{c}\bar{v}}{}^T\overline{\overline{B}}^T + \overline{\overline{B}}\,\overline{\overline{C}}_{\bar{c}\bar{v}} + \overline{\overline{C}}_{\bar{v}}\right)^{-1}\left(\overline{\overline{C}}_{\bar{c}}\overline{\overline{B}}^T + \overline{\overline{C}}_{\bar{c}\bar{v}}\right)^T. \tag{8.23b}$$

8.2.2 Simplified estimation algorithm

Except for the covariance matrices $\overline{\overline{C}}_{\bar{c}}$ and $\overline{\overline{C}}_{\bar{c}\bar{v}}$, equation (8.23a) can completely be determined for estimating the concentration vector $\hat{\bar{c}}$ from a measured set of conductivities $\bar{\Lambda}$. In order to eliminate these matrices some assumptions can be made [5]:

→ $\bar{c}$ and $\bar{v}$ are uncorrelated (the moment matrix $\overline{\overline{C}}_{\bar{c}\bar{v}} \equiv E\left(\bar{c}\bar{v}^T\right)$ is equal to zero);

→ the elements of $\bar{v}$ are uncorrelated and have equal standard deviations σ_v. This also implies that $\overline{\overline{C}}_{\bar{v}}$ is finite;

→ the true state of $\bar{c}$ is unknown so its moment matrix satisfies $\overline{\overline{C}}_{\bar{c}} \equiv E\left(\bar{c}\bar{c}^T\right) \to \infty$ (all variances are very large).

The linear minimum variance unbiased estimate $\hat{\bar{c}}$ of $\bar{c}$ given data $\bar{\Lambda}$ under these conditions is according to Gauss-Markoff theorem equal to

$$\hat{\bar{c}} = \left(\overline{\overline{B}}^T\overline{\overline{B}}\right)^{-1}\overline{\overline{B}}^T\cdot\bar{\Lambda} \tag{8.24a}$$

which reduces to (8.10) for a square matrix $\overline{\overline{B}}$. Because the variances σ_v^2 of the vector $\bar{v}$ are assumed to be equal, the moment matrix $\overline{\overline{C}}_{\bar{v}}$ can also be eliminated, and the error matrix can be expressed as

$$\overline{\overline{C}}_e = \left(\overline{\overline{B}}^T\overline{\overline{B}}\right)^{-1}\cdot\sigma_v{}^2 \tag{8.24b}$$

which contains all covariances of the fitted vector $\hat{\bar{c}}$ in its entries. So, the numbers on the diagonal of this error matrix are the variances of the fitted parameters. Using this knowledge, the standard deviation of the whole fit can be defined as

$$\sigma_c = \sqrt{\text{trace}\left(\overline{\overline{B}}^T\overline{\overline{B}}\right)^{-1}}\cdot\sigma_v \tag{8.25}$$

where the trace function is the summing of the elements on the diagonal of a matrix.

Experimental verification of the assumptions

The assumptions which justify the simplification to the estimation algorithm (8.24a/b), all refer to the measurement set-up. Some simple measurements for getting insight in the introduced system errors can verify these assumptions. The used set-up is the same as will be used later for doing the actual concentration determinations.

During some hours, a commercial conductivity meter (Radiometer CDM 210) is used for monitoring temperature and conductivity in stirred potassium chloride solutions. The solution is heated and cooled down several times between room temperature (18 °C) and about 55 °C. In a spreadsheet program, the data is collected and compared to the theoretical conductivities for these temperatures.

Table 8.1: Statistical information on KCl conductivity measurements at temperatures between 18 °C and 55 °C

Concentration KCl [mM]	Measured conductivity (20 °C) [mS/cm]	CDM210 range [mS/cm]	Mean error [mS/cm]	Standard deviation of error [mS/cm]
90	12.6	40	0.0009	0.05
309	38.5	400	0.0053	0.49
413	55.3	400	0.0183	0.50
615	86.2	400	0.0059	0.53

Notice that the conductivity meter is switched to the 40 mS range for the first sample which corresponds to a fixed operational frequency of 23.4 kHz, and to the 400 mS range for the other three samples (46.9 kHz). Obviously, the standard deviation is dependent on the chosen operational frequency and not on the electrolyte concentration. However, because the operational frequency is chosen according to the electrolyte concentration, the standard deviation is indirectly dependent on this concentration in practical applications.

All the measured errors of the three samples measured with the 400 mS range are collected into a single error distribution plot as shown in figure 8.1 which approaches the normal distribution shape.

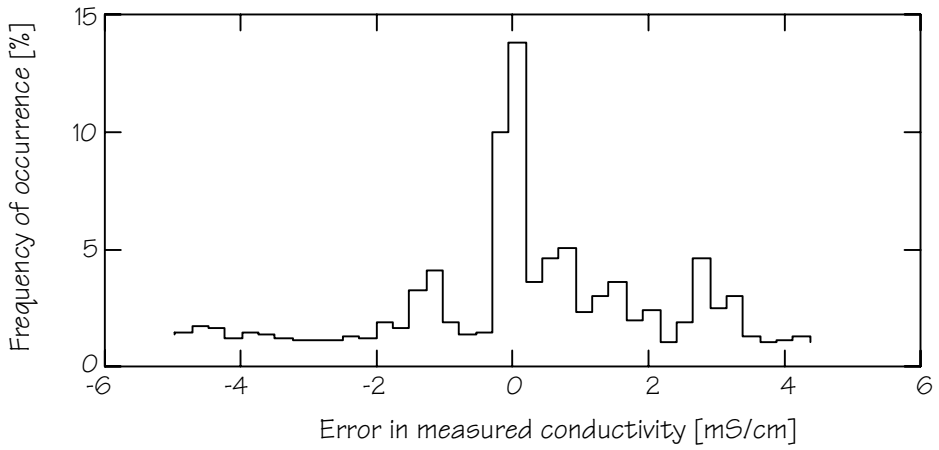

Figure 8.1: Error distribution in conductivity measurements

Discussion

Comparing column 4 to column 2 in table 8.1 it appears that the mean of the error is much lower than the observed conductivities. In other words

$$E(\bar{v}) = 0$$

which implies directly that the covariance with $\bar{c}$ is equal to zero as well:

$$\bar{\bar{C}}_{\bar{c}\bar{v}} \equiv E\left(\bar{c}\bar{v}^T\right) = 0 .$$

This proves the first assumption of $\bar{c}$ and $\bar{v}$ being uncorrelated.

The other two conditions, being $\bar{\bar{C}}_{\bar{c}} \to \infty$ and $\bar{\bar{C}}_{\bar{v}}$ is finite, are necessary to ensure that the moment matrix for $\bar{c}$ is much larger than the moment matrix for $\bar{v}$: $\bar{\bar{C}}_{\bar{c}} >> \bar{\bar{C}}_{\bar{v}}$. Since the standard deviations of $\bar{v}$ are finite and known (fifth column of table 8.1), its moment matrix will be small. More correctly, the moment matrix for $\bar{v}$ will go to zero in relation to the corresponding moment matrix for $\bar{c}$, which will go to infinite because its covariance goes to infinite [5].

The value for the standard deviation appears to be constant at a chosen operational frequency. This means that about 95% of the conductivity measurements is between the real conductivity plus/minus two times this standard deviation for the chosen operational range.

Besides being dependent on the operational frequency of the conductivity meter, the standard deviation might be dependent on temperature. Therefore, the data of the three measurements in the 400 mS range, is split into four sets: lower than 30 °C, between 30 °C and 40 °C, between 40 °C and 50 °C and higher than 50 °C. The calculated standard deviations are in table 8.2.

Table 8.2: Standard deviations calculated in several temperature ranges

Temperature range [°C]	Standard deviation [mS/cm]
< 30 °C	0.31
30 °C . . 40 °C	0.36
40 °C . . 50 °C	0.40
> 50 °C	0.42

Although there is a small temperature dependency, it might be concluded that no big error is introduced when assuming a temperature independent standard deviation.

Increasing the accuracy of estimation

Now the variance in the measurement error is practically determined, the propagation of this error through the estimation algorithm can be evaluated. This was done in subsection 8.1.4 for the situation where the number of applied temperatures is equal to the number of ions to be fitted (N = I). However, by using more than N measurements, a decrease in the final error can be expected because of suppression of measurement noise.

In figure 8.2 the normalised calculated standard deviation in the estimated concentration is represented for three different temperature ranges and estimations for N = 2 to 11. For this numerical example, the coefficients $k_{i,j}$ for a 100 mM sodium chloride solution are used.

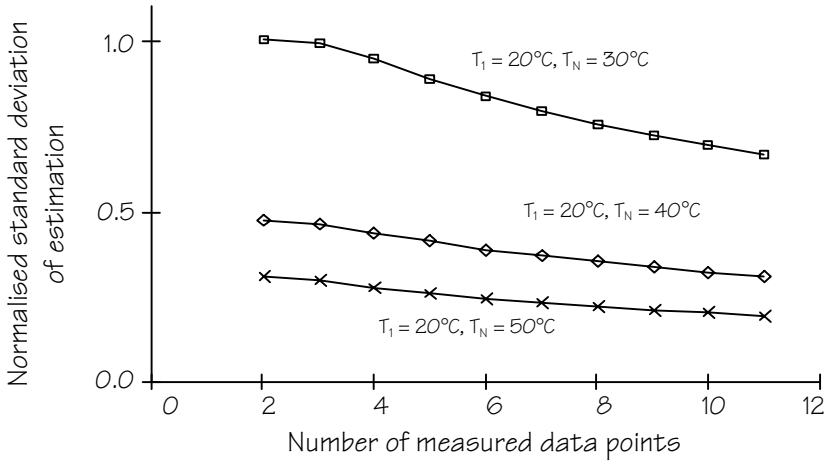

Figure 8.2: Effect of the temperature range and the number of measurements on the estimation accuracy

It can be seen that the accuracy of the estimation can be increased, either by increasing the number of measurements or the temperature range. The improvement in accuracy by increasing the temperature range is larger than the improvement obtained by using more measurements.

Summary

Reconsidering the original equation (8.9), describing the set of conductivity measurements at N temperatures, the ultimate method of determination should be

- Perform the measurements, by heating a solution while measuring the conductivity. Take more measurements (conductivities at known temperatures) than the number of ions to be fitted (N > I) since this will increase the accuracy of the estimation. Notice that the application of a large temperature sweep will increase the accuracy much more. Some conductivity meters have an automatic temperature compensation which must thus be switched off. Also the use of an auto range function will disturb the measurement since the variance in the measurement appeared to be constant per operational range;
- Assume a set of ions and calculate the matrix $\overline{\overline{B}}$ with the elements

  $$\overline{\overline{B}}_{n,i} = \sum_{j=0}^{J} k_{i,j}\left(T_n - T_0\right)^j$$

  with T_0 the reference temperature, T_n the temperature of measurement n, J the order of the polynomial fit and $k_{i,j}$ the polynomial fit coefficients for the temperature dependency of the mobilities (which can be found in literature [4]);
- Create the conductivity vector $\overline{\Lambda}$, which is a column of N conductivity measurements at N different temperatures;
- Use equation (8.24a) for finding the estimation vector $\hat{\bar{c}}$, which is a column of the $|z_i|c_i{\cdot}\lambda_i^0$ products for the I ions. Because the charge of the ions z_i and the limiting molar conductivity λ_i^0 are known, the concentrations of the individual ions can be calculated.

The size of the error in the estimated concentrations is represented by equation (8.25) in terms of the covariance of the measurement error. This covariance is determined for the Radiometer CDM210 conductivity meter to be about 0.5 mS/cm in the 400 mS operational range, and 0.05 mS/cm in the 40 mS range.

8.2.3 Error propagation

The absolute errors in the fitted concentrations due to random noise can be calculated using equation (8.24b). This equation gives the standard deviations in the fitted vector $\hat{\bar{c}}$ which contains the values $|z|c\,\lambda^0$ for all the fitted ions. So, when the error of a certain value is defined by two times its standard deviation (95% probability region), the resulting absolute error in the fitted ion concentration will be

$$e_{c,i} = \frac{2\sigma_v}{|z_i|\lambda_i^0}\sqrt{\left(\overline{\overline{B}}^T\overline{\overline{B}}\right)^{-1}\Big|_{i,i}} \qquad (8.26)$$

with

- $e_{c,i}$ the absolute error in the fitted ion concentration for ion i [10^{-3} mole / litre];
- z_i the ionic charge for ion i [no dimension];
- λ_i^0 the limiting molar ionic conductivity [m^2 S $mole^{-1}$];
- $\overline{\overline{B}}$ the matrix with the temperatures and coefficients $k_{i,j}$;
- σ_v the standard deviation in the measured conductivity [S / m];

Evaluation of equation (8.26) is easier with some numerical examples. When the conductivity meter is used in the 40 mS / cm range, which is equivalent to a maximum of about 300 mM KCl, the standard deviation of the measurement is approximately equal to 0.05 mS / cm as given in table 8.1. For N = 25 measurements, equidistantly distributed over a temperature range from 20 °C to 55 °C and using a polynomial approximation of J = 3 for the ion conductivities, the absolute errors in the fitted concentrations are calculated. In table 8.3, the results are summarised for combinations of two, three and four selected ions.

Table 8.3: Absolute errors in fitted concentrations due to random noise, for N = 25, T = 20 - 55 °C, J = 3, σ_v = 0.05 mS/cm

Fitted ion: / Solution:	Δ[Na^+] (mM)	Δ[H^+] (mM)	Δ[K^+] (mM)	Δ[Cl^-] (mM)
K^+ and Cl^-			32	30
H^+ and Cl^-		0.80		3.4
H^+, Na^+, and Cl^-	38	1.3		20
H^+, K^+ and Cl^-		12	253	215
H^+, K^+, Na^+ and Cl^-	90	28	1.2 M	0.9 M

On the average, the fitting of a larger number of ions increases the random noise propagation error. What can also be seen, is that the type of ion does matter. When the combination Cl^- and K^+ is present, the errors are bigger. In addition, the result for H^+ is more accurate, not only in the result for H^+ itself, but also for the other ions in the system. This could be expected since H^+ has a much more characteristic ionic conductivity and therefore ion discrimination is more easy.

Since table 8.3 is only valid when the meter is switched in the 40 mS / cm range, errors in the concentrations around the one molar limit will certainly exceed the actual concentrations. So, the fitting of four ions will probably be much too sensitive to errors.

Remarkable is that the absolute error is not dependent on the concentration, which is the result from the constant standard deviation of the conductivity measurement. It is important to choose the lowest

possible conductivity sensing range on the meter since then the standard deviation is the lowest as can be seen from table 8.1.

For errors in the measured conductivity which have not a random nature, the noise will not be filtered out by the estimation algorithm. An example which was already mentioned in subsection 8.1.4 is the presence of a background electrolyte, consisting of one or more ions which are not in the assumed set of ions.
When the error ε is assumed to be constant at every temperature, the relative error in the fitted concentration of ion i becomes

$$\frac{\overline{c}^{\varepsilon}_i - \overline{c}_i}{\overline{c}_i} = \frac{\left[\left(\overline{\overline{T}} \cdot \overline{\overline{K}}\right)^{-1}\right]_{Row\_i} \cdot \overline{\varepsilon}}{\left[\left(\overline{\overline{T}} \cdot \overline{\overline{K}}\right)^{-1}\right]_{Row\_i} \cdot \overline{\Lambda}} = \frac{\sum_{Row\_i}\left[\left(\overline{\overline{T}} \cdot \overline{\overline{K}}\right)^{-1}\right]}{\left[\left(\overline{\overline{T}} \cdot \overline{\overline{K}}\right)^{-1}\right]_{Row\_i} \cdot \overline{\Lambda}} \cdot \varepsilon \qquad (8.27)$$

where equation (8.14) is used and for simplicity N = I is taken. When later N > I is needed, the inverse of the $\overline{\overline{T}} \cdot \overline{\overline{K}}$ matrix can simply be substituted by the estimation matrix of equation (8.24a). The elements in the measured conductivity vector $\overline{\Lambda}$ can be normalised to the conductivity at for example 20 °C. The relative error in the fitted concentration becomes equal to

$$\frac{\overline{c}^{\varepsilon}_i - \overline{c}_i}{\overline{c}_i} = \frac{\sum_{Row\_i}\left[\left(\overline{\overline{T}} \cdot \overline{\overline{K}}\right)^{-1}\right]}{\left[\left(\overline{\overline{T}} \cdot \overline{\overline{K}}\right)^{-1}\right]_{Row\_i} \cdot \overline{\Lambda}_{20°C}} \cdot \frac{\varepsilon}{\Lambda_{20°C}} \qquad (8.28)$$

which means that the relative error in the fitted ion concentrations is proportional to the relative error due to an offset in the measured conductivity. In table 8.4 the factors which amplify the relative error in the measurement to relative errors in the fit are given for the same solutions as used in table 8.3. However, while the concentrations did not matter for the errors due to random noise, now concentrations must be assumed in order to find numerical values.

Table 8.4: Amplification factor for a relative error due to an offset in the measured conductivity to the relative error in the fitted ion concentrations, for N = 25, T = 20 - 55 °C, J = 3 and Λ_0 = 20 °C

Solution: Fitted ion:	Na^+	H^+	K^+	Cl^-
10 mM KCl			38	35
10 mM HCl		2.7		7.5
10 mM HCl + 10 mM NaCl	16	4.0		0.6
10 mM HCl + 10 mM KCl		8.7	206	82
10 mM NaCl + 10 mM KCl + 10 mM HCl	21	5.0	3.9	1.5

An entry in this table means that when estimating for example K^+ in a 10 mM KCl solution, a one percent offset in the measured conductivities will result into an 38% error in the fitted concentration.
Some remarks can be made. The error in the fitted H^+ concentration does not escalate excessively, but the error amplification seems to remain lower than ten. A factor ten means that for a 5% error in the fit, a 0.5% error in the measured conductivity is allowed. Roughly speaking, the allowed "background" normality may therefore not exceed 0.5% of the concentration of interest.
The real problem with this type of error is that it is unpredictable. For example the amplification of errors can range from 0.6 to 206. Without knowing, a small error due to a contamination in the system will be enormously amplified. The maximum amplification which empirically found here is 206. Although it is not guaranteed that no larger amplifications will be observed in other systems, a rough estimation of the possible detection limit of ions in demi water is possible. Using demi water with a purity of 0.5 μS/cm, for a 5% error in the fitted ion concentrations a conductivity of 2.0 mS/cm is the lower limit. This is equivalent to for example a 15 mM KCl solution. So, when trying to fit the ion concentration in solutions with a lower concentration, the impurity of the demi water might already disturb the estimation.

8.2.4 Implementing the zero charge condition

Because in practical solutions the total charge is equal to zero, the condition

$$\sum_{\text{Cations}} |z_i| c_i = \sum_{\text{Anions}} |z_i| c_i \tag{8.29}$$

can be implemented in the algorithm in order to increase accuracy and to avoid useless answers like negative concentrations. This equation can be implemented in the model (8.9) as

$$\begin{bmatrix} \Lambda_1 \\ \Lambda_2 \\ . \\ . \\ \Lambda_N \\ \hline 0 \end{bmatrix} = \begin{bmatrix} \sum_{j=0}^{J} k_{1,j}(T_1 - T_0)^j & \sum_{j=0}^{J} k_{2,j}(T_1 - T_0)^j & . & \sum_{j=0}^{J} k_{I,j}(T_1 - T_0)^j \\ \sum_{j=0}^{J} k_{1,j}(T_2 - T_0)^j & \sum_{j=0}^{J} k_{2,j}(T_2 - T_0)^j & . & . \\ . & . & . & . \\ \sum_{j=0}^{J} k_{1,j}(T_N - T_0)^j & . & . & \sum_{j=0}^{J} k_{I,j}(T_N - T_0)^j \\ \hline \frac{z_1}{|z_1|\lambda_1^0} & \frac{z_2}{|z_2|\lambda_2^0} & . & \frac{z_I}{|z_I|\lambda_I^0} \end{bmatrix} \cdot \begin{bmatrix} |z_1| c_1 \lambda_1^0 \\ |z_2| c_2 \lambda_2^0 \\ . \\ |z_I| c_I \lambda_I^0 \end{bmatrix} \tag{8.30}$$

were the $\overline{\overline{T}} \cdot \overline{\overline{K}}$ matrix has now become the augmented $\overline{\overline{T}} \cdot \overline{\overline{K}}$ matrix. The elements in the augmented vector $\overline{\Lambda}$ and the augmented matrix $\overline{\overline{T}} \cdot \overline{\overline{K}}$ do

not have an equal unity anymore. This does not make any difference for numerical evaluations, however.

This augmented model can be evaluated like the original model using the same estimation algorithm. However, the condition (8.29) will have the same priority as every single measurement and so its importance will be suppressed with an increasing number of applied temperatures N. Two options are available for increasing its priority:

- The first option is to give the last row of the augmented $\overline{\overline{T}} \cdot \overline{\overline{K}}$ matrix a weight factor equal to the number of measurements. The weighted least square form of (8.24) is [5]

$$\hat{\bar{c}} = \left(\overline{\overline{B}}^T \overline{\overline{W}}^{-1} \overline{\overline{B}}\right)^{-1} \overline{\overline{B}}^T \overline{\overline{W}}^{-1} \cdot \bar{\Lambda} \qquad (8.31)$$

  with $\overline{\overline{W}}$ the weight matrix. This weight matrix is of size (N+1) × (N+1) with on the diagonal the only non-zero entries being the weight factors. Since the matrix $\overline{\overline{B}}$ will be the augmented $\overline{\overline{T}} \cdot \overline{\overline{K}}$ matrix, the element on entry (N+1, N+1) will be the weight factor for the zero charge condition;
- Another possibility is obtained by first reducing the measured information and then implementing the zero charge condition. Concerning equation (8.8) it was concluded that the number of measurements is not in the $\overline{\overline{K}} \cdot \bar{c}$ matrix. The measured information (conductivities at N temperatures) can be reduced to J+1 points by first calculating an estimation for the vector $\overline{\overline{K}} \cdot \bar{c}$ by applying the simple algorithm (8.24a / b) to equation (8.7). The result, being equal to

$$\left.\overline{\overline{K}} \cdot \bar{c}\right|_{\text{Estimate}} = \left(\overline{\overline{T}}^T \overline{\overline{T}}\right)^{-1} \overline{\overline{T}}^T \cdot \bar{\Lambda} \qquad (8.32)$$

  is a vector with length J+1, independent on the number of measurements. This estimated vector is equal to the product of the coefficient matrix $\overline{\overline{K}}$ and the concentration vector $\bar{c}$ to be estimated as given by equation (8.8). The zero charge condition can now again be implemented by augmenting a matrix:

$$\begin{bmatrix} \left.\overline{\overline{K}} \cdot \bar{c}\right|_{\text{Estimate}} \\ \hdashline 0 \end{bmatrix} = \begin{bmatrix} k_{1,0} & k_{2,0} & . & k_{I,0} \\ k_{1,1} & k_{2,1} & . & . \\ . & . & . & . \\ k_{1,J} & k_{2,J} & . & k_{I,J} \\ \hdashline \frac{z_1}{|z_1|\lambda_1^0} & \frac{z_2}{|z_2|\lambda_2^0} & . & \frac{z_I}{|z_I|\lambda_I^0} \end{bmatrix} \cdot \begin{bmatrix} |z_1| c_1 \lambda_1^0 \\ |z_2| c_2 \lambda_2^0 \\ . \\ |z_I| c_I \lambda_I^0 \end{bmatrix} \qquad (8.33)$$

  To solve the concentrations from this equation, a second estimation step is necessary since the augmented $\overline{\overline{K}}$ matrix is not square.

The error coefficient matrix (8.24b) has now become meaningless, and so the standard deviation of the fit (8.25), since these are only valid when having equal variances $\bar{v}$ for all the measurements. The variances are not equal anymore, since the zero charge condition will have another variance than the actual conductivity measurements.

8.3 Experimental

The presented theory is verified using a Radiometer CDM210 commercial conductivity meter in a computer controlled set-up as shown in figure 8.3. This conductivity meter is capable of measuring conductivity, using a four points electrode (type Radiometer CDC565), and the solution temperature (using a Radiometer temperature probe type T201).

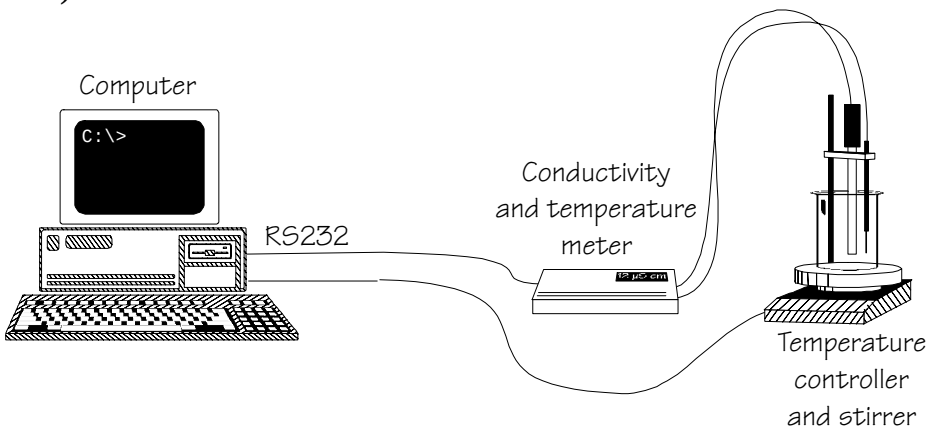

Figure 8.3: Measurement set-up

For this measurement, the automatic temperature compensation of the CDM210 must be switched off, and the automatic measurement range adaptation as well. Each measurement starts at room temperature. After a heating and stirring step, an equilibrium time of 5 seconds is used before measuring. This sequence is repeated until the temperature exceeds 55ºC.

The protocol is controlled by LabView 3.1 software, providing the user with an interactive interface. First the user is asked to prepare a solution and place it on the heater. The program switches on the heater and measures the conductivity equidistantly over the given range. After the measurement has finished, the menu shown in figure 8.4a asks to select the ions which are present in the solution. Figure 8.4b shows the result window with the measured curve, the fitted curve and fitted ion concentrations.

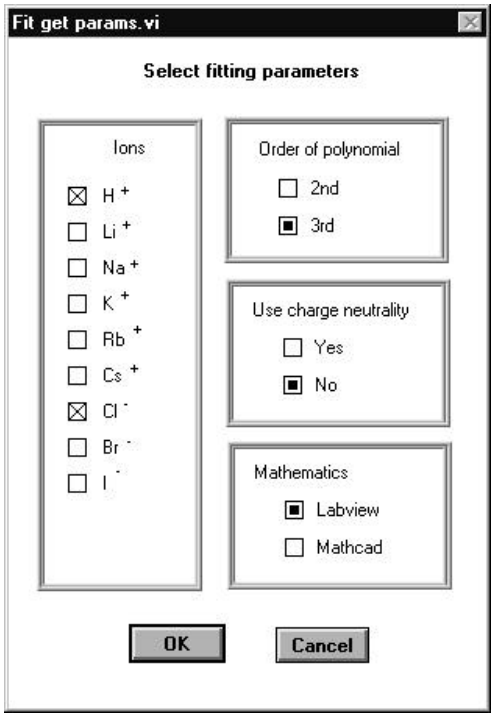

Figure 8.4a: Screen shot of the ion selection menu in the LabView 3.1 program

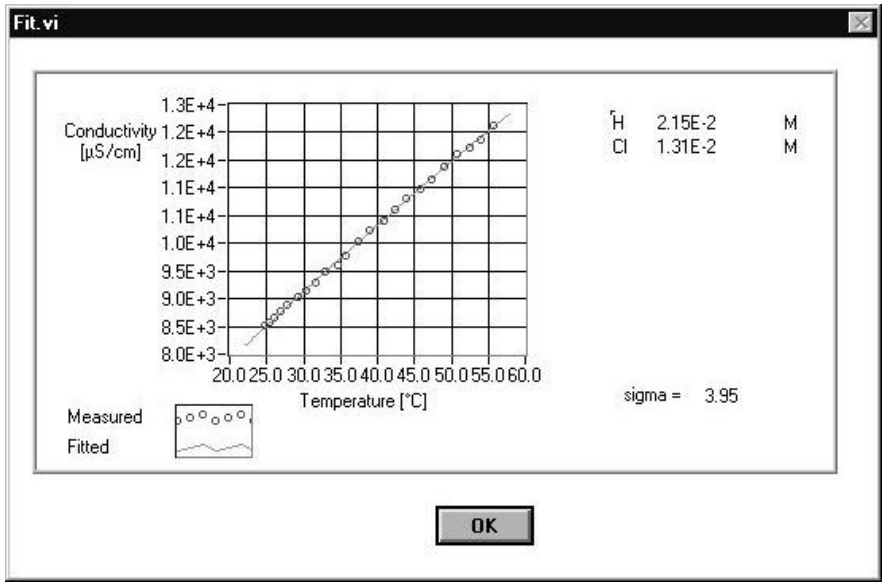

Figure 8.4b: Screen shot of the result window in the LabView 3.1 program

The implementation of the estimation algorithm, both for the normal and the zero charge case, is also done in LabView. The parameters for equation (8.2) are given by Harned and Owen [4] and are repeated in table 8.5.

Table 8.5: Coefficients for equation (8.2) [4], T_{Ref} = 25.0 °C

Ion	Molar conductivity λ^0 [10^{-4} m^2 S mol^{-1}]	k_1	k_2	k_3
H^+	349.85	$1.376576 \cdot 10^{-2}$	$-2.947692 \cdot 10^{-5}$	$-2.192368 \cdot 10^{-7}$
Li^+	38.64	$2.302950 \cdot 10^{-2}$	$1.140657 \cdot 10^{-4}$	$-5.284679 \cdot 10^{-7}$
Na^+	50.15	$2.176670 \cdot 10^{-2}$	$9.401795 \cdot 10^{-5}$	$-2.293121 \cdot 10^{-7}$
K^+	73.50	$1.949143 \cdot 10^{-2}$	$5.518776 \cdot 10^{-5}$	$-4.330612 \cdot 10^{-7}$
Rb^+	77.81	$1.901465 \cdot 10^{-2}$	$4.935098 \cdot 10^{-5}$	$-5.825729 \cdot 10^{-7}$
Cs^+	77.26	$1.874062 \cdot 10^{-2}$	$4.950815 \cdot 10^{-5}$	$-2.653378 \cdot 10^{-7}$
Cl^-	76.35	$2.017511 \cdot 10^{-2}$	$6.090373 \cdot 10^{-5}$	$-1.683039 \cdot 10^{-7}$
Br^-	78.17	$1.974799 \cdot 10^{-2}$	$5.718306 \cdot 10^{-5}$	$-2.942305 \cdot 10^{-7}$
I^-	76.90	$1.963498 \cdot 10^{-2}$	$5.689207 \cdot 10^{-5}$	$-2.821847 \cdot 10^{-7}$

8.3.1 An electrolyte with two ion types

First, the theory is tested for electrolytes having only one type of anion and one type of cation, both with and without using the zero charge condition as implemented in equation (8.33).
The number of applied temperatures per electrolyte is N = 25 and the polynomial fit is of order J = 3. Solutions are used of 20, 40, 60, 80 and 100 mM KCl and NaCl. Figure 8.5 shows the fitted concentrations.

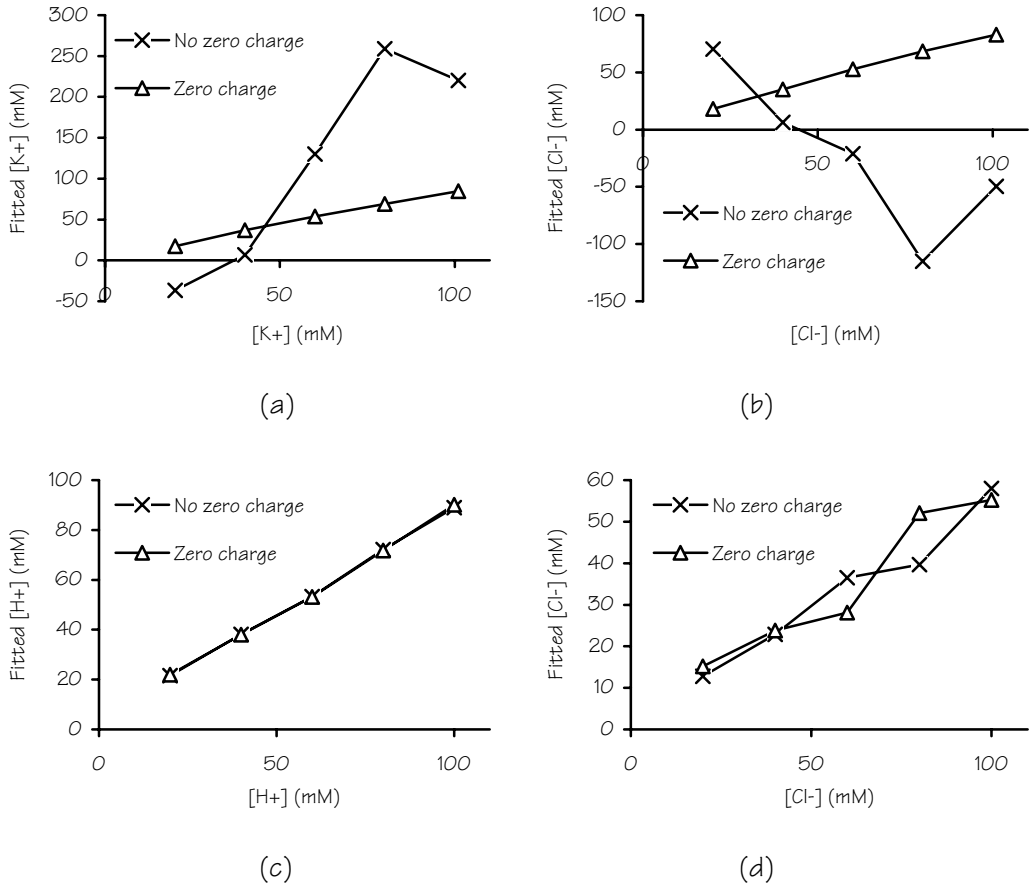

Figure 8.5: Fitted ion concentrations for (a, b) KCl and (c, d) HCl, both with and without the incorporation of the zero charge condition

It is not very surprising that the fitting of hydrogen chloride is much more accurate than that of potassium chloride because the mobilities, and also the temperature dependency of these mobilities, of potassium and chloride ions are almost equal. This property, which is exploited in conventional reference electrodes, is not observed with hydrogen chloride. The result is that for fitting KCl the usage of the zero charge condition is essential, while for HCl this is not strictly required. In figure 8.6 the fitted values using the zero charge condition are collected.

A proportional relationship between the fitted ion concentration and the actual concentration is certainly observed. However, the ratio between the imposed ion concentration and the calculated concentration is not equal to one. In figure 8.6 the fitted concentrations are only 80% of the real concentrations, while this is even lower for chloride in HCl. Such proportional errors where already mentioned in the subsections 8.1.4 and 8.2.3 as the result of a badly calibrated conductivity meter.
Other types of errors discussed in these subsections, are errors due to random noise and errors due to offsets in the measurements.While the effect of the error due to random noise in the observed conductivity is minimised by taking a large number of measurements, the size of the error due to offsets in the measured conductivity is unknown up to now. In subsection 8.3.3 the propagation of errors of this type will be discussed.

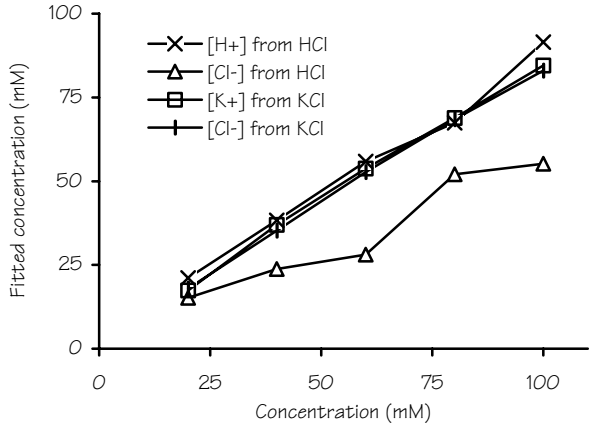

Figure 8.6: Summary of fits using the zero charge condition

Notice that the use of the zero charge condition together with the knowledge that only two ion types are present is already enough to know the actual separate ion concentrations. Nevertheless, a conclusion concerning the correctness of the introduced new method is allowed since the fitting is primarily based on the change in mobilities. Anyway, the real advantage of this method will be demonstrated when the separate concentrations of more than two different ions are fitted.

8.3.2 An electrolyte with three ion types

The advantage of the method presented here will be in solutions having more than two types of ions. As a test, a series of solutions is made having 25 mM sodium chloride and 10 to 70 mM hydrogen chloride or potassium chloride. The fitted results using the zero charge condition are presented in figure 8.7.

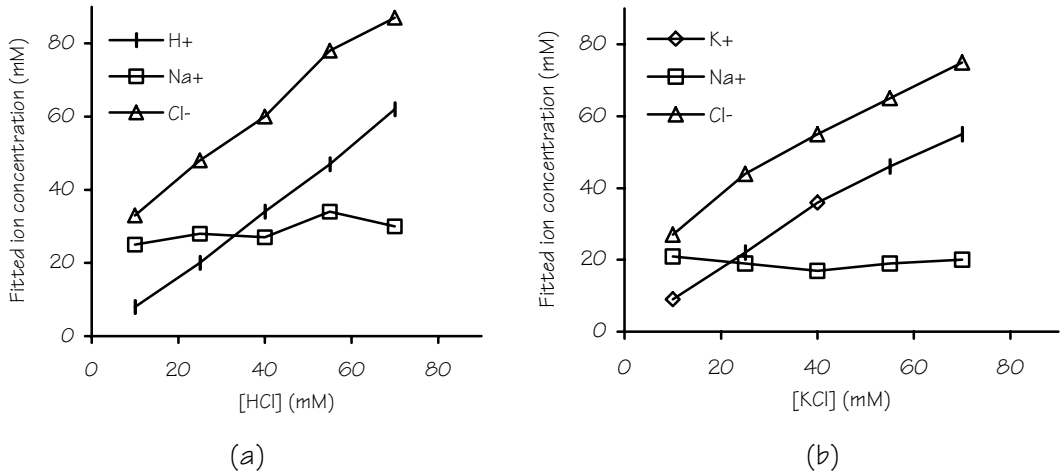

Figure 8.7: Result of fitting ions in 25 mM NaCl with various (a) HCl or (b) KCl concentrations, using the zero charge condition

As could be expected, the fitted sodium concentration remains constant while the other ion concentrations do change.

8.3.3 Error propagation

With the knowledge of the absolute errors introduced in subsection 8.2.3, error bars can be drawn in previously measured concentration plots. For example, figure 8.8 is repeated from figure 8.7a, but now with error bars and plotted in three separate graphs. Since there is no formula derived for the absolute errors when using the zero charge condition, the error bars for the non-zero charge method are placed in the graph with concentrations fitted using the zero charge condition. This will result into a worst case guess of the error. The dotted lines in the graphs are the imposed ion concentrations.

The error bars are obviously a bit too pessimistic for Na^+ and Cl^- since the correlation between fitted concentration and the real concentration is much larger than may be assumed according to these error bars.

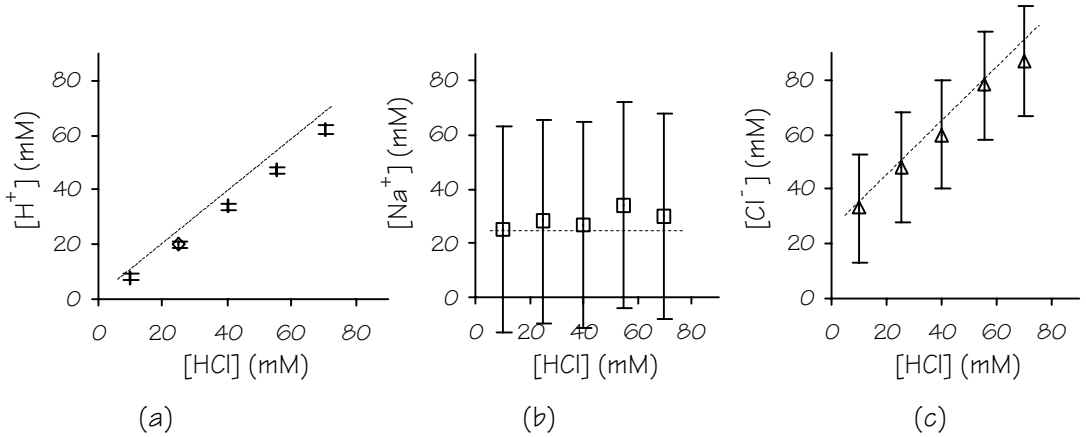

Figure 8.8: Fitted ion concentrations with error bars in solutions with 25 mM NaCl and several HCl concentrations. (a) H^+, (b) Na^+ and (c) Cl^-

When implementing the zero charge condition, the matching between anions and cations will be improved. Although no algorithm is given here for calculating the absolute errors in the fitted results when this condition is included, it may be assumed that the errors will decrease. Although this decrease is not known, it is probably meaningless to fit four ions, since table 8.3 shows that then the worst case error will exceed the one molar limit. Because the given values are only valid in the 40 mS/cm range, the errors are far more than the present ion concentrations.

8.3.4 A pH measurement

In some processes a pH measurement using an ISFET or a glass electrode is not possible. These problems often come from the reference electrode, for example because

- The sample is sensitive to chloride or potassium ions;
- The electrode dries out because it is not constantly immersed with water;
- The liquid junction is contaminated with proteins, oil or sulphide;
- Extremely high temperatures or low pH values are present.

In these situations the fitting method can still be applied because the heater and conductivity cell can be made of a solid state conductor on a chemically inert substrate.

Starting in 0.9 M HCl and diluting down to 2 µM, a series of pH's is created. The fitted hydrogen concentrations are presented in figure 8.9. Coming close to pH 5.5 the determination becomes worse. The explanation is that the measured conductivity is of the order of µS/cm while the used demineralised water was of the quality 0.59 µS/cm. So, clearly, the contamination with other ions disturbs the fit in this case.

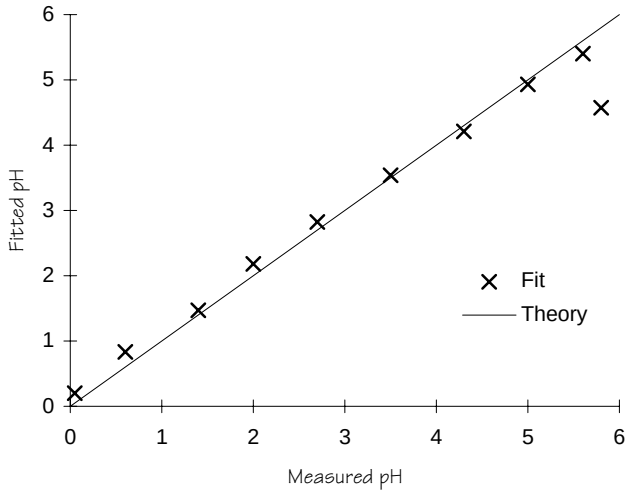

Figure 8.9: A measurement in HCl plotted as a pH determination

Although the fitting of two types of ions is quite trivial (a single conductivity measurement with the zero charge condition in mind would give the same result), this experiment did verify the possibility of applying the method in solutions with a very low pH.

8.4 Conclusions

From a non-selective conductivity measurement, it is possible to find specific ion concentrations by recording the conductivity at different temperatures. The key to this is that every ion has its own specific limiting molar conductivity which depends uniquely on temperature. This method needs an assumed set of ions: the electrolyte conductivity is a linear combination of the specific ionic conductivities of these ions.

The first condition needed for making the system solvable is that in order to fit I ions, at least N = I measurements at different temperatures are needed. However, to increase the accuracy, more measurements are preferred and subsequently an estimation algorithm is used to find the best fit. The second condition is that the characteristic polynomial used for the temperature dependencies of the limiting molar ionic conductivities is at least of order J = I - 1. Next, the coefficients $k_{i,j}$ in this polynomial must be unique for every single ion because the whole recognition is based on the difference in these coefficients. This is true since every single ion has a different size and mass and will therefore have another temperature dependency in its ionic conductivity. Finally, every ion which is significantly present in the solution must be included in the calculation, since the method is based on the conductivity being a linear combination of all the separate ionic conductivities.

In order to increase the accuracy of the calculated ion concentrations, either the temperature sweep or the number of points N can be increased. Increasing the temperature sweep, however, has a much more positive effective result on the accuracy.
For N = I, one unique solution for the ion concentrations is possible. For N > I, an estimation algorithm must be chosen. A linear estimation algorithm based on the minimum mean square error is introduced.
Actually, there is a third method for increasing the accuracy. The knowledge that the sum of all charges is zero in equilibrium can be included in the estimation algorithm as a boundary condition. Especially for “difficult” ion pairs (like chloride and potassium for example) the use of this condition appeared to be essential.
However, the use of an estimation algorithm can only decrease the errors due to random noise. An error in the observed conductivities due to the presence of an ion which is not in the assumed set, will propagate to an error in the fitted ion concentrations which can not be decreased by taking more measurements.

For only two ions in the solution, the introduced method is not necessary because then a single conductivity measurement already determines both ion concentrations. When there are four ions, the method is probably too sensitive to errors because a small error in the measured conductivity might result into an enormous error in the fitted ion concentration. A worst case analysis shows that the absolute error in the fitted concentration becomes sometimes more than one molar when the conductivity meter is switched in the 40 mS/cm range. So, in conclusion, the method will show the best results in systems having three different types of ions.

Although the experiments were carried out using bulk heating of the whole volume of electrolyte, it can also be done using the integrated sensor-actuator structure of chapter 4. In that case, however, only the local environment is heated which might shorten the time needed for measuring the conductivities at several temperatures. This experiment will be described in chapter 9.

Summarising, it can be said that the advantage of this method is that it introduces selectivity by smart data interpretation, and not by the sensor itself. In general, when a sensor is made selective, fragile and complex selective membranes are introduced. This results into transducers with a whole sandwich of membranes on top of it. Electrolyte conductivity sensing, on the other hand, is easy, chemically

inert and mechanically stable since it uses a solid metal structure. It is a reproducible technique since the cell constant which determines the sensitivity shows no drift in principle.

8.5 References

[1] D.M. Gray and A.C. Bevilacqua, Unique temperature compensation for conductivity and resistivity measurements, Ultrapure water, volume 13, 1996

[2] Toshiaki Isono, Density, viscosity, and electrolytic conductivity of concentrated aqueous electrolyte solutions at several temperatures. Alkaline-earth chlorides, $LaCl_3$, Na_2SO_4, $NaNO_3$, NaBr, KNO_3, KBr and $Cd(NO_3)_2$. Journal of chemical and engineering data, Vol. 29, No.1, 1984

[3] A.L. Horvath, Handbook of aqueous electrolyte solutions, physical properties, estimation and correlation methods, Ellis Horwood Limited, Chichester, 1985

[4] H.S. Harned and B.B. Owen, The physical chemistry of electrolytic solutions, Reinhold Publishing Corporation, New York, 1958

[5] P.B. Liebelt, An introduction to optimal estimation, Addison-Wesley Publishing Company, Reading, Massachusetts, 1967

CHAPTER 9

Supplementary results

This chapter comprises some results which were found during the development of the sensor array, but which did not fit in the previous chapters. The first section describes a technique which gives a new parameter, being the hardness of tap water, based on a statistical analysis. Next, an implementation of a conductivity cell is proposed which does not need the chosen silicon technology approach, but which can be fabricated using standard printed circuit board fabrication technology. Finally, the measurement technique which is described in chapter 8, is carried out using the integrated sensor-actuator device as introduced in chapter 4.

9.1 Hardness and conductivity of tap water

In chapter 2, the ions that determine the conductivity of tap water were given, based on a statistical analysis of the tap water in 44 Dutch cities in 1986 [1]. What could be seen from figure 2.3b is that the hardness ions, calcium and magnesium, determine the conductivity for 40%. The question rises whether it will be possible to approximate the tap water hardness by measuring the water conductivity. This could be interesting, since a conductivity sensor is already present in the integrated sensor-actuator device of chapter 4 and a hardness sensor is not.

Figure 9.1a shows a plot with the measured water conductivities on the horizontal axis, and the measured hardnesses on the vertical axis. The data is obtained from the same data source of the composition of Dutch tap water [1]. The hardness is expressed here as the total concentration of multivalent ions. To convert this to the more common calcium carbonate equivalent, the factor 100.1 g / mole must be used.
Using a least square algorithm, a line could be plotted in this figure. The observed correlation between hardness and conductivity appears to be 0.85. So, based on the measured conductivity, the hardness can be guessed using this line. The average error in the guessed hardness is 13% while the observed maximum error is 50%. Although this seems quite large, the estimated hardness can be used to reduce the excess amount of dosing, which is nowadays common. Without a conductivity measurement, the dosing should be adjusted to the largest possible water hardness which is about 3.0 mM. By a single conductivity measurement the dosing can be reduced. For example, when a

conductivity of 20 mS/m is observed, the hardness will not be larger than 1.2 mM using the correlation line with 50% overdosing compensating for the maximum error.

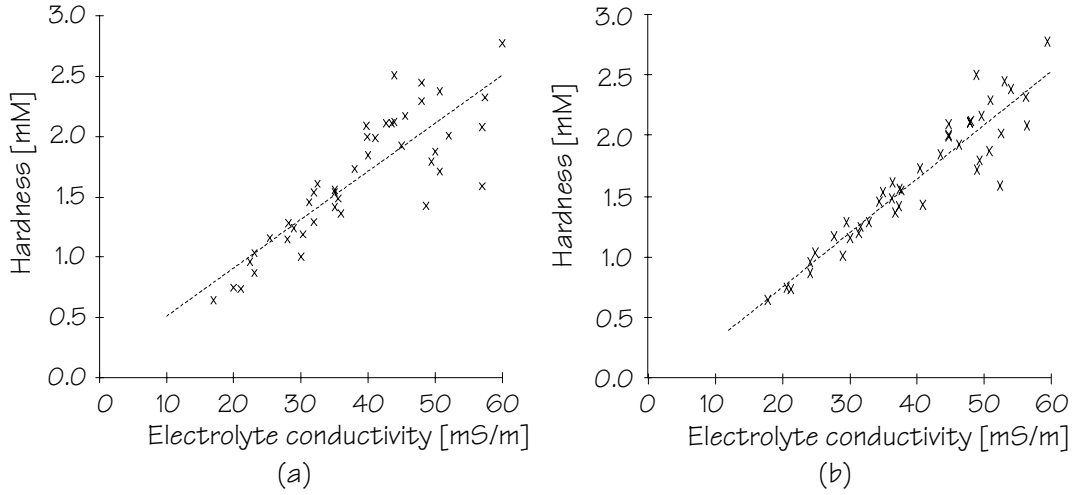

Figure 9.1: Correlation between water hardness and conductivity in 44 Dutch cities in 1986.
(a) Measured hardness and conductivity,
(b) the same, but after elimination of sodium from the conductivity

Any knowledge on other ions will increase the accuracy of the guessed hardness. For example, sodium sensors are easier to obtain than calcium sensors. By placing a sodium sensor in the same water as in which the conductivity is measured, the conductivity due to sodium can be subtracted from the total observed electrolyte conductivity. The result is a corrected conductivity which will have a larger correlation to the water hardness.
In figure 9.1b, the corrected conductivity is plotted on the horizontal axis for the same set of data which is used in figure 9.1a. The new correlation has become 0.94, which is obviously much larger. Also the average error in the approximated hardness has reduced to 7.8% and the maximum error is 38.4% now.
This example uses sodium, but knowledge concerning other ions will also increase the correlation. What can be seen from figure 2.3b, is that HCO_3^- has an even larger contribution to the conductivity of tap water than sodium. Therefore, knowing the concentration of this ion will increase the accuracy much stronger.

After applying the builder it is not possible any more to determine the hardness by measuring the conductivity while using a pre-defined slope. An exchange of one mole of calcium to two moles of sodium gives hardly a change in the conductivity of the liquid (in one litre an increase of 2×50.1 $\mu S\cdot cm^{-1}$ for sodium and a decrease of 119 $\mu S\cdot cm^{-1}$ for calcium) but the hardness decreases with one mole. Therefore, it is not

likely that the hardness can be guessed during washing based on the measured conductivity.

9.2 A conductivity cell on a PCB

The analysis of thermal properties, as carried out in chapter 6, gave the additional conclusion that printed circuit boards can be used as substrates for realising a planar heater. The very low thermal diffusion coefficient of printed circuit board materials might give a very efficient heating of water. However, in the context of this thesis, the realisation of the integrated sensor-actuator structure is preferably done using thin film technology. The reproducibility of fabricating small structures is extremely good using this technology. For thermoresistive measurements and heating, resistances can be defined with practical values, since the sheet resistance is in a convenient range.
As an alternative, printed circuit board technology can also be used to define planar metal structures, and is even more easy to apply. However, a PCB is provided with a copper layer which would be oxidised when used in wet applications. Therefore, it must be covered with a noble metal layer which can easily be applied by electro plating.
Since the sheet resistance of the copper layer is relatively low, making relatively high resistance values would require very narrow and long wires. This may become difficult because the wire width is limited by the photolithographic method used for defining the structures. Therefore, at first instance, no resistive structures have been made, but only a conductivity cell is produced.

9.2.1 Design and fabrication of the devices

The cell design as drawn in figure 9.2 is realised on a printed circuit board. The number of finger units is N = 5, the fingers have a width W = 0.2 mm and a spacing S = 0.16 mm. The total cell size is 2 × 2 mm², which is defined by casting with a Hysol® two component resin.

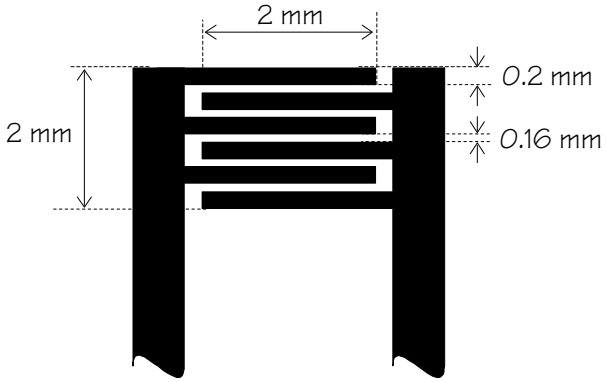

Figure 9.2: Layout of the conductivity cell on a PCB

Before the application of this resin, the tip of the sensor is electro plated with gold. These dimensions result into a theoretical cell constant of 2.308 cm^{-1} as can be calculated using equation 4.2.

9.2.2 Experimental

In figure 9.3a, the measured impedance sweeps recorded in potassium nitrate solutions of 0.5 to 100 mM are plotted. The curves are recorded using a HP4194A gain-phase analyser under unstirred conditions.

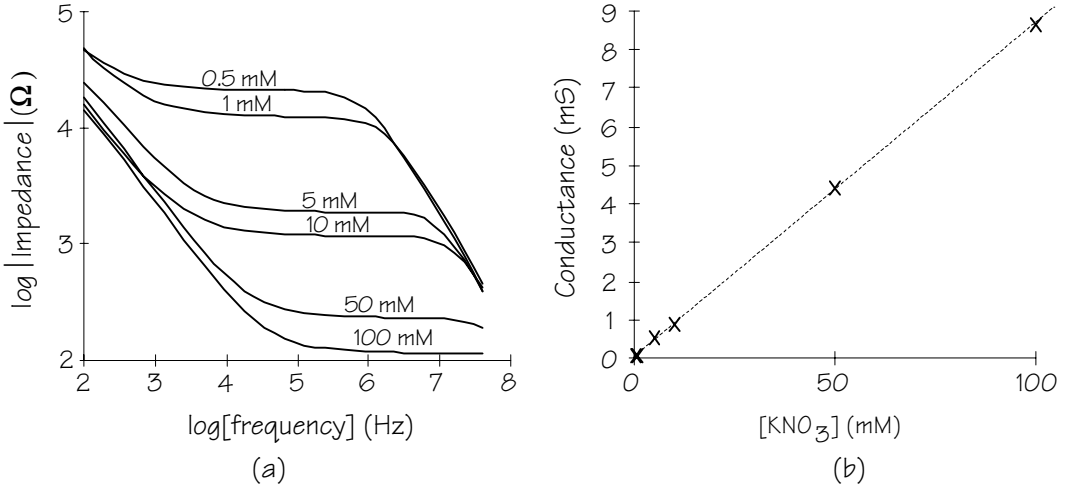

Figure 9.3: (a) Impedance versus frequency in various KNO_3 solutions and the (b) conductance at the plateau as a function of the KNO_3 concentration

Figure 9.3b is constructed by taking the reciproke of the impedance at the frequency independent regions in figure 9.3a. As described in chapter 4, this reciproke, which is equal to the conductance, is proportional to the electrolyte conductivity via the cell constant.

9.2.3 Discussion

The first remarkable point is the difference between the impedance sweeps, shown in figure 9.3a, and the sweeps recorded using the integrated sensor-actuator devices, as shown in figure 4.9. The observed widths of the frequency independent areas are much larger for the PCB sensors than when using the integrated sensors. This is probably the result of the larger size of the devices, shifting the low corner frequency to the left, according to equation 4.9. A frequency independent impedance is observed for almost two decades, which means that more than two decades of conductances (and also electrolyte conductivities) can be measured using a single operational frequency.
The measured conductances are perfectly proportional to the imposed potassium nitrate concentrations as can be seen in figure 9.3b. Since the conductivity of 100 mM KNO_3 is equal to 1.45 S/m [2], the measured

conductance of 8.66 mS results into a cell constant of 1.67 cm^{-1}. This is lower than the theoretical cell constant, probably because the model does not account for boundary effects.
So, the PCB conductivity cell can be used for determining conductivity. Although the cell constant could not be predicted very accurately, the performance is satisfying.

9.3 Integrated conductivity sensor - temperature actuator

Chapter 8 showed the interesting result, that it is in principle possible to use the integrated multi-purpose sensor-actuator structure of chapter 4 for determining specific ion concentrations. However, in that chapter the required technique of heating an electrolyte while monitoring the electrolyte conductivity was not applied using the integrated structure. The heating of a whole beaker filled with an electrolyte while monitoring the conductivity using a commercial conductivity meter was used instead.
An advantage of the integrated sensor-actuator device is that it can heat the environment locally, while the electrolyte conductivity can be monitored in the same local environment. This heating will be fast since this local volume is small. In addition, the temperature can be monitored simultaneously.
Up to now, the sensor and actuator functions present in the sensor structure were not used at the same time. The reason is that this was not yet necessary, since the processes monitored could be sampled sequentially which simplified the scheduling. However, for the conductivity versus temperature technique, the temperature must be known at exactly the same moment as the electrolyte conductivity. This requires a measurement technique capable of reading out two variables at the same time.

9.3.1 Measurement set-up

During some preliminary measurements, the integrated structure appeared to show (minor) permanent changes of its characteristics when it was used for heating. Although these changes are small, for the error sensitive conductivity versus temperature technique it would not be a good starting point to have a sensor which changes during a measurement. Therefore, heating during recording of the conductivity is not desired. A better idea is to heat first, and monitor temperature and conductivity during cooling down. Only then, possible permanent changes due to the heating are constant to every single conductivity and temperature sample.

Figure 9.4 shows the used measurement sequence. Starting with a device of type A as described in chapter 4, the local environment is heated. This is done by applying a 20 V top to top voltage of 10 kHz to one of the branches of the structure as shown in figure 9.4a. This heating power is maintained for a few seconds. Directly after switching off this power, the resistance of the other meander and the impedance at 1 MHz between the two meanders are measured simultaneously for about seven seconds. The resistance is a measure for the local temperature, and is calibrated before and after the experiment. The impedance at 1 MHz gives the electrolyte conductivity when the cell constant as determined in chapter 4 is used.

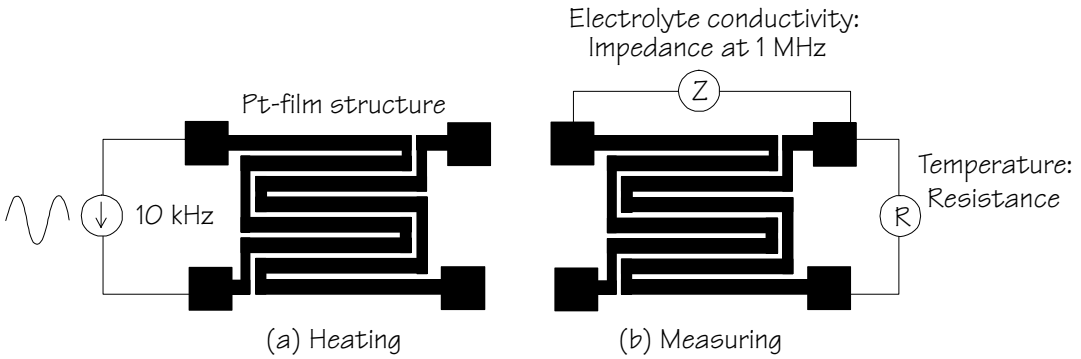

Figure 9.4: Measurement technique for determining the electrolyte conductivity at several temperatures. This technique uses (a) a heating step and (b) a measurement step

The control of this two step experiment is carried out by a LabView 3.1 program. Switching between the sine wave generator and the measurement equipment is done using four relays, switched using a control line of the serial computer port. The impedance is measured using a HP4194A gain-phase analyser, controlled and read out with the GPIB bus. Measuring the resistor is done using a HP34401A multimeter, also read out using the GPIB bus. No cross interference between the measurement of electrolyte conductivity and temperature is observed since these are recorded using different loops.
The solution, which consists of 100 mM KCl in demi water with a quality of 0.5 $\mu S/cm$, is not stirred during the measurement.

9.3.2 Experimental

Figure 9.5 shows the recorded transient responses of both the electrolyte conductivity and temperature just after switching off the heating power. For converting the recorded resistance into an equivalent temperature, the calibration data obtained by heating a beaker with water while monitoring the resistance is used as described in chapter 4. This appeared to give almost equal results before and after the actual experiment. The conductivity cell operation is not calibrated here, but

the cell constant, as determined with the experiments described in chapter 4, is used.

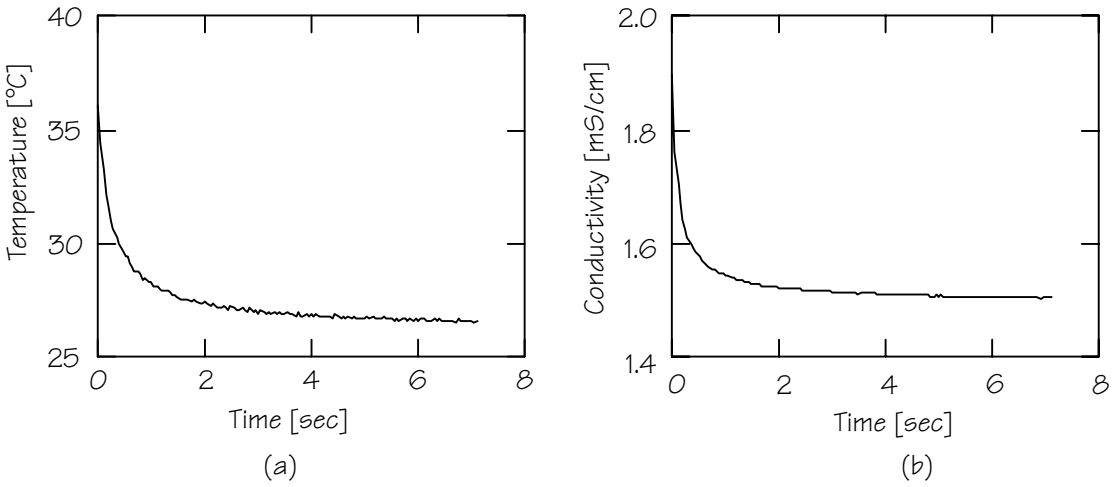

Figure 9.5: Measured (a) temperature and (b) conductivity while cooling down

The data plotted in figure 9.5 can be combined to form one single graph with the electrolyte conductivity as a function of temperature. This is shown in figure 9.6.

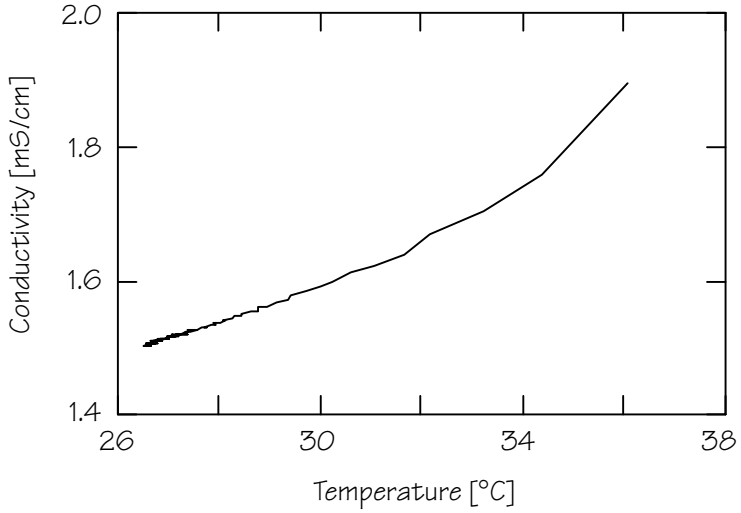

Figure 9.6: Electrolyte conductivity as a function of temperature as measured with the integrated sensor-actuator structure

The result is a curve which does not have an equidistant distribution of measurements points. In the range from 32 °C to 36 °C the number of points determining the curve is much lower than below 28 °C. The reason is that the points are measured at constant time intervals which results into unequal temperature intervals as can be seen in figure 9.5a.

9.3.3 Discussion

A curve necessary for applying the ion fitting theory of chapter 8 can be made using the integrated sensor-actuator structure as presented in chapter 4. However, the theory can not directly be applied since the polynomial coefficients, describing the temperature dependency of the ionic conductivities, as valid for bulk heating are no longer valid for local heating.

This is the result of the temperature which is not equal at every single place in the solution. The temperature as plotted on the horizontal axis in figure 9.6 is not the water temperature, but the temperature at the heater surface. In the vicinity of the heater, the temperature profile in the solution as given by figure 6.8 is observed. So, the conductivity cell will measure in an inhomogeneously heated volume of water. An impression of the measurement depth of a conductivity cell can be obtained by realising that 90% of the current flows in a layer thickness of $2/3$ times the finger width plus spacing (which can be calculated based on the theory presented in [3]). So, a conductivity cell with a finger width of 200 μm and a finger spacing of 5 μm measures the conductivity approximately up to a depth of $2/3 \times 205$ μm into the solution. According to figure 6.8 the temperature drops significantly across this depth.

It can be questioned whether the ion fitting method is valid at all when the temperature is not homogeneous. The validity can be proven by the following argument. Consider an infinitely large planar heater covered by water. During heating, a temperature profile will occur in the water. Nevertheless, at equidistant planes parallel to the heater, the temperature will be constant. The observed conductivity is the summation of the conductivities of these parallel planes with each their own instantaneous temperatures. To describe this by means of a formula, using a heater power P and defining each slice at a distance z to the heater, the total conductivity becomes

$$\Lambda(P) = \sum_{z=0}^{\infty} \Lambda_z\left(T_z\right) \tag{9.1}$$

where the power P is the cause of the temperature profile T_z. In chapter 8, the conductivity of an electrolyte with a uniform temperature was given by (8.4):

$$\Lambda(T) = \sum_{i=1}^{I}\left[\left|z_i\right| c_i \lambda_i^0 \sum_{j=0}^{J} k_{i,j}\left(T - T_0\right)^j\right].$$

Substitution of (8.4) into (9.1) and changing the order of summation yields

$$\Lambda(P) = \sum_{z=0}^{\infty}\sum_{i=1}^{I}\left[\left|z_i\right|c_i\lambda_i^0\sum_{j=0}^{J}k_{i,j}\left(T_z - T_0\right)^j\right]$$
$$= \sum_{i=1}^{I}\left[\left|z_i\right|c_i\lambda_i^0\sum_{j=0}^{J}\sum_{z=0}^{\infty}k_{i,j}\left(T_z - T_0\right)^j\right]$$

where the part of the expression which is dependent on the distance z can be changed to

$$\sum_{z=0}^{\infty}k_{i,j}\left(T_z - T_0\right)^j = k^*_{i,j}\left(T^* - T_0\right)^j$$

using a generalised temperature T^* and a new set of coefficients $k^*_{i,j}$. The generalised temperature is free to choose, but could be the temperature at the heater surface, for example. The new coefficients $k^*_{i,j}$ are not dependent on temperature. So, what is achieved by this manipulation is that it proves that a set of coefficients can be defined with which the conductivity at a generalised temperature can be calculated. This overall observed conductivity can be expressed by

$$\Lambda\left(T^*\right) = \sum_{i=1}^{I}\left[\left|z_i\right|c_i\lambda_i^0\sum_{j=0}^{J}k^*_{i,j}\left(T^* - T_0\right)^j\right] \qquad (9.2)$$

which is functionally equal to equation (8.4), but now in a non-homogeneously heated solution.

The presented evaluation does not account for the electrical field line distribution, which is not homogeneous either. A slice of water which is close to the conductivity cell, will affect the measured conductivity more than a slice which is located at a larger distance from the cell. Only when the temperature is not homogeneously distributed, this effect will be of interest. This confirms once more that the simple coefficients can not be used any more.

In conclusion, the ion fitting theory of chapter 8 can be applied to the situation where an electrolyte is heated locally by a dissipator, while the conductivity is monitored. However, the polynomial coefficients describing the temperature dependencies of the ionic conductivities are no longer valid. New coefficients have to be determined for this specific system.

9.4 References

[1] Statistiek wateronderzoek 1986, Vereniging van Exploitanten van Waterleidingbedrijven VEWIN, Rijswijk, 1986

[2] D.R. Lide, Handbook of chemistry and physics, 74th edition 1993 - 1994, CRC Press, Boca-Raton, Florida

[3] P. Jacobs, A. Varlan, W. Sansen, Design optimisation of planar electrolytic conductivity sensors, Medical & Biological Engineering & Computing, November 1995, page 802 - 810

CHAPTER 10

Concluding remarks and suggestions for further research

In this thesis, general concepts for integrating sensors into a single multi-purpose structure have been described, with the monitoring of washing processes as a practical application. This resulted into the integrated sensor-actuator structure of chapter 4 as an optimal design.
In the first section of this chapter, the conclusions are drawn of the most interesting achievements. The results are grouped based on the choice of implementation, used measurement techniques and the final set of variables which can be measured in washing processes. In the second section, some suggestions for further research are given.

10.1 Concluding remarks

An optimal reduction of the energy and water consumed with washing in a machine can be achieved when the process is adapted during washing. In addition, when the detergent can be applied in separate components, a reduction of consumed detergent is possible as well since only the components that are needed can be added. To optimise the process during washing by controlling detergent, water inlet, mechanical action and temperature, information concerning the washing is needed. So, for increasing the efficiency of washing in a machine, the use of sensors in the washing water is essential.
These sensors must give an impression of the state of the washing process. In other words: an array of sensors is desired from which outputs both information on the soil and the detergent effect can be deduced.
The scientific challenge of designing such an array of sensors, is to get a maximum amount of information from a sensor array which is as simple as possible. Therefore, the integration of sensors into a single multi-purpose structure is desired. The incorporation of actuators together with these sensors is interesting as well, since then dynamic measurements are possible which might give new information concerning the system.

10.1.1 The chosen fabrication technology and materials

The major part of the variables of interest appeared to be measurable with sensors consisting of planar, inert metal structures. Advantages of

planar, inert metal structures are that they will have a relatively long lifetime and that they can be cleaned easily without being destroyed. The first choice was to realise such structures using photolithographic techniques as known from silicon technology, since this technology is suitable for mass production and can be used to reproduce accurately the desired structures. Using this technology, a geometrically integrated sensor-actuator structure is developed and tested using platinum structures.

A thermal evaluation of heat absorption by both the substrate material and the water to be heated, yields that a quartz substrate will result into more efficient heating of water than in case a silicon substrate is used. For the practical realisation of the device, however, a cheaper alternative of quartz, being Hoya® SD-2 glass, is chosen.

Packaging of the device is preferably done on a strip of printed circuit board material. Such a strip turns the small device into a convenient dipstick, while also the electrical connection can be established using copper traces on the PCB. In addition, the counter/reference electrode necessary for amperometric experiments can easily be implemented on the back side of this strip by electro plating a copper area with gold.

10.1.2 Obtaining selectivity

When carrying out multiple experiments using a single structure, this structure must be as universal as possible. Therefore, selectivity in sensing is preferably not achieved by the definition of the structure and used material, but by smart control and mathematical evaluations.

Two major examples of selectivity which is not achieved by the sensor, but by the method of control, are reported in this thesis. The first example is the amperometric measurement of bleach activity. A method is introduced which uses the potential at which a current peak occurs as a marker. By measuring a current at this peak, a certain level of selectivity is obtained. The amperometric measurement of bleach activity also has another conceptually interesting aspect. Since the washing parameter, bleach activity, is measured in the way bleach is supposed to work, it has become a universal method, not dependent on the typical substance accounting for the bleach operation. Measuring bleach activity by observing the oxidising strength is therefore superior to the application of a selective sensor for, for example, hydrogen peroxide.

The second example is the fitting of specific ion concentrations by mathematical treatment of the electrolyte conductivity at several temperatures. While a conductivity measurement is not selective for specific ions, the response of the conductivity on heating does give ion specific information. This information can be extracted by assuming a set of ions (with known temperature dependencies of their specific conductivities) and estimating the best ion concentrations that fit with the measured conductivity-temperature relation.

10.1.3 Stimulus-response measurements

Both methods for creating selectivity, as mentioned in the previous subsection, are based on the application of a stimulus while measuring. Functional integration of sensors and actuators has proven its interest more than once.
The mentioned selectivity creating methods resulted into knowledge concerning new variables. Another example of a successful stimulus-response measurement which yields a new variable is the measurement of water movement (flow) by heating the local environment while monitoring temperature. A faster movement of the water results into a lowering of the observed local temperature. Theoretically, the application of a cloud of electrochemically generated H^+ ions while measuring the local electrolyte conductivity will also give a measure for the fluid motion.
Besides finding new variables, in some cases stimulus-response measurements give a reduction of noise. Using the integrated sensor-actuator device, the measurement before and after the stimulus is carried out using the same sensor. Therefore, the same offset (noise) will be observed which can be eliminated by subtracting the sensor outputs. This is referred to as a time differential measurement.

10.1.4 Measurable variables and washing parameters

The designed integrated sensor-actuator structure of chapter 4 has a small sensor area of 1×1 mm^2. Since all the variables are measured using the same sensor area, the measured information will be of the same local volume. The measurements which can be carried out using this structure do not need sample transport through a channel or other additional fluid handling, but can be carried out in the bulk of the sample solution.

The device has the possibility of directly measuring three variables, being temperature, bleach activity and electrolyte conductivity. In addition, the structure can heat its local environment and the local pH

can be changed by the electrolytical generation of H^+ or OH^- ions. When the information from the sensors is combined, together with the measured responses of the sample solution on the actuators, much more variables can be retrieved by smart data interpretation. Since the device will be used for monitoring washing processes, the measured variables must be interpreted as washing parameters.

In the tap water used for washing, the electrolyte conductivity can be measured. It appeared that the conductivity of tap water shows a large correlation to the water hardness. An estimation of the hardness based on the observed conductivity can be used for reducing the amount of added builder. Another option for determining the tap water hardness, is to apply the technique using the conductivity at several temperatures. Although this technique theoretically creates a much larger selectivity for calcium, it is probably too sensitive to errors since the number of ions observed in tap water is quite large.

After the laundry is soaked by the tap water, the conductivity can be measured again. Soluble parts of the soil present on the fabrics will dissolve in the water. Therefore, the new conductivity will be the result of both the conductivity of the tap water and charged soil particles.

Then, the detergent is added and the soil on the fabrics and in the water is affected. Directly after adding the detergent, there is not yet any washing effect, but slowly the added detergent is consumed by the soil. For example, when the bleach is monitored using the integrated sensor-actuator device switched as an amperometric working electrode, the decay of the bleaching component can be visualised. Based on the speed of this decay, the operator can decide to add more bleach or to stop the bleaching cycle. A similar monitoring of washing operation can be done based on the electrolyte conductivity. The builder component will capture charged particles from the washing water, which results into a lowering of the conductivity during washing. Either the addition of more builder, or stopping the main wash can be the appropriate action.

Monitoring temperature and flow speed is not needed in a normal washing machine. A machine can impose a desired temperature using its own thermostat and can apply a rotational speed of the tub resulting in a known mechanical washing action. Nevertheless, in some cases the sensor system is not capable of accessing the temperature and rotational speed control system of the washing machine for technical reasons. In that case, the subsystem containing the sensors must retrieve these variables itself. Then, based on the flow sensor, this subsystem can

determine itself whether the tub is rotating, and can use the temperature sensor for measuring the water temperature. In addition, for research purposes, the small flow sensor is a helpful tool for monitoring the local turbulence (mechanical washing operation) at any location in the tub.
Notice that although the knowledge of temperature itself might not always be of interest, the temperature sensing operation is needed for some sensor-actuator operations.
When, at the end of the main wash, the water and laundry in the tub do not consume added builder and bleach anymore, the washing process can probably be stopped. The next step is a series of rinsing cycles, in which the possible excesses of detergent and residues of washing are removed. The integrated sensor structure can then be switched into the conductivity sensing mode for determining when the residues are removed, and the rinsing can be stopped.

The tested ranges for measuring electrolyte conductivity, temperature and bleach activity using the proposed implementation of the integrated sensor-actuator structure cover the ranges observed in washing processes. These ranges are summarised in table 4.4. Therefore, the device can directly be applied for monitoring the washing process concerning these variables. The device, switched as a sensor for the local movement of washing water, is tested in a practical range as well, when assuming that the water will locally not move faster than imposed by rotation of the tub.

Only bleach activity has been measured in real detergent while the other sensor functions are tested in model solutions. Nevertheless, no fundamental problems are expected when measuring conductivity, temperature and flow in a washing machine, since the sensor design is based on a rigid structure and these three variables are in principle not affected by chemical interferences.

10.2 Suggestions for further research

The set of variables which can be measured with the described design for an integrated device does not completely cover the parameters determining a washing process. Future research on the integrated device should aim at the missing variables in order to employ it even more favourably in washing processes. Besides implementing missing variables, future research can focus at some inspirations which arose for extending the achievements.

10.2.1 Washing parameters not measurable with the existing device

The most important washing parameters which are not measurable directly using the integrated device are surfactant concentration, pH and hardness. The measurement of surfactant concentration has been carried out in an earlier Ph.D. project which has been conducted by Alex Volanschi [1, 2]. The developed sensor is capable of measuring dynamic surface tension which can be related to surfactant concentration. The technology for fabricating this sensor allows it to integrate it with the integrated sensor device without too much additional processing steps. Nevertheless, this was not done because no possibilities for functional integration are likely. The dynamic surface tension sensor will remain a sensor on itself because the integration with actuators and other sensor information will probably not increase its functionality.

The implementation of a pH sensing function in the integrated device will probably require some concessions which will affect the simplicity of the design. In general, determining pH requires an absolute reference potential which should be created using a reference electrode. Although a potentiometric pH electrode itself can be fabricated by oxidising a metal, the fabrication of a reference electrode does not fit within the chosen technology. So, for implementing a pH sensor, more research will be necessary on how to realise this efficiently.

An estimation of the water hardness can be done in tap water as reported in chapter 9. However, after the detergent is added this method can not be used anymore. Therefore, a method for determining hardness in washing water is still needed. The next subsection gives a preliminary measurement of a method which would be an optimal hardness determination.

10.2.2 Measuring hardness: a preliminary measurement

The integrated sensor-actuator structure can be used to increase the local pH by the reduction of water. At a certain pH, hardness ions will precipitate, which can be monitored with the same structure switched as a conductivity cell. This technique is a coulometric precipitation titration with conductivity sensing as the end point detecting method. Because the capability to precipitate is measured, this method gives the desired parameter, independent of what substance is actually responsible for the precipitation. In subsection 7.2.4 this idea has already been proposed, and a theoretical graph of a volumetric precipitation titration with a conductivity measurement is given there.

As a preliminary measurement, the precipitation titration of calcium nitrate with sodium hydroxide ions is performed. A volumetric titration is chosen because then the dosed amount of hydroxide ions can be controlled accurately, a coulometric titration would give an inhomogeneous OH^- profile.
The used conductivity meter is a Radiometer CDM210 which is used in combination with a Radiometer PP1311 two points conductivity probe. This is a special probe for precipitation titrations with the electrodes on the outside, ensuring that there are no dead volumes. The cell constant of this probe is equal to 2.27 cm^{-1}.
The titration is carried out using a burette filled with 1 M sodium hydroxide, from which volumes of 0.1 ml are dosed. The sample is 10 ml of either a 70, 80, 90 or 100 mM calcium nitrate solution, resulting in theoretical end points at 0.14, 0.16, 0.18 and 0.20 mole sodium hydroxide supplied per litre (when the volume change is not taken into account). The solution is stirred during the complete experiment, and the conductivity is measured 10 seconds after the addition of titrant.

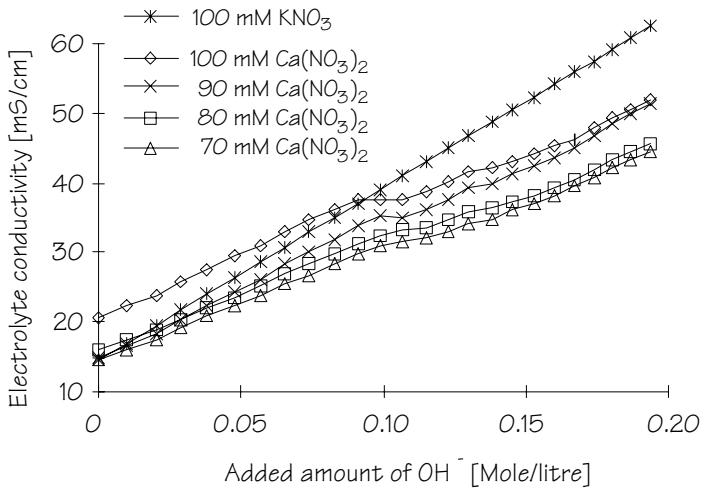

Figure 10.1: Volumetric titration of calcium by sodium hydroxide

The recorded curves are shown in figure 10.1. As a reference, a solution of 100 mM potassium nitrate is titrated as well, which should show a uniform increase in conductivity. On the horizontal axis, the added amount of OH^- ions is plotted, divided by the volume of the sample plus added titrant.

The curve for potassium nitrate shows the expected uniform increase in conductivity due to the added sodium hydroxide. On the other hand, the curves for the sample solutions, where calcium ions are present, show a discontinuity due to precipitation. However, the shape of these curves does not correspond to the theoretical curves as plotted in figure 7.5. Initially, the conductivity is of course equal to the conductivity of

calcium nitrate. But when adding sodium hydroxide, the conductivity increases proportionally to the conductivity corresponding to this amount of sodium hydroxide, even before reaching the theoretical end point. This indicates that precipitation does not take place which means that the solution is super-saturated. At a certain moment a discontinuity is observed. Although probably the precipitation of calcium hydroxide is initiated then, the measured curves are still not conform theory.

So, an effect due to the precipitation of calcium ions with hydroxide ions is observed, but the actual shape of the titration curve can not be explained by the theory based on complete precipitation. Instead of this, the conductivity measured 10 seconds after adding sodium hydroxide indicates a super saturation of the solution. This problem can probably be solved by the use of a nucleation core, since then the precipitation will be fastened. Only when this problem is solved for the volumetric titration, the same can be done with a coulometric titration using the integrated sensor-actuator device.

10.2.3 Conductivity and temperature

A method for fitting ion concentrations using the temperature dependency of the electrolyte conductivity is described in chapter 8. Although this method is successfully applied in simple solutions, direct success when applied in a washing process is not expected. The first reason is that the number of ions that can be fitted accurately is limited. A probably even more problematic shortcoming is that the method can not be applied in systems where the conductivity is changing due to other phenomena than the temperature dependency of the ion mobilities. An example of such an interfering phenomenon is the temperature dependency of equilibria like acid-base and solubilities. The response on the heating of water in a washing machine during washing is probably too complicated.

However, when a random set of ions is assumed, which are not necessarily the conductivity determining species, still “concentrations” of these ions can be fitted when the algorithm is applied. In that case, the resulting set of ions will not represent real concentrations but rather a characteristic fingerprint of the solution. The conclusions which can be made based on such a fingerprint should be evaluated.

Another approach is to try to define a local volume in which the composition is a simplification of the washing water. For example microdialysis or ultra filtration membranes will allow only a subset of the elements in the washing water to pass. An even higher level of

filtration is achieved using nanofiltration [3, 4]. Nanofiltration membranes are reported with molecular cut-offs of 200 to 1000 Da. So, a chamber covered with such a membrane will have a reduced set of particles when placed in a washing machine. It would be interesting to know if this subset is simple enough for the ion fitting method.

Sometimes, by using some pre-knowledge, the system is actually easier than it seems. When the ratio of two ion concentrations is constant, they can be taken together into one new polynomial. Or, sometimes, a whole category of ions can be represented by one generalised polynomial. For example, the ratio between calcium and magnesium in tap water is in practice equal to 4:1. Therefore, an imaginary ion can be used which is represented by four times the conductivity of calcium and one time the conductivity due to magnesium. This imaginary ion can be fitted as a single ion.

10.2.4 PCB sensors

From the thermal analysis carried out in chapter 6, printed circuit board materials appeared to be suitable substrate materials for realising a planar heater. However, although a PCB-based conductivity cell was successfully tested, the complete integrated sensor-actuator device is not yet produced using this very cheap material. The reason is that the thickness of the copper layer on PCBs is fixed resulting into a bad trimming possibility for defining planar resistors.
A solution to this problem can be the partial etching of the copper layer in an $Fe(Cl)_3$ solution. First, the planar structure is defined using photolithography on a strip of PCB material, with the sensor structure at the tip and copper connecting wires to the other side of this strip. Then, the strip is covered with resin, except for the sensor area and the pads to solder wires on. When subsequently the tip of this strip is placed in copper etchant, the copper defining the sensor area will become thinner. By monitoring the resistance while etching, the resistance can be trimmed. Afterwards, the tip is plated with gold.
Using this processing sequence, planar resistances can be defined without being limited by the default copper layer thickness.

10.2.5 Flow measurement using ions as a marker

A remarkable result of chapter 7 concerning sensor-actuator operations, refers to the determination of flow using either time of flight or indicator dilution methods. Based on the difference in diffusion speed of heat and ions in water, the use of an ionic marker for the detection of flow speed will be more efficient than when using heat as a marker. An

ionic marker will remain longer in a defined volume since the diffusion is relatively low. In addition, while leaking of heat out of the system is possible through the walls and via the sensor substrate, ions can not leave the water in principle. This will result into a larger signal to measure, and therefore lower flow rates can be detected.
The possibility to use an ionic marker was already mentioned in literature [5], but the advantage of the lower diffusion rate was not yet noticed.

10.3 References

[1] A. Volanschi, Dynamic surface tension measured with single nucleation site electrodes, thesis, University of Twente, 1996

[2] A. Volanschi, W. Olthuis, R.T.J.M. van der Heijden, P. Bergveld, European Patent Application nr. 94203609.6. deposited at the European Patent Office in Rijswijk, December 13, 1994

[3] Toshinori Tsuru, Shin-ichi Wada, Shuhei Izumi and Masashi Asaeda, Silica-zirconia membranes for nanofiltration, Journal of Membrane Science, vol. 149 (1998), page 127-135

[4] J.M.M. Peeters, J.P. Boom, M.H.V. Mulder and H. Strathmann, Retention measurements of nanofiltration membranes with electrolyte solutions, Journal of Membrane Science, vol. 145 (1998), page 199- 209

[5] B.H. van der Schoot and P. Bergveld, An ISFET-based microlitre titrator: integration of a chemical sensor-actuator system, Sensors and Actuators, 8 (1985), page 11 - 22

List of publications

G.R. Langereis, W. Olthuis and P. Bergveld, Measuring conductivity, temperature and hydrogen peroxide concentration using a single sensor structure, Proc. Transducers ’97, Chicago, June 16-19, 1997, page 543 - 546

G.R. Langereis, W. Olthuis and P. Bergveld, Using a single structure for three sensor operations and two actuator operations, Sensors and Actuators B, 53/3, page 197 - 203, April 1999

W. Olthuis, S. Böhm, G.R. Langereis and P. Bergveld, Selection in sensor and system, Proc. 217th American Chemical Society National Meeting, Devision of Environmental Chemistry, Anaheim, March 21-25, 1999

Multi-sensing method and device, G.R. Langereis, W. Olthuis and P. Bergveld, European patent application 98202690.8, Unilever N.V., filing date: August 11, 1998

Summary

Two actions are of interest when washing clothes in a washing machine. First, the electronics in the machine control two physical washing parameters, being movement and heating. By the rotation of the tub, both water and laundry is moved, which results into a mechanical washing. In addition, a heating coil can be switched on in order to control the water temperature. Second, the most important part of washing is determined by the detergent. In the detergent, several components are present which affect specific types of soil.
Because washing consumes much energy and water, and the detergent comes in the environment with the waste water, reducing the consumption of these is important. Although both the washing program and the dosing of detergent is controllable up to a certain limit, there is no mutual communication. To bring about an efficient reduction of consumed energy, water and detergent, intelligent co-operation between detergent dosing and the washing program is necessary. This can only be achieved by employing sensors for linking the chemical information to the electronic control in the machine.
This thesis deals with the development, realisation and testing of an array of sensors for determining the state of a washing process. To combine the sensors in a single array, some techniques are used.
First, the sensors which are integrated are chosen with respect to their fabrication materials and technique. By matching these, the sensors could be combined into a single multi-purpose structure. A reduction of the number of connecting wires is the result, and the single structure will measure all parameters at the same spot in the solution.
In addition, together with sensors, also actuators are integrated. This enables the possibility of performing stimulus-response measurements. Such experiments are based on recording the response of solution components on an imposed local disturbance. Sometimes, such dynamic measurements give new information on the solution.
Finally, the combination of sensor readings, together with the results of the stimulus-response measurements, yields a set of data which can be used for smart interpretation and decisions.
The final result is a system consisting of a small noble metal structure, applied on a carrier, with a size of only one square millimetre. By scheduling this structure in several operational modes, the following washing parameters can be measured: temperature, bleach activity, electrolyte conductivity, movement of the washing water and the

temperature dependency of the electrolyte conductivity. The latter one can give information on the individual types of charged particles in the solution.
Finally, some suggestions are given in order to implement washing parameters that are missing in the measurable set of variables.

Samenvatting

Bij het wassen van kleding in een wasmachine spelen twee processen een rol. Ten eerste voert de elektronica in de machine een programma uit dat zorg draagt voor een fysische waswerking. Door de trommel te bewegen komt een beweging van het wasgoed en waswater tot stand resulterend in mechanisch wassen. Ook zorgt de machine voor het doorlopen van een temperatuur programma van het waswater. Ten tweede resulteert het toegevoegde waspoeder in een chemische waswerking. In het waspoeder bevinden zich wascomponenten die ieder aangrijpen op een specifiek soort vuil.
Omdat wassen een aanzienlijke hoeveelheid energie en water verbruikt, en tevens het milieu belast met de afvoer van het waswater, is reductie hiervan van groot belang. Hoewel zowel het wasprogramma als de hoeveelheid gedoseerd waspoeder enigszins stuurbaar is, is er tussen beide stuurmechanismen geen wisselwerking. Voor een efficiënte afname van verbruikte energie, water en waspoeder is het noodzakelijk dat er een intelligente samenwerking is tussen de dosering van waspoeder en het mechanisch wassen. Dit kan slechts tot stand komen door sensoren in een wasmachine te plaatsen die informatie over de chemie aan het elektronisch brein van de wasmachine kunnen geven.
In dit proefschrift wordt beschreven hoe een sensorsysteem is ontworpen, vervaardigd en getest waarmee een indruk van de toestand van het wasproces verkregen kan worden. Hierbij is een aantal technieken gebruikt om de sensoren in het systeem te combineren.
Ten eerste zijn de sensoren die in het systeem geïntegreerd zijn zo gekozen dat ze gemakkelijk tot één multifunctionele structuur konden leiden op basis van materiaalkeuze en vervaardigingswijze. Dit leidt tot een afname van het aantal aansluitdraden tot vier, en tevens tot een structuur die steeds op hetzelfde punt in het waswater meet.
Daarbij komt, dat samen met de sensoren, ook actuatoren geïntegreerd zijn. Hiermee kunnen chemische experimenten uitgevoerd worden waarbij opzettelijk de chemische samenstelling van het waswater lokaal verstoord wordt, terwijl de respons op deze verstoring gemeten wordt. Een dergelijke meting wordt een stimulus-respons meting genoemd en heeft als voordeel dat soms nieuwe parameters gemeten kunnen worden.
Tenslotte levert het combineren van alle verkregen sensor uitlezingen met de resultaten van de stimulus-respons metingen nieuwe gegevens op na intelligente bewerking.

Het uiteindelijke resultaat is een sensor systeem dat bestaat uit een kleine metalen structuur op een drager met een totaal oppervlak van slechts één bij één millimeter. Hiermee kunnen, na uitlezing met de juiste elektronica, onder andere de volgende wasparameters bepaald worden: temperatuur, bleekactiviteit, elektrische geleidbaarheid en beweging van het waswater en tevens de temperatuur afhankelijkheid van de elektrische geleidbaarheid. Deze laatste kan informatie opleveren over de afzonderlijke soorten geladen deeltjes in het waswater.
Voor de wasparameters die nog niet direkt te meten zijn met de ontwikkelde structuur, worden tenslotte aanbevelingen gegeven om het geïntegreerde sensor systeem uit te breiden.

The author

Geert Langereis was born in Apeldoorn, the Netherlands, on April 11, 1970. He received the M.Sc. degree in Electrical Engineering from the University of Twente, Enschede, the Netherlands in 1994. During his study he achieved both a biomedical and an ergonomical endorsement. He conducted the Ph.D. project on integrated sensor arrays as described in this thesis in the Biosensor Group, part of the MESA Research Institute, of the University of Twente. In June 1999 he will start as a research scientist at Philips Research Laboratories, Eindhoven.

Dankwoord

“Hoe gaat het met je wasbol?” is de meest getoonde uiting van interesse in mijn werk zoals beschreven in dit proefschrift. Deze enigszins cynische uitlating is natuurlijk het gevolg van het lachwekkende imago van wasmiddelen zoals opgelegd door de reclamewereld. Toch hoop ik met dit proefschrift duidelijk te maken dat er achter het onderzoek naar wassystemen wel degelijk wetenschappelijke kennis schuilt. Misschien zullen jullie ooit eens durven te bevestigen dat jullie je schone onderbroeken voor een deel ook aan mij te danken hebben.

De wassensor was niet wat geworden zonder het juiste wasprogramma zoals afgedraaid binnen de leerstoel Biosensoren. Wie zich de taak van bleekmiddel en wasverzachter heeft toegeëigend weet ik zelf niet, maar het staat vast dat Piet Bergveld en Wouter Olthuis samen voor het grootste deel bepaald hebben wat er uiteindelijk van mijn tere weefsels geworden is. Voor zowel het verschaffen van inhoudelijke kennis als het begeleiden van mijn leerproces zijn zij van onschatbare waarde geweest.

Daarnaast is er de nodige kennis en interesse beschikbaar gesteld door enkele personen van Unilever te Vlaardingen. Achtereenvolgens Antoine Rocourt, René van der Heijden, Robert-Jan Uhlhorn, Jan-Paul Janssens, Jan-Peter Heida en tenslotte, onze ex-collega, Alex Volanschi zijn in de afgelopen vier jaar één voor één aangewezen geweest om toe te zien op de praktische bruikbaarheid van het was-meetsysteem.

Een andere bron van inhoudelijke kennis is 3T-BV, waarvan de werknemers bij onze leerstoel koffie dronken en taart aten. Albert Prak, Jeroen Wissink, Mirthe Wehrmeijer en Ke-Chun Ma om er maar enkele te noemen.

Een vierde groep personen die het project ondersteund heeft, bestaat uit een aantal personen van de gehele vloer 6. De meest opmerkelijke is toch wel Johan Bomer. Hij kan in de cleanroom meerdere processen tegelijk uitvoeren, terwijl hij de koffie zet en vervolgens niet klaagt wanneer deze opgedronken is als hij er zelf aan toe komt. Daarnaast was het prettig om de kantoor-tuinman Sjouke Hornstra en mini-fietsenmaker Ton Verloop altijd in te kunnen schakelen voor allerlei vragen en taken. Voor vragen over elektronica waren er altijd Ad Sprenkels en Ed Droog, ook al had ik daar niet altijd een antwoord op.

Truus Steijlen was zeker onmisbaar voor administratieve taken, en het oplossen van problemen die het gevolg waren van de keren dat ik zelf de administratieve taken probeerde uit te voeren.

Ties Bos van de vakgroep Chemische Analyse van de Chemische Technologie faculteit heeft zich meerdere malen bewezen als een handige vraagbaak op het gebied van chemische vraagstukken.

De grootste stappen in de voortgang vonden telkens plaats wanneer er een student begeleid moest worden bij een project of afstudeeropdracht. Sergio Botti, Radko Bankras, Christiaan Lievers, Erik Roos, Jasper van der Neut en Gideon Steijns, bedankt.

Tja, dan de kamergenoten. Door een vreselijke speling van het lot trof ik bij aankomst Joost Lötters en Jans Kruise samen in één kamer. Ik was getuige van het scrupuleuze beoordelingsvermogen van Jans hetgeen op mens-onterende wijze werd verbrijzeld door de onbenullige overmaat van kwetsende taal uitgestoten door Joost. Het dieptepunt vond plaats toen het proefschrift van Jans tot muismat werd vernederd. Ik deed niets toen Joost om zijn eigen actie lachte terwijl hij een boterham met sterk riekende salami met open mond vermaalde. Misschien was zijn meest vreselijke grap wel het vinden van een goede baan, een ware klap in het gezicht voor iedereen die wél zijn best doet.
Na het Jans en Joost tijdperk kwam de Hans Albers en Helma Kaptein periode. Pas toen bleek dat je met kamergenoten ook inhoudelijk over werk kon praten en dat je elkaar daarbij niet hoeft te kwetsen.

De paranimfen Bart Kooi en Joost Lötters (zie boven) dank ik voor het nalezen van het concept proefschrift en voor het uitvoeren van de belangrijke taak van decor-vulling op de dag van de promotie.

Tenslotte het thuisfront. Zonder Kitty zou ik zonder meer geëindigd zijn als een ziekelijke Willie Wortel en een genuanceerd beeld over de werkelijke zin van het leven gemakkelijk hebben kunnen verliezen. Ook de kinderen, Tara en Erin, lieten mij zien dat het moeilijkste vak niet het eerstejaars Elektromagnetisch Veld Practicum is, maar het levens-practicum peuter-opvoeding. Zij zijn de beste sensor-actuator systemen die ik tot nu toe gemaakt heb, ook al is het actueren voorlopig nog beperkt gebleven tot het vullen van luiers.

Geert Langereis, 8 april 1999

Stellingen

Behorende bij het proefschrift

1 - De modulaire opbouw van een chemisch analyse systeem volgens het µTAS concept vormt een beperking voor het integreren van sensor arrays.
D.J. Harrison and A. van den Berg, Micro Total Analysis Systems '98, Proceedings of the µTAS '98 workshop held in Banff, Canada, 13-16 October 1998; Dit proefschrift, hoofdstuk 4

2 - De variabele die men overweegt te meten om een proces te volgen, dient zo nauw mogelijk aan te sluiten bij het doel van dat proces.
Dit proefschrift, hoofdstuk 10

3 - Het is in principe mogelijk hardheid van water te meten met de voorgestelde geïntegreerde sensor structuur door middel van een coulometrische precipitatie titratie met een geleidbaarheidsmeting als eindpunt detectie.
Dit proefschrift, hoofdstuk 10

4 - H.S. Harned en B.B. Owen hebben een methode ontwikkeld voor temperatuurscompensatie van elektrische geleidbaarheidsmetingen in vloeistoffen op basis van polynomen. Het is opzienbarend dat het hun niet is opgevallen dat zij impliciet een analytische methode voor selectieve concentratiebepaling van ionen hebben beschreven.
H.S. Harned en B.B. Owen, The physical chemistry of electrolytic solutions, American Chemical Society monograph series, New York, 1958; Dit proefschrift, hoofdstuk 8

5 - Dat chemische selectiviteit niet slechts door een selectieve sensor, maar ook door een vernuftig meetprincipe kan worden verkregen, werd al in 1952 door Hodgkin en Huxley met de voltage-clamp techniek aangetoond.
A.L. Hodgkin and A.F. Huxley, A quantitative description of membrane current and its application to conduction and excitation in nerve, J. Physiol. (1952) 117, 500 - 544; Dit proefschrift, hoofdstuk 8

6 - Omdat het opvoeden en verzorgen van kinderen een vergelijkbare vaardigheid vereist op het gebied van planning en creatief denken als promoveren, dient het overwogen te worden het ouderschap als verplicht onderdeel in het promotie onderzoek op te nemen.

7 - De mate van emotie die een uitvoerend musicus in zijn spel kan leggen, is evenredig met de mate waarin zijn anatomie bij de generatie van klank is betrokken.

8 - Een stelling hoeft pas geformuleerd te worden als aan de inhoud ervan getwijfeld kan worden.

9 - In de discussie omtrent het samenvoegen van Hengelo, Enschede en Borne tot Twentestad gebruiken de tegenstanders doorgaans argumenten op basis van het directe belang van de burger, terwijl de voorstanders het algemeen economisch belang noemen. Het handhaven van verscheidene leefkernen binnen Twentestad kan beide partijen tevreden stellen.

Geert Langereis, 8 april 1999